Surface Reactivity of *Single Atom Alloys*: Model Studies Guiding the Design of Atom Efficient Nanoparticle Catalysts

A dissertation submitted by:
Felicia R. Lucci

In partial fulfillment of the requirements for the degree of:
Doctor of Philosophy, Chemistry

Tufts University
Department of Chemistry
Medford, MA
August 2016

Advisor:
E. Charles H. Sykes, Tufts University

Abstract

Catalysts are used in the majority of industrial chemical processes including the productions of $450 billion worth of chemicals. Heterogeneous catalysts often use precious metals such as Pt or Pd which have a high susceptibility to deactivation and unselective reactivity. By reducing the catalytic element to the minimum atomic ensemble, the catalytic reactivity, selectivity and stability can be optimized while using a reduced concentration of precious metal. This thesis focuses on developing atom efficient precious metal catalysts that exhibit enhanced reactivity and selectivity compared to monometallic surfaces for industrially important processes. In order to understand the capabilities of isolated atoms in inert Cu and Au hosts, the fundamental surface interactions of adsorbates with isolated reactive atoms were probed with a unique combination of atomic scale microscopy and desorption studies to elucidate the energetics of the catalyzed processes.

The majority of this work focused on Pt-Cu *single atoms alloys (SAAs)* where isolated Pt atoms, stable in a Cu surface, were identified as superior active sites for selective hydrogenation reactions. The bi-functional nature of Pt-Cu SAAs enables facile hydrogen activation without C-C bond scission and selective partial hydrogenations of butadiene on Cu terraces. In general, the weak adsorption of reactants and products to Pt-Cu SAAs yields improved selectivity and reduced susceptibility to CO poisoning and coke formation. The mechanistic details determined though surface studies on model catalysts guided the design of a new generation of Pt based catalysts for hydrogenation and methanol decomposition reactions under realistic reaction conditions.

The atom efficiency of Au based model catalysts were also studied to determine the atomic Pd ensemble in Au needed for diatomic molecule activation of H_2 and O_2. By systematically probing H_2 activation, isolated Pd atoms in Au were shown to activate H_2, a process previously thought to require to two Pd atoms. Unfortunately, the weak adsorption of hydrocarbons to Au impedes further hydrogenation reactivity in ultra-high vacuum. In order to expand the reactivity of SAAs, the potential of isolated Pd atoms for oxidation reactions was probed by examining the energetics of recombinative desorption of O_2 where dilute concentrations of Pd atoms alter the morphology of the oxidized Au surface. By understanding the surface structure of model catalysts and the energetics of probe reactions, this thesis highlights the viability of optimizing catalytic activity at the single atom limit.

Acknowledgments

"Learning is not attained by chance, it must be sought for with ardor and attended to with diligence." − Abigail Adams, 1780

Though graduate school was challenging at times, the encouragement and assistance of my family, mentors, friends, and colleagues made the last five years a rewarding and a successful experience. I am very grateful for all those who supported me during this endeavor.

These individuals begin with Prof. Charlie Sykes who was a constant source of motivation through his excitement for every single data point collected. He did his best to remove all extraneous obstacles so his students can successfully perform their research without unnecessary concerns. I am thankful for my fellow Sykes' lab members and basement associates who provided daily support. They were always available to lend a hand, provide an idea, disprove a theory, make a joke, or share a complaint. Particularly, I am indebted to those who patiently taught me their knowledge and expertise. Also, I express my gratitude to my colleagues at the *Northeastern Section of the American Chemical Society's Younger Chemists Committee* who became friends and trusted advisors that provided me with personal support and professional advice when I needed it most in graduate school.

Personally, I want to thank my family and friends for supporting me from afar in all the endeavors I decide to pursue. Throughout my life, my family has provided reassurance through a sense of stability and familiarity. On the other hand, my friends created an adventurous escape from everyday graduate student life and have shown me the significance of compassion for others.

Most importantly, I am thankful for my parents and sister who have lovingly instilled the importance of education and hard work. My parents have strived and sacrificed their entire lives to give me every opportunity possible to pursue both academic and personal passions. They always answer the phone (even though I usually don't) to share in my excitement or to provide comfort. Thus, I am eternally grateful, so I dedicate this work to you!

- Felicia R. Lucci

Table of Contents

List of Tables and Figures

Chapter 1: Introduction

1.1. Surface Science: A Guide for Heterogeneous Catalysis

In 2015, a coalition of Nobel Laureates declared that if the real and rising risk of climate change was not addressed, the demand for food, water, and energy would "overwhelm the Earth's ability to satisfy humanity's needs."[1] The declaration preceded the 2015 United Nations Climate Change Conference in Paris where a monumental agreement was reached between 196 countries that pledged to reduce their emissions of greenhouse gases and transition towards more sustainable technologies.[2]

Catalysts can play a vital role in reaching this goal by establishing processes that are environmentally cleaner and energetically efficient.[3–5] Currently, 85 % of all industrial processes utilize catalysts,[6] accounting for $450 billion per year.[3] Catalysts` are widely used because they facilitate chemical conversion at lower temperatures and pressures, thus utilizing less energy. Optimal catalysts exhibit three properties: high reactivity, strong preference to desired product, and long term stability. However, newer, more efficient catalysts are often discovered by trial and error due to the complexity of the catalysts' structures and the multi-step chemical reactions occurring on the catalysts. Thus, there is a need to understand the key properties of catalysts, such as the atomic composition and energetics of molecular interactions at the catalysts' active sites.

One viable approach to optimize catalysts is to determine the microscopic properties of a catalyst that dictate macroscopic catalytic performances. Surface science studies that use ordered surfaces can bridge the macroscopic catalytic properties, such as turn-over frequency and selectivity, with microscopic properties, such as the thermodynamics and kinetics of

elementary steps (Figure 1.1).[7–9] In this work, I studied highly controlled reactions on well-defined bimetallic alloyed surfaces to determine atomic scale parameters that control industrially relevant catalytic processes. Using atomic scale microscopy and spectroscopy, the fundamental energetics of isolated reactive catalytic atoms in noble metal hosts were identified as superior active sites.[10–14] The model catalysts then guided the design of nanoparticle catalysts that have enhanced reactivity, stability, and selectivity over monometallic catalysts at realistic operating conditions.[10,12,14]

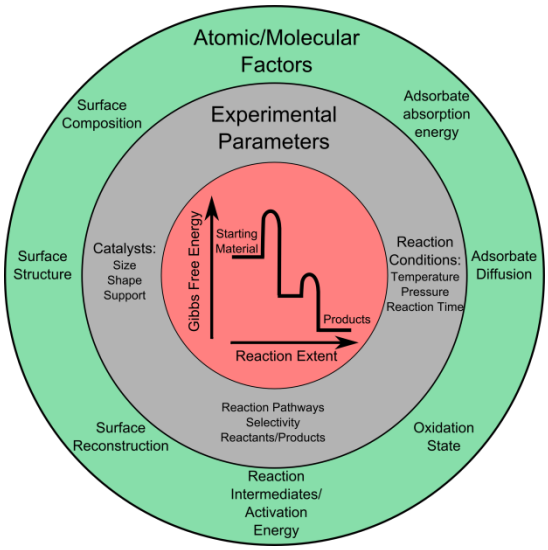

Figure 1.1. Microscopic and macroscopic properties that dictate a catalyst's activity
Adapted from Fechete et *al.*[7]

1.2. Fundamental Catalytic Surface Processes

Generally, the heterogeneous catalytic cycle is composed of a series of elementary steps starting with adsorption of molecules to the surface.[5] The adsorbed species diffuse, react, and/or desorb from the surface. The feasibility of these processes are governed by the activation barriers of each elementary step.[56] Thus, a catalyst enhances the rate of a reaction by lowering activation barriers for the rate determining step. For surface catalyzed reactions, microscopic reversibility states that the lowest energy pathway is the same for both the

forward and reverse reactions. Hence, the transition states for each elementary step are identical regardless of the reaction direction. Thus, for a reversible catalytic process, the energy profile for adsorption and desorption are identical, an important principle in experimentally elucidating the energy profile of a catalyzed reaction.

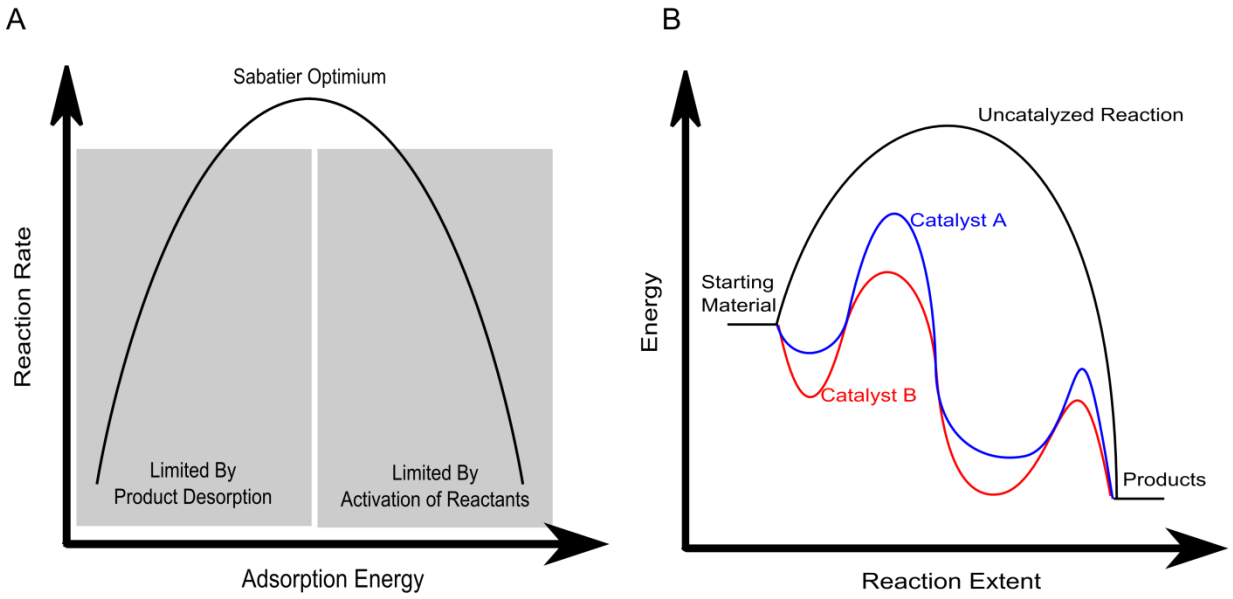

Figure 1.2. Sabatier Principle Schematic
Schematic of the (A) Sabatier Principle and (B) a general catalyzed reaction where catalyst A has higher activation barrier due to weak adsorption energy as opposed to catalyst B with the reverse relationship as predicted by the BEP relationship.

One of the most important descriptors of a catalytic surface is the adsorption strength of starting materials, intermediates, and products, as suggested by the Sabatier Principle. The Sabatier Principle relates the adsorption energy of intermediates on surfaces to the observed catalytic activity.[15] Graphical plots of catalytic activity and bond strength, called volcano plots, show a maximum in catalytic activity at intermediate adsorption strengths (Figure 1.2). Atoms or molecules must adsorb strongly enough to the surface to facilitate activation and reactivity of the reactants and intermediates, but weakly enough to allow for product desorption. The Sabatier Principle, however, is a qualitative concept that does not identify the

parameters or physical properties of transition metals necessary to predict activity and selectivity. The d-band model, proposed by Norskov, relates the adsorption strength of adsorbates to the d-band center of transition metals in relationship to the Fermi Level.[16–19]

The adsorption energy of atoms or molecules impacts the activation barriers for microscopic steps in the catalytic process including diffusion, reactivity, and desorption. The Brønsted-Evans-Polanyi (BEP) relationship theorizes a linear correlation between the barrier of a reaction and the change in enthalpy for elementary steps in a reaction.[15,20–22] For surface catalyzed reactions, the BEP relationship suggests that the activation energy (E_a) is proportional to adsorption energy (ΔE) of reactants and intermediates to a surface (Figure 1.3). As a result of the BEP relationship, strong adsorption of molecules to a surface can lower the barrier for multiple elementary steps thereby increasing the feasibility of multiple pathways. Thus, it can reduce the overall selectivity towards a given product.

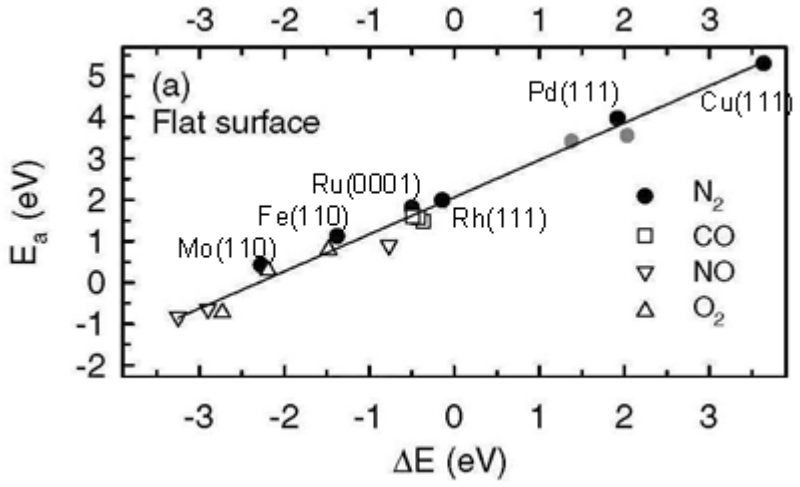

Figure 1.3. Brønsted-Evans-Polanyi (BEP) relationship
BEP relationship for N_2, CO, NO, and O_2 dissociation on metallic surfaces.[22]

Both the Sabatier Principle and BEP relationship present a challenge in catalyst design, specifically in designing catalysts that exhibit high reactivity, selectivity, and

stability. In order to have facile activation of reactants and intermediates, transition metal surfaces must bind molecules strongly. However, for surfaces that adsorb reactants and intermediates too strongly, they exhibit low selectivity, hinder desorption of products, and are often susceptible to poisoning, i.e. deactivation of the catalysts by CO adsorption[23] or coke formation.[24,25] Conversely, surfaces that weakly adsorb reactants and intermediates have higher selectivity, but barriers for activation are higher, thus resulting in lower conversion of a catalyzed reaction at a given temperature.

The inability to increase both reactivity and selectivity impacts hydrogenation and oxidation reactions where the rate limiting step is often activation of diatomic molecules which requires more reactive surfaces. When considering dissociative adsorption of molecular H_2 or O_2, generally, catalytic metals (group 10) exhibit facile activation of diatomic molecules while the noble metals (group 11) do not readily activate diatomic molecules.[16,22,26–28] For example, dissociative adsorption of H_2 is an activated process on Cu (E_a = 0.4 eV)[28] and a non-activated process on Pt (E_a = 0 eV)[29] (Figure 1.4). The energetics of H_2 activation obey the BEP relationship since the adsorption of H to Cu (ΔE = 0.2 eV) is weaker than that to Pt (ΔE = 0.6 eV). Thus, in order to have high selectivity, weak adsorption is preferred, although the barriers are often too high for activation. In this work, I show that a bi-functional model catalyst with different active sites for diatomic molecule activation and sequential hydrogenations allows for the simultaneous tuning of both reactivity and selectivity.

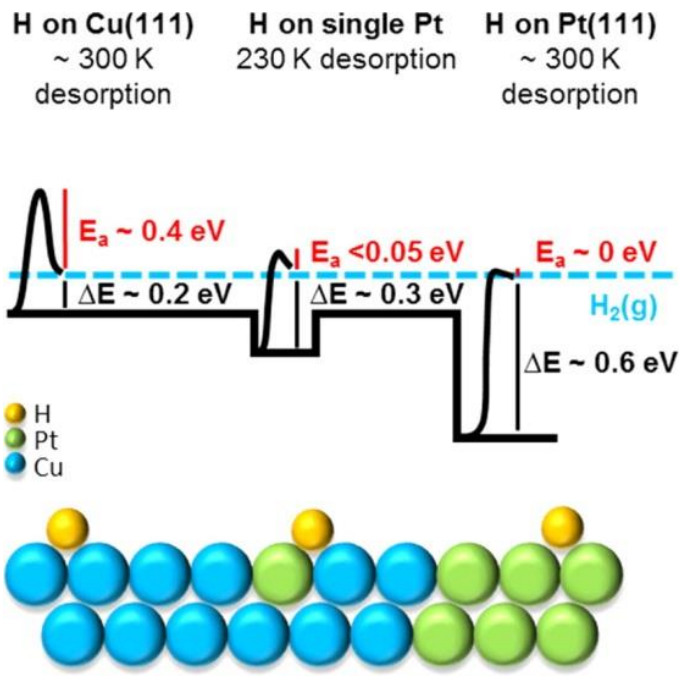

Figure 1.4. H_2 desorption from Cu(111), Pt-Cu(111) SAA and Cu(111)
Energy diagram for the adsorption and desorption of H_2 on Cu(111), Pt(111), and Pt-Cu(111) SAA[11,30,31]

1.3. Bimetallic Alloys

Since noble and catalytic group metals exhibit complementary properties in terms of weak adsorption energy and low activation barriers, it seems logical to use multiple metals to tune the reactivity, selectivity, and stability of catalysts. However, it is difficult to predict how bimetallic surfaces will compare to the parent metal.[32–34] Bimetallic alloys are known to have distinct chemical and electronic properties upon alloying.[35–39] With the advancements of atomic resolution techniques,[40–42] such as scanning tunneling microscopy and transition electron microscopy, it has been shown that the geometric arrangement of atoms in the alloy can greatly impact the observed chemical properties.[37,43–45]

Generally, the thermodynamic driving forces of alloy formation include surface free energy, mixing enthalpy, and elastic strain due to lattice size mismatch.[32–34] Bimetallic

surface alloys can form independently of bulk metal miscibilities[46] of two metals. Density Functional Theory (DFT) has predicted the miscibility of two metals by considering the segregation and mixing energies (Table 1.1 and 1.2).[32] The segregation energy is the energy of interchanging an impurity atom with a surface atom and the surface mixing energy considers the attractive/repulsive interaction between two impurity atoms. The partial concentrations of the metals affect the thermodynamic driving forces of alloy formation.[47,48] Thus, the ordering of surface atoms is highly variable depending on the preparation and reaction conditions since the kinetics of alloy formation are not fully understood or predictable. This gives rise to the necessity to characterize bimetallic alloys on the atomic scale to fully understand the composition of active sites of bimetallic catalysts for a given procedure since preparation temperature and atomic composition impact the observed structures.

Table 1.1. Segregation Energy (eV/atom) for bimetallic alloys
Shown is the energy of interchanging an impurity atom with a host surface atom where positive segregation energy predicts that the impurity atoms will diffuse into the bulk. The host atoms are in rows and the impurity atoms are in columns.[32]

	Cu	**Pd**	**Pt**	**Au**
Cu		-0.03	0.21	-0.14
Pd	0.13		0.23	-0.14
Pt	0.32	-0.01		-0.32
Au	0.26	0.15	0.21	

Table 1.2. Mixing Energy (eV/atom) for bimetallic alloys
The interaction energy between two impurity atoms where a positive energy indicates a repulsive interaction between impurity atoms.[32]

	Cu	**Pd**	**Pt**	**Au**
Cu		0.85	0.72	2.19
Pd	0.19		-0.03	0.22
Pt	0.16	0.03		-0.31
Au	0.65	0.73	0.22	

For bimetallic catalysts, changes in the reactivity and selectivity are often discussed in terms of ligand and/or ensemble effects.[35,49,50] Ligand effects refer to electronic interactions between the alloyed metals that alter their catalytic activity. When two metals are alloyed together, generally there is a shift in the d-band center which alters the adsorbate adsorption energy.[18,51] The d-band shift can be due to orbital overlap between the two metals or strain due to lattice size mismatch. For example, in the case of tensile strain, a smaller solute atom is incorporated into a larger host matrix. The d-band narrows because of a decrease in overlap of the d-orbitals and the center of the d-band becomes closer to the Fermi Level. The bond between the adsorbate and the transition metal becomes stronger. When the system is under compressive strain from a larger atom in a smaller host matrix, the reverse occurs and the overall adsorption energy decreases.[33,52]

The ensemble effects also influence bimetallic activity where changes in the catalytic activity is due to the structural or spatial arrangement of metallic atoms.[35,49] Clusters of atoms, e.g., monomers, dimers, and trimers, have been shown to exhibit distinct capabilities.[37,38,43,45,53–57] In order to optimize the atomic efficiency of catalysts, ensemble

effects are particularly interesting to investigate on the atomic level. By understanding and controlling ensemble effects, catalysts can be designed that maximize the number of active sites and minimize the amount of precious metal used.

Recently, single site catalysts have been shown to overcome the drawbacks of catalytic metals such as scarcity in nature, expense, and high susceptibility to CO poisoning and coke formation.[54] Single site catalysts have atomically dispersed species that can catalyze a number of reactions. It has been shown that single Pt and Au cations on various catalytic supports can be the active sites for water gas shift reactions,[58,59] CO oxidation,[60] steam reformation of methanol, and hydrogenation reactions.[61,62] Isolated Au atoms in Ni have been shown to suppress carbon deposition in the steam reforming of methanol.[37] Single Pd atoms in Au are required for the selective synthesis of vinyl acetate[36,63,64] and hydrogen peroxide.[65] Contiguous Pd dimers in Au are necessary for CO oxidation in order to activate diatomic O_2[43] and Pd-Ga intermetallic surfaces highlight the impact of the atomic arrangement on H_2 activation.[66] Thus, ensemble effects can greatly impact reactivity though it is challenging to determine the composition of real catalysts on the atomic scale due to the complexity of the surface structure of the catalysts.

1.4. Single Atom Alloys

The Sykes Research Group's early work focused on isolated Pd atoms in a Cu matrix.[44,67–69] The first studies showed that single Pd atoms stable in the surface of Cu enable the facile activation of H_2. H atoms then spill over from the Pd activation site to Cu terraces where they are weakly bound. The adsorbed H adatoms selectively hydrogenates styrene and acetylene. This unique class of alloys was termed *single atom alloy (SAA)*, where an isolated, more reactive atom exists in small concentrations in the surface layer of a noble metal host

(Figure 1.5). Other research groups have independently investigated the chemistry of isolated atoms in metallic hosts. Various studies examined the interaction of isolated atoms with probe molecules such as CO, CO_2 and H_2. [38,45,55,56,70–75] Fu *et al.* used DFT to compare H_2 activation barriers on Cu-based transition metal SAAs.[31] Both experiments and DFT calculations investigated the ability of isolated atoms to catalyze hydrogenation,[61,76–79] dehydrogenation,[80] oxidation,[81,82] hydrogenolysis,[83] and coupling reactions.[84] Furthermore, single atoms can potentially be used for the synthesis of hydrogen peroxide[65] and methanol.[85]

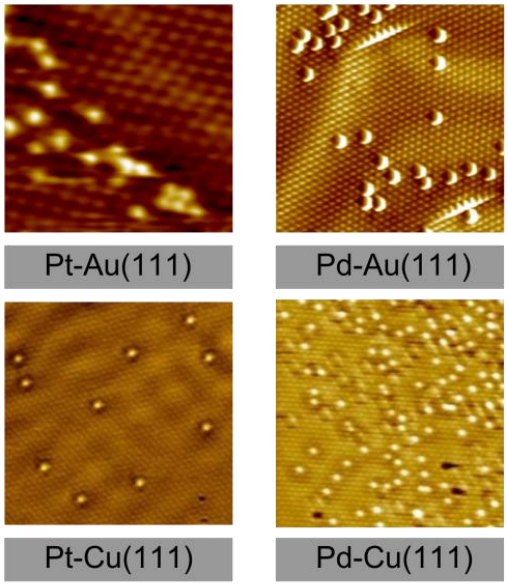

Figure 1.5. STM images of single atom alloys
The reactivity of Pd-Au(111), Pt-Cu(111), and Pd-Cu(111) SAAs and Pt-Au forms extended ensembles are probed in this dissertation.

This current work builds upon initial studies to show how SAAs can improve the overall catalytic activity under both ultra-high vacuum and realistic reaction conditions. By combing the catalytic metals, Pt or Pd, with the noble metals, Cu or Au, the activity of Cu/Au and selectivity of Pt/Pd were simultaneously increased. Unique to these studies, the catalytic metal existed in small concentrations (< 5 %) and as isolated atoms in the surface of noble

metal hosts. For these bi-functional catalysts, the isolated catalytic metals served to reduce the barrier for associative desorption of diatomic H_2 and O_2 and the adsorption energy of H, O, and CO. Also, the co-adsorption of probe molecules alter their desorption properties. In this thesis I show that SAAs are bi-functional, so the noble metal hosts perform the reactions resulting in high selectivity. The weak adsorption of reactants, intermediates and products to the host metals improves stability of the catalysts, reduces susceptibility to CO poisoning and coke formation, and selectively catalyzes butadiene hydrogenation and methanol dehydrogenation.

1.5. Descriptor Molecules

A key descriptor of a catalyst is the energetics associated with the interactions of diatomic molecules with the active site.[86] This work focused on the fundamental processes of adsorption, activation, diffusion, and desorption of diatomic molecules with SAAs to explain the improved reactivity of SAAs compared to monometallic catalysts (Table 1.3).

As a rate limiting step in hydrogenation reactions, H_2 activation by heterogeneous catalysts is of industrial interest.[87,88] Heterogeneous catalysts that allow facile activation of H_2 and weak binding of H adatoms exhibit the optimal efficiency for hydrogenation reactions. Moreover, the diffusion of H away from activation sites can be applied to H storage. The H spillover mechanism has been shown for bimetallic alloys as a useful approach to obtain weakly bound reactive H on coinage metal surfaces.[44,89] Spillover occurs when a chemical species is activated and migrates away from the active site to an alternate site that is not capable of activating the reactant under the same conditions.[90,91] Reactive metals such as Ru,[92] Ni,[71] Pd,[44,69,89] Pt,[11] and Co[93,94] alloyed with Cu dissociate H_2 and then H diffuses to the less reactive Cu host sites where it is weakly bonded. Experimental

evidence for H spillover with bimetallic surfaces focuses on Cu-based alloys, although H atoms on other surfaces including Au and Ag are of catalytic importance. This work shows H spillover readily occurs on Pt-Cu SAAs, while on Pd-Au SAAs, CO is needed to force H from the Pd activation site to the Au surface.

Another descriptor molecule is CO, a common poison for heterogeneous catalysts and PEM fuel cells.[23,95] Extensive research has investigated ways to prevent CO formation,[96,97] reduce the adsorption strength of CO,[38,56,98–100] or readily oxidize CO to CO_2.[100] When CO is co-adsorbed with H_2 onto metallic surfaces, its strong bonding can block H adsorption, alter the sticking probability, displace molecules, or alter the mixing/segregation.[12,13,64,67,93,101–106] Hence, an understanding of CO interaction with adsorbed molecules and competition for active sites is important when designing new catalysts. Also, the adsorption strength of CO can predict the ability of the surface to activate diatomic molecules or catalyst reactions as an extension of the BEP relationship.

For oxidation reactions, Au nanoparticle catalysts exhibit exceptional selectivity although Au is fairly inert towards O_2 activation.[16,119–122] The catalytic reactivity of Au can be increased by adding Pd for reactions such as vinyl acetate synthesis,[36] hydrogen peroxide synthesis,[123] hydrocarbon hydrogenation,[124,125] CO oxidation,[43] and oxidation of alcohols to aldehydes.[126] Ensemble effects are critical in controlling the overall selectivity of these reactions due to the ability to activate O_2. Thus, fundamental studies of O interactions with Pd-Au alloys can be used to fully understand the atomic interactions between O and the Pd-Au surface.

Table 1.3. Desorption temperature, adsorption energy, and activation energy of diatomic molecules of pure and SAA metallic surfaces

	Hydrogen			Carbon Monoxide		Oxygen		
	Desorption Temperature	Adsorption Energy[i]	Activation Energy[ı]	Desorption Temperature	Adsorption Energy	Desorption Temperature	Adsorption Energy[i]	Activation Energy[ı]
Pd(111)	300 K[107]	-0.58 eV[13,30,69]	0 eV[13,69]	450 K[108]	-1.58 eV[13]	800 K[109]	---	2.0 eV[110]
Pt(111)	300 K[26,27]	-0.6 eV[111]	0 eV[29]	410 K[27]	-1.893 eV[112]	720 K[110]	---	1.8 eV[110]
Cu(111)	300 K[28]	-0.2 eV[30,69]	0.4 eV[28,69]	200 K[99]	-0.922 eV[112]	---	---	---
Au(111)	110 K[13,113]	0.14 eV[13,16,69]	0.04 eV[13,16,69]	< 180 K[13,114]	-0.49 eV[13]	510 K [115]	0.20 eV[115,116]	0.93 eV[115,116]
Pd-Cu(111) SAA	210 K[44]	-0.35 eV[69]	0.02 eV[69]	270 K[67]	-1.283 eV[112]	---	---	---
Pt-Cu(111) SAA	235 K[11]	-0.3 eV[31]	0.05 eV[31,117]	350 K[12]	-1.607 eV[112]	---	---	---
Pd-Au(111) SAA	175 K[13]	-0.11 eV[13]	0.2 eV[13]	270 K[13]	-1.34 eV[13]	470 K[115]	0.25 eV[115,116]	1.12 eV[115,116]
Pt-Au(111) SAA	---	-0.360 eV[112]	0 eV[112]	385 K[37]	-1.77 eV[112]	---	---	---

[i] per H atom
[ı] per H_2 molecule neglecting quantum tunneling effects[118]
[i] per 2 O atoms
[ı] per O_2 molecule

1.6. Probe Reactions

Probe reactions were chosen based on their industrial importance. Hydrogenation reactions are widely used in the petrochemical, pharmaceutical and food industries.[87,88] Butadiene is of great interest to the polymer industry because it is a common impurity in propene and butenes feedstock. Annually, propene is used to produce 42.3 million tons of polypropylene.[127] In low concentrations (< 10 ppm), butadiene poisons alkene feedstocks.[128] Thus, the ability to selectively hydrogenate butadiene to butenes without hydrogenating alkenes would increase the purity of alkene feedstocks without reducing their overall concentration.[129–131] For this reaction, a selective catalyst would have a higher activation barrier for hydrogenation of butenes than their desorption. The

adsorption energy of butadiene has been shown to control the product distribution of the hydrocarbons. Comparing previous studies of Pt and Pd, it has been shown that weaker bonds direct product distribution in favor of butenes formation.[132,133] Butadiene adsorbs to Pt(111) via di-sigma bonds and results in multiple hydrogenation compounds.[129,132,134,135] On Cu, butadiene adsorbs in a weaker pi bond[136] which is known to direct the product distribution in favor of butenes formation. Thus, by synthesizing SAAs with predominately Cu sites and very few Pt atoms can allow for the utilization of Cu to perform the partial hydrogenation. Pt-Cu and Pd-Au alloys have been shown to catalyze selective partial hydrogenations of butadiene[125,137] and cyclohexadiene,[138] however, these studies do not consider the atomic ensembles of the alloy.

Another molecule of industrial importance is methanol due to its potential to produce both clean hydrogen gas and the commodity chemical, formaldehyde. Additionally, due to the transportability and high carbon to hydrogen ratio, methanol conversion can be used for on demand hydrogen production in PEM fuel cells. In the presence of O, methanol can be readily dehydrogenated, however, the availability of O drives the reaction.[139,140] Thus, a catalyst that can efficiently and selectively dehydrogenate methanol to formaldehyde in the absence of O is of great interest.

1.7. Pt-Cu Single Atom Alloys

The first half of this dissertation is dedicated to rationally designing a new generation of Pt-based catalysts. Pt is ubiquitous in the chemical and fuel production sectors, although its scarcity in nature and high price can limit future proliferation of platinum-

catalyzed reactions. Due to fairly strong interaction with intermediates and susceptibility to CO poisoning, Pt is often mixed with other elements. Given the catalytic differences between Pt and Cu, in these studies small amounts of Pt were alloyed into Cu and show that the surface composition and geometry of Pt-Cu alloys has a large influence on adsorbate interactions with the surface.

Extensive characterization of bulk $Pt_3Cu(111)$[141–145] alloys has been performed; however, none have examined the atomic scale surface structure of Pt-Cu and its interactions with descriptor molecules. Outlined in Chapter 3[146], the local surface structure of Pt-Cu alloys was determined using STM where it was revealed that Pt atoms alloy directly into the Cu surface distinguishing this alloy from other systems where atoms primarily alloy in at step edges. Thus, Pt atoms exist as individual isolated features well dispersed across the surface. Systematically, the uptake, spillover, and release of H as a function of surface concentration and structure was studied in Chapter 4[11]. I show both low temperature activation (< 85 K) and desorption (230 K) from Pt-Cu SAA compared to monometallic Cu (300 K) or Pt (300 K). Overall, dilute Pt-Cu alloys containing only isolated Pt atoms are most favorable for H_2 activation, spillover and release at greatly reduced concentrations of the precious metal. In Chapter 7, I probe the co-adsorption of H with catalytic poison CO to reveal that CO traps H_2 on the surface beyond its typical desorption temperature from SAAs.

In Chapters 5, 6, and 8, this dissertation shows how atomic level microscopy and spectroscopy can guide the design of a new generation of Pt-Cu nanoparticle catalysts. In collaboration with the Stephanopoulos Research Group, who synthesized γ-alumina

supported SAA nanoparticle catalysts, we transferred the concepts of SAAs from UHV model studies to realistic reaction conditions. In Chapter 5[10], Pt-Cu SAA selectively hydrogenates butadiene, an industrial important reaction. Isolated Pt atom geometries enable H_2 activation and spillover but are incapable of C-C bond scission that leads to loss of selectivity and deactivation of catalysts. Chapter 6[12] further probes the high stability of SAAs using the catalytic poison, CO. On the model SAAs surfaces, CO desorbs at low temperatures (350 K) which enables the continual exchange of H_2 and D_2 and acetylene hydrogenation under realistic conditions. Finally, in Chapter 8[14], SAAs are extended from hydrogenation reactions to methanol dehydrogenation where water is a co-catalyst to produce formaldehyde in the absence of O in UHV.

1.8. Pd-Au Single Atom Alloys

The remainder of this dissertation is dedicated to Pd-Au SAAs. Although Pd-Au alloys are well characterized in literature, the nature of the active sites for H_2 and O_2 activation are not well understood, specifically the minimum Pd ensemble needed for activation. It is proposed in the literature that contiguous Pd atoms are necessary for activation of diatomic molecules.[43,75] In Chapter 9[13], I show that single Pd atoms in Au can indeed activate H_2 at 85 K and observe an intermediate desorption temperature (175 K) of H from Pd-Au SAAs compared to Au(111) (110 K) and Pd(111) (300 K). The H atoms reside at the Pd sites, but the co-adsorption of CO forces H to spillover to the Au terraces. Though Pd-Au SAAs can activate H_2, they are unable to perform hydrogenation reactions in UHV due to the low desorption temperature of H_2 from Au (Chapter 10). In Chapter 11, I extend the reactivity of SAA to O_2 surface interactions where my research demonstrates that dilute concentration of Pd atoms alter the morphology of the Au(111) surface, thereby reducing the

desorption temperature of O_2. Since neither Au(111) or Pd-Au(111) SAA are capable of activating O_2 in UHV, in this study ozone was used to obtain O adatoms on the surfaces in order to probe the desorption properties from SAAs.

The final alloy system investigated in Chapter 12 was Pt-Au(111) to determine its feasibility as a SAA. Since higher reactivity was observed on Pt-Cu(111) compared to Pd-Cu(111),[14] it is reasonable to anticipate Pt-Au(111) would exhibit higher activity than Pd-Au(111). However, preliminary results suggest that Pt atoms do not exist as isolated atoms and form linear clusters near the Au edge dislocations.

1.9. Summary

This dissertation demonstrates the exceptional reactivity and selectivity of isolated precious metal atoms in inert metallic hosts. Through atomic-scale studies of the surface structure and adsorbate-surface interactions, this thesis shows that the catalytic element can be reduced to the single atom level. At the ultimate level of atom efficiency, model catalysts accurately predict facile H_2 activation, weak adsorption of poisonous CO, and selective hydrogenation and methanol decomposition reactivity of Pt-Cu SAAs. The reactivity of isolated atoms is then expanded to the recombinative desorption of O_2 from Pd-Au SAAs to begin to probe the use of SAAs in oxidation reactions. By systematically considering microscopic properties of SAAs, we can better explain the macroscopic reactivity experimentally observed with analogous SAA nanoparticle catalysts. Due to the bi-functional nature of SAAs which enables low temperature activation, selective reactivity, and high tolerance to coke formation and CO poising, SAAs satisfy the criteria of an ideal catalyst as an alternative approach for the use of expensive precious metal catalysts.

1.10. References

(1) Agre, P. Mainau Declaration 2015 on Climate Change, 2015.
(2) United Nations. Paris Agreement, 2015.
(3) Catalysis for Energy: Fundamental Science and Long-Term Impacts of the U. S. Department of Energy Basic Energy Science Catalysis Science Program, 2009.
(4) Bell, A. T.; Gates, B. C.; Ray, D. Basic Research Needs: Catalysis for Energy, 2007, 1–254.
(5) Bowker, M. *The Basis and Applications of Heterogeneous Catalysis*; New York, 1998.
(6) Chorkendorff, I.; Niemantsverdriet, J. W. *Concepts of Modern Catalysis an Kineticss*; WILEY-VCH Verlag: Weinheim, 2003.
(7) Fechete, I.; Wang, Y.; Vedrine, J. C. The Past, Present and Future of Heterogeneous Catalysis. *Catal. Today* **2012**, *189*, 2–27.
(8) Freund, H. J. Model Studies in Heterogeneous Catalysis. *Chem. - A Eur. J.* **2010**, *16*, 9384–9397.
(9) Yu, W.; Porosoff, M. D.; Chen, J. G. Review of Pt-Based Bimetallic Catalysis: From Model Surfaces to Supported Catalysts. *Chem. Rev.* **2012**, *112*, 5780–5817.
(10) Lucci, F. R.; Liu, J.; Marcinkowski, M. D.; Yang, M.; Allard, L. F.; Flytzani-Stephanopoulos, M.; Sykes, E. C. H.; Liu, J.; Marcinkowski, M. D.; Yang, M.; et al. Selective Hydrogenation of 1,3-Butadiene on Platinum–Copper Alloys at the Single-Atom Limit. *Nat. Commun.* **2015**, *6*, 8550.
(11) Lucci, F. R.; Marcinkowski, M. D.; Lawton, T. J.; Sykes, E. C. H. H_2 Activation and Spillover on Catalytically Relevant Pt-Cu Single Atom Alloys. *J. Phys. Chem. C* **2015**, *119*, 24351–24357.
(12) Liu, J.; Lucci, F. R.; Yang, M.; Lee, S.; Marcinkowski, M. D.; Therrien, A. J.; Williams, C. T.; Sykes, E. C. H.; Flytzani-Stephanopoulos, M. Tackling CO Poisoning with Single Atom Alloy Catalysts. *J. Am. Chem. Soc.* **2016**, No. 138, 6396–6399.
(13) Lucci, F. R.; Darby, M. T.; Mattera, M. F. G.; Ivimey, C. J.; Therrien, A. J.; Michaelides, A.; Stamatakis, M.; Sykes, E. C. H. Controlling Hydrogen Activation, Spillover, and Desorption with Pd-Au Single Atom Alloys. *J. Phys. Chem. Lett.* **2016**, *7*, 480–485.
(14) Shan, J.; Lucci, F. R.; Liu, J.; El-Soda, M.; Marcinkowski, M. D.; Allard, L. F.; Sykes, E. C. H.; Flytzani-Stephanopoulos, M. Water Co-Catalyzed Selective Dehydrogenation of Methanol to Formaldehyde and Hydrogen. *Surf. Sci.* **2016**, No. 650, 121–129.
(15) Bligaard, T.; Nørskov, J. K.; Dahl, S.; Matthiesen, J.; Christensen, C. H.; Sehested, J. The Brønsted–Evans–Polanyi Relation and the Volcano Curve in Heterogeneous Catalysis. *J. Catal.* **2004**, *224*, 206–217.
(16) Hammer, B.; Nørskov, J. K. Why Gold Is the Noblest of All the Metals. *Nature* **1995**, *376*, 238–240.
(17) Nørskov, J. K.; Abild-Pedersen, F.; Studt, F.; Bligaard, T. Density Functional Theory in Surface Chemistry and Catalysis. *PNAS* **2011**,

108, 937.
(18) Hammer, B.; Nørskov, J. K. Electronic Factors Determining the Reactivity of Metal Surfaces. *Surf. Sci.* **1995**, *343*, 211–220.
(19) Hammer, B. Norskov, J. K. Theoretical Surface Science and Catalysis-Calculations and Concepts. *Adv. Catal.* **2000**, *45*, 71–129.
(20) Santen, R. a Van; Neurock, M.; Shetty, S. G. Reactivity Theory of Transition-Metal Surfaces: A Brønsted-Evans- Polanyi Linear Activation Energy-Free-Energy Analysis. *Chem. Rev.* **2010**, *110*, 2005–2048.
(21) Nørskov, J. K.; Rossmeisl, J.; Logadottir, A.; Lindqvist, L.; Kitchin, J. R.; Bligaard, T.; Jónsson, H. Origin of the Overpotential for Oxygen Reduction at a Fuel-Cell Cathode. *J. Phys. Chem. B* **2004**, *108*, 17886–17892.
(22) Nørskov, J. K.; Bligaard, T.; Logadottir, A.; Bahn, S.; Hansen, L. B.; Bollinger, M.; Bengaard, H.; Hammer, B.; Sljivancanin, Z.; Mavrikakis, M.; et al. Universality in Heterogeneous Catalysis. *J. Catal.* **2002**, *209*, 275–278.
(23) Cheng, X.; Shi, Z.; Glass, N.; Zhang, L.; Zhang, J.; Song, D.; Liu, Z.; Wang, H.; Shen, J. A Review of PEM Hydrogen Fuel Cell Contamination: Impacts, Mechanisms, and Mitigation. *J. Power Sources* **2007**, *165*, 739–756.
(24) Barbier, J. Deactivation of Reforming Catalysts by Coking. *Appl. Catal.* **1986**, *23*, 225–243.
(25) Bitter, J. H.; Seshan, K.; Lercher, J. A. Deactivation and Coke Accumulation during CO2/CH4 Reforming over Pt Catalysts. *J. Catal.* **1999**, *343*, 336–343.
(26) Olsen, R. A.; Kroes, G. J.; Baerends, E. J. Atomic and Molecular Hydrogen Interacting with Pt(111). *J. Phys. Chem. C* **1999**, *111*, 11155–11163.
(27) Collins, D. M.; Spicer, W. E. The Adsorption of CO, O_2 and H_2 on Pt. *Surf. Sci.* **1977**, *69*, 85–113.
(28) Anger, G.; Winkler, A.; Rendulic, K. D. Adsorption and Desorption Kinetics in the Systems H_2/Cu(111), H_2/Cu(110) and H_2/Cu(100). *Surf. Sci.* **1989**, *220*, 1–17.
(29) Park, N.; Choi, K.; Hwang, J.; Kim, D. W.; Kim, D. O.; Ihm, J. Progress on First-Principles-Based Materials Design for Hydrogen Storage. *Proc. Natl. Acad. Sci.* **2012**, *109*, 19893–19899.
(30) Greeley, J.; Mavrikakis, M. Surface and Subsurface Hydrogen: Adsorption Properties on Transition Metals and near-Surface Alloys. *J. Phys. Chem. B* **2005**, *109*, 3460–3471.
(31) Fu, Q.; Luo, Y. Catalytic Activity of Single Transition-Metal Atom Doped in Cu(111) Surface for Heterogeneous Hydrogenation. *J. Phys. Chem. C.* **2013**, *117*, 14618–14624.
(32) Christensen, A.; Ruban, A. V.; Stoltze, P.; Jacobsen, K. W.; Skriver, H. L.; Nørskov, J. K.; Besenbacher, F. Phase Diagrams for Surface Alloys. *Phys. Rev. B* **1997**, *56*, 5822–5834.

(33) Groß, A. Reactivity of Bimetallic Systems Studied from First Principles. *Top. Catal.* **2006**, *37*, 29–39.
(34) Rodriguez, J. A.; Rodriguex, J. A. Physical and Chemical Properties of Bimetallic Surfaces. *Surf. Sci. Rep.* **1996**, *24*, 223–287.
(35) Ponec, V. Alloy Catalysts: The Concepts. *Appl. Catal. A* **2001**, *222*, 31.
(36) Chen, M.; Kumar, D.; Yi, C.; Goodman, D. W. The Promotional Effect of Gold in Catalysis by Palladium-Gold. *Science* **2005**, *310*, 291–293.
(37) Besenbacher, F.; Chorkendorff, I.; Clausen, B. S.; Hammer, B.; Molenbroek, A. M.; Nørskov, J. K.; Stensgaard, I. Design of a Surface Alloy Catalyst for Steam Reforming. *Science* **1998**, *279*, 1913–1915.
(38) Pedersen, M. Ø.; Helveg, S.; Ruban, A.; Stensgaard, I.; Lægsgaard, E.; Nørskov, J. K.; Besenbacher, F. How a Gold Substrate Can Increase the Reactivity of a Pt Overlayer. *Surf. Sci.* **1999**, *426*, 395–409.
(39) Greeley, J.; Mavrikakis, M. Alloy Catalysts Designed from First Principles. *Nat. Mater.* **2004**, *3*, 810–815.
(40) Bell, A. The Impact of Nanoscience on Heterogeneous. *Science* **2003**, *299*, 1688–1691.
(41) Bowker, M. Catalysis Resolved Using Scanning Tunnelling Microscopy. *Chem. Soc. Rev.* **2007**, *36*, 1656–1673.
(42) Varga, P.; Schmid, M. Chemical Discrimination on Atomic Level by STM. *Appl. Surf. Sci.* **1999**, *141*, 287–293.
(43) Gao, F.; Wang, Y.; Goodman, D. W. CO Oxidation over AuPd(100) from Ultrahigh Vacuum to near-Atmospheric Pressures: The Critical Role of Contiguous Pd Atoms. *J. Am. Chem. Soc.* **2009**, *131*, 5734–5735.
(44) Kyriakou, G.; Boucher, M. B.; Jewell, A. D.; Lewis, E. A.; Lawton, T. J.; Baber, A. E.; Tierney, H. L.; Flytzani-Stephanopoulos, M.; Sykes, E. C. H. Isolated Metal Atom Geometries as a Strategy for Selective Heterogeneous Hydrogenations. *Science* **2012**, *335*, 1209–1212.
(45) Maroun, F.; Ozanam, F.; Magnussen, O. M.; Behm, R. J. The Role of Atomic Ensembles in the Reactivity of Bimetallic Electrocatalysts. *Science* **2001**, *293*, 1811–1814.
(46) Hansen, M. *Constitution of Binary Alloys*, 2nd Ed.; McGraw-Hill: New York, 1958.
(47) Brune, H.; Röder, H.; Bromann, K.; Kern, K.; Jacobsen, J.; Stoltze, P.; Jacobsen, K.; Nørskov, J. K. Anisotropic Corner Diffusion as Origin for Dendritic Growth on Hexagonal Substrates. *Surf. Sci.* **1996**, *6028*, L115–L122.
(48) Hwang, R. Q.; Schroder, J.; Gunther, C.; Behm, R. J. Fractal Growth of Two-Dimensional Islands: Au on Ru(0001). *Phys. Rev. Lett.* **1991**, *67*, 3279–3282.
(49) Sachtler, W. M. H. Ensemble and Ligand Effects in Metal Catalysis. **2003**, 313–320.
(50) Liu, P.; Nørskov, J. K. Ligand and Ensemble Effects in Adsorption on Alloy Surfaces. *Phys. Chem. Chem. Phys.* **2001**, *3*, 3814–3818.
(51) Liu, P.; Nørskov, J. K. Ligand and Ensemble Effects in Adsorption on Alloy Surfaces. *Phys. Chem. Chem. Phys.* **2001**, *3*, 3814–3818.

(52) Rodriguez, J. A. Physical and Chemical Properties of Bimetallic Surfaces. *Surf. Sci. Rep.* **1996**, *24*, 223–287.
(53) Thomas, J. M. The Concept, Reality and Utility of Single-Site Heterogeneous Catalysts (SSHCs). *Phys. Chem. Chem. Phys.* **2014**, *16*, 7647–7661.
(54) Thomas, J. M.; Saghi, Z.; Gai, P. L. Can a Single Atom Serve as the Active Site in Some Heterogeneous Catalysts? *Top. Catal.* **2011**, *54*, 588–594.
(55) Takehiro, N.; Liu, P.; Bergbreiter, A.; Nørskov, J. K.; Behm, R. J. Hydrogen Adsorption on Bimetallic PdAu(111) Surface Alloys: Minimum Adsorption Ensemble, Ligand and Ensemble Effects, and Ensemble Confinement. *Phys. Chem. Chem. Phys.* **2014**, *16*, 23930–23943.
(56) Ruff, M.; Takehiro, N.; Liu, P.; Nørskov, J. K.; Behm, R. J. Size-Specific Chemistry on Bimetallic Surfaces: A Combined Experimental and Theoretical Study. *ChemPhysChem* **2007**, *8*, 2068–2071.
(57) Cuesta, A. At Least Three Contiguous Atoms Are Necessary for CO Formation during Methanol Electrooxidation on Platinum. *J. Am. Chem. Soc.* **2006**, *128*, 13332.
(58) Zhai, Y.; Pierre, D.; Si, R.; Deng, W.; Ferrin, P.; Nilekar, A. U.; Peng, G.; Herron, J. A.; Bell, D. C.; Saltsburg, H.; et al. Alkali-Stabilized Pt-OH_x Species Catalyze Low-Temperature Water-Gas Shift Reactions. *Science* **2010**, *329*, 1633–1636.
(59) Fu, Q.; Saltsburg, H.; Flytzani-Stephanopoulos, M. Active Nonmetallic Au and Pt Species on Ceria-Based Water-Gas Shift Catalysts. *Science* **2003**, *301*, 935–938.
(60) Qiao, B.; Wang, A.; Yang, X.; Allard, L. F.; Jiang, Z.; Cui, Y.; Liu, J.; Li, J.; Zhang, T. Single-Atom Catalysis of CO Oxidation Using Pt_1/FeO_x. *Nat. Chem* **2011**, *3*, 634–641.
(61) Vilé, G.; Albani, D.; Nachtegaal, M.; Chen, Z.; Dontsova, D.; Antonietti, M.; López, N.; Pérez-Ramírez, J. A Stable Single-Site Palladium Catalyst for Hydrogenations. *Angew. Chemie - Int. Ed.* **2015**, *54*, 11265–11269.
(62) Zhang, X.; Shi, H.; Xu, B.-Q. Catalysis by Gold: Isolated Surface Au3+ Ions Are Active Sites for Selective Hydrogenation of 1,3-Butadiene over Au/ZrO_2 Catalysts. *Angew. Chem. Int. Ed. Engl.* **2005**, *44*, 7132–7135.
(63) Neurock, M.; Tysoe, W. T. Mechanistic Insights in the Catalytic Synthesis of Vinyl Acetate on Palladium and Gold/Palladium Alloy Surfaces. *Top. Catal.* **2013**, *56*, 1314–1332.
(64) Calaza, F.; Stacchiola, D.; Neurock, M.; Tysoe, W. T. Coverage Effects on the Palladium-Catalyzed Synthesis of Vinyl Acetate: Comparison between Theory and Experiment. *J. Am. Chem. Soc.* **2010**, *132*, 2202–2207.
(65) Beletskaya, A. V; Pichugina, D. A.; Shestakov, A. F.; Kuz ’menko, N. E. Formation of H_2O_2 on Au_20 and $Au_{19}Pd$ Clusters: Understanding the Structure Effect on the Atomic Level.
(66) Prinz, J.; Gaspari, R.; Pignedoli, C. A.; Vogt, J.; Gille, P.; Armbrüster, M.;

Brune, H.; Gröning, O.; Passerone, D.; Widmer, R. Isolated Pd Sites on the Intermetallic PdGa(111) and PdGa(111) Model Catalyst Surfaces. *Angew. Chem.* **2012**, *124*, 9473–9477.

(67) Marcinkowski, M. D.; Jewell, A. D.; Stamatakis, M.; Boucher, M. B.; Lewis, E. A.; Murphy, C. J.; Kyriakou, G.; Sykes, E. C. H. Controlling a Spillover Pathway with the Molecular Cork Effect. *Nat. Mater.* **2013**, *12*, 523–528.

(68) Boucher, M. B.; Marcinkowski, M. D.; Liriano, M. L.; Murphy, C. J.; Lewis, E. A.; Jewell, A. D.; Mattera, M. F. G.; Kyriakou, G.; Flytzani-Stephanopoulos, M.; Sykes, E. C. H. Molecular-Scale Perspective of Water-Catalyzed Methanol Dehydrogenation to Formaldehyde. *ACS Nano* **2013**, *7*, 6181–6187.

(69) Tierney, H. L.; Baber, A. E.; Kitchin, J. R.; Sykes, E. C. H. Hydrogen Dissociation and Spillover on Individual Isolated Palladium Atoms. *Phys. Rev. Lett.* **2009**, *103*, 246102–1 – 4.

(70) Ramos, M.; Martínez, A. E.; Busnengo, H. F. H_2 Dissociation on Individual Pd Atoms Deposited on Cu(111). *Phys. Chem. Chem. Phys.* **2012**, *14*, 303–310.

(71) Yao, Y.; Goodman, D. W. Direct Evidence of Hydrogen Spillover from Ni to Cu on Ni–Cu Bimetallic Catalysts. *J. Mol. Catal. A Chem.* **2014**, *383-384*, 239–242.

(72) Serrate, D.; Moro-Lagares, M.; Piantek, M.; Pascual, J. I.; Ricardo Ibarra, M. Enhanced Hydrogen Dissociation by Individual Co Atoms Supported on Ag(111).

(73) Qiu, M.; Fang, Z.; Li, Y.; Zhu, J.; Huang, X.; Ding, K.; Chen, W.; Zhang, Y. First-Principles Investigation of the Activation of CO_2 Molecule on TM/Cu (TM=Fe, Co and Ni) Surface Alloys. *Appl. Surf. Sci.* **2015**.

(74) Linke, R.; Schneider, U.; Busse, H.; Becker, C.; Schröder, U.; Castro, G. R.; K., W. Interaction of Hydrogen with Cu_3Pt(111): Dissociation via Isolated Platinum Atoms. *Surf. Sci.* **1994**, *307 - 309*, 407–411.

(75) Yu, W. Y.; Mullen, G. M.; Mullins, C. B. Hydrogen Adsorption and Absorption with Pd-Au Bimetallic Surfaces. *J. Phys. Chem. C* **2013**, *117*, 19535–19543.

(76) Pei, G. X.; Liu, X. Y.; Wang, A.; Li, L.; Huang, Y.; Zhang, T.; Lee, J. W.; Jang, B. W. L.; Mou, C.-Y. Promotional Effect of Pd Single Atoms on Au Nanoparticles Supported on Silica for the Selective Hydrogenation of Acetylene in Excess Ethylene. *New. J. Chem.* **2014**, *38*, 2043–2051.

(77) Pei, G. X.; Liu, X, Y.; Liu, Y.; Wang, A.; Lee, A. F.; Isaacs, M. A.; Li, L.; Pan, X.; Yang, X.; Wang, X.; et al. Ag Alloyed Pd Single-Atom Catalysts for Efficient Selective Hydrogenation of Acetylene to Ethylene in Excess Ethylene. *ACS Catal.* **2015**, *5*, 3717–3725.

(78) Aich, P.; Wei, H.; Basan, B.; Kropf, A. J.; Schweitzer, N. M.; Marshall, C. L.; Miller, J. T.; Meyer, R. Single-Atom Alloy Pd–Ag Catalyst for Selective Hydrogenation of Acrolein.

(79) McCue, A. J.; Gibson, A.; Anderson, J. A. Palladium Assisted Copper/alumina Catalysts for the Selective Hydrogenation of Propyne,

Propadiene and Propene Mixed Feeds. *Chem. Eng. J.* **2016**, *285*, 384–391.
(80) Cao, X.; Ji, Y.; Luo, Y. Dehydrogenation of Propane to Propylene by a Pd/Cu Single-Atom Catalyst: Insight from First-Principles Calculations. *J. Phys. Chem. C* **2015**, *119*, 1016–1023.
(81) Zhang, H.; Kawashima, K.; Okumura, M.; Toshima, N. Colloidal Au Single-Atom Catalysts Embedded on Pd Nanoclusters. *J. Mater. Chem.* **2014**, *2*, 13498.
(82) Cheng, X.; Zhao, Y.; Li, F.; Liu, Y. Catalytic Mechanisms of Au11 and Au_{11}-nPt_n (n=1–2) Clusters: A DFT Investigation on the Oxidation of CO by O_2. *J. Mol. Model.* **2015**, *21*, 230.
(83) Yao, Y.; Goodman, D. W. New Insights into Structure–activity Relationships for Propane Hydrogenolysis over Ni–Cu Bimetallic Catalysts.
(84) Zhang, L.; Wang, A.; Miller, T.; Liu, X.; Yang, X.; Wang, W.; Li, L.; Huang, Y.; Mou, C.; Zhang, T. Efficient and Durable Au Alloyed Pd Single-Atom Catalyst for the Ullmann Reaction of Aryl Chlorides in Water. *ACS Catal.* **2014**, *4*, 1546–1553.
(85) Yang, Y.; White, M. G.; Liu, P. A Theoretical Study of Methanol Synthesis from CO_2 Hydrogenation on Metal-Doped Cu(111) Surfaces. *J. Phys. Chem. C* **2012**, *116*, 248–256.
(86) Knudsen, J.; Nilekar, A. U.; Vang, R. T.; Schnadt, J.; Kunkes, E. L.; Dumesic, J. A.; Mavrikakis, M.; Besenbacher, F. A Cu/Pt Near-Surface Alloy for Water-Gas Shift Catalysis. *J. Am. Chem. Soc.* **2007**, *129*, 6485–6490.
(87) Hagen, J. *Industrial Catalysis*; WILEY-VCH Verlag: Germany, 2006.
(88) Ritter, J. A.; Ebner, A. D. State-of-the-Art Adsorption and Membrane Separation Processes for Hydrogen Production in the Chemical and Petrochemical Industries. *Sep. Sci. Technol.* **2007**, *42*, 1123–1193.
(89) Boucher, M. B.; Zugic, B.; Cladaras, G.; Kammert, J.; Marcinkowski, M. D.; Lawton, T. J.; Sykes, E. C. H.; Flytzani-Stephanopoulos, M. Single Atom Alloy Surface Analogs in $Pd_{0.18}Cu_{15}$ Nanoparticles for Selective Hydrogenation Reactions. *Phys. Chem. Chem. Phys.* **2013**, *15*, 12187–12196.
(90) Prins, R. Hydrogen Spillover. Facts and Fiction. *Chem. Rev.* **2012**, *112*, 2714–2738.
(91) Conner, W. C.; Falconer, J. L. Spillover in Heterogeneous Catalysis. *Chem. Rev.* **1995**, *95*, 759–788.
(92) Citrin, P. H.; Wertheim, G. K.; Baer, Y. Surface-Atom X-Ray Photoemission from Clean Metals: Cu, Ag, and Au P. *Phys. Rev. B* **1983**, *27*, 3160.
(93) Lewis, E. A.; Le, D.; Jewell, A. D.; Murphy, C. J.; Rahman, T. S.; Sykes, E. C. H. Visualization of Compression and Spillover in a Coadsorbed System: Syngas on Cobalt Nanoparticles. *ACS Nano* **2013**, *7*, 4384–4392.
(94) Lewis, E. A.; Marcinkowski, M. D.; Murphy, C. J.; Liriano, M. L.; Sykes, E.

C. H. Hydrogen Dissociation, Spillover, and Desorption from Cu-Supported Co Nanoparticles. *J. Phys. Chem. Lett.* **2014**, *5*, 3380–3385.
(95) Baschuk, J. J.; Li, X. Carbon Monoxide Poisoning of Proton Exchange Membrane Fuel Cells. *Int. J. Energy Res.* **2001**, *25*, 695–713.
(96) Tanaka, K.; Shimizu, A.; Fujimori, M.; Kodama, S.; Sawai, S. Deactivation of a Cu/Al_2O_3 Catalyst in a N_2O Decomposition Reaction. *Appl. Catal. A* **1999**, *179*, 21–29.
(97) Lindström, B. Hydrogen Generation by Steam Reforming of Methanol over Copper-Based Catalysts for Fuel Cell Applications. *Int. J. Hydrogen Energy* **2001**, *26* (9), 923–933.
(98) Eyrich, M.; Diemant, T.; Hartmann, H.; Bansmann, J.; Behm, R. J. Interaction of CO with Structurally Well-Defined Monolayer PtAu/Pt(111) Surface Alloys. *J. Phys. Chem. C* **2012**, *116*, 11154–11165.
(99) Kirstein, W.; Krüger, B.; Thieme, F. CO Adsorption Studies on Pure and Ni-Covered Cu(111) Surfaces. *Surf. Sci.* **1986**, *176*, 505–529.
(100) Hashmi, A. S. K.; Hutchings, G. J. Gold Catalysis. *Angew. Chemie - Int. Ed.* **2006**, *45*, 7896–7936.
(101) Montano, M.; Bratlie, K.; Salmeron, M.; Somorjai, G. A. Hydrogen and Deuterium Exchange on Pt(111) and Its Poisoning by Carbon Monoxide Studied by Surface Sensitive High-Pressure Techniques. *J. Am. Chem. Soc.* **2006**, *128*, 13229–13234.
(102) Johansson, M.; Lytken, O.; Chorkendorff, I. The Sticking Probability for H_2 in Presence of CO on Some Transition Metals at a Hydrogen Pressure of 1 Bar. *Surf. Sci.* **2008**, *602*, 1863–1870.
(103) Tang, D. C.; Hwang, K. S.; Salmeron, M.; Somorjai, G. A. High Pressure Scanning Tunneling Microscopy Study of CO Poisoning of Ethylene Hydrogenation on Pt(111) and Rh(111) Single Crystals. *J. Phys. Chem. B* **2004**, *108*, 13300–13306.
(104) Hoge, D.; Tushaus, M.; Bradshaw, a. M. Island Formation during CO/H Coadsorption on Pt{111} Studied by IR Reflection-Absorption Spectroscopy. *Surf. Sci.* **1988**, *207*, L935–L942.
(105) Richter, L. J.; Gurney, B. A.; Ho, W. The Influence of Adsorbate–adsorbate Interactions on Surface Structure: The Coadsorption of CO and H_2 on Rh(100). *J. Chem. Phys.* **1987**, *86*, 477–490.
(106) Morkel, M.; Rupprechter, G.; Freund, H. J. Ultrahigh Vacuum and High-Pressure Coadsorption of CO and H_2 on Pd(111): A Combined SFG, TDS, and LEED Study. *J. Chem. Phys.* **2003**, *119*, 10853–10866.
(107) Gdowski, G. E.; Felter, T. E.; Stulen, R. H. Effect of Surface Temperature on the Sorption of Hydrogen on Pd(111). *Surf. Sci.* **1987**, *181*, L147–L155.
(108) Guo, X.; Yates, J. T. Dependence of Effective Desorption Kinetic Parameters on Surface Coverage and Adsorption Temperature: CO on Pd(111). *J. Chem. Phys.* **1989**, *90*, 6761–6766.
(109) Zheng, G.; Altman, E. I. The Oxidation of Pd(111). *Surf. Sci.* **2000**, *462*, 151–168.

(110) Miller, S. D.; Pushkarev, V. V.; Gellman, A. J.; Kitchin, J. R. Simulating Temperature Programmed Desorption of Oxygen on Pt(111) Using DFT Derived Coverage Dependent Desorption Barriers. *Top. Catal.* **2014**, *57*, 106–117.
(111) Hanh, T. T. T.; Takimoto, Y.; Sugino, O. First-Principle Thermodynamic Description of Hydrogen Electroadsorption on Pt(111) Surface. *Surf. Sci.* **2014**, *625*, 104–111.
(112) Unpublished from Matthew T. Darby and the Stamatakis Group from University College London.
(113) Pan, M.; Flaherty, D. W.; Mullins, C. B. Low-Temperature Hydrogenation of Acetaldehyde to Ethanol on H-Precovered Au(111). *J. Phys. Chem. Lett.* **2011**, *2*, 1363–1367.
(114) Kim, J.; Samano, E.; Koel, B. E. CO Adsorption and Reaction on Clean and Oxygen-Covered Au(211) Surfaces. *J. Phys. Chem. B* **2006**, *110*, 17512–17517.
(115) Unpublished from Graeme Henkelman from The University of Texas at Austin as Shown in Chapter 11.
(116) Yu, W. Y.; Zhang, L.; Mullen, G. M.; Henkelman, G.; Mullins, C. B. Oxygen Activation and Reaction on Pd–Au Bimetallic Surfaces. *J. Phys. Chem. C* **2015**, *119* (21), 11754–11762.
(117) Schröder, U.; Linke, R.; Boo, J.; Wander, K. Adsorption Properties and Formation of Pt/Cu Surface Alloys. *Surf. Sci.* **1996**, *354*, 211–217.
(118) Kyriakou, G.; Davidson, E. R. M.; Peng, G.; Roling, L. T.; Singh, S.; Boucher, M. B.; Marcinkowski, M. D.; Mavrikakis, M.; Michaelides, A.; Sykes, E. C. H. Significant Quantum Effects in Hydrogen Activation. *ACS Nano* **2014**, *8*, 4827–4835.
(119) Claus, P. Heterogeneously Catalysed Hydrogenation Using Gold Catalysts. *Appl. Catal.* **2005**, *291*, 222–229.
(120) Mcewan, L.; Julius, M.; Roberts, S.; Fletcher, J. C. Q. A Review of the Use of Gold Catalysts in Selective Hydrogenation Reactions. *Gold Bull.* **2010**, *43*, 298–306.
(121) Haruta, M. Size- and Support-Dependency in the Catalysis of Gold. *Catal. Today* **1997**, *861*, 153–166.
(122) Mohr, C.; Hofmeister, H.; Radnik, J.; Claus, P. Identification of Active Sites in Gold-Catalyzed Hydrogenation of Acrolein. *J. Am. Chem. Soc.* **2003**, *103*, 178–180.
(123) Edwards, J. K.; Solsona, B.; Ntainjua N, E.; Carley, A. F.; Herzing, A. A.; Kiely, C. J.; Hutchings, G. J. Switching off Hydrogen Peroxide Hydrogenation in the Direct Synthesis Process. *Science* **2009**, *323*, 1037–1041.
(124) Choudhary, T. V; Sivadinarayana, C.; Datye, A. K.; Kumar, D.; Goodman, D. W. Acetylene Hydrogenation on Au-Based Catalysts. *Catal. Letters* **2003**, *86*, 1–8.
(125) Hugon, A.; Delannoy, L.; Krafft, J. M.; Louis, C. Selective Hydrogenation of 1,3-Butadiene in the Presence of an Excess of Alkenes over Supported Bimetallic Gold−palladium Catalysts. *J. Phys. Chem. C.* **2010**,

114, 10823–10835.
(126) Enache, D. I.; Edwards, J. K.; Landon, P.; Solsona-Espriu, B.; Carley, A. F.; Herzing, A. A.; Watanabe, M.; Kiely, C. J.; Knight, D. W.; Hutchings, G. J. Solvent-Free Oxidation of Primary Alcohols to Aldehydes Using Au-Pd/TiO_2 Catalysts. *Science* **2006**, *311*, 362–365.
(127) GBI Research. *Polypropylene Global Market to 2020 - Developing Regions of Asia-Pacific and Middle East and Africa to Drive Polypropylene Market Growth*; 2013.
(128) Derrien, M. L. Selective Hydrogenation Applied to the Refinging of Petrochemical Raw Materials Produced by Steam Cracking. *Stud. Surf. Sci. Catal.* **1986**, *27*, 613–666.
(129) Yoon, C.; Yang, M. X.; Somorjai, G. A. Hydrogenation of 1,3-Butadiene on Platinum Surfaces of Different Structures. *Catal. Lett.* **1997**, *46*, 37–41.
(130) Zaera, F.; Somorjai, G. A. Hydrogenation of Ethylene over Platinum (111) Single-Crystal Surfaces. *J. Am. Chem. Soc.* **1984**, *106*, 2288–2293.
(131) Guo, X.; Madix, R. J. . Selective Hydrogenation and H-D Exchange of Unsaturated Hydrocarbons on Pd(100)-p(1x1)-H(D). *J. Catal.* **1995**, *155*, 336–344.
(132) Mittendorfer, F.; Thomazeau, C.; Raybaud, P.; Toulhoat, H. Adsorption of Unsaturated Hydrocarbons on Pd(111) and Pt(111): A DFT Study. *J. Phys. Chem. B* **2003**, *107*, 12287–12295.
(133) Valcárcel, A.; Clotet, A.; Ricart, J. M.; Delbecq, F.; Sautet, P. Selectivity Control for the Catalytic 1,3-Butadiene Hydrogenation on Pt (111) and Pd (111) Surfaces: Radical versus Closed-Shell Intermediates. *J. Phys. Chem. B* **2005**, *109*, 14175–14182.
(134) Zhao, H.; Welch, L. A.; Koel, B. E. Site-Blocking Effects of Preadsorbed H on Pt(111) Probed by 1,3-Butadiene Adsorption and Reaction. *Surf. Sci.* **2009**, *603*, 3355–3360.
(135) Michalak, W. D.; Krier, J. M.; Komvopoulos, K.; Somorjai, G. A. Structure Sensitivity in Pt Nanoparticle Catalysts for Hydrogenation of 1,3-Butadiene: In Situ Study of Reaction Intermediates Using SFG Vibrational Spectroscopy. *J. Phys. Chem. C* **2013**, *117*, 1809–1817.
(136) Huang, W.; Wei, W.; Zhao, W.; White, J. M. Two-Photon Photoemission Spectroscopy Study of 1 , 3-Butadiene on Cu (111): Electronic Structures and Excitation Mechanism. *J. Phys. Chem. B* **2006**, *110*, 5547–5552.
(137) Lonergan, W. W.; Xing, X.; Zheng, R.; Qi, S.; Huang, B.; Chen, J. G. Low-Temperature 1,3-Butadiene Hydrogenation over Supported Pt/3d/γ-Al_2O_3 Bimetallic Catalysts. *Catal. Today* **2011**, *160*, 61–69.
(138) Qi, S.; Yu, W.; Lonergan, W. W.; Yang, B.; Chen, J. G. General Trends in the Partial and Complete Hydrogenation of 1,4-Cyclohexadiene over Pt-Co, Pt-Ni and Pt-Cu Bimetallic Catalysts. *Chem. Cat. Chem* **2010**, *2*, 625–628.
(139) Takagi, K.; Morikawa, Y.; Ikawa, T. Catalytic Activities of Coppers in the Various Oxidation States for the Dehydrogenation of Methanol.

Chem. Lett. **1985**, 527–530.
(140) Wachs, I. E.; Madix, R. J. Selective Oxidation of CH_3OH to H_2CO on a Copper(110) Catalyst. *J. Catal.* **1978**, *53* (2), 208–227.
(141) Miura, S.; Mitsui, K.; Tanaka, Y.; Mishima, Y.; Suzuki, T. Positive Temperature Dependence of Strength Observed in Ordered Cu_3Pt Single Crystals. *Philos. Mag. A* **1992**, *65*, 737–747.
(142) Shen, Y. G.; O'Connor, D. J.; Wandelt, K.; Macdonald, R. J. Studies of Surface Composition and Structure of $Cu_3Pt(111)$ by Low Energy Alkali Ion Scattering. *Surf. Sci.* **1995**, *328*, 21–31.
(143) Castro, G. R.; Schneider, U.; Busse, H.; Janssens, T.; Wandelt, K. The Interaction of CO with the $Cu_3Pt(111)$ Surface. *Surf. Sci.* **1992**, *270*, 321–325.
(144) Shen, Y. G.; O'Connor, D. J.; Wandelt, K.; MacDonald, R. J. Thin Film Growth of Pt on Cu(111): A LEIS Study. *Surf. Sci.* **1996**, *357 - 358*, 921–925.
(145) Shen, Y. G.; O'Connor, D. J.; Wandelt, K. The Surface Composition, Structure and Oxygen-Induced (2×1) Reconstruction of CuPt(110). *Surf. Sci.* **1998**, *410*, 1–14.
(146) Lucci, F. R.; Lawton, T. J.; Pronschinske, A.; Sykes, E. C. H. Atomic Scale Surface Structure of Pt/Cu(111) Surface Alloys. *J. Phys. Chem. C* **2014**, *118*, 3015–3022.

Chapter 2: Experimental Methods

In order to comprehensively characterize the chemistry of single atom alloys, bimetallic catalysts were modeled using well defined metallic surfaces in ultra-high vacuum (UHV). The (111) facet of Cu or Au were used since it is the predominant crystal facet on nanoparticles. Bimetallic surface alloys were then prepared by physical vapor deposition of Pt or Pd onto Au(111) or Cu(111) single crystals (Figure 2.1A and 2.2A). The unique coupling of scanning tunneling microscopy (STM), temperature programmed desorption/reactions (TPD/R), and x-ray photoelectron spectroscopy (XPS) provided the ability to probe both morphology and reactivity on the atomic scale at surface concentrations < 1 %. STM characterized the local electronic and topographical morphology of the surface, and XPS gave chemical identity and oxidation states. TPD/R quantified reaction kinetics, surface structure and reactivity/selectivity of adsorbates on the surface.

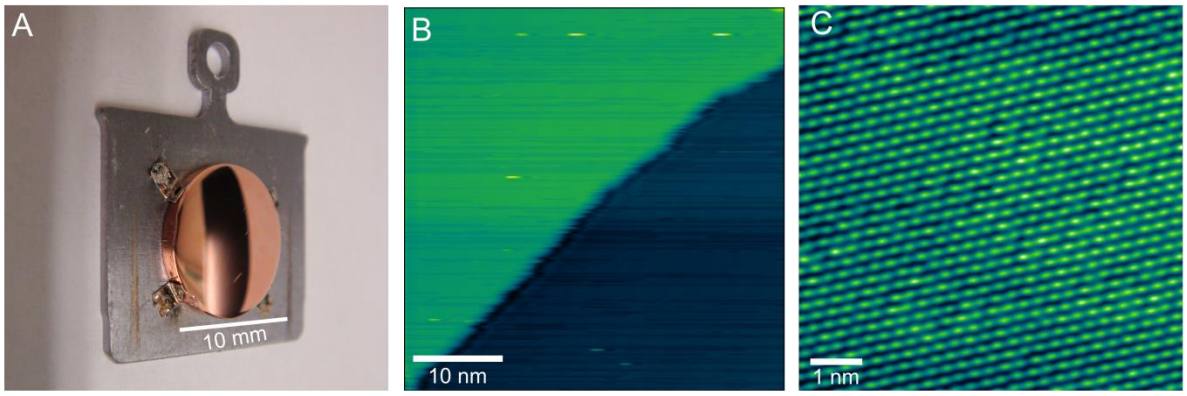

Figure 2.1. STM of Cu(111) single crystal
Shown is a curved Cu(111)[7] single crystal and STM images of (B) monoatomic Cu steps and (C) atomic lattice.

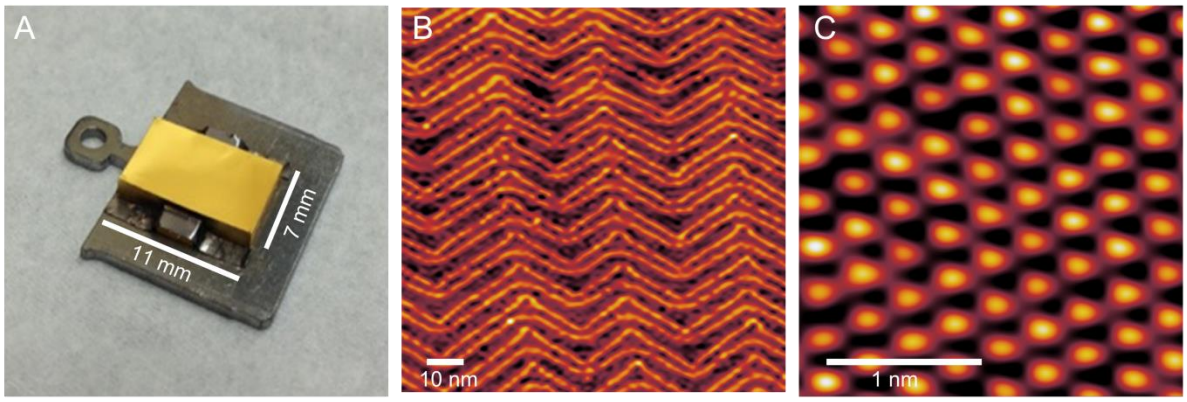

Figure 2.2. STM of Au(111) single crystal
Shown is a Au(111) single crystal and STM images of the (B) Au(111) herringbone reconstruction and (C) atomic lattice.

2.1. Techniques

2.1.1. Scanning Tunneling Microscopy (STM)

STM is a tool used to investigate surface structure on the atomic scale and manipulate atoms or molecules.[1–3] A topographical map of the surface is obtained by rastering an atomically sharp tip across a conductive surface and fixing the tunneling current between the materials while monitoring the tip height. A W or Pt/Ir tip is brought within nanometers of the surface, since the surface and tip are not in electrical contact, classically, there should be no flow of electrons. However, due to quantum mechanics, the wave functions of the tip and surface overlap allowing electrons to transverse the small separation between the two conductive materials. The observed tunneling current (I) is exponentially related to the separation between the conductive points (d) as described in the equation:

$$I \propto e^{-2\kappa \mathrm{d}}$$

$$\kappa = \sqrt{\frac{2m}{\hbar}(eU_B - E)}$$

Where m is the mass of an electron, $\hbar$ is Planck's constant divided by 2 π, E is the energy state from which the electron tunnels, and eU_B is the barrier height of the tunneling gap. Thus, a small change in the separation between the tip and sample yields an exponential change in current. Additionally, applying a potential to either the sample or tip controls the direction of electron flow since electrons flow from occupied to unoccupied electronic states. Thus, STM specifically images the density of states of the surface. Since electrons are localized around the atomic nuclei, the position of atoms can be inferred. For example, STM is capable of resolving monoatomic steps of Cu(111) (Figure 2.2B), the Au(111) herringbone reconstruction[4,5] (Figure 2.3B), and individual atoms (Figure 2.2C and 2.3C). Although STM can determine the local structure of the surface, it does not provide chemical identification.[6]

2.1.2. Temperature Programmed Desorption/Reaction (TPD/R)

TPD is a simple technique that can be used to extrapolate both thermodynamic and kinetic parameters such as desorption rate, desorption energy and reactions orders.[2,8] It can also be used to determine surface composition/coverage, adsorption sites, and relative sticking probabilities. Additionally, the co-adsorption of molecules in Temperature Programmed Desorption /Reactions (TPD/R) can be used to extrapolate reaction pathways, selectivity, active sites, and the rate limiting steps of surface catalyzed reactions. TPD is performed by exposing a surface to a combination of gases and then applying a linear heating rate to the sample to react or desorb the surface species (Figure 2.3A). A mass spectrometer (MS) is used to monitor desorption of molecules as a function of temperature as shown in a typical TPD trace (Figure 2.3B). With sufficient pumping speed, the rate of desorption is related to the pressure increase in the chamber.

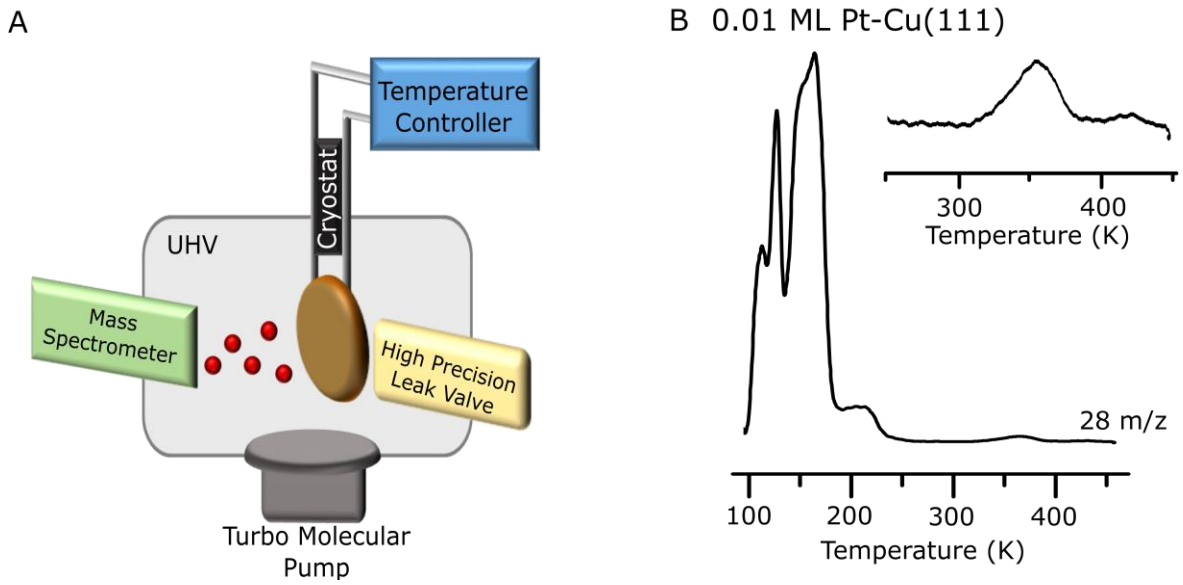

Figure 2.3. Temperature programmed desorption schematic
(A) Schematic of TPD setup and (B) TPD trace for the desorption of CO from 0.01 ML Pt-Cu(111).

A thermal desorption trace can be used to extrapolate surface kinetics based on the Polanyi-Wigner Equation:

$$r_{des} = \frac{\partial \Theta}{\partial t} = v_n \Theta^n e^{-\frac{E_{des}}{RT}}$$

Where r_{des} is the rate of desorption, θ is surface coverage, t is time, $v_n\theta^n$ is the pre-exponential factor of chemical process of n order (i.e. attempt frequency), E_{des} is the activation energy of desorption, R is the universal gas constant, and T is temperature.

The Polanyi-Wigner equation can be derived from the rate of desorption (r_{des}) of an adsorbate from a surface as expressed in the general form:

$$r_{des} = \frac{\partial \Theta}{\partial t} = k_{des} \Theta^n$$

where $\frac{\partial \Theta}{\partial t}$ is the change in coverage with respect to t and k_{des} is the rate constant for desorption. When applying a linear heating rate ($T = T_0 + \beta t$), the heating rate (β) can be described as $\beta = dT/dt$. Thus, the rate of desorption can be written as:

$$r_{des} = \frac{\partial \Theta}{\partial T} = \frac{k_{des}}{\beta} \Theta^n$$

Since desorption is an activated process, the rate constant (k_{des}) can be expressed in the Arrhenius form:

$$k_{des} = v_n e^{-\frac{E_{des}}{RT}}$$

Thus, the rate of desorption is :

$$r_{des} = \frac{\partial \Theta}{\partial T} = \frac{v_n \Theta^n}{\beta} e^{-\frac{E_{des}}{RT}}$$

From the Polanyi-Wigner equation, we can determine parameters such as rate of desorption and kinetic order of desorption.

Additional methods can be used to determine the energy of desorption from the thermal desorption traces[9] including Complete Analysis, Leading Edge Analysis, Redhead Analysis, and Varied Heating Rate Analysis. The Redhead Analysis[10] is commonly used to approximate the energy of desorption for first order processes from the Polanyi-Wigner equation. The Redhead equation shows that the energy of desorption is related to the peak temperature (T_p):

$$E_{des} = RT_P \left[\ln \frac{vT_p}{\beta} - 3.65\right]$$

Redhead can only be applied to first order processes and utilizes multiple assumptions including E_{des} and *v* are coverage independent. Furthermore, *v* must be independently calculated or assumed. Typically, a standard pre-exponential factor (*v*) is assumed to be 10^{13} s^{-1} characteristic of a vibrational frequency of atom in a potential well. However, recently, it has been shown 10^{15} s^{-1} is a more accurate estimation since it accounts for the adsorbates interaction with the surface.[11,12]

2.1.3. X-ray Photoelectron Spectroscopy (XPS)

Chemical identification and oxidation state of surface atoms can be provided by XPS due to characteristic binding energy of core level electrons.[2] XPS is based on the photoelectric effect where a monochromatic x-ray source (Mg or Al) ejects core level electrons from the surface. Based on the Einstein equation, the kinetic energy of the ejected electrons is dependent on the energy of the incident photon ($h\upsilon$), the binding energy of the electron (E_B) and the work function (ϕ).

$$E_{kin} = h\upsilon - E_B - \phi$$

The number of electrons ejected as function of kinetic energy is detected using an electrostatic energy analyzer. A potential is applied across a hemispherical analyzer so that only the electrons of a given kinetic energy reach the detector. The constant pass energy maintains a constant resolution regardless of kinetic energy. Although core level electrons are less susceptible then valence electrons to binding interactions, the binding energy is dependent on the chemical environment. Since charge transfer alters the columbic attraction between core electrons and the nucleus, chemical shifts in the binding energy can be used to determine the oxidation state of the surface species.

2.2. Ultra-high Vacuum Chambers

In order to maintain the well-defined surfaces and cleanliness of the samples over extended periods of time, experiments on model catalytic surfaces were performed in four separate ultra-high vacuum (UHV) chamber depending on the chamber's capabilities to perform TPD/R, STM, or XPS experiments (Figure 2.4, Table 2.1). All UHV chambers had base pressures < 5 * 10^{-10} mbar that were monitored using Iridium Filament ion gauge (VG Scienta).

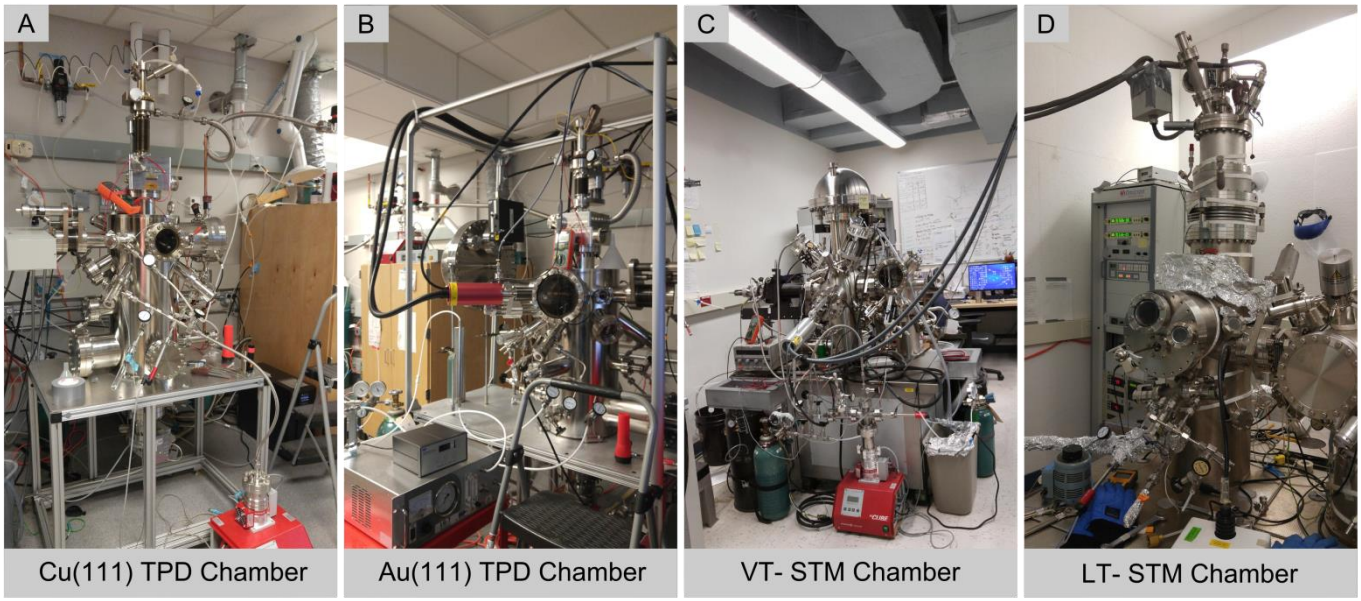

Figure 2.4. Sykes Research Group's ultra-high vacuum chambers
Shown are the four separate UHV chambers used in this work including (A) Cu(111) TPD1, (B) Au(111) TPD2, (C) VT-STM, and (D) LT-STM.

Table 2.1. Capabilities of Sykes Research Group's ultra-high vacuum chambers

	Instrumentation	**STM Temperature Capabilities**	**Manipulator Temperature Capabilities**	**Metal Deposition Sources**
Cu(111) TPD1	MS, LEED, Auger	n/a	85 K – 750 K	Pt
Au(111) TPD2	MS, XP	n/a	85 K – 750 K	Pt
VT-STM	XPS, STM	30 – 500 K	110 K –1100 K	Pd and Pt
LT-STM	STM	5 K, 85 K, 293K	293 K – 1170 K	Pd or Pt

For TPD experiments two different UHV chambers were used which contained either a Cu(111) or Au(111) single crystal. Both chambers were equipped with a quadrupole mass spectrometer (Hidden Hal/3F 301 RC system, Hidden Analytical) with a mass range of 300 amu. The mass spectrometers had a dual Faraday/single channel electron multiplier detector. In order to maintain UHV conditions, the TPD chambers used turbo molecular pumps (Pfeiffer Vacuum) and titanium sublimation pumps (TSPs). The single crystals were 11 mm in diameter and were mounted to a manipulator that could be translated in the x (± 10 mm), y (± 10 mm), and z (± 50 mm) directions, and rotated 360 °. The manipulator was equipped with a liquid nitrogen cryostat allowing the crystal to be cooled to 85 K. The single crystals were suspended using Ta wires (0.25 mm) and a k-type thermocouple was pressure fitted directly into the crystal. The sample could be resistively heated from 85 K to 750 K. For TPD experiments, the sample was heated at a rate of 1 K/s.

The quadrupole mass spectrum monitored multiple ions including base and parent peaks of experimentally relevant molecules and the background gases H_2 (*m/z* 2), H_2O (*m/z* 18), and CO (*m/z* 28). The *m/z* values monitored accounted for the offset of each mass

spectrometer. The mass spectrometers are offset by *m/z* 0.3 and *m/z* -0.2 for the Cu(111) and Au(111) TPD chambers, respectively. The mass spectrometers utilize 70 eV ionization energy.

The Au(111) TPD chamber was also equipped with a PSP Vacuum Technology XPS. The x-ray system has dual anode x-ray source that was operated at 100 W. The anodes were Al Kα (1486.6 eV) and Mg Kα (1253.6 eV). The ejected electrons were monitored with a concentric hemispherical electron energy analyzer as a function of electron kinetic energy.

STM experiments were primarily performed on a variable temperature STM (VT-STM) (Omicron NanoTechnology). The chamber was equipped with an identical XPS system as described above. The VT-STM system had a preparation and scanning chamber separated by a gate valve. Samples were spotted welded to Ta plates and thus transportable between preparation and scanning chambers via a wobble stick. The base pressure in the VT was $< 5 * 10^{-11}$ mbar and the preparation chamber $< 5 * 10^{-10}$ mbar. In order to reduce vibrations during scanning, UHV conditions were maintained with ion getter pumps and TSPs in both the preparation and scanning chambers. The preparation chamber also had a turbo molecular pump (Pfeiffer Vacuum) for high vacuum procedures.

The preparation chamber had a liquid nitrogen cooled manipulator (McAllister) allowing the sample to be cooled to 110 K by constantly flowing liquid nitrogen through the manipulator. The VT-STM could image samples between 30 – 500 K using a flow cryostat with liquid helium that was in thermal contact with the STM stage. Since the STM tip was at room temperature during scanning, etched W tips were degassed to 370 K prior to use. Bare alloyed surfaces could be imaged at either room temperature or 30 K. In order to obtain

atomic resolution or image adsorbates, the samples were cooled to 30 K to reduce the rate of diffusion, particularly atoms from step edges. Generally, the activation energy for diffusion can be estimated to be 12 % of the binding energy of the adsorbate.[13] Typical bare alloys were imaged at sample biases between ± 0.01 and 0.05 V and tunneling currents between 1.5 and 2.0 nA. For atomic resolution, tunneling currents between 50 and 200 nA were used.

In order to observe H adatoms, a low temperature STM (LT-STM) (Omicron NanoTechnology) was utilized. In this system, the sample could be cooled to 5 K, thus reducing rate of diffusion of the adsorbed species. Imaging at 5 K was achieved by storing liquid helium in a static cryostat. In order to facilitate the spillover of H atoms from the Pt activation site, the prepared alloyed surface was exposed to H_2 at 85 K. After exposure to H_2, the sample was cooled to 5 K for imaging. H adatoms were imaged at non- perturbative conditions (< 30 mV, < 30 pA).

2.3. Sample Preparation in Ultra-High Vacuum

Samples were prepared in a similar manner in all four UHV chambers. Cu(111) single crystals, Au(111) single crystals or Au(111)/mica substrates were cleaned with cycles of Ar^+ sputtering (1.0 – 1.5 KeV, ~15 μA) and annealing to 750 – 850 K. Flux monitored EFM 3 electron beam evaporators (Omicron Nanotechnology, GmbH) were used to reproducibly deposit Pd (Goodfellow, 99.95 %) or Pt (Goodfellow, 99.95 %) onto the cleaned surfaces using the condition described in Table 2.2. For all single atom alloy experiments, the single crystals were held at 380 K during deposition of Pt or Pd with the exception of Chapter 3. The deposition rate of Pd or Pt was ~0.02 monolayer (ML) per min.

Table 2.2. Metal deposition conditions
Typical power needed to deposit Pd and Pt with Flux monitored EFM 3 electron beam evaporators.

	Flux (nA)	Filament Current (A)	Emission (mA)	Voltage (V)	Deposition Rate (ML/min)
Pd	10.4	1.9	15	950	0.01
Pt	30.0	1.9	30	950	0.0097
	50.0	2.2	40	950	0.013

In TPD experiments, Pd or Pt coverages were determined via CO titration assuming CO binds atop to isolated Pd[14,15] or Pt[16–18]atoms in Cu or Au. For Pt-Cu(111), the ratio between CO desorption from Cu sites (< 200 K) and Pt sites (> 300 K) (Figure 2.3B) was used to determine the Pt concentration after accounting for the known saturation packing density of CO on Cu(111) (0.52 ML) (Figure 2.5).[19] For Pd-Au, the area of the Pd peak at 270 K was divided by saturation coverage of CO desorbing from Pd multi-layers (Figure 2.6). Pd multi-layers were deposited on Au(111) and were assumed to terminate as Pd(111) with a 0.75 ML saturation coverage of CO.[20] For STM experiments, Pt or Pd coverages were determined by counting individual atoms from STM images. Calibration curves were attempted using XPS, however, at the 0.01 ML limits, the calibrations were overestimated.

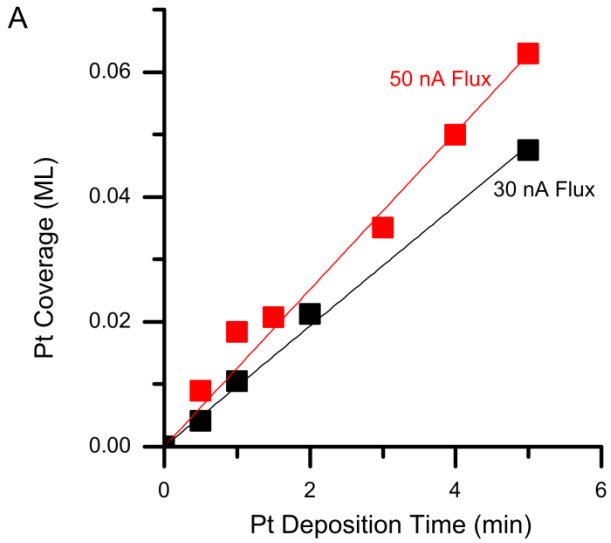

Figure 2.5. Pt-Cu(111) TPD calibration curve
Shown Pt coverage from the resulting Pt deposition time with the Cu(111) at 380 K. Note: The above calibration accounts for the misalignment of crystal. The linear fitting for 50 nA flux Pt coverage (ML) = 0.013* t (min) and 30 nA flux Pt coverage (ML) = 0.0097 * t (min).

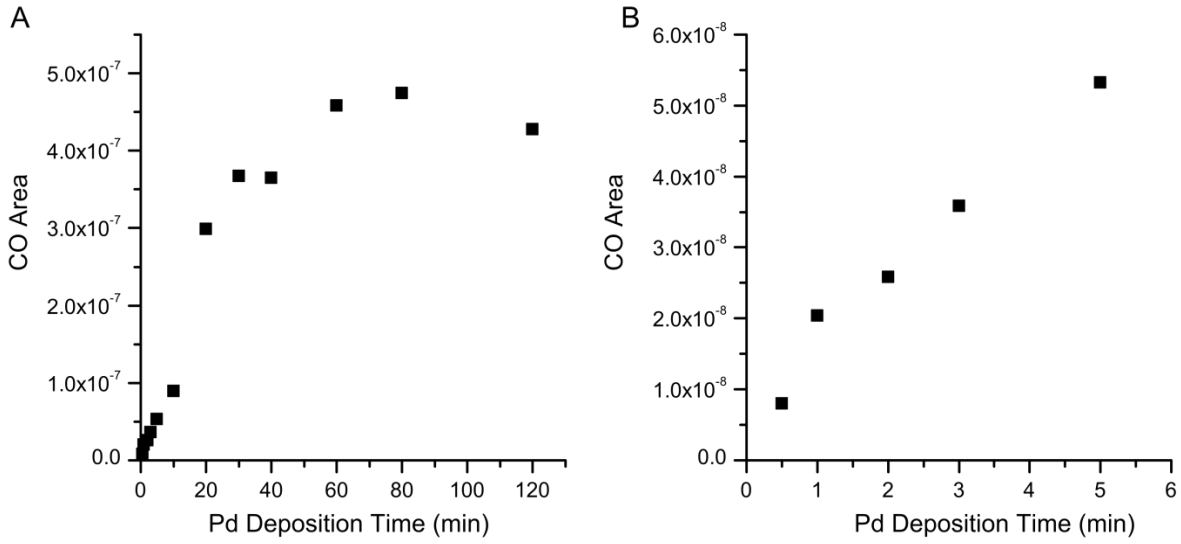

Figure 2.6. Pd-Au(111) TPD calibration curve
The area under the CO (*m/z* 28) peak versus deposition time of Pd with the Au(111) crystal held at 380 K. (A) Shows Pd coverage saturates at 60 min and (B) shows CO uptake is linear for shorter deposition times.

Care was taken to reduce the adsorption of background gases H, CO, and H_2O onto Pt-Cu(111) and Pd-Au(111) alloys. This was especially important for Pt-Cu(111) alloys where CO desorption occurs above room temperature at 350 K. Thus, prior to experiments, TSPs were routinely flashed to reduce the base pressure of the chamber. In TPD experiments, the amount of time between temperature ramps was minimized (< 15 min) and the manipulator was cooled to 85 K prior to deposition of Pt or Pd to prevent cryopumping of background gases onto the sample. Likewise, the VT-STM stage was pre-cooled to 30 K prior to introduction of the sample. In both the TPD and VT-STM chambers, the sample could be quickly flashed to > 350 K to remove any adsorbed CO without altering the alloyed surface. Since, it was not possible to resistively heat the sample while in the LT-STM stage, the manipulator was kept > 350 K while moving the sample from the preparation chamber to the STM chamber to prevent adsorption of CO due to pressure spikes from moving the manipulator.

At 85 K, surfaces were exposed to relevant gases including H_2 (Airgas, 99.9 %), D_2 (Airgas, 99.999 %), CO (Airgas, 99.99 %), O_2 (Airgas, 99.9 %) butadiene (Aldrich, ≥99.5 %) and/or butene (Aldrich, ≥ 99 %) by backfilling the chamber using high precision leak valves. Liquid samples including methanol (Alfa Aesar, ultrapure HPLC grade 99.8 %), water (deionized H_2O), and methanol-D (Sigma-Aldrich, 99.5 %) were further purified via freeze-pump-thaw cycles prior to deposition via high precision leak valves. All exposures are quoted in Langmuirs (L) (1 L = 1 * 10^{-6} torr · s). Coverages for adsorbates were determined as the ratio of peak area to area of the saturated monolayer. Hydrogen coverages were determined by the saturation coverage of unity for H adsorbed onto Pd or Pt multilayers.

2.4. Ozone Deposition

In order to adsorb O atoms onto Au(111), a laboratory ozone generator (LG-7, Ozone Engineering) created ozone that was directly introduced into the UHV chamber (Figure 2.7). O_2 was continuously flowed (0.5 L/min) through Teflon or stainless steel tubing to the ozone generator which applied 5.5 V to produce ozone. The line was directly connected to a high precision leak valve on the UHV chamber. The sample was 2 - 5 in from the collimator on the leak valve. In order to monitor ozone generation, a process ozone UV-monitor (Model 454, Teledyne Instruments) used UV spectrometer to determine grams of ozone per normal cubic meter ($g/N \cdot m^3$). The ozone exhaust passed through an ozone reducing catalysts and then exhausted into a fume hood.

Due to the short life time of ozone, the Au(111) crystal needed to be directly in front of the leak valve and the lines (including the collimator in vacuum), which needed to be passivated for > 15 hours. After initial passivation of the system, the system was purged daily by introducing into the chamber $5 * 10^{-6}$ mbar ozone for 30 min. Typical ozone exposures ranged from $5 * 10^{-7}$ mbar for 1 min to $5 * 10^{-6}$ mbar ozone for 30 min.

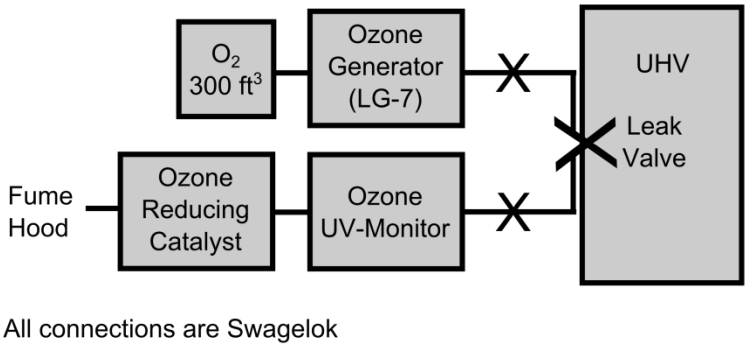

Figure 2.7. Schematic for introduction of ozone into UHV chamber

2.5. References

(1) Binning, G.; Rohrer, H.; Gerber, C.; Weibel, E. Surface Studies by Scanning Tunneling Microscopy. *Phys. Rev. Lett.* **1993**, *49*, 57–61.

(2) Kolasinski, K. W. *Surface Science*, 3rd ed.; Wiley: West Chester, 2012.

(3) Schmid, M.; Stadler, H.; Varga, P. Direct Observation of Surface Chemical Order by Scanning Tunneling Microscopy. *Phys. Rev. Lett.* **1993**, *70*, 1441–1444.

(4) Barth, J. V.; Brune, H.; Ertl, G.; Behm, R. J. Scanning Tunneling Microscopy Observations on the Reconstructed Au(111) Surface: Atomic Structure, Long-Range Superstructure, Rotational Domains, and Surface Defects. *Phys. Rev. B* **1990**, *42*, 9307–9318.

(5) Woll, C.; Chiang, S.; Wilson, R. J.; Lippel, P. H. Determination of Atom Positions at Stacking-Fault Dislocations on Au(111) by Scanning Tunneling Microscopy. *Phys. Rev. B* **1989**, *39*, 7988–7991.

(6) Varga, P.; Schmid, M. Chemical Discrimination on Atomic Level by STM. *Appl. Surf. Sci.* **1999**, *141*, 287–293.

(7) De Alwis, A.; Holsclaw, B.; Pushkarev, V. V.; Reinicker, A.; Lawton, T. J.; Blecher, M. E.; Sykes, E. C. H.; Gellman, A. J. Surface Structure Spread Single Crystals (S_4C): Preparation and Characterization. *Surf. Sci.* **2013**, *608*, 80–87.

(8) King, D. A. Thermal Desorption from Metal Surfaces: A Review. *Surf. Sci.* **1975**, *47*, 384–402.

(9) de Jong, A. M.; Niemantsverdriet, J. W. Thermal Desorption Analysis: Comparative Test of Ten Commonly Applied Procedures. *Surf. Sci.* **1990**, *233*, 355–365.

(10) Redhead, P. A. Thermal Desorption of Gases. *Vacuum* **1962**, 203–211.

(11) Campbell, C. T.; Sellers, J. R. V. The Entropies of Adsorbed Molecules. *J. Am. Chem. Soc.* **2012**, *134*, 18109–18115.

(12) Campbell, C. T.; Sellers, J. R. V. Enthalpies and Entropies of Adsorption on Well-Defined Oxide Surfaces : Experimental Measurements. *Chem. Rev.* **2013**, *113*, 4106–4135.

(13) Nilekar, A. U.; Greeley, J.; Mavrikakis, M. A Simple Rule of Thumb for Diffusion on Transition-Metal Surfaces. *Angew. Chemie - Int. Ed.* **2006**, *45* (42), 7046–7049.

(14) Pedersen, M. Ø.; Helveg, S.; Ruban, A.; Stensgaard, I.; Lægsgaard, E.; Nørskov, J. K.; Besenbacher, F. How a Gold Substrate Can Increase the Reactivity of a Pt Overlayer. *Surf. Sci.* **1999**, *426*, 395–409.

(15) Eyrich, M.; Diemant, T.; Hartmann, H.; Bansmann, J.; Behm, R. J. Interaction of CO with Structurally Well-Defined Monolayer PtAu/Pt(111) Surface Alloys. *J. Phys. Chem. C* **2012**, *116*, 11154–11165.

(16) Marcinkowski, M. D.; Jewell, A. D.; Stamatakis, M.; Boucher, M. B.; Lewis, E. A.; Murphy, C. J.; Kyriakou, G.; Sykes, E. C. H. Controlling a Spillover Pathway with the Molecular Cork Effect. *Nat. Mater.* **2013**, *12*, 523–528.

(17) Maroun, F.; Ozanam, F.; Magnussen, O. M.; Behm, R. J. The Role of

Atomic Ensembles in the Reactivity of Bimetallic Electrocatalysts. *Science* **2001**, *293*, 1811–1814.

(18) Liu, J.; Lucci, F. R.; Yang, M.; Lee, S.; Marcinkowski, M. D.; Therrien, A. J.; Williams, C. T.; Sykes, E. C. H.; Flytzani-Stephanopoulos, M. Tackling CO Poisoning with Single Atom Alloy Catalysts. *J. Am. Chem. Soc.* **2016**, *138*, 6396–6399.

(19) Raval, R.; Parker, S. F.; Pemble, M. E.; Hollins, P.; Pritchard, J.; Chesters, M. A. FT-RAIRS EELS LEED Studies of the Adsorption of Carbon Monoxide on Cu(111). *Surf. Sci.* **1988**, *203*, 353–377.

(20) Rose, M.; Mitsui, T.; Dunphy, J.; Borg, A.; Ogletree, D. .; Salmeron, M.; Sautet, P. Ordered Structures of CO on Pd(111) Studied by STM. *Surf. Sci.* **2002**, *512*, 48–60.

Chapter 3: Atomic Scale Surface Structure of Pt-Cu(111) Surface Alloys

This chapter was modified from an original publication of the same title by F. R. Lucci et al. from the Journal of Physical Chemistry C, volume 118, pages 3015-3022.

3.1. Introduction

Noble metal alloys have been extensively studied due to their use in heterogeneous catalysis. The addition of a second metal into a host can dramatically improve reactivity and/or selectivity in surface catalyzed reactions.[1–3] These changes can be described by ligand and/or ensemble effects. A ligand effect is a change in catalytic activity due to electronic interactions between the elements, while an ensemble effect is related to the spatial arrangement of atoms.[4] Understanding these interactions may lead to the design of more efficient catalysts by tuning the activity and selectivity for a given reaction.[5–7] Ensemble effects are particularly attractive to study because understanding and controlling these effects allows for the design of catalysts that maximize the number of active sites and minimize the amount of precious metals.

Ensemble effects play a significant role in a number of catalytic systems.[5,8–11] Gao *et al.* showed that two adjacent Pd atoms in PdAu(100) are required for the oxidation of CO.[8] Linke *et al* demonstrated that isolated Pt atoms in $Cu_3Pt(111)$ dissociate H_2,[9] and Borovkov *et al.* attributed the selective dechlorination of 1,2-dichloroethane to ethylene to small Pt ensembles in Pt-Cu/SiO_2 catalysts.[10] Recently, using temperature programmed desorption (TPD) and scanning tunneling microscopy (STM), we related the selective hydrogenation of styrene and acetylene to the local atomic structure of Pd-Cu(111) alloys.[11] Specifically, individual, isolated Pd atoms dissociated H_2 and allowed spillover onto Cu. Hydrogen was

bound weakly to Cu and could selectively hydrogenate alkenes and alkynes.[11] As shown in these systems, the number of atoms that constitutes the active site varies depending on the reaction. Thus, the atomic structure of the surface can influence both the reaction selectivity and reactivity. In this study, we will focus on the geometric arrangement of Pt atoms in a Cu(111) host surface.

Pt-Cu alloys catalyze CO oxidation, hydrogenation, and hydrocarbon and dechlorination reactions.[9,12–14] Therefore, an understanding of the atomic scale structure of Pt-Cu alloys is important for a number of reactions. Pt is miscible in Cu and exists in three bulk ordered phases: Cu_3Pt, CuPt, and $CuPt_3$.[15] The thermodynamically stable phase of Cu_3Pt is the $L1_2$ phase.[16] Ideal termination of the $L1_2$ phase along the (111) plane leads to a p(2x2) ordering of the Pt atoms. LEED experiments showed that Pt atoms in the (111) surface of the $L1_2$ phase exist in both an ordered p(2x2) and amorphous structure depending on the preparation conditions.[17,18] In terms of surface and near surface alloys, earlier studies determined a layer-by-layer growth mode of Pt films on Cu(111).[19,20] Annealing of the films formed Cu_3Pt surface alloys due to the intermixing of Pt and Cu.[21,22] At submonolayer coverage of Pt, Cu step edges were shown to enable the intermixing of Pt and Cu.[23] Theoretical studies have indicated that a combination of the surface free energy difference between Pt and Cu, negative mixing enthalpy between the two metals and elastic strain relief drives the alloying process.[24–27]

Although a range of surface science techniques have been used to characterize Pt-Cu bimetallic alloys, the atomic scale structure of the surface alloy and its evolution as a function of both coverage and alloying temperature is unknown. Here we directly characterize the local atomic arrangement of submonolayer coverages of Pt atoms in Cu(111)

using STM. We demonstrate the ability to tune the arrangement of Pt in the surface by controlling the temperature of the Cu(111) crystal during deposition of Pt and show that it alloys with high dispersion.

3.2. Results and Discussion

STM was used to determine the morphology of submonolayer coverages of Pt deposited on Cu(111) as a function of sample temperature. Pt and Cu atoms are distinguished from one another due to topographical and electronic differences that are discernible with STM.[7,28,29] Prior to the deposition of Pt, there was less than one impurity per $(50\ nm)^2$ observed on the clean Cu surface. After deposition of Pt, protrusions within the surface were imaged appearing 25 ± 5 pm higher than the surrounding Cu lattice (Figure 3.1). The STM tip state affects the observed height of the Pt atoms, therefore, depending on the tip state, Pt atoms imaged as either protrusions or depressions. However, the Pt atoms predominately imaged as protrusions at most tunneling conditions. The height of the observed protrusions was consistent with Pt atoms being substituted into the surface due to Pt atoms (diameter = 277 pm) being ~20 pm larger than Cu atoms (diameter = 256 pm) and also due to electronic differences between the elements.[7] Previous STM and DFT studies showed that Pt atoms appear brighter than Cu atoms when Cu atoms were substituted into Pt(111).[7] An increase in the concentration of the localized brighter features that we observed correlated with longer deposition times of Pt; therefore, we conclude that the features are due to Pt atoms substituted into the surface layer. This is consistent with medium energy ion scattering (MEIS) data indicating that at 315 K the vast majority of the Pt alloys into the surface layer of Cu(111).[23]

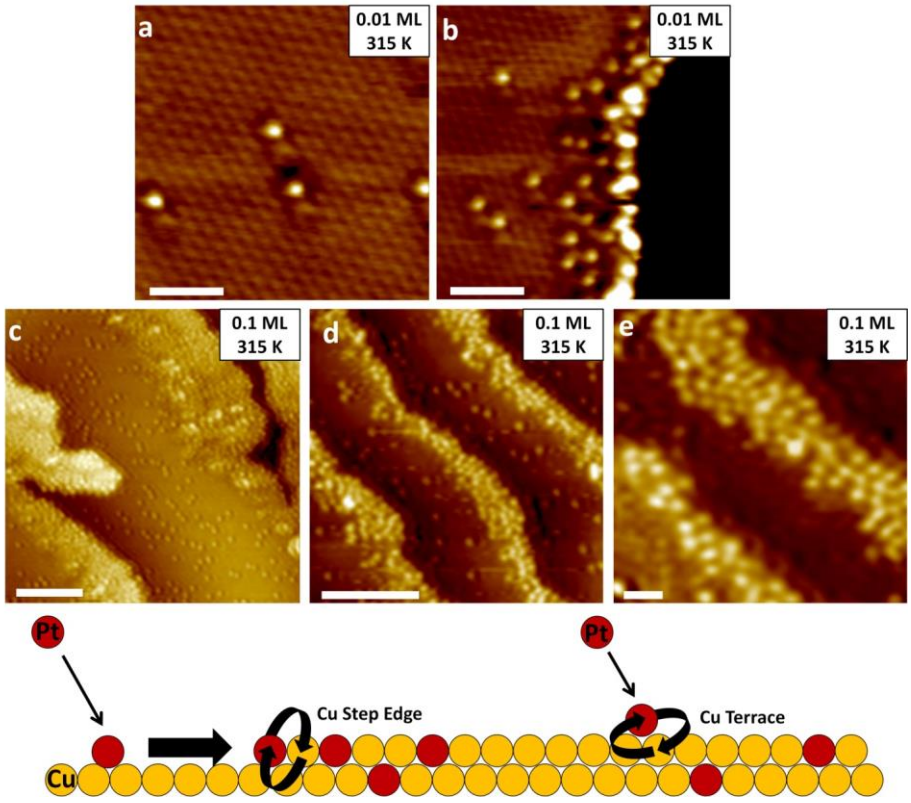

Figure 3.1. STM images of Pt-Cu alloys formed at 315 K
STM images of Pt-Cu alloys formed by deposition of (A, B) 0.01 ML and (C-D) 0.1 ML of Pt on Cu(111) at 315 K. Atomic resolution images reveal that Pt alloys into the surface both at (A) the terraces and (B) ascending step edges. (C-E) At a higher coverage of Pt deposited at 315 K, Pt atoms form Pt-rich brims and fingers at step edges as well as dispersing in the terraces. (E) High-resolution image of disordered Pt atoms densely packed at step edges. Schematic shows the proposed alloying mechanisms. Scale bars are (A, B, E) 1 nm and (C, D) 5 nm.

STM images illustrate that at 315 K, Pt atoms alloy in the vicinity of step edges and throughout the Cu(111) terraces. The formation of Pt-rich brims indicates that alloying at ascending step edges occurs via place exchange.[30–33] Our data revealed that the amount of Pt deposited, the size of the lower terrace, and the temperature of the surface during deposition influenced the width and Pt density in these step edge brims. Each effect will be discussed throughout the paper. At 315 K, deposition of 0.1 ML of Pt yielded larger and denser brims than the deposition of 0.01 ML of Pt (Figure 3.1). Wider brims were also observed for step edges that had larger lower terraces, indicating that the lower terrace acts as a catchment area

for Pt. The variation in the size of the fingers due to the area of the lower terrace is apparent in Figure 3.3A, where larger fingers are observed for larger lower terraces. These results agree well with previous MEIS studies which indicated that step edges facilitated the incorporation of Pt atoms into the surface and subsurface layers of Cu(111).[23] Our STM images show that at the upper terrace side of the brims, the density of Pt atoms dramatically decreased further from the step edge. However, beyond the brim, there was a homogeneous distribution of Pt atoms across the terraces (Figure 3.1A and 3.1C). This observed morphology for the surface prepared at 315 K suggests that Pt preferentially alloys into Cu at ascending step edges and that Pt is also capable of incorporation into the terraces far from steps. Figure 3.1F shows a schematic of the proposed alloying processes. Pt atoms adsorb on the surface and then diffuse across a terrace until coming into contact with an ascending step edge. At the step edge, Pt place exchanges with Cu atoms. An additional alloying channel involves Pt atoms exchanging with Cu atoms and alloying directly into the terraces. The densely populated step edges suggest kinetic limitations of alloying at 315 K, where Pt atoms diffuse across the surface and aggregate in the vicinity near steps faster than they are able to alloy into the terraces.

Previous work on the Pd-Cu(111) alloy proposed a similar alloying mechanism involving the exchange of Pd atoms into Cu(111) at ascending step edges.[30–32] Aaen *et al.* showed that the width of the Pd rich brims was dependent on the width of the lower terrace.[30] DFT calculations by Bellisario *et al.* indicated that Pd atoms exchange into the Cu terrace at step edges and once a Pd atom coordinates to the step edge it is unlikely to overcome the activation energy needed to detach from the step edge.[32] Hence, the dense Pt brims we observe are indicative of the exchange mechanism at ascending step edges. Regardless of the

preparation conditions for the Pd-Cu system, Pd atoms did not alloy into the Cu terrace beyond the brim region. In this study, the Pt atoms not only alloy at Cu step edges, but are apparently able to directly exchange into the Cu terraces at 315 K. We postulate that this ability of Pt atoms to readily place exchange with Cu atoms into the terrace is due to a greater difference in surface free energy between Pt (2.204 J/m^2) and Cu (1.566 J/m^2) compared to Pd (1.743 J/m^2) and Cu.[34]

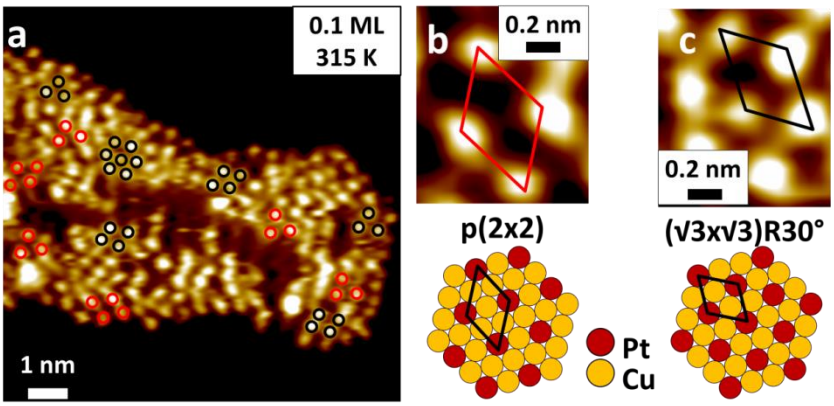

Figure 3.2. STM image of local Pt order on densely packed Pt-Cu finger
STM image of a densely packed Pt-Cu finger protruding from a step edge. Pt atoms form small ordered regions corresponding to local (B) p(2 x 2) and (C) (√3 x √3)R30° structures. STM images were taken at room temperature and scale bars are (A) 1 nm and (B, C) 0.2 nm.

At higher Pt coverages (Figure 3.2 and 3.3), we observed finger-like-protrusions emanating from step edges. Based on the contrast differences of Pt and Cu atoms in STM images, these structures are composed of Cu atoms (darker) with dense clusters of Pt atoms (brighter) predominantly at the peripheries of the fingers. The outer location of the Pt atoms presumably relieves the compressive strain from intermixing larger Pt atoms with Cu and while still increasing the number of favorable heteroatom bonds which are the driving force for the ordering of Cu_3Pt bulk alloys.[26]

In the dense Pt regions, there was no long-range order but small clusters of Pt atoms exhibited short-range order (Figure 3.2). Figure 2B and 2C show small patches of the ordered structures observed in the finger-like-protrusions. The Pt atoms assemble in both p(2 x 2) and (√3 x √3)R30° arrangements with a local surface stoichiometry of Cu_3Pt and Cu_2Pt, respectively. These packing arrangements are energetically preferred because they optimize the number of favorable Pt-Cu heteroatom bonds and minimize the compressive strain of the larger Pt atoms within the smaller Cu lattice.[25] A combination of p(2 x 2) and (√3 x √3)R30° is observed due to the thermodynamic stability of both the $L1_2$ bulk phase of Cu_3Pt alloys[21,25] and maximization of isolated Pt atoms in the surface layer, respectively.[35–37]

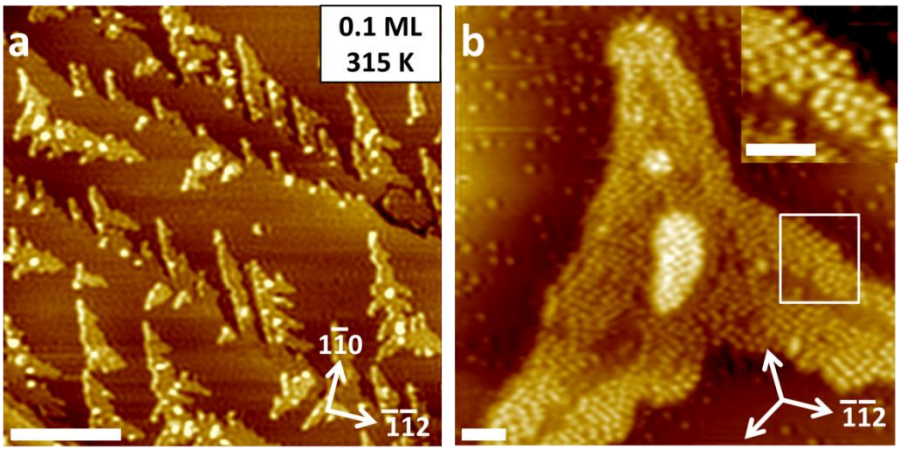

Figure 3.3. STM images of Pt rich islands and fingers
STM images of Pt rich islands and fingers formed after deposition of higher coverages of Pt at 315 K. (A) Both fingers and islands grow on the Cu(111) surface preferentially in the $< \bar{1}\bar{1}2 >$ and equivalent directions. (B) The islands consist of a mixture of Pt and Cu atoms and the inset shows atomically resolved Pt atoms at the edge of the Pt-Cu islands. The individual protrusions in the inset correspond to single Pt atoms in the surface layer and the flat areas are unresolved Cu atoms. The Pt atoms in the islands are concentrated at the edges of the islands and the inset shows atomically resolved denser Pt regions at the edge of the island. Images were taken at room temperature and scale bars are (A) 50 nm and (B) 2 nm.

One atom-high islands on the Cu(111) terraces and one atom-high fingers protruding from step edges were observed when higher coverages of Pt was deposited at 315 K (Figure 3.3A-B). The islands and fingers are composed of Cu and Pt atoms. We postulate that the

source of the Cu atoms are Cu atoms expelled by Pt atoms entering the surface or Cu atoms diffusing from step edges. The mobile Cu and Pt atoms aggregate to form islands or diffuse to step edges and form fingers. The three-pointed islands observed at higher Pt coverage grew along the $< \bar{1}\bar{1}2 >$ and equivalent directions (Figure 3.3). This type of anisotropic growth is typically attributed to differences in step energies or adatom diffusion barriers between steps resulting in the formation of triangular islands as opposed to hexagonal islands.[38,39] Despite the equivalent surface free energy of (111) and (100) microfaceted Cu steps,[40] one might expect the predominant microfaceted step edge to be (111) due to the lower surface free energy of (111) microfaceted Pt steps compared to (100) [38,41] and the lower diffusion barriers from (111) to (100) microfaceted steps as observed for Pt on Ru(0001).[39,42] Pt atoms are expected to occupy fcc hollow adsorption sites since Pt films grown on Cu(111) follow the fcc structure of the underlying Cu lattice.[21] This preference for the occupation of fcc hollow adsorption sites and (111) microfaceted steps leads the triangular islands to grow predominately in only one of the two possible epitaxial orientations on Cu(111). This postulate was supported by our experiments, although we observed more dendritic growth as opposed to perfect triangular islands.[43] Dendritic growth from fingers and islands suggests kinetically limited growth, however, our experiments demonstrate that the thermodynamic stability of (111) type steps and the occupation of fcc hollow adsorption sites further contribute to the metastable surface structures observed. Annealing the samples could elucidate the thermodynamically preferred state; however, this causes the subsurface diffusion of the Pt atoms.

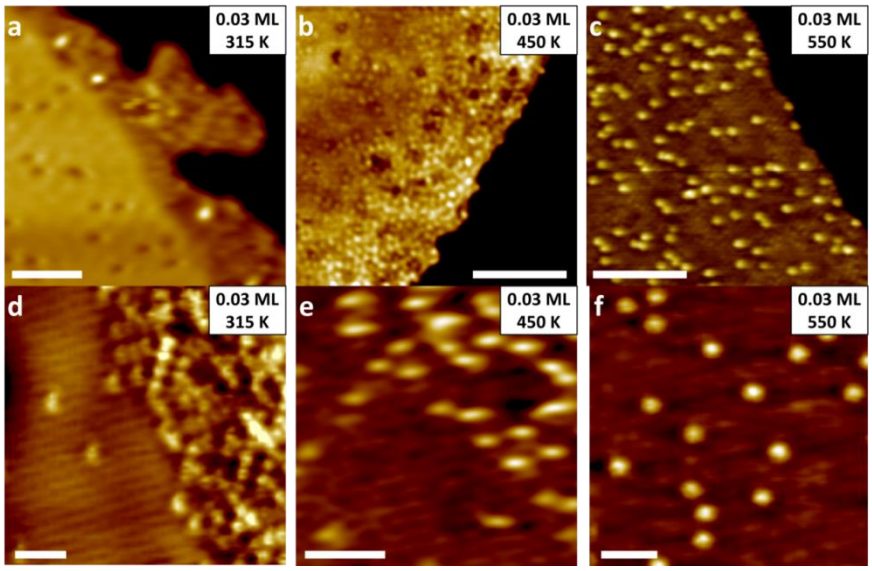

Figure 3.4. STM images of Pt-Cu(111) alloyed formed at 315 K, 450 K, 550 K
STM images of Pt-Cu(111) alloys formed by depositing Pt at a range of surface temperatures. (A) At 315 K, fingers and islands are observed along with single Pt atoms substituted into the Cu terraces. (B) At 450 K, Pt rich brims are formed along with single Pt atoms in the terraces. (C) At 550 K, the Pt atoms are evenly dispersed across the terrace and Pt rich brims at step edges are no longer observed. (D, E, F) High resolution images of the interface of brims and terraces as a function of temperature. As the alloying temperature increases, the Pt atom arrangement changes from densely packed brims/fingers at 315 K (D) to a highly dispersed distribution across the terrace at 550 K (f). All images were taken at 30 K and scale bars are (A, B, C) 5 nm and (C, D, E) 1 nm.

We investigated the effect of temperature on the alloying of Pt with Cu(111). Depositing Pt onto a Cu surface at elevated temperatures (450 K and 550 K) resulted in the formation of a more homogeneous surface alloy. The greater dispersion of individual, well isolated Pt atoms into Cu terraces at higher temperatures is accompanied by the disappearance of the brims and fingers (Figures 3.4A-C) and a gradual loss of the interface between the brims and terraces (Figure 3.4D-F). Alloying Pt at 315 K and cooling to 30 K for imaging lead to step edges with dense brims and fingers. The density was such that the majority of the deposited Pt aggregated in extended structures with Pt-Pt bonds rather than solely Pt-Cu bonds, which were observed at higher temperatures. The limited time above 300 K in this set of experiments did not allow all the deposited Pt to alloy into the Cu, but trapped it in a metastable state at the edge of steps and islands. This resulted in STM images with an

abrupt boundary between the Pt rich brim and Cu terrace as seen in Figure 3.4A and D. At 450 K, an intermediate state was observed. The step edges were smoother and no longer exhibited finger growth but there was still a visible interface between the dense Pt brims and Cu terraces as seen in Figure 3.4B and E. The local density of Pt atoms in the brims at 450 K was lower than the density at 315 K. At 550 K there was an even distribution of Pt atoms across the surface and an interface between the brim and Cu terrace was no longer present as seen in Figure 3.4C and F.

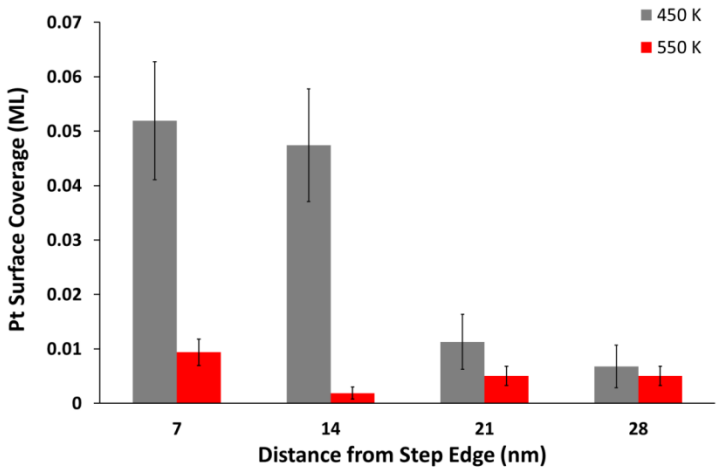

Figure 3.5. Local surface Pt atom concentration as function of distance from step-edge
Local surface Pt atom concentration as a function of distance from the step-edge as a function of alloying temperature (450 K vs. 550 K).

Figure 3.5 shows the concentration of Pt atoms (ML) in the surface layer as a function of distance from the step edge for alloying at 450 K and 550 K. The data at 450 K and 550 K support that there are two alloying mechanisms; Pt attachment at step edges followed by exchange into the terraces, and direct place exchange into the terraces. At 450 K, alloying via ascending step edge and subsequent exchange into the terraces is apparent due to the clear existence of a Pt rich brim where the local concentration is 0.05 ML for a distance of up to 14 nm from the step edge. Beyond the Pt rich brim, the local concentration of Pt atoms drops to

0.01 ML. At 550 K, the concentration of surface Pt atoms is the same regardless of the distance from the step edge. If the sole alloying mechanism were Pt attachment at step edges and exchange into the terraces, then a continuous decrease in the concentration of Pt from the step edges would be expected at 450 K. The loss of the interface between the Pt rich-brim and Cu terraces is seen in Figure 3.4C. In Figure 3.5, the absolute Pt coverage in the surface layer at 550 K is less than the absolute Pt coverage at 450 K. The observed decrease in Pt coverage from 0.03 ML to 0.005 ML at higher temperatures is due to the subsurface diffusion of Pt atoms at higher temperatures as well as the effect of the catchment area as previously discussed. At 450 K, ~70 % of the Pt atoms exist in the surface layer and at 550 K, only ~20 % of the Pt atoms are in the surface.

The progressive loss of fingers and brims is reflective of the formation of more thermodynamically stable alloys which maximize favorable Pt-Cu bonds.[24] At lower temperatures, Pt atoms are kinetically limited to alloy at step edges where the observed morphology is reflective of a metastable state that locally decreases the compressive surface strain by locating the larger Pt atoms at the perimeter of the structures. The high density of Pt atoms in the dendritic structures supports this behavior. Dendritic growth occurs where the local density of Pt atoms is higher, as dendritic growth releases the strain generated by the incorporation of larger Pt atoms into a Cu lattice. At higher temperatures, Pt atoms can overcome the activation energy to alloy directly into the Cu terrace. This was evident by an increase in concentration of Pt atoms in the terraces at 450 K and 550 K compared to 315 K. Also, the increased mobility of Cu and Pt atoms at higher temperatures facilitates the intermixing of Pt and Cu driven by their negative mixing enthalpy. Thus, although the Pt rich brims have regions of local order, increasing the temperature of the surface during the

deposition of low coverages of Pt does not result in long-range order of the Pt atoms: the elevated temperatures provide thermal energy necessary for the dispersion and subsurface segregation of Pt atoms. Alloying Pt throughout the terraces leads to well separated isolated Pt atoms in the surface layer surrounded by Cu and a reduction in compressive strain as compared to the regions of higher Pt density at the step edges. The dispersion of solute atoms across the surface at higher temperatures was also observed for the alloying of Pb and Cu(111).[33] Like Pt-Cu(111), at higher temperatures, Pb has a random dispersion across the terrace instead of establishing long-range order. Dispersion was observed despite the immiscibility of Cu with Pb; however, Pb was shown to remain in the surface layer.[15,33]

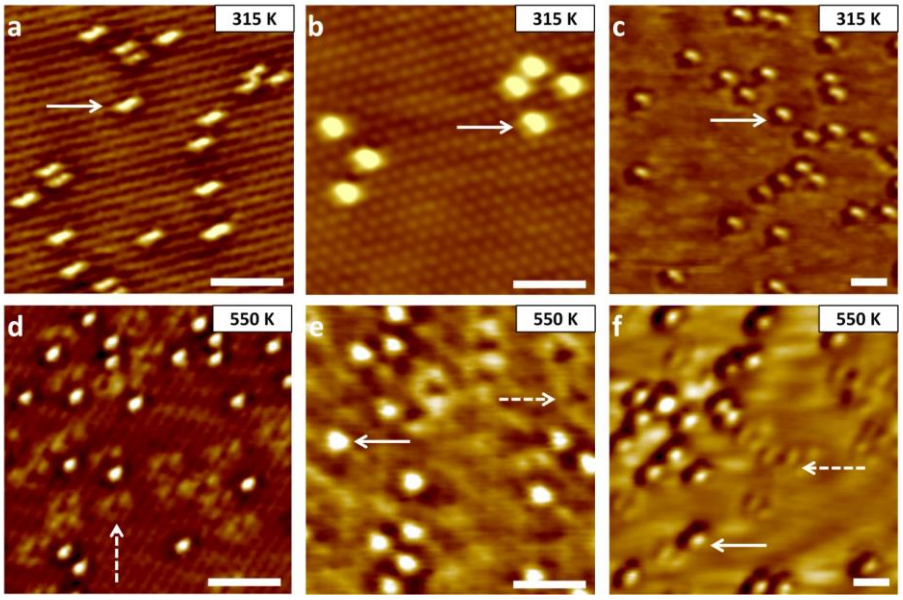

Figure 3.6. Atomically resolved images of surface and subsurface Pt atoms
Atomically resolved images of surface and subsurface Pt atoms in a Cu(111) surface with different STM tip states. (A-C) Alloying at 315 K yields only a single feature (protrusions) (solid arrow) in the Cu lattice corresponding to Pt atoms substituted into the surface layer. The oblong shape of the Pt atoms in image (A) derives from an asymmetric STM tip shape. (D-F) At 550 K, both protrusions (solid arrow) and depressions (dashed arrow) are observed in the same image corresponding to Pt atoms in the surface and subsurface layers respectively. Scale bars are 1 nm.

In addition to affecting the surface arrangement of Pt, the surface temperature during deposition also influences the depth profile of the Pt atoms in Cu.[23] Our atomically-resolved

STM images reveal single atom protrusions (25 ± 5 pm) corresponding to Pt atoms in the surface layer after the deposition of Pt at 315 K (Figure 3.6A). At higher surface deposition temperatures of 450 and 550 K, both protrusions and depressions (30 ± 10 pm) are observed (Figure 3.6E). Previous studies have shown that subsurface Pd atoms in Cu(111) and subsurface Cu atoms in Pt(111) perturb the electronic structure of overlying surface atoms.[7,31] Therefore, the depressions we observe are assigned as subsurface Pt atoms. The percentage of surface Pt atoms located in the terraces at 315, 450, and 550 K are > 99 %, ~70 % and ~20 %, respectively. Regardless of the state of the STM tip, only a single characteristic feature of Pt atoms was observed at 315 K. Figure 3.6A-Cshow images of alloys prepared at 315 K in which depressions were not observed for three different STM tip states. At higher alloying temperatures, both protrusions and depressions were observed. The depressions exist independently of distinct protrusions; therefore, they are not an artifact of the STM tip. Two distinct features observed with several different STM tip states are shown in Figure 3.6D-F. Blunt STM tips or asymmetrical STM tips result in larger or elongated features.

The presence of subsurface Pt atoms formed at higher temperatures is also consistent with the aforementioned medium and low energy ion scattering studies of Pt-Cu near-surface alloys prepared by deposition of submonolayer and multilayer amounts of Pt.[21,23] Using MEIS, Dastoor *et al.* quantified the concentration of Pt atoms in the first three layers of the Pt-Cu(111) alloy and showed that on a stepped Cu surface, at 525 K, ~70 % of the Pt atoms alloyed below the surface layer. The results agree well with the trend we observe that the concentration of subsurface atoms increases with higher substrate temperatures during alloying. At even higher temperatures, Pt segregates below the surface due to the greater

surface energy of Pt compared to Cu.[34] Dastoor *et al.* demonstrated differences in the amount of surface and subsurface Pt alloyed in stepped versus flat Cu surfaces as a function of alloying temperature.[23] Their data indicated that step edges facilitate the subsurface intermixing since on the stepped surface there was an increase in the Pt occupation of subsurface sites. They proposed that either Pt alloys into the subsurface layers at step edges or migration of Cu atoms over the Pt rich brims allows for the capping of the step edges and an increase in subsurface occupancy. Our results indicate that there appears to be two separate alloying mechanisms occurring at the step edges and terraces and at higher temperature the predominant mechanism is the incorporation of Pt atoms into the Cu terraces.

Subsurface segregation was also observed at elevated temperatures for Pd in Cu(111) and Au(111).[30,31,44] However, unlike Pt-Cu(111), Pd-Cu(111) has no intermediate phase in which Pd is dispersed across the whole Cu(111) terrace. Both systems preferentially alloy at step edges and at higher temperatures subsurface alloying is observed for both. Pd-Cu(111) has the majority of Pd atoms localized in brims at step edges independent of the temperature of the surface during alloying.[30,31] In contrast, we find that Pt is capable of alloying at all regions of the Cu(111) terraces. At higher substrate temperatures, the local density of Pt atoms at step edges decreases due to an increase in Pt atoms alloying across the terraces. The ability for Pt to disperse and segregate into the surface allows for more individual, isolated Pt atoms to be incorporated into the surface layer of a Cu host. Given Pt's ability to catalyze a number of important chemical reactions the Pt-Cu(111) system discussed in this paper provides a platform for interrogating the surface chemistry of individual, isolated Pt atoms in Cu.[11,45–47]

3.3. Summary

Given the reactivity differences between Pt and Cu, the surface stoichiometry and geometry of catalytically important Pt-Cu alloys are expected to have a major influence on their surface chemistry. We examined the local atomic arrangement of submonolayer amounts of Pt atoms alloyed into Cu(111) at a range of temperatures with variable temperature STM. We observed several metastable structures that formed due to kinetic limitations during the alloying process. Given enough thermal energy during alloying, Pt alloys with high dispersion in the surface layer of Cu with the subsurface being populated at higher temperatures. The high dispersion of Pt in Cu surface layer is driven by the negative mixing enthalpy of Pt in Cu and by the strain relief caused by the larger size of Pt as compared to Cu. This work reveals Pt atom's tendency to alloy into the entire Cu surface layer with high dispersion making this system a useful model with which to probe Pt's hydrogenation chemistry at the single atom level.

3.4. References

(1) Chen, J. G.; Menning, C. A.; Zellner, M. B. Monolayer Bimetallic Surfaces: Experimental and Theoretical Studies of Trends in Electronic and Chemical Properties. *Surf. Sci. Rep.* **2008**, *63*, 201–254.

(2) Rodriguez, J. A. Physical and Chemical Properties of Bimetallic Surfaces. *Surf. Sci. Rep.* **1996**, *24*, 223–287.

(3) Greeley, J.; Mavrikakis, M. Alloy Catalysts Designed from First Principles. *Nat. Mater.* **2004**, *3*, 810–815.

(4) Liu, P.; Nørskov, J. K. Ligand and Ensemble Effects in Adsorption on Alloy Surfaces. *Phys. Chem. Chem. Phys.* **2001**, *3*, 3814–3818.

(5) Besenbacher, F.; Chorkendorff, I.; Clausen, B. S.; Hammer, B.; Molenbroek, A. M.; Nørskov, J. K.; Stensgaard, I. Design of a Surface Alloy Catalyst for Steam Reforming. *Science* **1998**, *279*, 1913–1915.

(6) Pedersen, M. Ø.; Helveg, S.; Ruban, A.; Stensgaard, I.; Lægsgaard, E.; Nørskov, J. K.; Besenbacher, F. How a Gold Substrate Can Increase the Reactivity of a Pt Overlayer. *Surf. Sci.* **1999**, *426*, 395–409.

(7) Knudsen, J.; Nilekar, A. U.; Vang, R. T.; Schnadt, J.; Kunkes, E. L.; Dumesic, J. A.; Mavrikakis, M.; Besenbacher, F. A Cu/Pt Near-Surface Alloy for Water-Gas Shift Catalysis. *J. Am. Chem. Soc.* **2007**, *129*, 6485–

6490.
(8) Gao, F.; Wang, Y.; Goodman, D. W. CO Oxidation over AuPd(100) from Ultrahigh Vacuum to near-Atmospheric Pressures: The Critical Role of Contiguous Pd Atoms. *J. Am. Chem. Soc.* **2009**, *131*, 5734–5735.
(9) Linke, R.; Schneider, U.; Busse, H.; Becker, C.; Schröder, U.; Castro, G. R.; K., W. Interaction of Hydrogen with $Cu_3Pt(111)$: Dissociation via Isolated Platinum Atoms. *Surf. Sci.* **1994**, *307 - 309*, 407–411.
(10) Borovkov, V. Y.; Luebke, D. R.; Kovalchuk, V. I.; Itri, J. L. Hydrogen-Assisted 1,2-Dichloroethane Dechlorination Catalyzed by $Pt\text{-}Cu/SiO_2$: Evidence for Different Functions of Pt and Cu Sites. *J. Phys. Chem. B* **2003**, *107*, 5568–5574.
(11) Kyriakou, G.; Boucher, M. B.; Jewell, A. D.; Lewis, E. A.; Lawton, T. J.; Baber, A. E.; Tierney, H. L.; Flytzani-Stephanopoulos, M.; Sykes, E. C. H. Isolated Metal Atom Geometries as a Strategy for Selective Heterogeneous Hydrogenations. *Science* **2012**, *335*, 1209–1212.
(12) Kummer, J. T. Laboratory Experiments Evaluating the Effects of S and Cu on a $Pt\text{-}A1_2O_3$ Auto Exhaust Oxidation Catalysts. *J. Catal.* **1975**, *38*, 166–171.
(13) de Jongste, H. C.; Ponec, V. Role of Cu in the Hydrogenolysis of Pentane on Cu Alloy Catalysts. *J. Catal.* **1980**, *63*, 389–394.
(14) Vadlamannati, L. S.; Kovalchuk, V. I.; Itri, J. L. Dechlorination of 1,2-Dichloroethane Catalyzed by Pt–Cu/C : Unraveling the Role of Each Metal. *Catal. Lett.* **1999**, *58*, 173–178.
(15) Hansen, M. *Constitution of Binary Alloys*, 2nd Ed.; McGraw-Hill: New York, 1958.
(16) Miura, S.; Mitsui, K.; Tanaka, Y.; Mishima, Y.; Suzuki, T. Positive Temperature Dependence of Strength Observed in Ordered Cu_3Pt Single Crystals. *Philos. Mag. A* **1992**, *65*, 737–747.
(17) Shen, Y. G.; O'Connor, D. J.; Wandelt, K.; Macdonald, R. J. Studies of Surface Composition and Structure of $Cu_3Pt(111)$ by Low Energy Alkali Ion Scattering. *Surf. Sci.* **1995**, *328*, 21–31.
(18) Castro, G. R.; Schneider, U.; Busse, H.; Janssens, T.; Wandelt, K. The Interaction of CO with the $Cu_3Pt(111)$ Surface. *Surf. Sci.* **1992**, *270*, 321–325.
(19) Belkhou, R.; Barrett, N. T.; Guillot, C.; Barbier, A.; Eugène, J.; Carrière, B.; Naumovic, D.; Osterwalder, J. Growth of Pt/Cu(111) Characterized by Auger Electron Spectroscopy, Core Level Photoemission and X-Ray Photoelectron Diffraction. *Appl. Surf. Sci.* **1993**, *65*, 63–70.
(20) Belkhou, R.; Barrett, N. T.; Guillot, C.; Fang, M.; Barbier, A.; Eugène, J.; Carrière, B.; Naumovic, D.; Osterwalder, J. Formation of a Surface Alloy by Annealing of Pt/Cu(111). *Surf. Sci.* **1993**, *297*, 40–56.
(21) Shen, Y. G.; O'Connor, D. J.; Wandelt, K.; MacDonald, R. J. Thin Film Growth of Pt on Cu(111): A LEIS Study. *Surf. Sci.* **1996**, *357 - 358*, 921–925.
(22) Shen, Y. G.; O'Connor, D. J.; Wandelt, K. The Surface Composition, Structure and Oxygen-Induced (2×1) Reconstruction of CuPt(110). *Surf.*

Sci. **1998**, *410*, 1–14.
(23) Dastoor, P. C.; O'Connor, D. J.; MacLaren, D. A.; Allison, W.; Noakes, T. C. Q.; Bailey, P. Step Mediated Surface Alloy Formation of Pt/Cu(111). *Surf. Sci.* **2005**, *588*, 101–107.
(24) Christensen, A.; Ruban, A. V.; Stoltze, P.; Jacobsen, K. W.; Skriver, H. L.; Nørskov, J. K.; Besenbacher, F. Phase Diagrams for Surface Alloys. *Phys. Rev. B* **1997**, *56*, 5822–5834.
(25) Yuge, K.; Seko, A.; Kuwabara, A.; Oba, F.; Tanaka, I. Ordering and Segregation of a $Cu_{75}Pt_{25}$(111) Surface: A First-Principles Cluster Expansion Study. *Phys. Rev. B* **2007**, *76*, 0454071–045407.
(26) Luyten, J.; Schurmans, M.; Creemers, C.; Bunnik, B. S.; Kramer, G. J. Construction of Modified Embedded Atom Method Potentials for Cu, Pt and Cu–Pt and Modeling Surface Segregation in Cu_3Pt Alloys. *Surf. Sci.* **2007**, *601*, 2952–2961.
(27) Schurmans, M.; Luyten, J.; Creemers, C.; Declerck, R.; Waroquier, M. Surface Segregation in CuPt Alloys by Means of an Improved Modified Embedded Atom Method. *Phys. Rev. B* **2007**, *76*, 1742081–17420817.
(28) Schmid, M.; Stadler, H.; Varga, P. Direct Observation of Surface Chemical Order by Scanning Tunneling Microscopy. *Phys. Rev. Lett.* **1993**, *70*, 1441–1444.
(29) Varga, P.; Schmid, M. Chemical Discrimination on Atomic Level by STM. *Appl. Surf. Sci.* **1999**, *141*, 287–293.
(30) Aaen, A. B.; Lægsgaard, E.; Ruban, A. V; Stensgaard, I. Submonolayer Growth of Pd on Cu(111) Studied by Scanning Tunneling Microscopy. *Surf. Sci.* **1998**, *408*, 43–56.
(31) Tierney, H. L.; Baber, A. E.; Sykes, E. C. H. Atomic-Scale Imaging and Electronic Structure Determination of Catalytic Sites on Pd/Cu near Surface Alloys. *J. Phys. Chem. C* **2009**, *113*, 7246–7250.
(32) Bellisario, D. O.; Han, J. W.; Tierney, H. L.; Baber, A. E.; Sholl, D. S.; Sykes, E. C. H. Importance of Kinetics in Surface Alloying: A Comparison of the Diffusion Pathways of Pd and Ag Atoms on Cu (111). *J. Phys. Chem. C* **2009**, *113*, 12863–12869.
(33) Nagl, C.; Haller, O.; Platzgummer, E.; Schmid, M.; Varga, P. Submonolayer Growth of Pb on Cu(111) Surface Alloying and De-Alloying. *Surf. Sci.* **1994**, *321*, 237–248.
(34) Tyson, W. R.; Miller, W. A. Surface Free Energies of Solid Metals Estimation from Liquid Surface Tension Measurments. *Surf. Sci.* **1977**, *62*, 267–276.
(35) Canzian, A.; Mosca, H. O.; Bozzolo, G. Atomistic Modeling of Pt Deposition on Cu(111) and Cu Deposition on Pt(111). *Surf. Rev. Lett.* **2004**, *11*, 235–243.
(36) Overbury, S. H.; Ku, Y. Formation of Stable, Two-Dimensional Alloy-Surface Phases: Sn on Cu(111), Ni(111), and Pt(111). *Phys. Rev. B* **1992**, *46*, 7868–7872.
(37) Gambardella, P.; Kern, K. Ni Growth on Vicinal Pt(111): Low Temperature Exchange and Formation of Ordered Surface Alloys. *Surf.*

Sci. **2001**, *475*, L229–L234.
(38) Michely, T.; Comsa, G. Temperature Dependence of the Sputtering Morphology of Pt(111). *Surf. Sci.* **1991**, *256*, 217–226.
(39) Brune, H.; Röder, H.; Bromann, K.; Kern, K.; Jacobsen, J.; Stoltze, P.; Jacobsen, K.; Nørskov, J. K. Anisotropic Corner Diffusion as Origin for Dendritic Growth on Hexagonal Substrates. *Surf. Sci.* **1996**, *6028*, L115–L122.
(40) Giesen, M.; Steimer, C.; Ibach, H. What Does One Learn from Equilibrium Shapes of Two-Dimensional Islands on Surfaces? *Surf. Sci.* **2001**, *471*, 80–100.
(41) Kalff, M.; Comsa, G.; Michely, T. How Sensitive Is Epitaxial Growth to Adsorbates? *Phys. Rev. Lett.* **1998**, *81*, 1255–1258.
(42) Käsberger, U.; Jakob, P. Growth and Thermal Evolution of Submonolayer Pt Films on Ru(0001) Studied by STM. *Surf. Sci.* **2003**, *540*, 76–88.
(43) Negulyaev, N.; Stepanyuk, V.; Bruno, P.; Diekhöner, L.; Wahl, P.; Kern, K. Bilayer Growth of Nanoscale Co Islands on Cu(111). *Phys. Rev. B* **2008**, *77*, 1254371–1254377.
(44) Baber, A. E.; Tierney, H. L.; Sykes, E. C. H. Atomic-Scale Geometry and Electronic Structure of Catalytically Important Pd/Au Alloys. *ACS Nano.* **2010**, *4*, 1637–1645.
(45) Tierney, H. L.; Baber, A. E.; Kitchin, J. R.; Sykes, E. C. H. Hydrogen Dissociation and Spillover on Individual Isolated Palladium Atoms. *Phys. Rev. Lett.* **2009**, *103*, 246102–1 – 4.
(46) Baber, A. E.; Tierney, H. L.; Lawton, T. J.; Sykes, E. C. H. An Atomic-Scale View of Palladium Alloys and Their Ability to Dissociate Molecular Hydrogen. *Chem. Cat. Chem* **2011**, *3*, 607–614.
(47) Marcinkowski, M. D.; Jewell, A. D.; Stamatakis, M.; Boucher, M. B.; Lewis, E. A.; Murphy, C. J.; Kyriakou, G.; Sykes, E. C. H. Controlling a Spillover Pathway with the Molecular Cork Effect. *Nat. Mater.* **2013**, *12*, 523–528.

Chapter 4: H_2 Activation and Spillover on Catalytically Relevant Pt-Cu *Single Atom Alloys*

This chapter was modified from an original publication of the same title by F. R. Lucci et al. from the Journal of Physical Chemistry C, volume 119, pages 24351-24357.

4.1. Introduction

Hydrogenation reactions are critical to the petrochemical, pharmaceutical, and food industries.[1,2] Heterogeneous catalysts that allow facile activation of H_2 and weak binding of H_a exhibit the optimal efficiency for these reactions. However, for a monometallic surface, the Brønsted-Evans-Polanyi (BEP) relationship dictates that these properties are mutually exclusive because the activation energy of a reaction is inversely proportional to the adsorption strength of the intermediates.[3,4] Some bimetallic catalysts exhibit electronic changes upon alloying and present multiple binding sites that enables them to overcome the BEP relationship and provide both low activation energies for H_2 dissociation and weak binding of H atoms.[5–10] Generally, the catalytic properties of bimetallic alloys are described by ligand and ensemble effects. An ensemble effect refers to changes in the catalytic activity due to the structural and spatial arrangement of the catalytic metal atoms. Ligand effects refer to electronic interactions between the alloyed metals that alter their catalytic activity. Furthermore, surface strain can also alter the catalytic properties of metals via an electronic effect.[11,12] By understanding and then controlling these effects in catalysts containing precious metal alloys, we can reduce the concentration of expensive reactive metal by supporting it in a cheaper more inert host, thus reducing the overall cost of the catalyst.

Pt readily activates H_2 [13,14] which is often the rate-limiting step of industrial hydrogenation reactions; however, its high cost is a major factor in its proliferation.[15]

Although H_2 activation on Pt is a non-activated process, Pt catalysts are highly susceptible to CO poisoning and coke formation.[16–18] In contrast, Cu is known to perform highly selective hydrogenation reactions, though the observed catalytic activity is lower than Pt because of the high activation barrier for H_2 dissociation on Cu.[19] Alloying offers a new set of catalytic properties and Pt-Cu alloys have been shown to be capable of highly selective partial hydrogenation of cyclohexadiene and butadiene.[20,21] However, the atomic scale structure of the active sites for these reactions is unknown; therefore, a fundamental knowledge of the surface composition of Pt-Cu alloys and their interaction with hydrogen is a key step toward designing new alloy catalysts.

Approaching the limit of atom efficiency, single site catalysts offer exciting opportunities both in terms of superior chemistry and lower cost.[22–24] Isolated Pt atoms on Al_2O_3 and FeO_3 supports have been shown to catalyze CO oxidation.[25,26] Recently, we have shown that isolated Pd atoms in a Cu surface dissociate H_2 and enable the spillover of H atoms to Cu sites.[7,27] Theoretical simulations predict that isolated Pt atoms are also capable of similar chemistry;[6,28] however, this has not been shown experimentally. The energetic landscape for activation of small molecules on metal alloys depends critically on the atomic geometry of the surface atoms. For example, the Goodman group demonstrated that contiguous Pd atoms in Au are required for O_2 activation.[29] Related to the current work; a recent study of PdGa intermetallic surfaces highlights how the atomic arrangement affects the barrier for H_2 activation.[30] Therefore, a fundamental understanding of the influence of Pt ensemble sizes in Cu on H_2 activation, spillover and desorption will contribute to the rational design of catalysts that use trace amounts of expensive Pt in more inert, cheaper host metals.

In this study, we link hydrogen uptake, spillover and release to the surface structure of Pt-Cu alloys for both dilute Pt surfaces which contain dispersed Pt monomers and Pt rich surfaces with extended Pt ensembles. Combining scanning tunneling microscopy (STM) with temperature programmed desorption (TPD) enables us to explore the relationship of H_2 desorption and H atom spillover to the atomic arrangement of Pt atoms in Cu. At low Pt coverages (< 0.05 monolayer), Pt exists in the Cu surface as individual, isolated atoms that are thermally stable with respect to bulk segregation to ~450 K. The Pt monomers in Cu allow for facile H_2 dissociation and enable H atom spillover onto the Cu terraces which we directly visualize with STM. We observe higher desorption temperatures of H_2 from Pt rich surface alloys than for those containing only isolated Pt atoms. The low temperature adsorption, spillover and desorption of H_2 from Pt monomers in an inexpensive Cu host show great promise for improving the efficiency and reducing the overall cost of Pt alloy catalysts.

4.2. Results and Discussion

Figure 4.1 summaries the results of our initial experiments which focused on low Pt loading Cu alloys (0.01 ML Pt-Cu(111)). Extensive STM imaging showed that the surface of these dilute alloys is composed of Cu(111) terraces with monatomic steps (Figure 4.1B) and atomic resolution images revealed isolated protrusions within the Cu lattice which are Pt monomers (Figure 4.1C). TPD traces demonstrated that these individual, isolated Pt atoms in Cu activate the dissociation of H_2 (Figure 4.1A). Specifically, after uptake at 85 K we observed the desorption of H_2 at 230 K in TPD traces (Figure 4.1A). Since molecular desorption of H_2 from metal surfaces occurs below 20 K,[31,32] desorption of H_2 at 230 K indicates the adsorption is dissociative. Furthermore, and most importantly, the H_2 desorption temperature is lower than H_2 desorption from both pure metal surfaces where H_2 recombinant

desorption from both Pt(111) and Cu(111) occurs at ~300 K.[13,14,19,33] As the exposure of H_2 increased, the desorption temperature decreases from 260 K to 230 K suggestive of second order desorption kinetics.

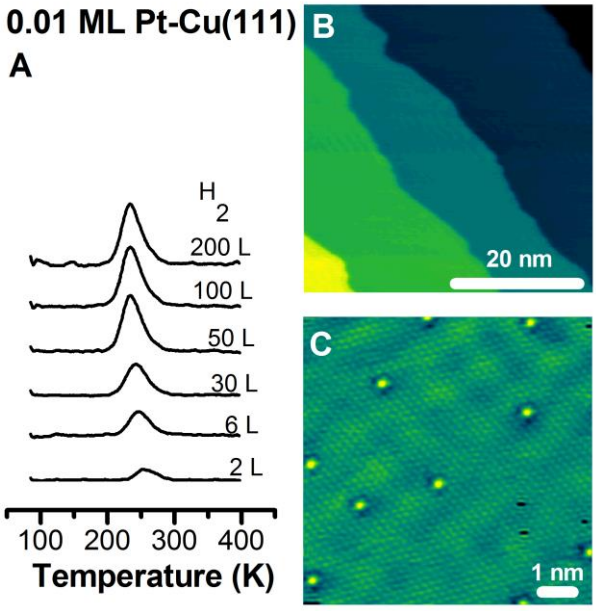

Figure 4.1. H_2 desorption from Pt-Cu(111) SAA
(A) TPD spectra of H_2 uptake on a 0.01 ML Pt-Cu(111) surface. (B, C) STM images of 0.01 ML Pt surfaces in which the Pt atoms appear in STM images as isolated protrusions substituted into the Cu surface lattice. All STM images were recorded at 30 K.

Of particular note is the fact that H_2 uptake on 0.01 ML SAA Pt-Cu(111) surfaces yields ~10 % H surface coverage indicating that the concentration of H atoms is not limited by the number of Pt active sites; therefore the Pt-Cu SAA is capable of spillover. Using STM, we observed the H atoms that migrate from the Pt atom dissociation sites to the Cu surface, directly visualizing the spillover H atoms (Figure 4.2). After exposing a clean 0.01 ML Pt-Cu(111) surface to H_2 at 85 K and cooling to 5 K for STM imaging, we observed the appearance of depressions on the Cu terraces. The locations of the depressions are independent of substituted Pt sites which appear as protrusions in STM images. Figure 4.2A-

B are consecutive STM images showing the motion of H atoms on the surface. Since imaging was performed at 5 K using non-perturbative tunneling conditions, the mobility of the clusters provides further evidence that they are composed of H atoms as it has previously been shown that H atoms undergo quantum tunneling mediated diffusion at low temperature.[34,35]

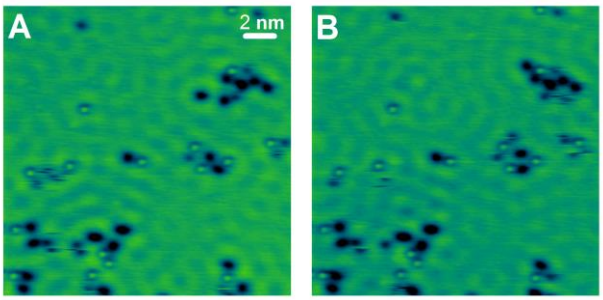

Figure 4.2. Low-temperature STM images of H atom motion on the 0.01 ML SAA Pt-Cu(111) surface
Panels A and B show consecutive STM images in which the H atom clusters (depressions) change position. All images were taken at 5 K at 30 pA and 30 mV.

Our TPD experiments indicate that H_2 desorption from Pt-Cu SAAs is ~60 K lower than observed on Cu(111)[19] or Pt(111)[14] surfaces (Figure 4.1). We hypothesize that this low temperature desorption is due to the weak binding energy of H to the Pt-Cu surface and a low activation barrier for H_2 dissociation (Figure 4.3). Due to microscopic reversibility, molecules adsorb and desorb via the same pathway. In this system H_2 adsorbs and desorbs at the isolated Pt atom sites as Cu(111) is not capable of dissociating H_2 in UHV.[19] In terms of the desorption temperature of H_2, hydrogen must overcome both its binding energy to the Pt site and the recombination barrier as shown in Figure 4.3. For Cu, the desorption temperature accounts for both the binding energy of H atoms to Cu and the activation energy for H_2 recombinant desorption.[19] For Pt, however, the desorption barrier is primarily due to the stronger binding energy of H atoms since H_2 dissociation is a non-activated process on

Pt.[36] We hypothesize that the low temperature desorption that we observe for the Pt-Cu SAA is a result of a weaker H atom binding energy compared to continuous Pt and a lower activation energy compared to Cu. We postulate the binding energy of H to a single Pt site is lower than bulk Pt since H prefers to adsorb to 3-fold hollow sites containing 1 Pt atom and 2 Cu atoms. These ideas are consistent with recent theoretical calculations which reported that the adsorption energy of H to Pt-Cu SAAs as 0.3 eV[6] and that H_2 dissociation on Pt-Cu alloys has an activation barrier <0.05 eV, which is consistent with our results.[6,28]

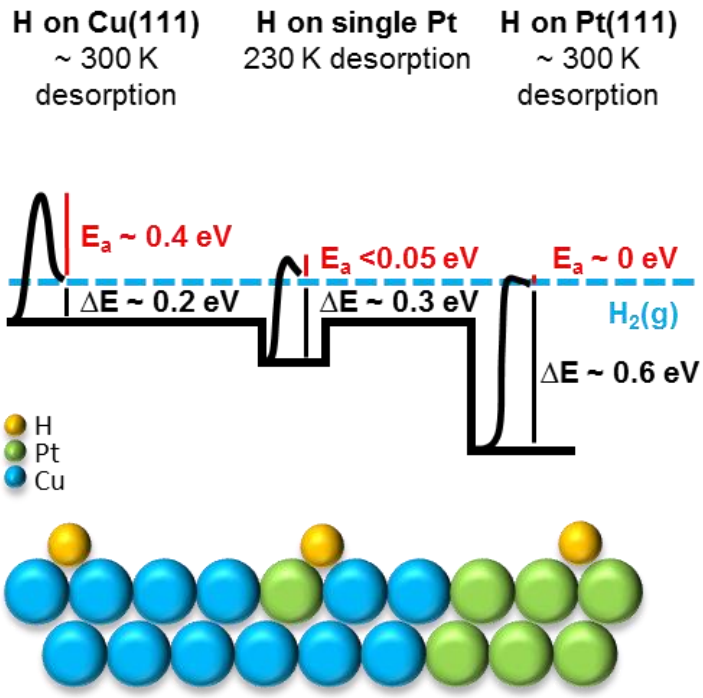

Figure 4.3. Energetic landscape of H_2 desorption
Schematic of the energetic landscape for dissociation and desorption of H_2 on Pt-Cu SAAs as compared to monometallic Cu and Pt surfaces.[6,19,27,36]

Multiple H_2 adsorption/desorption experiments indicate that Pt-Cu SAA are stable with respect to both hydrogen exposure and thermal annealing (Figure 4.4). After 13 trials of exposing a 0.01 ML Pt-Cu(111) sample to a coverage of H below saturation (1 L of H_2), the amount of H uptake remained constant at 0.08 ± 0.02 ML as shown in Figure 4.4. We find

that individual, isolated Pt atoms remain in the surface layer and active for H_2 dissociation and spillover when ramped to catalytically relevant temperatures of 450 K multiple times. Canzian *et al.* have shown with Monte Carlo simulations that two competing effects impact the subsurface diffusion of Pt into Cu.[37] The size mismatch between Pt (277 pm) and Cu (256 pm) disfavors subsurface diffusion of Pt , but the greater surface free energy of Pt (2.204 J/m^2) than Cu (1.566 J/m^2)[38] favors subsurface diffusion. While no evidence of subsurface diffusion of Pt is a promising attribute of the UHV system, looking forward, in higher pressure environments the composition of the gas phase affects the segregation behavior of the metallic atoms in a way that is not related to just their surface free energies. For Pt-Cu alloys, adsorbate binding often induces changes in the local composition and surface structure as seen with Pt segregating to the surface in a H_2 atmosphere and segregating subsurface in a CO atmosphere.[39,40]

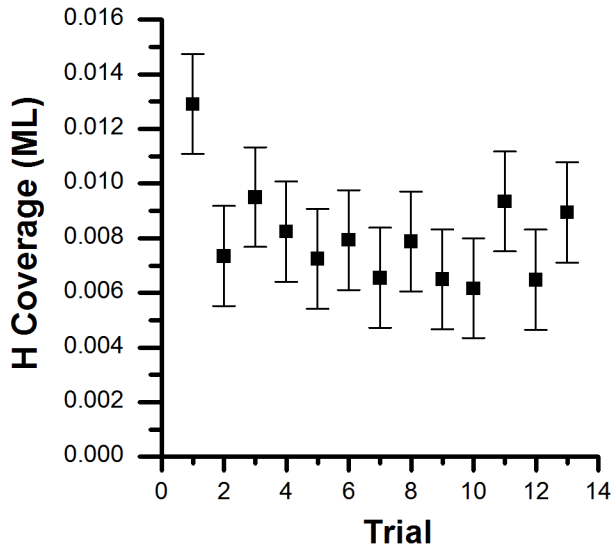

Figure 4.41. Pt-Cu SAA performance during multiple H_2 adsorption/desorption cycles
Pt-Cu SAA performance during multiple H_2 adsorption/desorption cycles. In each trial 1 L of H_2 is deposited on the sample at 85 K and the temperature ramped to 450 K. Error bars are one standard deviation.

In order to understand the geometric effect of Pt ensembles on the energetics of H_2 uptake and release, STM imaging was performed on a variety of coverages of Pt deposited onto a Cu(111) surface held at 380 K (Figure 4.5). At low Pt coverage (< 0.1 ML), the Pt-Cu(111) surface exhibited straight step edges similar to steps observed on Cu(111) (Figure 5 A,B). At Pt coverages > 0. 1 ML, finger like growth parallel to step-edges was observed (Figure 5 C,D, and E). Prior to completion of the first Pt layer, growth of a second layer demonstrates 3D growth of the Pt-Cu alloy.[41] This structural progression agrees with previous studies reporting low coverage formation of the $Cu_3Pt(111)$ alloy.[42] Our high resolution STM images show interesting geometric changes on the atomic scale with increasing Pt coverage. At lower Pt coverage (< 0.05 ML), the Pt atoms exist as isolated species (Figure 5F). In the terraces, the Pt atoms are homogeneously distributed and higher concentrations of Pt atoms exist near step edges.[43] Figure 5F shows the interface between a

terrace and a Pt rich area near a step edge. When alloyed at 380 K, Pt atoms exist as isolated species, even in regions of locally higher Pt concentrations. As the concentration of Pt atoms increase (> 0.05 ML), larger clusters of Pt atoms begin to develop within the finger-like growths at step edges (Figure 4.5G-H). The larger Pt clusters exist as linear chains and run preferentially in the close-packed directions of the Cu(111) surface. As the concentration of Pt increases, the predominance and size of the clusters increases. Larger Pt ensembles with higher Pt density are present near the step edges and gradually decrease in density transitioning from the finger-like growth back to the position of the original Cu step-edges. At Pt coverages > 0.5 ML, Pt(111) like regions are present at the edges of the finger-like growths. On the terraces, Pt still exists as well dispersed, isolated atoms. The local ordering of Pt and Cu atoms in regions of high Pt density demonstrates the strong tendency of Pt and Cu atoms to intermix compared to segregating into regions of pure Pt and Cu atoms.[44–47]

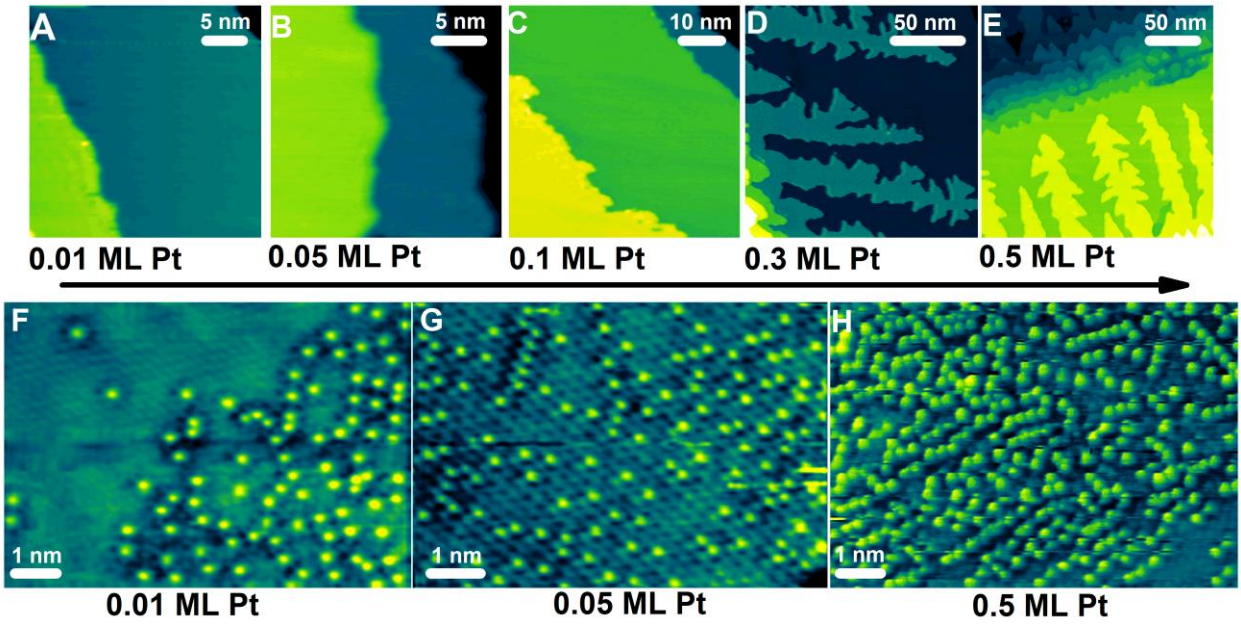

Figure 4.5. Effect of Pt surface coverage on the distribution of Pt ensembles in the Cu(111) surface
High resolution STM images near Cu step edges showing the appearance of 1D chains at coverages > 0.05 ML. Alloys were prepared by depositing Pt at 380 K. All images were recorded at 30 K.

Previously, we have shown that Pt alloys with Cu via two mechanisms.[43] Briefly, the predominant alloying mechanism is place-exchange via ascending step edges. Pt atoms bind to under coordinated atoms at step-edges and then progressively place exchange into terraces resulting in localized higher concentrations of Pt atoms at step edges. The development of finger-like growths at step edges is a kinetic limitation of the process, due to the diffusion of Pt atoms across the surface to the step edges being faster than incorporation into Cu terraces. The second alloying mechanism is direct place-exchange into Cu terraces which itself yields a homogeneous dispersion of Pt atoms across terraces. At the alloying temperatures we examine here, both mechanisms contribute to the final distribution of Pt atoms.

Using our knowledge of the alloying behavior of Pt with Cu(111) as a function of Pt coverage, we selectively prepared alloys with isolated Pt atoms in the surface for coverages < 0.05 ML by holding the temperature of Cu(111) at 380 K during deposition of Pt. At low coverages Pt atoms preferentially exist as isolated species because Pt-Cu bonds are stronger than Pt-Pt bonds.[48] The incorporation of larger Pt atoms into the smaller Cu lattice generates compressive strain and the dispersion of the atoms reduces the strain. Additionally, for Pt based alloys, relativistic effects alter the orbital overlap between Pt and Cu impacting the ordering of Pt-Cu bulk alloys yielding segregation of Pt and Cu into alternating layers which we postulate drives the formation of the 1D chains we observe.[37,44,46,47]

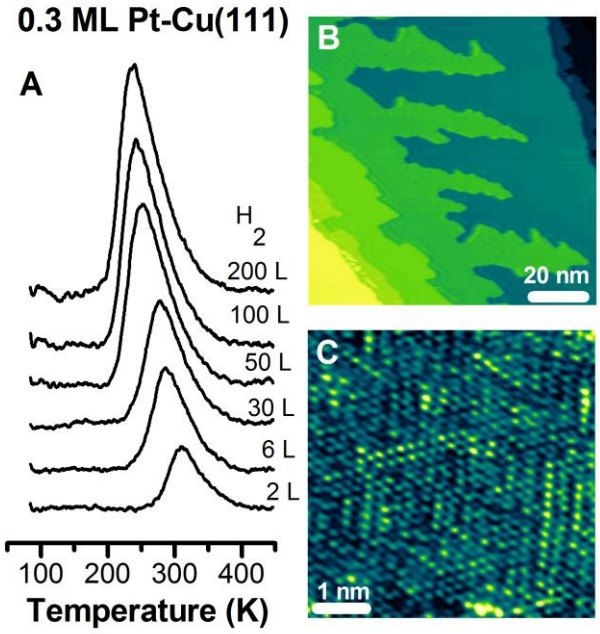

Figure 4.6. H_2 desorption from Pt-Cu(111) alloys with extended Pt ensembles
(A) TPD spectra for the desorption of H_2 from Pt-Cu(111) surface alloys with 0.3 ML Pt. (B-C) STM images of 0.3 ML Pt-Cu surface including (C) atomic resolution where Pt atoms appear in STM images as protrusions within the Cu surface lattice. STM images were obtained at 30 K.

In additional TPD experiments, we examined the effect of higher Pt loading on H_2 uptake, spillover and desorption (Figure 4.6A). Compared to the 0.01 ML Pt-Cu(111) surface, the higher Pt coverage desorption traces are asymmetrical with a higher temperature tail (Figure 4.1A and Figure 4.6A). At saturation coverage of H, desorption from 0.3 ML Pt begins below 200 K and finishes above 300 K in a broad peak. Since our STM images reveal that a higher Pt coverage (0.3 ML) yields a heterogeneous surface structure, the observed increase in the desorption temperature of H_2 as measured by TPD is due to presence of larger Pt ensembles (Figure 4.6 B and C). These 0.3 ML Pt surfaces contain isolated Pt atoms in the Cu terraces, 1D chains of Pt atoms, and also extended Pt arrays at sites where two chains are present next to one another. The broad H_2 desorption trace that we observe with TPD of saturated hydrogen at 0.3 ML Pt is due to desorption from these multiple surface sites. We postulate since H atoms bind at 3-fold hollow sites on metals, the H atoms bound to sites

containing 1 to 3 Pt atoms give rise to the progressively higher desorption temperatures measured in TPD.

To fully investigate the effect of Pt concentration and ensemble size on H_2 uptake, spillover and desorption, H_2 TPD were recorded as a function of Pt coverage (Figure 4.7). As the concentration of Pt increases, the intensity of the H_2 desorption peak increases and the peak broadens. At low coverages, a narrow symmetrical peak is observed indicative of H_2 desorption from a single site; the Pt SAA. The peak progressively broadens and the peak center is shifted to 290 K at 0.6 ML Pt. The progressive broadening suggests desorption from a variety of different surface sites including single Pt atoms, short linear Pt chains, and large Pt clusters as observed in the STM images (Figures 4.5). Given that the H_2 dissociation barrier is low at isolated Pt sites and essentially zero on Pt(111), the shift in desorption peak temperature indicates the increase in binding strength of H to larger Pt clusters as the Pt coverage is increased. At the highest Pt coverage (> 1 ML), desorption at 290 K is consistent with desorption from Pt(111) like sites.[14] The variation in H_2 desorption profiles from the progression of alloy surface structures particularly highlights the fact that individual, isolated Pt atoms (SAAs) bind H considerably more weakly than 1D and 2D Pt ensembles.

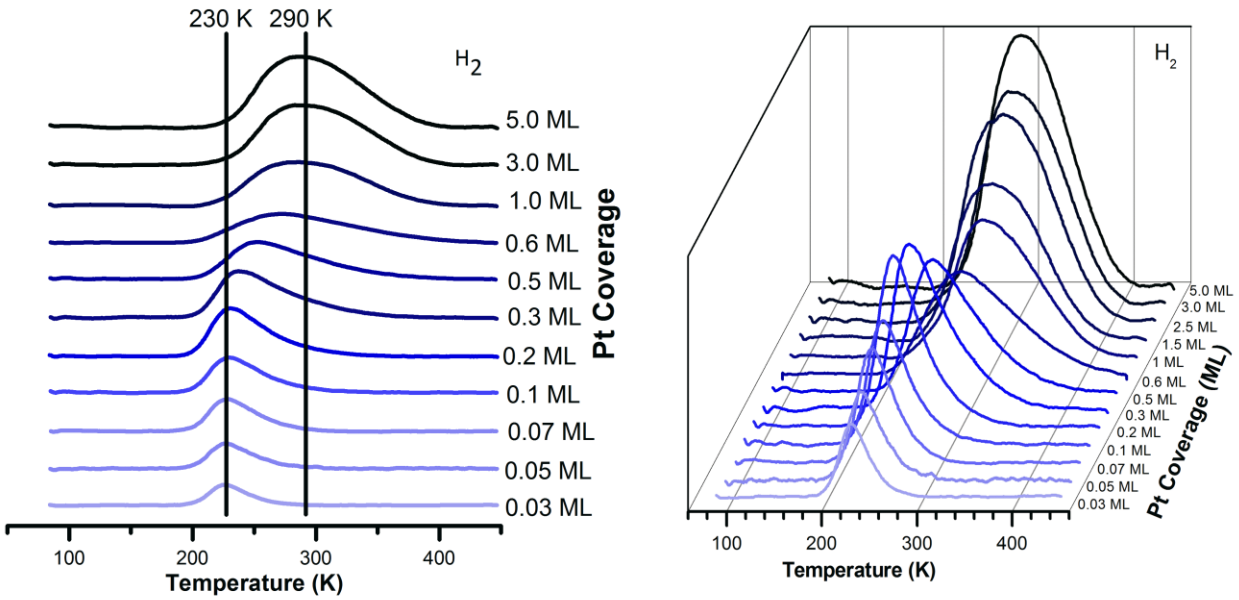

Figure 4.7. H_2 desorption from Pt-Cu(111) surface alloys
TPD spectra of 50 L H_2 uptake of multiple coverages of Pt. The varying stoichiometry of Pt-Cu surface was achieved by alloying well defined amounts of Pt in Cu(111) at 380 K. The TPD plots highlight both (A) the shift in desorption temperature with increasing Pt coverage and (B) changes in the desorption peak shape. The color change from light to dark blue reflects increasing Pt coverage.

By measuring the H uptake as a function of Pt-Cu alloy stoichiometry, we observe as the Pt coverage increases from 0.3 ML to 5 ML, the uptake and the desorption temperature of H_2 both increase. This supports Pt atoms as being both the active sites for dissociation/recombination and the preferred binding sites for H (Figure 4.8). If there was no spillover of H to Cu a linear increase of H coverage with Pt surface loading would be expected since only the Pt atoms are responsible for H_2 activation. However, for low coverages of Pt (< 0.2 ML) a non-linear trend was observed (Figure 4.8). Therefore, H uptake is not limited by the number of Pt sites, which supports and quantifies our STM results where we observe H atom spillover onto Cu (Figure 4.2). The H_2 coverage plateaus between 0.2 ML - 0.5 ML Pt where STM shows that the surface is dominated by 1D Pt chains. The single atom sites are more efficient at H spillover than the larger clusters due to

the stronger binding of H to Pt chains. H_2 saturation does not occur until ~2 ML of Pt due to 3D alloy growth prior to Pt termination.[12]

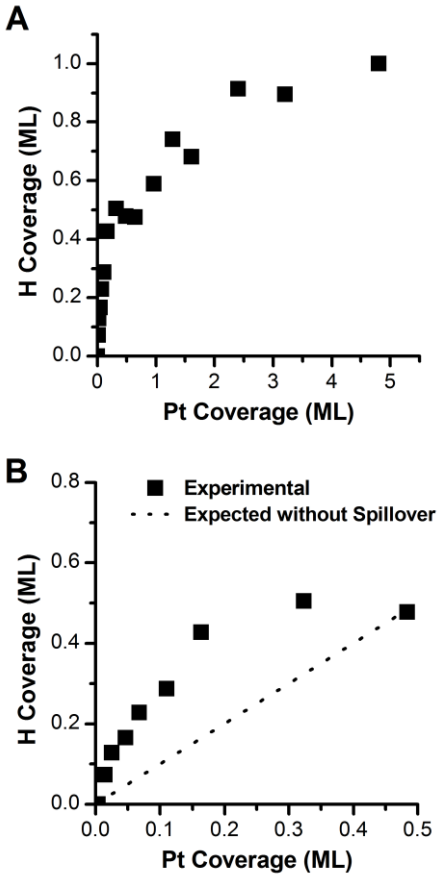

Figure 4.8. H_2 uptake (50 L) on Pt-Cu alloys as a function of Pt coverage
Panel B shows data for low coverages of Pt and the anticipated H coverage that would be expected if H spillover onto Cu did not occur.

Previously, we have reported that H atoms are capable of spilling over from single Pd atom active sites to Cu terraces.[7,8,27] The distinguishing feature of the Pt-Cu alloy compared to Pd-Cu alloy is the enhanced stability in the surface layer. For Pt-Cu alloys, H_2 uptake remained constant after repeated ramps to 450 K, however, ~70 % drop in H_2 uptake was observed for Pd-Cu alloys ramped repeatedly to 300 K (13 trials). Additionally, Pt is able to alloy directly into the terraces leading to a higher overall dispersion. Different alloying mechanisms are observed for Pt-Cu and Pd-Cu alloys, but both alloys behave very similarly

in terms of H_2 activation in that both SAAs reduce the activation energy of H_2 dissociation, allow spillover to Cu and exhibit lower recombination barriers than the pure metals. Therefore, the SAA concept we developed for Pd appears to hold in the Cu-Pt system which turns out to be more stable with respect to annealing than Pd-Cu.[7,8,27,49–53]

4.3. Summary

By combining STM and TPD we probed H_2 activation, spillover and desorption on a range of Pt-Cu alloy surfaces. We observed that single Pt atoms substituted into the Cu(111) surface enable H_2 to undergo facile dissociation at 85 K. The H atoms are then able to migrate from Pt atoms to Cu sites at 85 K revealing an efficient spillover mechanism. H_2 desorbs from the alloy surface at temperatures significantly lower than either pure metal. We find these SAAs surfaces are robust to multiple heating cycles to 450 K. Our STM measurements show the evolution of the alloy surface structure as the Pt content is raised, from isolated atoms to 1D Pt chains and extended Pt ensembles. Our TPD studies reveal how the H coverage and desorption temperature track with the alloy surface structure. This work provides a fundamental understanding of ensemble effects in Pt-Cu alloys on the uptake and release of H_2. This in turn yields guiding principles for the design of Pt-Cu alloy catalysts that maximize the efficient low-temperature uptake, spillover and release of hydrogen while minimizing the amount of precious metal required to activate hydrogen.

4.4. Additional Experimental Details

Surfaces were exposed to H_2 (99.9 % Airgas) by backfilling the chamber to the required pressure through high precision leak valves while the sample was held at 85 K. H_2 coverages were determined by the saturation coverage of unity for H_2 adsorbed on 5 ML of Pt, assuming the surface terminates as Pt(111). Pt coverages were quantified by CO (99.99 % Airgas) titration by saturating with CO (10 L) and comparing the ratio between CO desorption from Cu sites (<200 K) and Pt sites (>300 K). CO binds atop to isolated Pt atoms in Cu similar to CO binding to isolated Pt atoms in Au[54,55] and isolated Pd atoms in Cu.[49] We also accounted for the known saturation packing density of CO on Cu(111) (0.52 ML). [56]

4.5. References

(1) Hagen, J. *Industrial Catalysis*; WILEY-VCH Verlag: Weinheim, 2006.

(2) Ritter, J. A.; Ebner, A. D. State-of-the-Art Adsorption and Membrane Separation Processes for Hydrogen Production in the Chemical and Petrochemical Industries. *Sep. Sci. Technol.* **2007**, *42*, 1123–1193.

(3) Nørskov, J. K.; Rossmeisl, J.; Logadottir, A.; Lindqvist, L.; Kitchin, J. R.; Bligaard, T.; Jónsson, H. Origin of the Overpotential for Oxygen Reduction at a Fuel-Cell Cathode. *J. Phys. Chem. B* **2004**, *108*, 17886–17892.

(4) Nørskov, J. K.; Bligaard, T.; Logadottir, A.; Bahn, S.; Hansen, L. B.; Bollinger, M.; Bengaard, H.; Hammer, B.; Sljivancanin, Z.; Mavrikakis, M.; et al. Universality in Heterogeneous Catalysis. *J. Catal.* **2002**, *209*, 275–278.

(5) Greeley, J.; Mavrikakis, M. Alloy Catalysts Designed from First Principles. *Nat. Mater.* **2004**, *3*, 810–815.

(6) Fu, Q.; Luo, Y. Catalytic Activity of Single Transition-Metal Atom Doped in Cu(111) Surface for Heterogeneous Hydrogenation. *J. Phys. Chem. C.* **2013**, *117*, 14618–14624.

(7) Kyriakou, G.; Boucher, M. B.; Jewell, A. D.; Lewis, E. A.; Lawton, T. J.; Baber, A. E.; Tierney, H. L.; Flytzani-Stephanopoulos, M.; Sykes, E. C. H. Isolated Metal Atom Geometries as a Strategy for Selective Heterogeneous Hydrogenations. *Science* **2012**, *335*, 1209–1212.

(8) Boucher, M. B.; Zugic, B.; Cladaras, G.; Kammert, J.; Marcinkowski, M. D.; Lawton, T. J.; Sykes, E. C. H.; Flytzani-Stephanopoulos, M. Single Atom Alloy Surface Analogs in $Pd_{0.18}Cu_{15}$ Nanoparticles for Selective Hydrogenation Reactions. *Phys. Chem. Chem. Phys.* **2013**, *15*, 12187–12196.

(9) Skoplyak, O.; Barteau, M. A.; Chen, J. G. Reforming of Oxygenates for H_2 Production: Correlating Reactivity of Ethylene Glycol and Ethanol on Pt(111) and Ni/Pt(111) with Surface D-Band Center. *J. Phys. Chem. B* **2006**, *110*, 1686–1694.
(10) Alayoglu, S.; Nilekar, A. U.; Mavrikakis, M.; Eichhorn, B. Ru-Pt Core-Shell Nanoparticles for Preferential Oxidation of Carbon Monoxide in Hydrogen. *Nat. Mater.* **2008**, *7*, 333–338.
(11) Groß, A. Reactivity of Bimetallic Systems Studied from First Principles. *Top. Catal.* **2006**, *37*, 29–39.
(12) Rodriguez, J. A. Physical and Chemical Properties of Bimetallic Surfaces. *Surf. Sci. Rep.* **1996**, *24*, 223–287.
(13) Olsen, R. A.; Kroes, G. J.; Baerends, E. J. Atomic and Molecular Hydrogen Interacting with Pt(111). *J. Phys. Chem. C* **1999**, *111*, 11155–11163.
(14) Collins, D. M.; Spicer, W. E. The Adsorption of CO, O_2 and H_2 on Pt. *Surf. Sci.* **1977**, *69*, 85–113.
(15) Yu, W.; Porosoff, M. D.; Chen, J. G. Review of Pt-Based Bimetallic Catalysis: From Model Surfaces to Supported Catalysts. *Chem. Rev.* **2012**, *112*, 5780–5817.
(16) Barbier, J. Deactivation of Reforming Catalysts by Coking. *Appl. Catal.* **1986**, *23*, 225–243.
(17) Bitter, J. H.; Seshan, K.; Lercher, J. A. Deactivation and Coke Accumulation during CO_2/CH_4 Reforming over Pt Catalysts. *J. Catal.* **1999**, *343*, 336–343.
(18) Pettersson, L.; Westerholm, R. State of the Art of Multi-Fuel Reformers for Fuel Cell Vehicles: Problem Identification and Research Needs. *Int. J. Hydrog. Energy* **2001**, *26*, 243–264.
(19) Anger, G.; Winkler, A.; Rendulic, K. D. Adsorption and Desorption Kinetics in the Systems H_2/Cu(111), H_2/Cu(110) and H_2/Cu(100). *Surf. Sci.* **1989**, *220*, 1–17.
(20) Qi, S.; Yu, W.; Lonergan, W. W.; Yang, B.; Chen, J. G. General Trends in the Partial and Complete Hydrogenation of 1,4-Cyclohexadiene over Pt-Co, Pt-Ni and Pt-Cu Bimetallic Catalysts. *Chem. Cat. Chem* **2010**, *2*, 625–628.
(21) Lonergan, W. W.; Xing, X.; Zheng, R.; Qi, S.; Huang, B.; Chen, J. G. Low-Temperature 1,3-Butadiene Hydrogenation over Supported Pt/3d/γ-Al_2O_3 Bimetallic Catalysts. *Catal. Today* **2011**, *160*, 61–69.
(22) Thomas, J. M. The Concept, Reality and Utility of Single-Site Heterogeneous Catalysts (SSHCs). *Phys. Chem. Chem. Phys.* **2014**, *16*, 7647–7661.
(23) Neurock, M.; Tysoe, W. T. Mechanistic Insights in the Catalytic Synthesis of Vinyl Acetate on Palladium and Gold/Palladium Alloy Surfaces. *Top. Catal.* **2013**, *56*, 1314–1332.
(24) Calaza, F.; Stacchiola, D.; Neurock, M.; Tysoe, W. T. Coverage Effects on the Palladium-Catalyzed Synthesis of Vinyl Acetate: Comparison between Theory and Experiment. *J. Am. Chem. Soc.* **2010**, *132*, 2202–2207.

(25) Qiao, B.; Wang, A.; Yang, X.; Allard, L. F.; Jiang, Z.; Cui, Y.; Liu, J.; Li, J.; Zhang, T. Single-Atom Catalysis of CO Oxidation Using Pt_1/FeO_x. *Nat. Chem* **2011**, *3*, 634–641.

(26) Peterson, E. J.; DeLaRiva, A. T.; Lin, S.; Johnson, R. S.; Guo, H.; Miller, J. T.; Kwak, J.; Peden, C. H. F.; Kiefer, B.; Allard, L. F.; et al. Low-Temperature Carbon Monoxide Oxidation Catalysed by Regenerable Atomically Dispersed Palladium on Alumina. *Nat. Commun.* **2014**, *5*, 1–11.

(27) Tierney, H. L.; Baber, A. E.; Kitchin, J. R.; Sykes, E. C. H. Hydrogen Dissociation and Spillover on Individual Isolated Palladium Atoms. *Phys. Rev. Lett.* **2009**, *103*, 246102–1 – 4.

(28) Diño, W.; Kasai, H.; Okiji, A. Dissociative Adsorption Dynamics of H_2 at the atop-Pt, atop-Cu, and Cu-Pt Bridge Sites of an Ordered $Cu_3Pt(111)$ - Orientational Effects. *Appl. Surf. Sci.* **2001**, *169-170*, 36–41.

(29) Gao, F.; Wang, Y.; Goodman, D. W. CO Oxidation over AuPd(100) from Ultrahigh Vacuum to near-Atmospheric Pressures: The Critical Role of Contiguous Pd Atoms. *J. Am. Chem. Soc.* **2009**, *131*, 5734–5735.

(30) Prinz, J.; Gaspari, R.; Pignedoli, C. A.; Vogt, J.; Gille, P.; Armbrüster, M.; Brune, H.; Gröning, O.; Passerone, D.; Widmer, R. Isolated Pd Sites on the Intermetallic PdGa(111) and PdGa(111) Model Catalyst Surfaces. *Angew. Chem.* **2012**, *124*, 9473–9477.

(31) Andersson, S.; Persson, M. Crystal-Face Dependence of Physisorption Potentials. *Phys. Rev. B* **1993**, *48*, 5685–5688.

(32) Sugimoto, T.; Fukutani, K. Effects of Rotational-Symmetry Breaking on Physisorption of Ortho- and Para- H_2 on Ag(111). *Phys. Rev. Lett.* **2014**, *112*, 146101–1 – 5.

(33) Linke, R.; Schneider, U.; Busse, H.; Becker, C.; Schröder, U.; Castro, G. R.; K., W. Interaction of Hydrogen with $Cu_3Pt(111)$: Dissociation via Isolated Platinum Atoms. *Surf. Sci.* **1994**, *307 - 309*, 407–411.

(34) Jewell, A. D.; Peng, G.; Mattera, M. F. G.; Lewis, E. A.; Murphy, C. J.; Kyriakou, G.; Mavrikakis, M.; Sykes, E. C. H. Quantum Tunneling Enabled Self-Assembly of Hydrogen Atoms on Cu(111). *ACS Nano* **2012**, *6*, 10115–10121.

(35) Lauhon, L. J.; Ho, W. Direct Observation of the Quantum Tunneling of Single Hydrogen Atoms with a Scanning Tunneling Microscope. *Phys. Rev. Lett.* **2000**, *85*, 4566–4569.

(36) Hanh, T. T. T.; Takimoto, Y.; Sugino, O. First-Principle Thermodynamic Description of Hydrogen Electroadsorption on Pt(111) Surface. *Surf. Sci.* **2014**, *625*, 104–111.

(37) Canzian, A.; Mosca, H. O.; Bozzolo, G. Atomistic Modeling of Pt Deposition on Cu(111) and Cu Deposition on Pt(111). *Surf. Rev. Lett.* **2004**, *11*, 235–243.

(38) Tyson, W. R.; Miller, W. A. Surface Free Energies of Solid Metals Estimation from Liquid Surface Tension Measurments. *Surf. Sci.* **1977**, *62*, 267–276.

(39) Andersson, K. J.; Calle-Vallejo, F.; Rossmeisl, J.; Chorkendorff, I.

Adsorption-Driven Surface Segregation of the Less Reactive Alloy Component. *J. Am. Chem. Soc.* **2009**, *131*, 2404–2407.

(40) Bondarenko, A. S.; Stephens, I. E. L.; Chorkendorff, I. A Cell for the Controllable Thermal Treatment and Electrochemical Characterisation of Single Crystal Alloy Electrodes. *Electrochem. commun.* **2012**, *23*, 33–36.

(41) Belkhou, R.; Barrett, N. T.; Guillot, C.; Barbier, A.; Eugène, J.; Carrière, B.; Naumovic, D.; Osterwalder, J. Growth of Pt/Cu(111) Characterized by Auger Electron Spectroscopy, Core Level Photoemission and X-Ray Photoelectron Diffraction. *Appl. Surf. Sci.* **1993**, *65*, 63–70.

(42) Dastoor, P. C.; O'Connor, D. J.; MacLaren, D. A.; Allison, W.; Noakes, T. C. Q.; Bailey, P. Step Mediated Surface Alloy Formation of Pt/Cu(111). *Surf. Sci.* **2005**, *588*, 101–107.

(43) Lucci, F. R.; Lawton, T. J.; Pronschinske, A.; Sykes, E. C. H. Atomic Scale Surface Structure of Pt/Cu(111) Surface Alloys. *J. Phys. Chem. C* **2014**, *118*, 3015–3022.

(44) Christensen, A.; Ruban, A. V.; Stoltze, P.; Jacobsen, K. W.; Skriver, H. L.; Nørskov, J. K.; Besenbacher, F. Phase Diagrams for Surface Alloys. *Phys. Rev. B* **1997**, *56*, 5822–5834.

(45) Hansen, M. *Constitution of Binary Alloys*, 2nd Ed.; McGraw-Hill: New York, 1958.

(46) Lu, Z. W.; Wei, S. H.; Zunger, A. Long-Range Order in Binary Late-Transition Metal Alloys. *Phys. Rev. Lett.* **1991**, *66*, 13–16.

(47) Sanyal, B.; Bose, S. K.; Drchal, V.; Kudrnovský, J. Ordering and Segregation in X Pt (X =V, Cu, and Au) Random Alloys. *Phys. Rev. B* **2001**, *64*, 134111.

(48) Yuge, K.; Seko, A.; Kuwabara, A.; Oba, F.; Tanaka, I. Ordering and Segregation of a $Cu_{75}Pt_{25}$(111) Surface: A First-Principles Cluster Expansion Study. *Phys. Rev. B* **2007**, *76*, 0454071–045407 – 8.

(49) Marcinkowski, M. D.; Jewell, A. D.; Stamatakis, M.; Boucher, M. B.; Lewis, E. A.; Murphy, C. J.; Kyriakou, G.; Sykes, E. C. H. Controlling a Spillover Pathway with the Molecular Cork Effect. *Nat. Mater.* **2013**, *12*, 523–528.

(50) Boucher, M. B.; Marcinkowski, M. D.; Liriano, M. L.; Murphy, C. J.; Lewis, E. A.; Jewell, A. D.; Mattera, M. F. G.; Kyriakou, G.; Flytzani-Stephanopoulos, M.; Sykes, E. C. H. Molecular-Scale Perspective of Water-Catalyzed Methanol Dehydrogenation to Formaldehyde. *ACS Nano* **2013**, *7*, 6181–6187.

(51) Tierney, H. L.; Baber, A. E.; Sykes, E. C. H. Atomic-Scale Imaging and Electronic Structure Determination of Catalytic Sites on Pd/Cu near Surface Alloys. *J. Phys. Chem. C* **2009**, *113*, 7246–7250.

(52) Baber, A. E.; Tierney, H. L.; Lawton, T. J.; Sykes, E. C. H. An Atomic-Scale View of Palladium Alloys and Their Ability to Dissociate Molecular Hydrogen. *Chem. Cat. Chem* **2011**, *3*, 607–614.

(53) Baber, A. E.; Tierney, H. L.; Sykes, E. C. H. Atomic-Scale Geometry and Electronic Structure of Catalytically Important Pd/Au Alloys. *ACS Nano.* **2010**, *4*, 1637–1645.

(54) Pedersen, M. Ø.; Helveg, S.; Ruban, A.; Stensgaard, I.; Lægsgaard, E.; Nørskov, J. K.; Besenbacher, F. How a Gold Substrate Can Increase the Reactivity of a Pt Overlayer. *Surf. Sci.* **1999**, *426*, 395–409.
(55) Eyrich, M.; Diemant, T.; Hartmann, H.; Bansmann, J.; Behm, R. J. Interaction of CO with Structurally Well-Defined Monolayer PtAu/Pt(111) Surface Alloys. *J. Phys. Chem. C* **2012**, *116*, 11154–11165.
(56) Raval, R.; Parker, S. F.; Pemble, M. E.; Hollins, P.; Pritchard, J.; Chesters, M. A. FT-RAIRS EELS LEED Studies of the Adsorption of Carbon Monoxide on Cu(111). *Surf. Sci.* **1988**, *203*, 353–377.

Chapter 5: Selective Hydrogenation of Butadiene on Pt-Cu Alloys at the Single Atom Limit

This chapter was modified from an original publication of the same title by F. R. Lucci, J. Liu* et al. from Nature Communications, volume 6, page 8550.*

5.1. Introduction

Pt is one of the most widely used transition metal catalysts due to its superior catalytic performance for both oxidation and hydrogenation reactions. It is used extensively in electrochemical and heterogeneous catalysts with applications in fuel cells, automotive catalytic converters, and industrial hydrocarbon cracking processes.[1,2] Pt will also undoubtedly play a large role in the ongoing development of clean energy technologies. Despite its favorable reactivity, there are two major drawbacks of Pt catalysts. First, Pt is very expensive and scarce in nature which imposes major limitations on its future role in catalysis. Second, Pt is susceptible to CO poisoning in polymer electrolyte membrane (PEM) fuel cells because CO binds strongly to metallic Pt.[3,4] Therefore, a key step towards the next generation catalysts will be the development of hybrid systems that retain the high activity of Pt, while improving its selectivity and increasing its tolerance to CO poisoning.

One approach is to design catalysts that contain only the Pt sites necessary to perform or to assist a target reaction. Recently "single-site heterogeneous catalysts" containing atomically dispersed active metal species have been shown to be effective in catalyzing a number of reactions.[5] Single-site Pt and Au cations stabilized by -O- linkages on various supports with vicinal -OH groups have been identified as the active sites for the water-gas shift reaction.[6,7] In a similar fashion, isolated precious metal-O_x species on various support matrices have shown superior activity for CO oxidation,[8] and the steam reforming of

methanol.[9,10] Atomically dispersed Au atoms in metallic Ni have been shown to dramatically suppress carbon deposition in the steam reforming of methane,[11] while isolated Pd atoms in metallic copper host catalyze selective hydrogenation reactions.[12–14] Though Pt and Pd are often interchangeable in terms of catalytic activity, they have different physical properties that impact their alloying behavior, surface segregation, and electronic structure that can potentially impact their ability to activate H_2 and catalyze hydrogenation reactions.[15–19] Pt-Cu bimetallic alloys offer an alternative method for reducing the amount of Pt and potentially enhancing catalyst selectivity for partial hydrogenation reactions,[20–23] but to date it has not been reported that single metallic Pt atoms are capable of such chemistry. Theory work has shown that by simultaneously optimizing the activation of reactants and binding strength of intermediates, the catalyst activity for hydrogenation reactions should be controllable.[24]

Herein we show that very low concentrations of individual, isolated Pt atoms in a Cu surface catalyze the industrially important butadiene hydrogenation reaction with high selectivity to butenes. Butadiene poisons polymerization catalysts even at low concentrations (< 10 ppm) in industrial alkene streams.[25] Of particular interest is the butadiene impurity in propene feedstocks used to produce 42.3 million tons of polypropylene annually.[26] The selective hydrogenation of butadiene to butene serves to increase the purity of alkene feedstocks without reducing their overall concentration. Therefore, catalysts that selectively hydrogenate butadiene to butenes and prevent the hydrogenation of butenes to butane are of great interest. It has been proposed that the observed product distribution is controlled by the adsorption energy of butadiene to the catalytic surface and weaker binding is known to direct the product distribution in favor of the formation of butenes.[27,28] Our surface science experiments show that Cu binds butadiene weaker than Pt, but the dissociation of molecular

H_2 on Cu surfaces and nanoparticle systems is often the rate limiting step. We have used high-resolution microscopy to interrogate the atomic geometry of Pt-Cu alloys and have discovered the minimum ensemble of Pt, a single atom, embedded in Cu(111) single crystal surface will dissociate H_2 thus enabling selective hydrogenation reactions. Our surface science experiments revealed that isolated Pt atom geometries, unlike continuous Pt ensembles, exhibit weak binding of CO and maintain activity after many hydrogenation cycles. Guided by these model catalyst experiments, we prepared highly diluted Pt-Cu nanoparticles using this single atom alloy (SAA) principle.[12,13] Nanoparticle Cu catalysts, with Pt as the minority species, were found to exhibit high activity and selectivity for butadiene hydrogenation to butenes under relatively mild conditions.

5.2. Results and Discussion

Hydrogen Uptake and Desorption from Pt-Cu(111) Surfaces

Model Pt-Cu surfaces with a range of Pt coverages were prepared using physical vapor deposition of Pt onto a clean Cu(111) surface held at 380 K. Scanning tunneling microscopy (STM) imaging (Figure 5.1B) shows that at low Pt coverages (0.02 monolayer (ML)) Pt atoms exist as individual, isolated species substituted in the Cu surface lattice which we refer to as a SAA.[19] The STM images indicate that Pt atoms incorporate both directly into Cu(111) terraces and in areas above surface step edges via place exchange. Even in regions of higher local concentration near step edges, the Pt atoms are always isolated from one another and do not form dimer or trimer clusters. This high dispersion of individual Pt atoms is driven by the negative mixing enthalpy of Pt in Cu and elastic strain relief of incorporating a larger Pt atom into a smaller Cu lattice.[15]

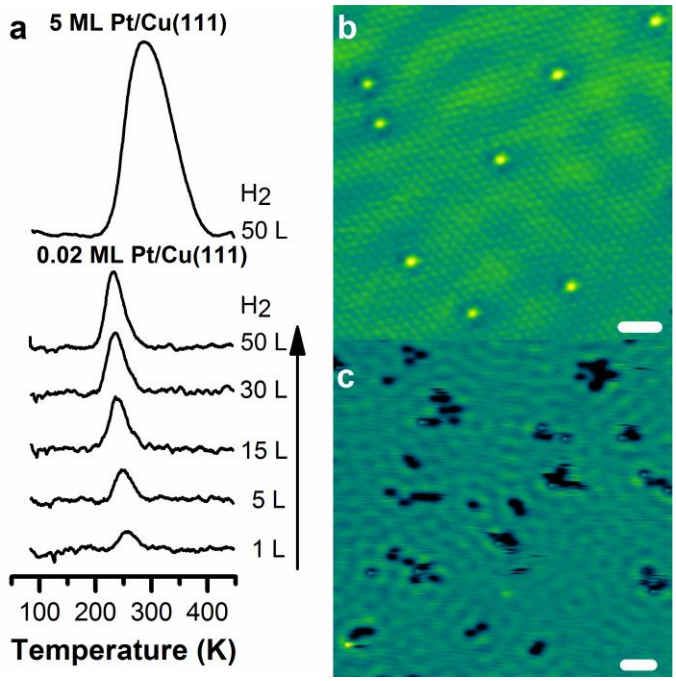

Figure 5.1. H_2 dissociation and spillover on a Pt-Cu(111) SAA
(A) Temperature program desorption (TPD) traces of H_2 uptake on 0.02 ML and 5 ML Pt-Cu(111) surface exposed to H_2 at 85 K. (B) STM image of 0.02 ML Pt-Cu(111) SAA surface where the Pt atoms appear as isolated protrusions substituted into the Cu(111) surface. Scale bars are 1 nm. (C) STM image showing H atom spill over onto Cu in which the H atoms appear as depressions and cluster into small mobile islands. Pt sites appear in STM images as protrusions. Scale bars are 3 nm.

By quantifying surface coverages of both Pt and H, our temperature programmed desorption (TPD) experiments (Figure 5.1A) reveal that trace amounts of Pt make H available on the more inert Cu surface by dissociating H_2 and allowing spillover of H atoms to Cu sites. Importantly, the H_2 desorption temperature on the Pt-Cu(111) SAA of 230 K is significantly lower than H_2 desorption from either a Pt(111) or Cu(111) surfaces which occurs at ~300 K[29–31] meaning that the H atoms also recombine and desorb from the Pt atom sites. This is consistent with the principle of microscopic reversibility which states the forward and reverse reactions follow the same lowest energy pathway. With increasing exposure to H_2, the desorption temperature shifts to lower temperatures characteristic of second order desorption kinetics. Therefore, the Pt atoms in Cu act as both entrance and exit

sites for H_2 dissociation and recombination. Calculations predict that Pt exhibits a negligible barrier for H_2 dissociative adsorption which is consistent with the facile dissociative adsorption of H_2 that we observe at 85 K.[32] Notably, the concentration of H_2 desorbing from the surface is much higher than the the Pt coverage, demonstrating that the H atoms must spill over from the Pt sites to Cu. Low-temperature STM allows us to directly image these H atoms. STM images of Pt-Cu(111) SAA surfaces exposed to H_2 show mobile depressions on the Cu surface that Jewell *et al.* previously assigned as H atoms diffusing across a Cu surface.[33] The presence of H atoms on Cu(111) demonstrates that H atoms do indeed spill over onto the Cu surface (Figure 5.1C). This spillover process allows for an increase in weakly bound H on Cu (~20 kJ/mol)[34] which is a prerequisite for selective hydrogenation chemistry.

The low temperature desorption of H_2 from the Pt-Cu(111) SAA surface is a result of a decrease in the H_2 recombination barrier as compared to a Cu surface and a decrease in H atom binding energy compared to a pure Pt surface. These experimental results are consistent with theoretical studies that predict a minimal activation energy (< 0.05 eV) for H_2 dissociation at individual, isolated Pt sites in Cu and much weaker binding of H atoms to the Cu surface as opposed to pure Pt.[32,35] The weaker binding of H atoms at the single Pt atom dissociation sites compared to Pt(111) results from the preferential adsorption of H at 3-fold hollow sites, which in the SAAs are composed of 1 Pt atom and 2 Cu atoms. By combining complementary energetic landscapes for H_2 dissociation and spillover, we later show that Pt-Cu bimetallic catalysts exhibit enhanced reactivity since Pt readily activates H_2 and Cu exhibits weak binding of reaction intermediates. Thus, the Pt-Cu bimetallic combination

addresses both the reduced selectivity of Pt catalysts and the barrier for H_2 activation on Cu.[30,36]

Additionally, our experiments reveal that Pt-Cu(111) SAAs bind CO significantly weaker than Pt as evidenced by the lower desorption temperature of CO from single Pt atoms (350 K) compared to Pt(111)[32] (450 K) (Figure S1 and Note S1[37]). This result holds great promise for the utility of Pt-Cu SAAs given problems like CO poisoning of the Pt anodes of PEM fuel cells.[4]

Butadiene Hydrogenation on Pt-Cu(111) Alloys

In order to probe the chemical reactivity of Pt-Cu SAAs, we performed temperature programmed desorption/reaction (TPD/R) studies on the model catalyst systems. Figure 5.2A shows TPD/R traces resulting from adsorption of 50 L H_2 (which results in 0.2 ML of adsorbed H atoms (H_a)) and 0.1 L butadiene (0.2 ML) on a 0.02 ML Pt-Cu(111) SAA. The sole product of co-adsorption of H_a and butadiene is butenes at 25 % conversion with no detectable yield of butane. The hydrogenation reaction is facile on the SAA as evidenced by reactively formed butenes desorbing from the surface below room temperature (240 K). Unreacted butadiene desorbs from Cu terraces (220 K), Pt sites (290 K), and Cu steps (330 K) and unreacted H_2 desorbs from Pt sites (230 K) (Figure 2S and 3S and Note 2S[37]). The desorption temperature of these unreacted species is consistent with desorption from a clean Pt-Cu(111) surface demonstrating that the co-adsorption of butadiene and H_a does not alter the desorption behavior. In the absence of H_a, butadiene reversibly adsorbs and desorbs from the surface without decomposing or inducing self-hydrogenation to unwanted butane (Figure S3[37]). Reactively formed butenes desorb at the same temperature as adsorbed 1-butene

(Figure S4) [37], indicating that the reaction is desorption rate limited and the selective hydrogenation must occur at a temperature below 240 K.[38–40] Desorption of butane is never observed and co-adsorption of H_a and 1-butene did not yield the fully hydrogenated product butane (Figure S5[37]) indicating that weak binding to Cu enables selective hydrogenation to the desired product.

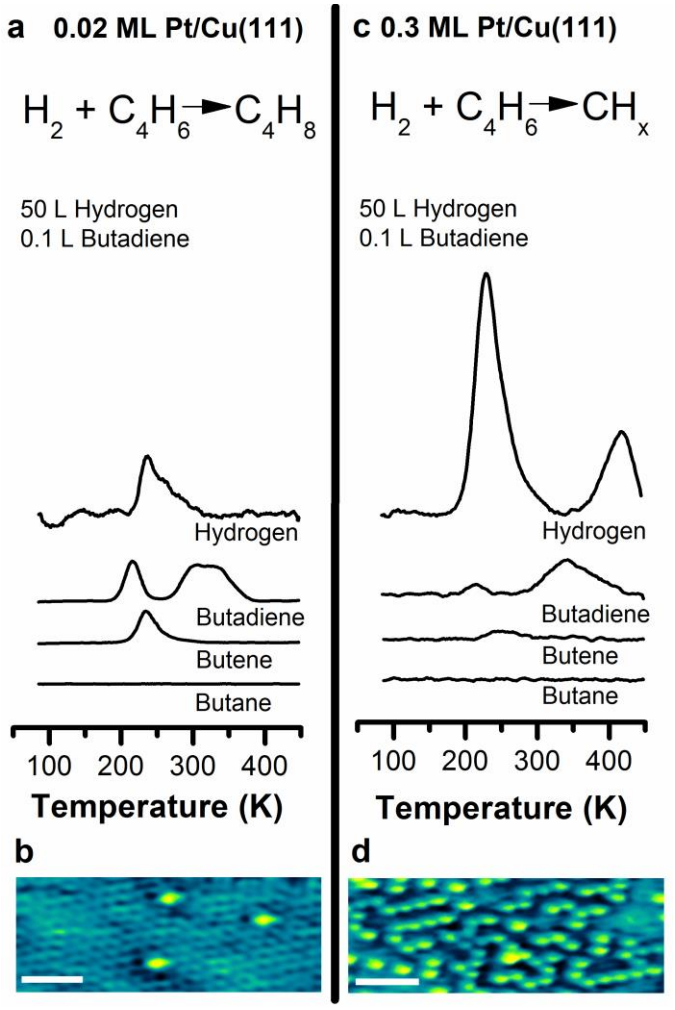

Figure 5.2. Selective hydrogenation of butadiene on Pt-Cu(111) SAAs vs. larger Pt ensembles TPD/R traces from the adsorption of H_2, and butadiene on (A) 0.02 ML Pt-Cu(111) SAA and (C) 0.3 ML Pt-Cu(111). STM image of (B) 0.02 ML and (D) 0.3 ML Pt-Cu(111). Scale bars are 1 nm.

Increasing the concentration of Pt to 0.3 ML decreased the selectivity of the surface to butenes. With increased Pt content, we predominantly observe decomposition of

hydrocarbons resulting in surface bound hydrocarbon fragments as evidenced by desorption of H_2 at higher temperatures (Figure 5.2C).[41] High temperature desorption of H_2 (420 K) is indicative of the decomposition of butadiene and butenes into surface CH_x fragments that further decompose to C and release additional H_2 at higher temperatures as previously observed for decomposed butenes on Pd catalysts.[41] STM images of 0.3 ML Pt-Cu(111) reveal the cause of this effect; in addition to single Pt atoms the 0.3 ML Pt surface is composed of extended linear chains (2-10 atoms) of Pt atoms (Figure 5.2D). Unlike individual Pt atoms, these larger Pt ensembles within the Cu matrix are capable of breaking C-C and C-H bonds that leads to decomposition and active site poisoning. These Pt sites exhibit reduced selectivity similar to Pt(111) on which the decomposition of butadiene is preferred over hydrogenation due to strong binding of butadiene to Pt(111) and facile decomposition.[42–45]

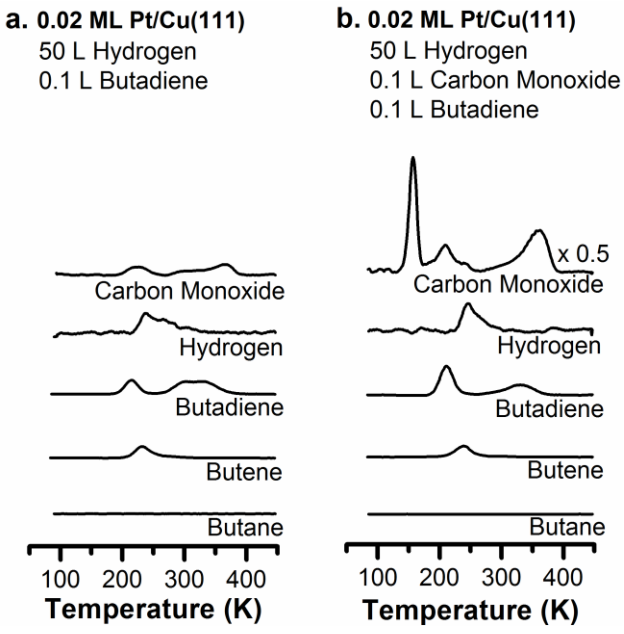

Figure 5.3. Butadiene hydrogenation in the presence of CO
TPD/R traces for the co-adsorption of H_2 and butadiene (A) without and (B) with CO on 0.02 ML Pt-Cu(111). H_2 was adsorbed on the surface prior to adsorption of CO.

In order to determine the active sites for hydrogenation, CO was used to selectively block Pt sites as the hydrogenation was performed. First, H was adsorbed onto a Pt-Cu(111) SAA and then small amounts of CO were adsorbed (Figure 5.3). Due to the stronger binding energy of CO to Pt than Cu, CO selectively adsorbs atop to the isolated Pt atoms.[46,47] H was adsorbed onto the surface prior to CO since CO blocks the adsorption of H. The surface was then exposed to butadiene and the temperature ramped to perform the hydrogenation reaction. Since CO desorbs from Pt sites at higher temperature (350 K) than butenes or H_2, CO inhibits any hydrogenation from occurring at the Pt sites. CO also blocks the adsorption of butadiene at Pt sites as seen by the disappearance of its desorption peak at 290 K. Our results indicate that the conversion of butadiene to butenes is unaffected by the CO adsorption at the Pt atom sites meaning that the selective hydrogenation of butadiene occurs predominately on the Cu sites.

Pt-Cu(111) SAAs exhibit excellent stability after multiple TPD/R cycles as shown by the steady and selective conversion of butadiene to butenes. Cycles of the co-adsorption of hydrogen and butadiene followed by CO titration and H_2 uptake showed no change in reactivity (Figure 5.4). After 6 cycles, the conversion of butadiene to butenes remained constant at 25 ± 1 % as determined by the amount of butenes desorbing at 240 K. The number of Pt atoms in the surface was also quantified via CO titration between each reaction. After each TPD/R cycle, the concentration of Pt atoms in the surface layer was 1.4 ± 0.2 %, consistent with the number of Pt atoms present prior to each hydrogenation reaction. Since the Pt atoms serve as the entrance routes of H_a onto the surface, the ability for the surface to uptake H_a remained constant at 15 ± 1 %. Loss of Pt sites or decrease in H_2 activation was not observed because Pt atoms are neither poisoned by decomposition of hydrocarbon

fragments nor lost by sub-surface migration. Since multiple hydrogenation runs result in no decrease in activity or selectivity, single isolated Pt atoms in Cu are capable of H_2 activation and spillover but not of breaking of C-C bonds, thus preventing the butadiene decomposition and surface poisoning that occur at higher Pt coverage. The robust nature of the Pt-Cu system further highlights the durability of SAAs.

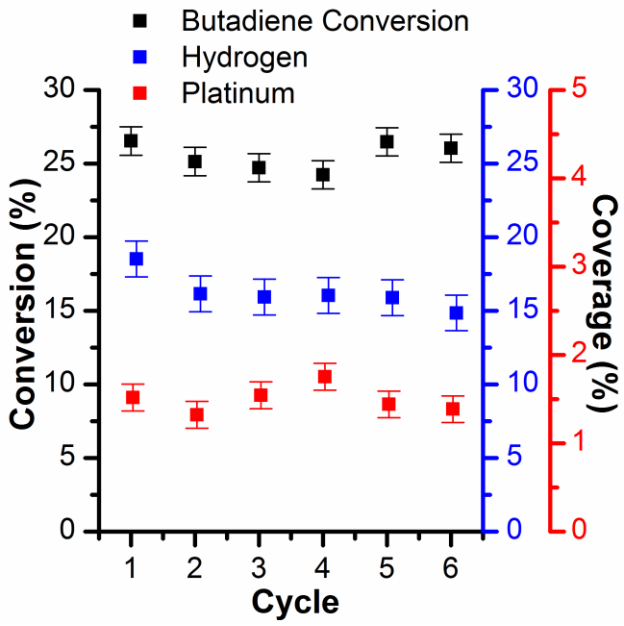

Figure 5.4. Repeated cycles of butadiene hydrogenation on a Pt-Cu(111) SAA
Repeated cycles of butadiene hydrogenation on a Pt-Cu(111) SAA reveals no loss in activity Multiple cycles of TPD/R after the co-adsorption 50 L H_2 + 0.1 L butadiene, followed by TPD of 50 L H_2 and then TPD of 1 L CO on 0.02 ML Pt-Cu(111) SAA. Multiple co-adsorptions of H_2 and butadiene lead to no decrease in the amount of butenes produced. The Pt atom concentration in the surface after each reaction cycle was quantified by CO titration. In each reaction cycle the temperature was ramped from 85 K to 450 K. Error bars are 1 s.d. of the data.

Pt-Cu Single Atom Alloy Nanoparticles

Inspired by the performance and stability of highly dispersed Pt atoms in the model catalyst system, we applied our SAA strategy to prepare Pt-Cu bimetallic nanoparticles (NPs) and examined them at atmospheric pressure under several realistic reaction conditions. Three

different Pt-Cu NP compositions were prepared by the galvanic replacement (GR) method,[48] in which a controlled amount of Pt was exchanged with Cu on pre-formed Cu NPs supported on γ-Al_2O_3. Low concentrations of Pt in solution form SAA $Pt_{0.1}Cu_{14}/Al_2O_3$ and $Pt_{0.2}Cu_{12}/Al_2O_3$ NPs, while higher concentrations of Pt form Pt_2Cu_6/Al_2O_3. A detailed description of the synthesis and characterization of all Pt-Cu alloy NPs is given in the Supplementary Information[37] (Figure S6 -14, Table S1-2, and Note S3).

Elemental mapping by energy dispersive X-ray spectroscopy (EDS) reveals that the Pt-Cu NPs are all bimetallic. Pt, Cu, Al, and O elemental mapping by EDS shows that Pt is distributed over the Cu NPs and is not deposited on the γ-Al_2O_3 support (Figure S10[37]). *In situ* EXAFS performed at room temperature at the Pt-L_{III} edge reveals the coordination of Pt in Pt-Cu alloys (Figure 5.5E and Table S2[37]). No Pt-Pt bonds are detected in $Pt_{0.1}Cu_{14}/Al_2O_3$ and $Pt_{0.2}Cu_{12}/Al_2O_3$, which provides direct evidence for individual, isolated Pt atoms in the Pt-Cu bimetallic NPs. The Pt-Cu first shell interaction distance is 2.63 Å which is between Pt-Pt (2.77 Å) and Cu-Cu bond lengths (2.56 Å),[49] further supporting SAA formation. The existence of Pt-Pt bonds in Pt_2Cu_6/Al_2O_3 suggests that Pt islands and/or clusters are formed in the NPs with this higher Pt loading.

Figure 5.5 shows aberration- corrected high-angle annular dark-field scanning transmission electron microscope (HAADF-STEM) images of $Pt_{0.1}Cu_{14}/Al_2O_3$. Aberration-corrected HAADF imaging can distinguish isolated Pt atoms due to differences in Z-contrast.[50,51] In this work, we observed a number of bright, atom-sized features within the Cu lattice (Figure 5.5). Our EXAFS results indicate that these features are isolated Pt atoms in Cu. Additionally, the lattice spacing of Pt-Cu is comparable to the pure Cu lattice spacing which also supports dilute dispersion of Pt atoms (Figure 5.5D). Variations in the

background structure of the Cu NPs make imaging of isolated atoms difficult, but in Figure 5.5D the single Pt atoms are more apparent due to the uniform background.[51] STEM and EXAFS analysis demonstrate the formation Pt-Cu SAA NPs, which provides a new catalytic system to study selective hydrogenation reactions.

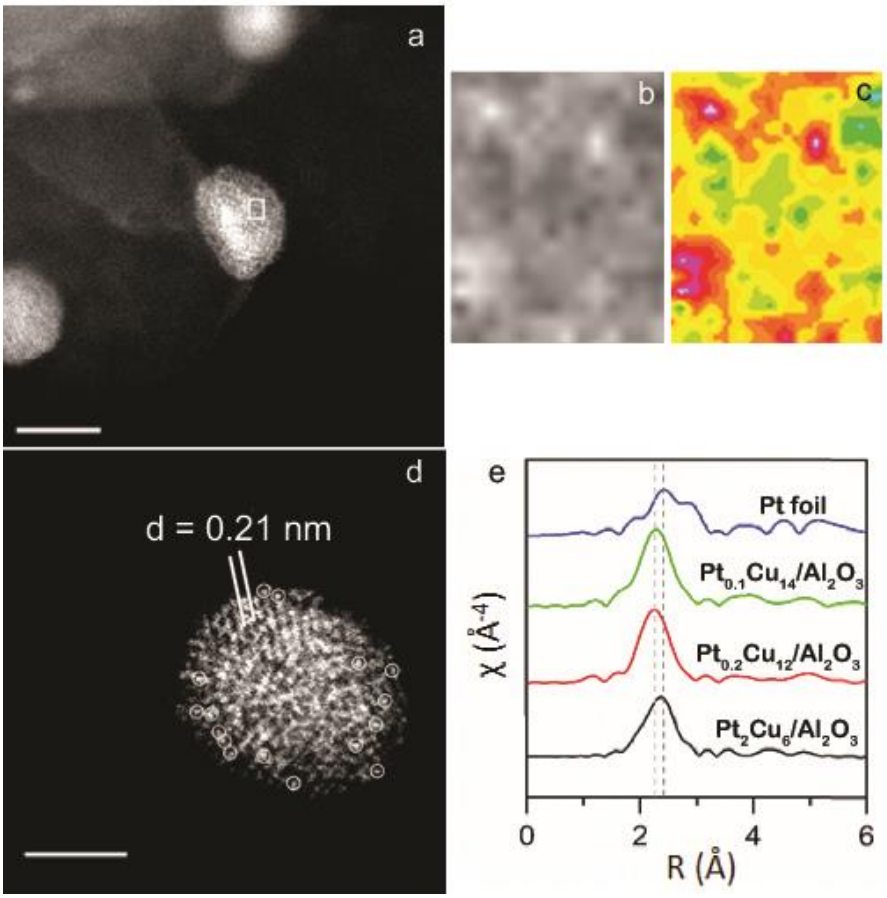

Figure 5.5. Characterization of Pt-Cu SAA NPs
(A-D) HAADF-STEM images with (C) colored intensity map from selected region, and (E) EXAFS k^3 – weighted Fourier transforms. (A, D) typical regions of the sample $Pt_{0.1}Cu_{14}/Al_2O_3$, showing Cu metal particles with isolated Pt atoms. Isolated Pt atoms are highlighted with circles. The lattice spacing of Cu(111) is 0.21 nm. Scale bars are (A) 5 nm and (D) 2 nm. (B) Enlarged image and (C) colorized intensity map of highlighted region showing isolated Pt atoms. (E) EXAFS data was collected at Pt-L_{III} edge at room temperature from Pt foil and in H_2 atmosphere at Pt-L_{III} edge at room temperature from pre-reduced $Pt_{0.1}Cu_{14}/Al_2O_3$, $Pt_{0.2}Cu_{12}/Al_2O_3$ and Pt_2Cu_6/Al_2O_3.

Our catalytic data reveals that adding trace amounts of Pt to Cu NPs significantly enhances hydrogenation. The butadiene hydrogenation activity and selectivity as a function of temperature on $Pt_{0.1}Cu_{14}/Al_2O_3$, $Pt_{0.2}Cu_{12}/Al_2O_3$, and Cu_{15}/Al_2O_3 NPs are shown in Figure 5.6 and Figure S15.[37] Under the conditions employed, $Pt_{0.1}Cu_{14}/Al_2O_3$ has a hydrogenation reaction onset at 40 °C, which is 35 °C lower than that of the monometallic Cu catalyst. The reaction rate over the $Pt_{0.1}Cu_{14}/Al_2O_3$ at 60 °C is an order of magnitude higher than the monometallic Cu catalyst. $Pt_{0.2}Cu_{12}/Al_2O_3$ exhibits greater hydrogenation activity than $Pt_{0.1}Cu_{14}/Al_2O_3$ due to a higher Pt atom surface amount at the increased Pt loading. However, the selectivity remains unaffected because the Pt atoms continue to be isolated in $Pt_{0.2}Cu_{12}/Al_2O_3$, as found by EXAFS model fitting (Table S2[37]).

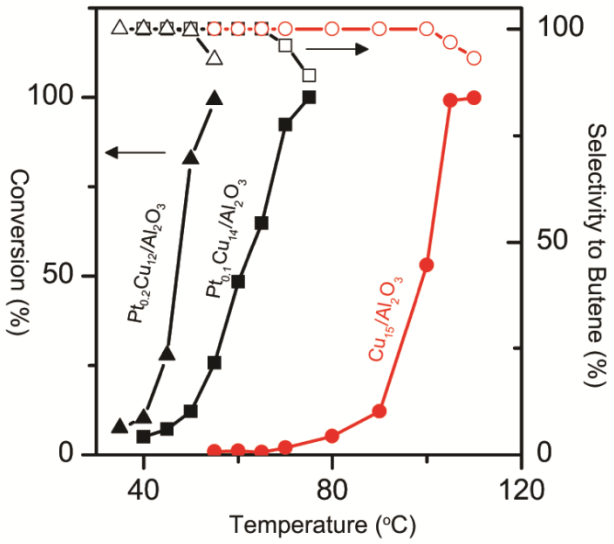

Figure 5.6. Selective hydrogenation of butadiene
Hydrogenation shown as a function of temperature over Cu_{15}/Al_2O_3, $Pt_{0.1}Cu_{14}/Al_2O_3$, and $Pt_{0.2}Cu_{12}/Al_2O_3$ NPs (1,3-butadiene (1.25 %), H_2 (20 %) and He (balance), GHSV=1,200 h^{-1}).

Notably, the SAA catalysts maintain the high selectivity to butenes exhibited by Cu. At full conversion, there is over 90% selectivity towards butenes isomers. The selectivity of SAA NPs ($Pt_{0.1}Cu_{14}/Al_2O_3$ and $Pt_{0.2}Cu_{12}/Al_2O_3$) was comparable to Cu_{15}/Al_2O_3 whereas Pt monometallic catalysts fully converted butadiene to butane under these conditions. Monometallic Pt is known for over-hydrogenating dienes and alkynes.[52,53] Therefore, by combining the hydrogen activation ability of Pt with the weak binding of butadiene on Cu and the latter's selectivity to butenes, Pt-Cu SAA catalysts exhibit superior performance for this important industrial reaction (Figure S15 – 20 and Note S4[37]). Various other alloy surfaces, including Pd-Au and Sn-Pt, have been shown to improve selective hydrogenation reactions.[54,55] However, this is the first report that single Pt atoms can enhance selective hydrogenation reactions on a less active metal, such as Cu.

To demonstrate the ability of Pt-Cu SAAs to selectively hydrogenate alkadiene impurities in alkene feedstocks,[25] we tested the selective hydrogenation activity of $Pt_{0.1}Cu_{14}/Al_2O_3$ catalysts in the presence of excess propylene and found that butadiene is preferentially hydrogenated on the Pt-Cu SAA NPs (Figure S19[37]). Below 120 °C, conversion of propylene was not observed. At 100 % conversion of butadiene, less than 1 % of propylene was converted to propane. Comparing these results to the hydrogenation activity of $Pt_{0.1}Cu_{14}/Al_2O_3$ in propylene-free condition, we found the propylene has no effect on the activity and selectivity of Pt-Cu SAAs for the hydrogenation of butadiene. At 160 °C and 145 °C, butadiene is fully converted and > 95 % converted, respectively, over $Pt_{0.1}Cu_{14}/Al_2O_3$ without significant propylene hydrogenation (1.2 % at 160 °C and 0.5 % at 145 °C) for > 12 h on-stream at each temperature (Figure 5.7) demonstrating high stability of the catalysts at full conversion of butadiene.

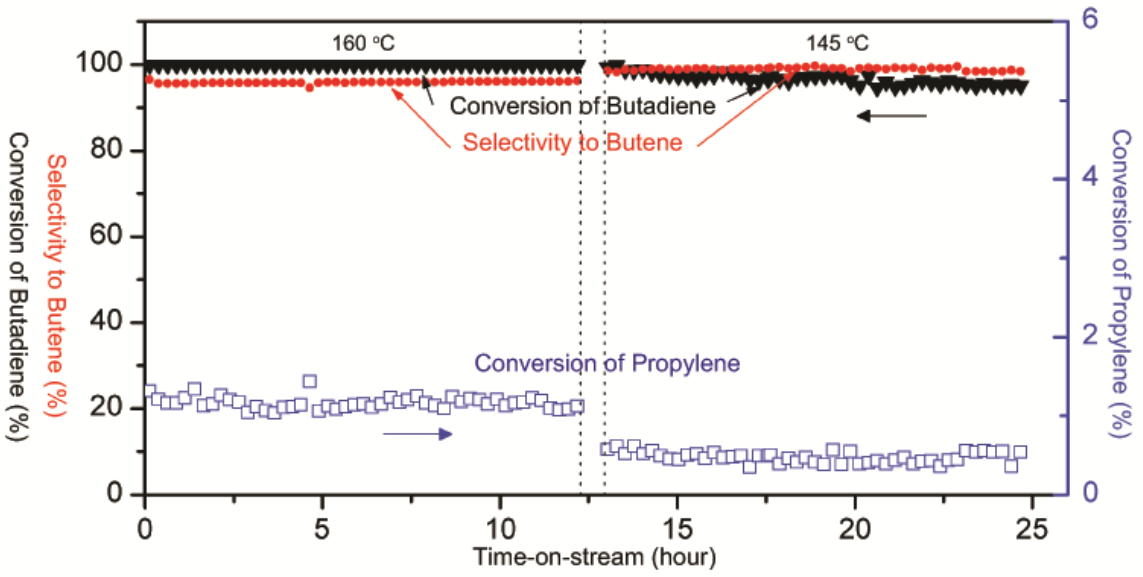

Figure 5.7. Butadiene conversion in the presence of excess propylene
Conversion and selectivity in long-time steady state selective hydrogenation of butadiene at 160 and 145 °C (~ 0.1 g catalyst $Pt_{0.1}Cu_{14}/Al_2O_3$, flow rate = 50 ml min^{-1}, 2 % 1, 3-butadiene, 20 % propylene, 16 % H_2 and balance He. GHSV=12,000 h^{-1}).

Pt-Cu SAAs exhibit high stability and selectivity under realistic hydrogenation conditions (Figure S16 – S20[37]). The Pt-Cu SAAs maintain stable butadiene conversion for more than 46 h at 160 °C (Figure S16[37]). Temperature-programmed oxidation (TPO) studies of the catalysts after hydrogenation show negligible CO_2 formation (Figure S20[37]) demonstrating the robustness of SAA catalysts to butadiene decomposition, oligomerization, and coke formation. Based on our model catalyst studies, the increase in the selectivity of SAAs is due to the inhibition of hydrocarbon decomposition commonly observed with Pt catalysts because SAAs do not offer extended Pt ensembles where these unfavorable reactions occur. Additionally, it is known that Cu or Pd catalysts for diene and alkyne hydrogenation are affected by oligomer formation at mild temperatures, which leads to instability in their hydrogenation activity.[56] By running the reaction at higher temperatures, we do not observe any instability in the catalysts due to oligomerization (Figure S16[37]). We found that after performing the reaction at near ambient temperatures, the hydrogenation

activity declines due to adsorption of hydrocarbon species. However, the activity can be fully recovered by heating in H_2 at 350 °C, which effectively desorbs the hydrocarbons (Figure S17[37]). Running at the higher temperatures shown in Figure 5.7 preserved the catalyst activity without affecting its selectivity.

5.3. Summary

In this work, surface science and atomic resolution microscopy studies of the selective hydrogenation of butadiene to butenes on model Pt-Cu(111) alloy surfaces have shown that individual, isolated Pt atoms in the Cu(111) surface are all that is required to ensure stable activity and 100 % selectivity. We have extended these findings to realistic pressures (1 bar) by synthesizing and testing Pt-Cu SAA nanoparticle catalysts. At low loadings, Pt exists as individual, isolated atoms substituted into the Cu(111) surface. These single Pt atoms activate the dissociation and spillover of H to Cu. The weak binding of butadiene to Cu allows for the highly selective hydrogenation to butenes. No decomposition or poisoning of these alloys was observed which can be attributed to the lack of extended Pt surface sites. At higher Pt content in Pt-Cu alloy surfaces, we directly visualized extended Pt ensembles responsible for the reduced selectivity. Isolated Pt atoms also bind CO significantly more weakly than metallic Pt which is an important consideration in many Pt catalyzed reactions. This combined model system/NP catalyst strategy is a powerful approach to the design of new alloy catalysts. This approach is especially useful for highly diluted single-site systems in which identification of the active sites and elucidation of the surface chemistry is very challenging. Furthermore, this work reveals that, in addition to their promising selective hydrogenation properties, SAAs provide the ultimate limit for the most efficient use of costly catalytic elements like Pt.

5.4. Additional Experimental Methods

Ultra-high vacuum studies

Pt-Cu(111) surfaces were cooled to 85 K with liquid nitrogen and exposed to H_2 (99.9 % Airgas), CO (99.99 % Airgas), 1-butene (≥99 % Aldrich), and/or 1,3-butadiene (≥99.5 % Aldrich). H_2 coverages were determined by the saturation coverage of (1x1) H adsorbed on 5 ML of Pt, assuming the surface terminates as Pt(111).

Synthesis and characterization

Pt-Cu nanoparticles (NPs) with different Pt-loadings were synthesized using the galvanic replacement (GR) method on the pre-reduced Cu NPs as described by Boucher et al.13 The Cu NPs were pre-formed and supported on γ-Al2O3 (ultra-pure grade 99.9 %, surface area 70-100 m^2/g, Inframat Advanced Materials; heat treated in air at 400 °C), followed by calcination in air at 350 °C. GR took place in aqueous solution under nitrogen protection with constant stirring and refluxing at 100 °C. Desired amounts of Pt precursor (H2PtCl6 · x H_2O, Sigma - Aldrich) were added to a suspension of Cu NPs in an aqueous solution containing HCl (2 mM). After 20 min, the resulting material was filtered, washed and dried in vacuum.

Aberration-corrected high-angle annular dark-field (HAADF) STEM images of Pt-Cu NPs were obtained at a nominal resolution of 0.07 nm using a JEOL 2200FS-AC STEM/TEM equipped with a hexapole corrector (CEOS GmbH, Heidelberg, Germany) at Oak Ridge National Laboratory. EDS imaging was conducted with a Bruker-AXS 30 mm2 silicon-drift detector system and Pt, Cu, Al and O elemental maps were collected. The instrument was operated at 200 kV for all imaging and EDS work.

X-ray absorption spectroscopy (XAS) measurements at the Pt LIII-edge were made at Argonne National Laboratory and Brookhaven National Laboratory in fluorescence mode at room temperature. All samples were reduced in H_2 in situ prior to the measurements. Experimental and analysis details on the XAS are described in the Supplementary Methods37.

Catalytic activity measurements

The selective hydrogenation activity of the catalysts was tested in a quartz-bed flow reactor for 1,3-butadiene hydrogenation with 400 mg of catalyst diluted by 1.5 g of quartz particles. The as synthesized Pt-Cu catalysts were reduced in H_2 at 350 °C for 4 h prior to the reaction, the Cl-residues were removed in H_2 as well. A gas mixture of 1.25 % 1,3-butadiene, 20 % H_2 and balance He (flow rate=20 ml min^1, GHSV=1,200 h^{-1}) was introduced at 120 °C, followed by descending temperature testing. Gas chromatograph (GC) injections were done at each temperature after the temperature was stabilized for at least 10 min. The exit gas stream was analyzed by a HP6890 GC equipped with a 30 ft. column (1/8 in, filled with Sebaconitrile 20 % Chromosorb Paw 80/100).

The activity tests with added propylene were conducted with a gas mixture of 2 % 1,3-butadiene, 20 % propylene, 16 % H_2 and balance He at a flow rate of 50 ml/min (100 mg catalyst, GHSV=12,000 h^{-1}). After the activity tests with ascending temperature up to 170 °C (Figure S12[37]), the long-time stability tests were performed isothermally at 160 °C and 145 °C for 12 h at each temperature.

5.5. References

(1) Stamenkovic, V. R.; Mun, B. S.; Arenz, M.; Mayrhofer, K. J. J.; Lucas, C. A.; Wang, G.; Ross, P. N.; Markovic, N. M. Trends in Electrocatalysis on Extended and Nanoscale Pt-Bimetallic Alloy Surfaces. *Nat. Mater.* **2007**, *6*, 241–247.

(2) Weitkamp, J.; Jacobs, P. A.; Martens, J. A. Isomerization and Hydrocracking of C_9 through C_{16} N-Alkanes on Pt/HZSM-5 Zeolite. *Appl. Catal. B* **1983**, *8*, 123–141.

(3) Cheng, X.; Shi, Z.; Glass, N.; Zhang, L.; Zhang, J.; Song, D.; Liu, Z.; Wang, H.; Shen, J. A Review of PEM Hydrogen Fuel Cell Contamination: Impacts, Mechanisms, and Mitigation. *J. Power Sources* **2007**, *165*, 739–756.

(4) Pettersson, L.; Westerholm, R. State of the Art of Multi-Fuel Reformers for Fuel Cell Vehicles: Problem Identification and Research Needs. *Int. J. Hydrog. Energy* **2001**, *26*, 243–264.

(5) Thomas, J. M. The Concept, Reality and Utility of Single-Site Heterogeneous Catalysts (SSHCs). *Phys. Chem. Chem. Phys.* **2014**, *16*, 7647–7661.

(6) Zhai, Y.; Pierre, D.; Si, R.; Deng, W.; Ferrin, P.; Nilekar, A. U.; Peng, G.; Herron, J. A.; Bell, D. C.; Saltsburg, H.; et al. Alkali-Stabilized Pt-OHx Species Catalyze Low-Temperature Water-Gas Shift Reactions. *Science* **2010**, *329*, 1633–1636.

(7) Yang, M.; Li, S.; Wang, Y.; Herron, J. A.; Xu, Y.; Allard, L. F.; Lee, S.; Huang, J.; Mavrikakis, M.; Flytzani-Stephanopoulos, M. Catalytically Active Au-$O(OH)_x$-Species Stabilized by Alkali Ions on Zeolites and Mesoporous Oxides. *Science* **2014**, *346*, 1498–1501.

(8) Qiao, B.; Wang, A.; Yang, X.; Allard, L. F.; Jiang, Z.; Cui, Y.; Liu, J.; Li, J.; Zhang, T. Single-Atom Catalysis of CO Oxidation Using Pt_1/FeO_x. *Nat. Chem* **2011**, *3*, 634–641.

(9) Yi, N.; Si, R.; Saltsburg, H.; Flytzani-Stephanopoulos, M. Steam Reforming of Methanol over Ceria and Gold-Ceria Nanoshapes. *Appl. Catal. B* **2010**, *95*, 87–92.

(10) Boucher, M. B.; Goergen, S.; Yi, N.; Flytzani-Stephanopoulos, M. Shape Effects in Metal Oxide Supported Nanoscale Gold Catalysts. *Phys. Chem. Chem. Phys.* **2011**, *13*, 2517–2527.

(11) Besenbacher, F.; Chorkendorff, I.; Clausen, B. S.; Hammer, B.; Molenbroek, A. M.; Nørskov, J. K.; Stensgaard, I. Design of a Surface Alloy Catalyst for Steam Reforming. *Science* **1998**, *279*, 1913–1915.

(12) Kyriakou, G.; Boucher, M. B.; Jewell, A. D.; Lewis, E. A.; Lawton, T. J.; Baber, A. E.; Tierney, H. L.; Flytzani-Stephanopoulos, M.; Sykes, E. C. H. Isolated Metal Atom Geometries as a Strategy for Selective Heterogeneous Hydrogenations. *Science* **2012**, *335*, 1209–1212.

(13) Boucher, M. B.; Zugic, B.; Cladaras, G.; Kammert, J.; Marcinkowski, M. D.; Lawton, T. J.; Sykes, E. C. H.; Flytzani-Stephanopoulos, M. Single Atom Alloy Surface Analogs in $Pd_{0.18}Cu_{15}$ Nanoparticles for Selective

Hydrogenation Reactions. *Phys. Chem. Chem. Phys.* **2013**, *15*, 12187–12196.

(14) McCue, A. J.; McRitchie, C. J.; Shepherd, A. M.; Anderson, J. a. $Cu/A_{l2}O_3$ Catalysts Modified with Pd for Selective Acetylene Hydrogenation. *J. Catal.* **2014**, *319*, 127–135.

(15) Christensen, A.; Ruban, A. V.; Stoltze, P.; Jacobsen, K. W.; Skriver, H. L.; Nørskov, J. K.; Besenbacher, F. Phase Diagrams for Surface Alloys. *Phys. Rev. B* **1997**, *56*, 5822–5834.

(16) Tyson, W. R.; Miller, W. A. Surface Free Energies of Solid Metals Estimation from Liquid Surface Tension Measurments. *Surf. Sci.* **1977**, *62*, 267–276.

(17) Santana, J. A.; Rösch, N. Hydrogen Adsorption on and Spillover from Au- and Cu-Supported Pt_3 and Pd_3 Clusters: A Density Functional Study. *Phys. Chem. Chem. Phys.* **2012**, *14*, 16062–16069.

(18) Tierney, H. L.; Baber, A. E.; Sykes, E. C. H. Atomic-Scale Imaging and Electronic Structure Determination of Catalytic Sites on Pd/Cu near Surface Alloys. *J. Phys. Chem. C* **2009**, *113*, 7246–7250.

(19) Lucci, F. R.; Lawton, T. J.; Pronschinske, A.; Sykes, E. C. H. Atomic Scale Surface Structure of Pt/Cu(111) Surface Alloys. *J. Phys. Chem. C* **2014**, *118*, 3015–3022.

(20) Yu, W.; Porosoff, M. D.; Chen, J. G. Review of Pt-Based Bimetallic Catalysis: From Model Surfaces to Supported Catalysts. *Chem. Rev.* **2012**, *112*, 5780–5817.

(21) Prinz, J.; Gaspari, R.; Pignedoli, C. A.; Vogt, J.; Gille, P.; Armbrüster, M.; Brune, H.; Gröning, O.; Passerone, D.; Widmer, R. Isolated Pd Sites on the Intermetallic PdGa(111) and PdGa(111) Model Catalyst Surfaces. *Angew. Chem.* **2012**, *124*, 9473–9477.

(22) Lonergan, W. W.; Xing, X.; Zheng, R.; Qi, S.; Huang, B.; Chen, J. G. Low-Temperature 1,3-Butadiene Hydrogenation over Supported Pt/3d/γ-Al_2O_3 Bimetallic Catalysts. *Catal. Today* **2011**, *160*, 61–69.

(23) Qi, S.; Yu, W.; Lonergan, W. W.; Yang, B.; Chen, J. G. General Trends in the Partial and Complete Hydrogenation of 1,4-Cyclohexadiene over Pt-Co, Pt-Ni and Pt-Cu Bimetallic Catalysts. *Chem. Cat. Chem* **2010**, *2*, 625–628.

(24) Greeley, J.; Mavrikakis, M. Alloy Catalysts Designed from First Principles. *Nat. Mater.* **2004**, *3*, 810–815.

(25) Derrien, M. L. Selective Hydrogenation Applied to the Refinging of Petrochemical Raw Materials Produced by Steam Cracking. *Stud. Surf. Sci. Catal.* **1986**, *27*, 613–666.

(26) GBI Research. *Polypropylene Global Market to 2020 - Developing Regions of Asia-Pacific and Middle East and Africa to Drive Polypropylene Market Growth*; 2013.

(27) Mittendorfer, F.; Thomazeau, C.; Raybaud, P.; Toulhoat, H. Adsorption of Unsaturated Hydrocarbons on Pd(111) and Pt(111): A DFT Study. *J. Phys. Chem. B* **2003**, *107*, 12287–12295.

(28) Valcárcel, A.; Clotet, A.; Ricart, J. M.; Delbecq, F.; Sautet, P. Selectivity

Control for the Catalytic 1,3-Butadiene Hydrogenation on Pt (111) and Pd (111) Surfaces: Radical versus Closed-Shell Intermediates. *J. Phys. Chem. B* **2005**, *109*, 14175–14182.

(29) Collins, D. M.; Spicer, W. E. The Adsorption of CO, O2 and H2 on Pt. *Surf. Sci.* **1977**, *69*, 85–113.

(30) Anger, G.; Winkler, A.; Rendulic, K. D. Adsorption and Desorption Kinetics in the Systems H_2/Cu(111), H_2/Cu(110) and H_2/Cu(100). *Surf. Sci.* **1989**, *220*, 1–17.

(31) Linke, R.; Schneider, U.; Busse, H.; Becker, C.; Schröder, U.; Castro, G. R.; K., W. Interaction of Hydrogen with Cu_3Pt(111): Dissociation via Isolated Platinum Atoms. *Surf. Sci.* **1994**, *307 - 309*, 407–411.

(32) Fu, Q.; Luo, Y. Catalytic Activity of Single Transition-Metal Atom Doped in Cu(111) Surface for Heterogeneous Hydrogenation. *J. Phys. Chem. C.* **2013**, *117*, 14618–14624.

(33) Jewell, A. D.; Peng, G.; Mattera, M. F. G.; Lewis, E. A.; Murphy, C. J.; Kyriakou, G.; Mavrikakis, M.; Sykes, E. C. H. Quantum Tunneling Enabled Self-Assembly of Hydrogen Atoms on Cu(111). *ACS Nano* **2012**, *6*, 10115–10121.

(34) Greeley, J.; Nørskov, J. K. Large-Scale, Density Functional Theory-Based Screening of Alloys for Hydrogen Evolution. *Surf. Sci.* **2007**, *601*, 1590–1598.

(35) Diño, W.; Kasai, H.; Okiji, A. Dissociative Adsorption Dynamics of H2 at the atop-Pt, atop-Cu, and Cu-Pt Bridge Sites of an Ordered Cu_3Pt(111) - Orientational Effects. *Appl. Surf. Sci.* **2001**, *169-170*, 36–41.

(36) Chen, B.; Dingerdissen, U.; Krauter, J. G. E.; Lansink Rotgerink, H. G. J.; Möbus, K.; Ostgard, D. J.; Panster, P.; Riermeier, T. H.; Seebald, S.; Tacke, T.; et al. New Developments in Hydrogenation Catalysis Particularly in Synthesis of Fine and Intermediate Chemicals. *Appl. Catal. A* **2005**, *280*, 17–46.

(37) Lucci, F. R.; Liu, J.; Marcinkowski, M. D.; Yang, M.; Allard, L. F.; Flytzani-Stephanopoulos, M.; Sykes, E. C. H.; Liu, J.; Marcinkowski, M. D.; Yang, M.; et al. Selective Hydrogenation of 1,3-Butadiene on Platinum–Copper Alloys at the Single-Atom Limit. *Nat. Commun.* **2015**, *6*, 8550.

(38) Zaera, F.; Somorjai, G. A. Hydrogenation of Ethylene over Platinum (111) Single-Crystal Surfaces. *J. Am. Chem. Soc.* **1984**, *106*, 2288–2293.

(39) Stacchiola, D.; Azad, S.; Burkholder, L.; Tysoe, W. T. An Investigation of the Reaction Pathway for Ethylene Hydrogenation on Pd(111). *J. Phys. Chem. B* **2001**, *105*, 11233–11239.

(40) Guo, X.; Madix, R. J. . Selective Hydrogenation and H-D Exchange of Unsaturated Hydrocarbons on Pd(100)-p(1x1)-H(D). *J. Catal.* **1995**, *155*, 336–344.

(41) Brandt, B.; Fischer, J.-H.; Ludwig, W.; Libuda, J.; Zaera, F.; Schauermann, S.; Freund, H.-J. Isomerization and Hydrogenation of Cis-2-Butene on Pd Model Catalyst. *J. Phys. Chem. C.* **2008**, *112*, 11408–11420.

(42) Zhao, H.; Welch, L. A.; Koel, B. E. Site-Blocking Effects of Preadsorbed H on Pt(111) Probed by 1,3-Butadiene Adsorption and Reaction. *Surf. Sci.* **2009**, *603*, 3355–3360.
(43) Yoon, C.; Yang, M. X.; Somorjai, G. A. Hydrogenation of 1,3-Butadiene on Platinum Surfaces of Different Structures. *Catal. Lett.* **1997**, *46*, 37–41.
(44) Michalak, W. D.; Krier, J. M.; Komvopoulos, K.; Somorjai, G. A. Structure Sensitivity in Pt Nanoparticle Catalysts for Hydrogenation of 1,3-Butadiene: In Situ Study of Reaction Intermediates Using SFG Vibrational Spectroscopy. *J. Phys. Chem. C* **2013**, *117*, 1809–1817.
(45) Zhao, H.; Koel, B. Hydrogenation of 1,3-Butadiene on Two Ordered Sn/Pt(111) Surface Alloys. *J. Catal.* **2005**, *234* (1), 24–32.
(46) Marcinkowski, M. D.; Jewell, A. D.; Stamatakis, M.; Boucher, M. B.; Lewis, E. A.; Murphy, C. J.; Kyriakou, G.; Sykes, E. C. H. Controlling a Spillover Pathway with the Molecular Cork Effect. *Nat. Mater.* **2013**, *12*, 523–528.
(47) Schröder, U.; Linke, R.; Boo, J.; Wander, K. Adsorption Properties and Formation of Pt/Cu Surface Alloys. *Surf. Sci.* **1996**, *354*, 211–217.
(48) Lu, X.; Chen, J.; Skrabalak, S. E.; Xia, Y. Galvanic Replacement Reaction: A Simple and Powerful Route to Hollow and Porous Metal Nanostructures. *J. Nanoeng. Nanosci.* **2007**, *221*, 1–16.
(49) Yamamoto, T. A.; Nakagawa, T.; Seino, S.; Nitani, H. Bimetallic Nanoparticles of PtM (M=Au, Cu, Ni) Supported on Iron Oxide: Radiolytic Synthesis and CO Oxidation Catalysis. *Appl. Catal. A* **2010**, *387*, 195–202.
(50) Yang, M.; Allard, L. F.; Flytzani-Stephanopoulos, M. Atomically Dispersed Au-$(OH)_x$ Species Bound on Titania Catalyze the Low-Temperature Water-Gas Shift Reaction. *J. Am. Chem. Soc.* **2013**, *135*, 3768–3771.
(51) Peterson, E. J.; DeLaRiva, A. T.; Lin, S.; Johnson, R. S.; Guo, H.; Miller, J. T.; Kwak, J.; Peden, C. H. F.; Kiefer, B.; Allard, L. F.; et al. Low-Temperature Carbon Monoxide Oxidation Catalysed by Regenerable Atomically Dispersed Palladium on Alumina. *Nat. Commun.* **2014**, *5*, 1–11.
(52) Dobrovolná, Z.; Kačer, P.; Červený, L. Competitive Hydrogenation in Alkene – Alkyne – Diene Systems with Palladium and Platinum Catalysts. *J. Mol. Catal. A* **1998**, *130*, 279–284.
(53) Boitiaux, J. P.; Cosyns, J.; Robert, E. Liquid Phase Hydrogenation of Unsaturatued Hydrogcarbons on Palladium, Platinum and Rodium Catalysts. *Appl. Catal.* **1987**, *32*, 145–168.
(54) Kolli, N. El; Delannoy, L.; Louis, C. Bimetallic Au–Pd Catalysts for Selective Hydrogenation of Butadiene: Influence of the Preparation Method on Catalytic Properties. *J. Catal.* **2013**, *297*, 79–92.
(55) Zhao, H.; Koel, B. E. Adsorption and Reaction of 1,3-Butadiene on Pt(111) and Sn/Pt(111) Surface Alloys. *Surf. Sci.* **2004**, *572*, 261–268.
(56) Delannoy, L.; Thrimurthulu, G.; Reddy, P. S.; Méthivier, C.; Nelayah, J.; Reddy, B. M.; Ricolleau, C.; Louis, C. Selective Hydrogenation of

Butadiene over TiO_2 Supported Copper, Gold and Gold-Copper Catalysts Prepared by Deposition-Precipitation. *Phys. Chem. Chem. Phys.* **2014**, *16*, 26514–26527.

5.6. Collaborations

Nanoparticle catalysts experiments were performed by Jilei Liu and the Stephanopoulos Group from the Department of Chemical and Biological Engineering at Tufts University.

Chapter 6: Tackling CO Poisoning with *Single Atom Alloy* Catalysts

This chapter was modified from an original publication of the same title by J. Liu, F. R. Lucci* et al. from Journal of the American Chemical Society, volume138, pages 6396 – 6399.*

6.1. Introduction

Pt is widely used for fuel cell anodes and hydrocarbon processing due to its superior catalytic performance. Pt metals are highly active for H_2 dissociation, but are very susceptible to CO poisoning.[1] Due to its strong binding to Pt, even trace amounts of CO impurity, which is always present in H_2 gas produced from fuel reforming, can diminish H_2 activation and reactivity.[2] This strong CO adsorption also hinders the fast conversion of CO to CO_2 at low temperatures (< 200 ^oC), and becomes a technical challenge for efficient emission control and water-gas shift (WGS) for hydrogen upgrading. Recently, atomically dispersed Pt_1 (or Pd_1) -O_x- stabilized on a variety of supports, such as silica,[3] titania,[4] KLTL-Zeolite,[4,5] MCM-41,[4] alumina,[6] and iron oxide,[7] were found to be highly active in WGS and CO oxidation reactions and $Pd_1/g\text{-}C_3N_4$ was reported to be active and stable in the selective hydrogenation of 1-hexyne to 1-hexene.[8] The single platinum atom sites have a cationic nature that results in weak CO adsorption,[3] thus becoming the exclusive sites for the low temperature CO conversion. Although single-atom catalytic sites in Pt_1 (or Pd_1)-O_x-oxides possess the desired property of weaker CO adsorption, they may not be stable enough under hydrogenation conditions.

Alternatively, SAA catalysts were also shown to be active for a variety of selective hydrogenation[9–11] and dehydrogenation reactions,[12,13] including the Pd-Cu SAA for the selective hydrogenation of styrene,[9] acetylene,[9] and phenylacetylene.[10] Moreover, the Pt-Cu

SAA was shown by Lucci *et al*. to selectively hydrogenate 1,3-butadiene to butenes under realistic flow reactor conditions.[10] For Pt-Cu SAAs, H_2 dissociation occurs at the single atom Pt sites followed by spillover of atomic hydrogen to the Cu surface where selective hydrogenation takes place.[11,14] Both Pt-Cu(111) SAAs in ultra-high vacuum (UHV) and Pt-Cu SAA nanoparticle catalysts in flow conditions at 1 bar exhibit highly selective and stable butadiene hydrogenation reactivity.[11] As the natural expansion of the SAA concept, herein we tackle the CO poisoning issue of platinum catalysts with Pt-based SAAs in which the Pt atoms are embedded in a host metal surface, such as copper. The situation for isolated Pt atoms may be different than traditional bimetallic alloys, where ensemble effects have been shown to increase the CO binding strength at extended catalytic metal sites.[15–17] From a fundamental perspective, metal alloys that alter the adsorption geometry of CO can exhibit weaker CO binding and enhanced CO tolerance. Isolated Pt atoms enable exclusively atop adsorption configuration of CO, which we show is weaker than CO adsorption on extended Pt sites. Herein, we investigate the interaction between CO and Pt sites on a Pt-Cu SAA and demonstrate improved CO tolerance of Pt-Cu SAA catalysts under realistic working conditions for H_2 activation and acetylene hydrogenation reaction.

6.2. Results and Discussion

By using model Pt-Cu SAAs, we first determined the binding strength of CO to isolated Pt atoms in the surface of Cu(111) (Figure 6.1A). Weakly bound CO desorbs from Cu(111) below 200 K and after deposition of 0.01 ML Pt, a CO desorption peak was observed in TPD traces at 350 K. At an increased coverage of 0.3 ML Pt, CO desorbed at 360 K with a high temperature tail. The high temperature tail developed into an additional

peak at 480 K at a Pt coverage of 0.6 ML. At 5 ML, a desorption feature was observed at 410 K and the surface is assumed to be terminated as Pt(111).

In agreement with the Pt surface structure observed by scanning tunneling microscopy (STM),[14,18] the CO desorption traces reveal the development of 3 distinct Pt-Cu alloyed structures with increasing Pt coverage (Figure 6.1B-D). With atomic resolution, the Pt atoms image ~20 pm taller than the surrounding Cu lattice and appear as brighter protrusions. At low Pt coverages, CO desorbs from isolated Pt atoms (peak at 350 K) and at intermediate coverages, CO desorbs from extended ensembles of Pt atoms (peak at 480 K). At 5 ML Pt, the surface layer is composed primarily of continuous ordered Pt atoms and CO desorbs at 410 K. At low CO coverages, CO desorption from Pt(111) is reported at 450 K and with increasing CO coverage desorption is observed at 400 K due to the repulsion between co-adsorbed CO molecules.[19] In Pt-Cu alloys, CO adsorbs weakest on the Pt-Cu SAA and strongest on the extended Pt clusters.

To apply this surface science and microscopy knowledge to the design of heterogeneous catalysts, Pt-Cu alloy nanoparticles (NPs) were prepared by galvanic replacement (GR) of Pt for Cu on preformed Cu NPs (Table S1[20]).[10,11] $Pt_{0.008}Cu$ supported on γ-Al_2O_3 is a SAA as confirmed by aberration-corrected high angle annular dark field scanning transmission electron microscopy and extend X-ray absorption fine structure (EXAFS) studies.[11] Importantly, with CO in the gas phase, no Pt-Pt interactions were found by EXAFS in $Pt_{0.008}Cu$-SAA (Table S2, Figure S5[20]), which demonstrates the stability of the isolated Pt atoms in the presence of CO.

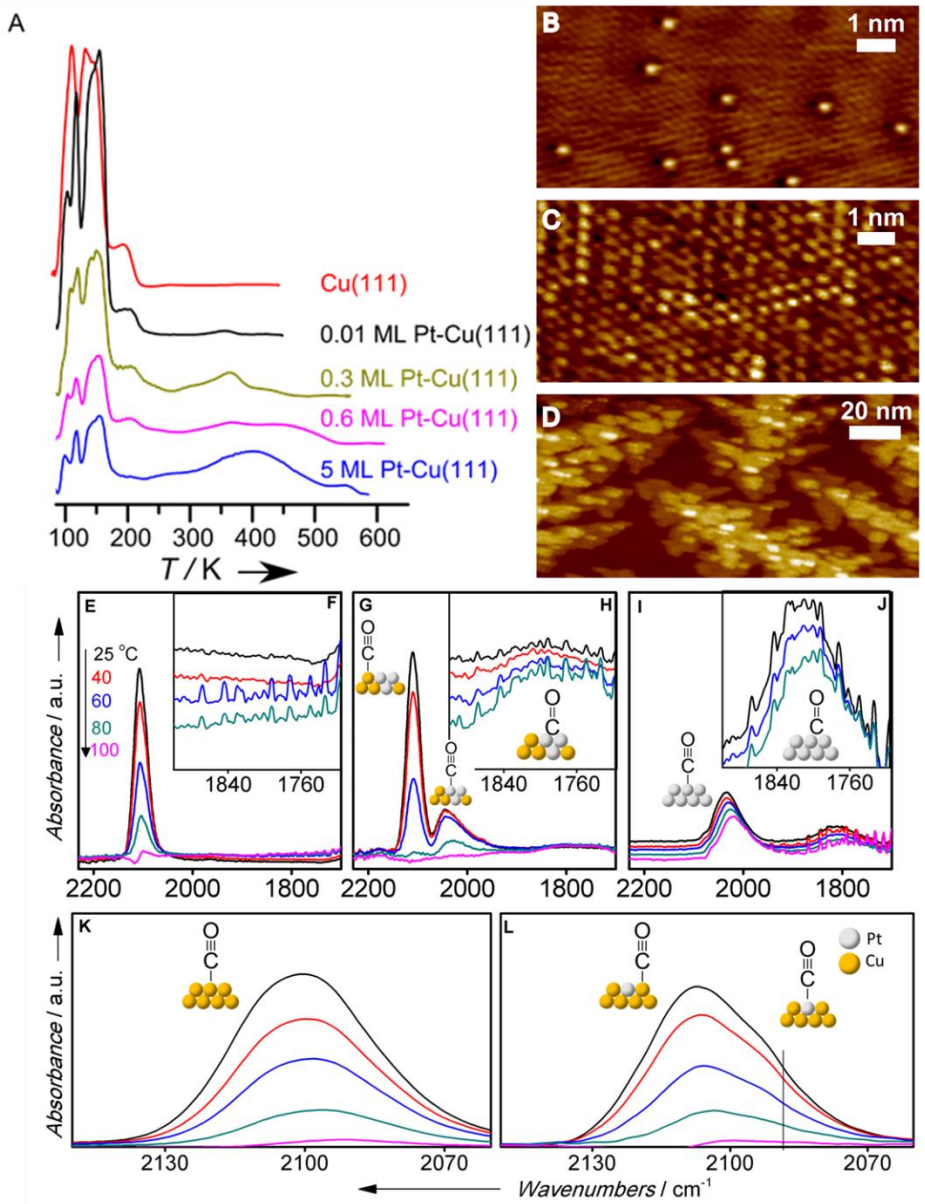

Figure 6.1. Binding strength of CO to Pt-Cu SAAs vs. pure Pt
(A) CO desorption and STM images of (B) 0.01 ML, (C) 0.3 ML and (D) 1 ML Pt-Cu(111) alloys prepared at 380 K. Scanning conditions (B) -10 mV and 150 nA (C) -10 mV and 250 nA (D) 500 mV and 10 nA. IR spectra in the carbonyl range of pre-reduced (E, F, L) Pt0.008Cu-SAA, (G, H) Pt0.39Cu-bimetallic, (I, J) Pt-NP, and (K) Cu-NP.

The binding strength of CO on Pt-Cu alloys and their monometallic counterparts in NP forms was investigated at ambient pressure by IR spectroscopy. The bridged-adsorbed CO to two adjacent Pt atoms between 1900 and 1700 cm^{-1} was observed on the Pt-NP and $Pt_{0.39}Cu$-bimetallic, but not seen on the $Pt_{0.008}Cu$-SAA (Figure 6.1F,H and J). This is consistent with the fact that exclusively isolated Pt atoms are in the surface of $Pt_{0.008}Cu$-SAA,

unlike the existence of a mixed phase of Pt atoms, clusters and particles on the Pt-NP and $Pt_{0.39}$Cu-bimetallic. Overlapping peaks between 2150 and 2060 cm^{-1} are seen for $Pt_{0.008}$Cu-SAA, as indicated by the asymmetric absorption band (Figure 6.1L). The unique absorption band centered at ca. 2088 cm^{-1} is distinct from atop CO on the Cu or Pt NPs, and is assigned to the linearly adsorbed CO on the isolated single Pt atoms. The absorption band of linearly adsorbed CO is at ca. 2020 cm^{-1} on Pt-NP, 2031 cm^{-1} on the Pt ensembles on $Pt_{0.39}$Cu-bimetallic and 2093 cm^{-1} on Cu-NP (Figure 6.1G,I and K). As for the different Pt species characterized by CO-IR, their formal charges and coordination numbers are essentially the same, and dipole-dipole coupling has little effect on $Pt_{0.008}$Cu-SAA due to the weak CO-metal bonds on isolated Pt atoms and Cu surfaces.[21] Hence, the strength of CO binding indicates the relative CO-metal π backbonding strength, that is the stronger the CO-metal bond, the lower the C-O vibrational frequency. We conclude that Pt-CO bond is weakest on $Pt_{0.008}$Cu-SAA and strongest on Pt-NP while the Pt cluster in $Pt_{0.39}$Cu-bimetallic has an intermediate binding strength for CO. Moreover, the adsorption strength of CO on the $Cu_3Pt(111)$ alloy, is lower than Pt(111) according to DFT calculations.[22]

To probe the interaction of CO and H with the Pt catalytic sites at the atomic-scale, H and CO were co-adsorbed onto 0.01 ML Pt-Cu(111) (Figure 6.2). We used the STM tip to interrogate the nature of the H and CO adsorption sites. Initially, we observed clusters of mobile depressions on the Cu terraces previously identified as H adatoms due to their characteristic diffusion rate at 5 K (Figure 6.2A).[23] Increasing the bias applied to the STM tip removed these H atoms (Figure 6.2B). Select immobile depressions remained on the surface that could only be removed by individual pulses locally delivered by the STM tip (5 V) (Figure 6.2C), hence, the dark immobile depressions are CO molecules as also previously

reported[24]. After removal of the CO molecules, stationary surface protrusions were observed where the CO molecules were previously located. We identify the ~20 pm high protrusions as Pt atoms substituted into the Cu lattice, thus, providing further evidence of the selective adsorption of CO on the Pt sites. These STM experiments also demonstrate that H adatoms are capable of diffusing onto Cu sites and away from the Pt dissociation sites yielding H atom coverage of 0.10 ML from 0.01 ML Pt.

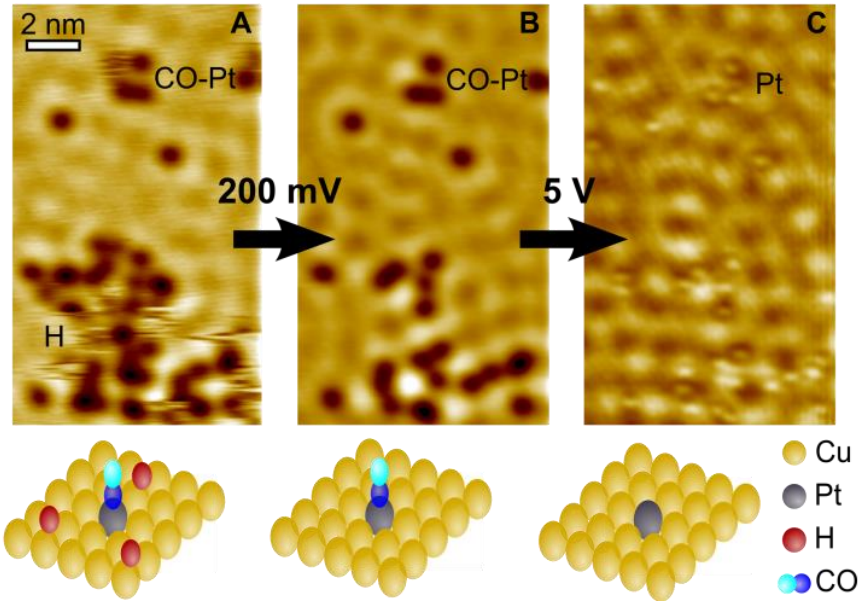

Figure 6.2. STM images showing the co-adsorption of H and CO on a Pt-Cu(111) SAA surface and STM tip-induced adsorbate removal to reveal the binding sites beneath
(A) H and CO adsorbed on Pt-Cu(111) SAA. (B) Image of same area following scanning at 200 mV to remove adsorbed H. (C) After 5 V pulses to remove adsorbed CO, individual Pt atoms are seen underneath each removed CO molecule. Scanning conditions (A, B) 30 mV, 30 pA and (D) 10 mV and 50 nA.

The next question is how does the weaker CO-Pt binding on Pt-Cu SAA contribute to its CO tolerance. We conducted H_2-D_2 exchange experiments to evaluate the effect of CO on H_2 activation on Pt-Cu SAAs and monometallic Pt catalysts. The mobility of H atoms on Pt-Cu SAAs was demonstrated in UHV by co-adsorption of H_2 and D_2 onto SAA Pt-Cu(111) (Figure 6.3A). We observed desorption of HD (*m/z* 3) which provides evidence of the

dissociation of H_2 and migration of H atoms away from the dissociation site. When equal amounts of H and D atoms are adsorbed on the surface, we observe complete scrambling of H and D with ratio of H_2:HD:D_2 of 1:2:1 due to H atom spillover and the facile diffusion on Cu.

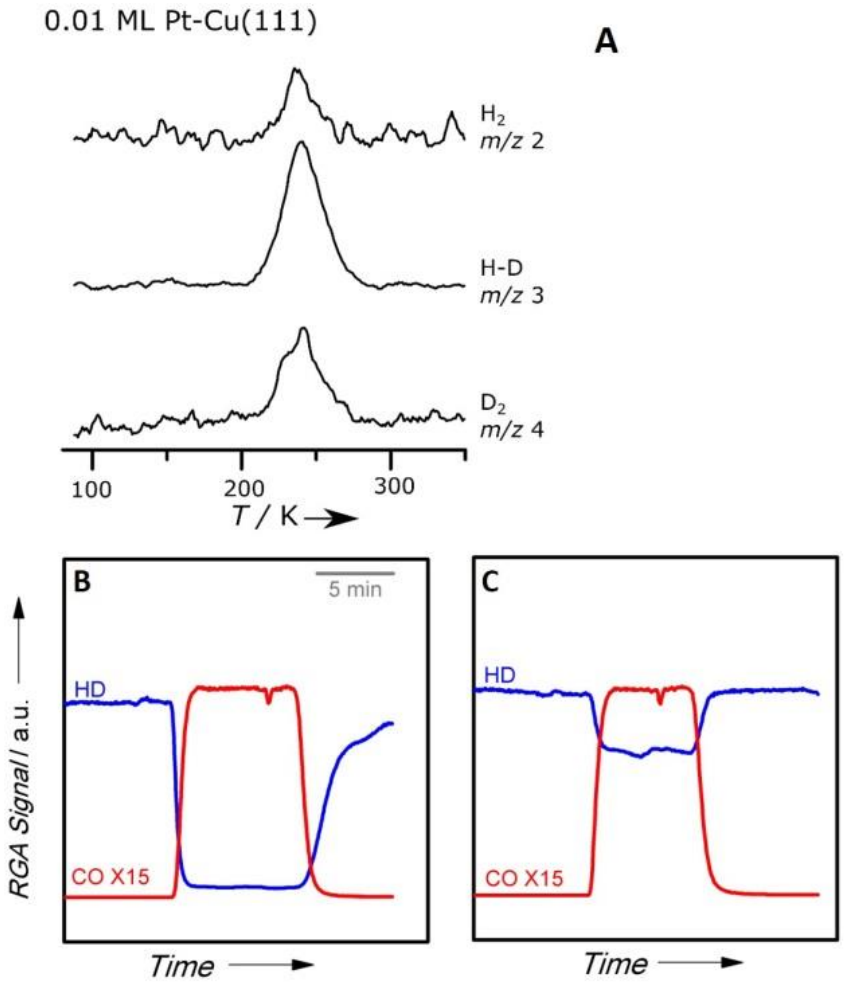

Figure 6.3. H-D scrambling on Pt-Cu SAA
(A) H-D scrambling on a model Pt-Cu(111) SAA surface. Desorption traces are shown resulting from adsorption of equivalent amounts of H_2 and D_2. Real catalyst data for isothermal H_2-D_2 exchange over (B) Pt-NP and (C) $Pt_{0.008}$Cu-SAA at 150°C. Gas composition: 33 % H_2, 33 % D_2, 3.3 % CO and balance Argon. Total flow rate=50 ml/min. 90 mg catalyst load. Same Pt loading was applied in both samples (Table S1[20]).

Extending this common principle, H_2-D_2 exchange was employed to characterize the H_2 dissociation activity on the corresponding nanocatalysts at ambient pressure in a flow reactor setup. As shown in Figure 6.3B and C, HD is initially produced when H_2 and D_2 are co-fed into the reactor. Once CO is introduced, the HD production decreases due to CO poisoning. With the same CO concentration in the gas phase, $Pt_{0.008}$Cu-SAA yields 12 times more HD than Pt-NP at 150 °C. Since the CO coverage is a function of binding strength, and we have shown that CO binds to Pt-Cu SAAs more weakly compared to pure Pt, the reduced binding strength of CO to $Pt_{0.008}$Cu-SAA yields more CO-free sites that are available for H_2 activation and hence HD production.

To investigate the CO-tolerance of Pt-Cu SAA under realistic catalytic reaction conditions, we conducted the selective hydrogenation of acetylene over $Pt_{0.008}$Cu-SAA and Pt-NP with and without CO in a flow reactor. We found about half of the reaction rate was retained for $Pt_{0.008}$Cu-SAA with 200 ppm CO, which is a typical CO concentration found in industrial H_2 gas (Figure 6.4, S4). However, the hydrogenation activity of Pt-NP decreased 15-fold with 200 ppm CO. The H_2-D_2 exchange and acetylene hydrogenation activity of Cu-NP was at least one order of magnitude lower than that of $Pt_{0.008}$Cu-SAA at these temperatures. Our results demonstrate that Pt-Cu SAAs offer a new approach to design CO tolerant materials for industrial applications.

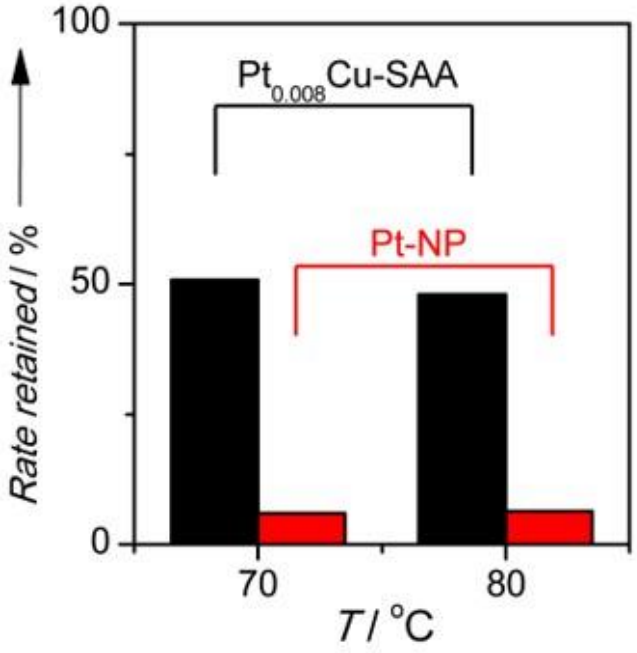

Figure 6.4. Ratio of retained reaction rate of acetylene hydrogenation in CO over $Pt_{0.008}$Cu-SAA and Pt-NP at different temperatures
Rate retained = reaction rate with CO/rate without CO in the reaction gas. Gas composition: 20 % H_2, 2.2 % C_2H_2, 200 ppm CO, 10 % Argon, balance He.

6.3. Summary

To summarize, we investigated the fundamentals of CO adsorption on Pt-Cu alloys using a variety of surface science and catalysis techniques. We found that CO binds weaker to single Pt atoms in Cu compared to larger Pt ensembles or monometallic Pt. Thus, when CO is present in the gas phase, more CO-free Pt sites are available on the SAA than the monometallic Pt, yielding higher H_2 activation reactivity and sequential hydrogenation activity under realistic conditions which we demonstrated for SAA catalysts. We postulate that this SAA approach in other metal combinations can be used for the design of novel CO-tolerant catalysts for other industrially important reactions such as hydrocarbon and alcohol

oxidation reactions, and for the present generation, low-temperature hydrogen fuel cells where the platinum electrocatalystis prone to CO-poisoning.

6.4. Additional Experimental Methods

For TPD experiments, samples were cooled to 85 K with liquid nitrogen prior to exposure to H_2 (99.9 % Airgas), D_2 (99.999 % Airgas) and/or CO (99.99 % Airgas). CO desorption traces were obtained after saturation exposure of CO at 10 Langmuirs (L) (1 L = 1 * 10^{-6} torr · s). STM experiments were performed on both variable and low temperature STMs. Images of bare Pt-Cu(111) were obtained using a variable temperature STM at 30 K with tunneling conditions of 100–200 nA and biases between 0.01 and 0.05 V. Atom manipulation studies in Figure 6.2 were performed on a low temperature STM. The samples were exposed to 20 L H_2 followed by 0.05 L CO at 85 K. The samples were then cooled to 5 K for imaging. STM images were obtained at 30 pA currents and 30 mV. Voltages were increased to 200 mV to remove H adatoms and 5 V localized pulses to remove CO molecules.

6.5. References

(1) Cheng, X.; Shi, Z.; Glass, N.; Zhang, L.; Zhang, J.; Song, D.; Liu, Z.; Wang, H.; Shen, J. A Review of PEM Hydrogen Fuel Cell Contamination: Impacts, Mechanisms, and Mitigation. *J. Power Sources* **2007**, *165*, 739–756.

(2) Baschuk, J. J.; Li, X. Carbon Monoxide Poisoning of Proton Exchange Membrane Fuel Cells. *Int. J. Energy Res.* **2001**, *25*, 695–713.

(3) Zhai, Y.; Pierre, D.; Si, R.; Deng, W.; Ferrin, P.; Nilekar, A. U.; Peng, G.; Herron, J. A.; Bell, D. C.; Saltsburg, H.; et al. Alkali-Stabilized Pt-OH_x Species Catalyze Low-Temperature Water-Gas Shift Reactions. *Science* **2010**, *329*, 1633–1636.

(4) Yang, M.; Liu, J.; Lee, S.; Zugic, B.; Huang, J.; Allard, L. F.; Flytzani-Stephanopoulos, M. A Common Single-Site Pt(II)-$O(OH)_x$- Species Stabilized by Sodium on “active” and “inert” Supports Catalyzes the Water-Gas Shift Reaction. *J. Am. Chem. Soc.* **2015**, *137*, 3470–3473.

(5) Kistler, J. D.; Chotigkrai, N.; Xu, P.; Enderle, B.; Praserthdam, P.; Chen,

C. Y.; Browning, N. D.; Gates, B. C. A Single-Site Platinum CO Oxidation Catalyst in Zeolite KLTL: Microscopic and Spectroscopic Determination of the Locations of the Platinum Atoms. *Angew. Chemie - Int. Ed.* **2014**, *53*, 8904–8907.

(6) Peterson, E. J.; DeLaRiva, A. T.; Lin, S.; Johnson, R. S.; Guo, H.; Miller, J. T.; Kwak, J.; Peden, C. H. F.; Kiefer, B.; Allard, L. F.; et al. Low-Temperature Carbon Monoxide Oxidation Catalysed by Regenerable Atomically Dispersed Palladium on Alumina. *Nat. Commun.* **2014**, *5*, 1–11.

(7) Qiao, B.; Wang, A.; Yang, X.; Allard, L. F.; Jiang, Z.; Cui, Y.; Liu, J.; Li, J.; Zhang, T. Single-Atom Catalysis of CO Oxidation Using Pt_1/FeO_x. *Nat. Chem* **2011**, *3*, 634–641.

(8) Vilé, G.; Albani, D.; Nachtegaal, M.; Chen, Z.; Dontsova, D.; Antonietti, M.; López, N.; Pérez-Ramírez, J. A Stable Single-Site Palladium Catalyst for Hydrogenations. *Angew. Chemie - Int. Ed.* **2015**, *54*, 11265–11269.

(9) Kyriakou, G.; Boucher, M. B.; Jewell, A. D.; Lewis, E. A.; Lawton, T. J.; Baber, A. E.; Tierney, H. L.; Flytzani-Stephanopoulos, M.; Sykes, E. C. H. Isolated Metal Atom Geometries as a Strategy for Selective Heterogeneous Hydrogenations. *Science* **2012**, *335*, 1209–1212.

(10) Boucher, M. B.; Zugic, B.; Cladaras, G.; Kammert, J.; Marcinkowski, M. D.; Lawton, T. J.; Sykes, E. C. H.; Flytzani-Stephanopoulos, M. Single Atom Alloy Surface Analogs in $Pd_{0.18}Cu_{15}$ Nanoparticles for Selective Hydrogenation Reactions. *Phys. Chem. Chem. Phys.* **2013**, *15*, 12187–12196.

(11) Lucci, F. R.; Liu, J.; Marcinkowski, M. D.; Yang, M.; Allard, L. F.; Flytzani-Stephanopoulos, M.; Sykes, E. C. H. Selective Hydrogenation of 1,3-Butadiene on Platinum – Copper Alloys at the Single-Atom Limit. *Nat. Commun.* **2015**, *6*, 8550.

(12) Boucher, M. B.; Marcinkowski, M. D.; Liriano, M. L.; Murphy, C. J.; Lewis, E. A.; Jewell, A. D.; Mattera, M. F. G.; Kyriakou, G.; Flytzani-Stephanopoulos, M.; Sykes, E. C. H. Molecular-Scale Perspective of Water-Catalyzed Methanol Dehydrogenation to Formaldehyde. *ACS Nano* **2013**, *7*, 6181–6187.

(13) Shan, J.; Lucci, F. R.; Liu, J.; El-Soda, M.; Marcinkowski, M. D.; Allard, L. F.; Sykes, E. C. H.; Flytzani-Stephanopoulos, M. Water Co-Catalyzed Selective Dehydrogenation of Methanol to Formaldehyde and Hydrogen. *Surf. Sci.* **2016**, No. 650, 121–129.

(14) Lucci, F. R.; Marcinkowski, M. D.; Lawton, T. J.; Sykes, E. C. H. H_2 Activation and Spillover on Catalytically Relevant Pt-Cu Single Atom Alloys. *J. Phys. Chem. C* **2015**, *119*, 24351–24357.

(15) Pedersen, M. Ø.; Helveg, S.; Ruban, A.; Stensgaard, I.; Lægsgaard, E.; Nørskov, J. K.; Besenbacher, F. How a Gold Substrate Can Increase the Reactivity of a Pt Overlayer. *Surf. Sci.* **1999**, *426*, 395–409.

(16) Ruff, M.; Takehiro, N.; Liu, P.; Nørskov, J. K.; Behm, R. J. Size-Specific Chemistry on Bimetallic Surfaces: A Combined Experimental and Theoretical Study. *ChemPhysChem* **2007**, *8*, 2068–2071.

(17) Kirstein, W.; Krüger, B.; Thieme, F. CO Adsorption Studies on Pure and Ni-Covered Cu(111) Surfaces. *Surf. Sci.* **1986**, *176*, 505–529.
(18) Lucci, F. R.; Lawton, T. J.; Pronschinske, A.; Sykes, E. C. H. Atomic Scale Surface Structure of Pt/Cu(111) Surface Alloys. *J. Phys. Chem. C* **2014**, *118*, 3015–3022.
(19) Collins, D. M.; Spicer, W. E. The Adsorption of CO, O_2 and H_2 on Pt. *Surf. Sci.* **1977**, *69*, 85–113.
(20) Liu, J.; Lucci, F. R.; Yang, M.; Lee, S.; Marcinkowski, M. D.; Therrien, A. J.; Williams, C. T.; Sykes, E. C. H.; Flytzani-Stephanopoulos, M. Tackling CO Poisoning with Single Atom Alloy Catalysts. *J. Am. Chem. Soc.* **2016**, *138*, 6396–6399.
(21) Castro, G. R.; Doyen, G. Electronical and Structural Effects in CO Chemisorption on Cu_3Pt(111). *Surf. Sci.* **1994**, *307*, 384.
(22) Zhang, C. J.; Baxter, R. J.; Hu, P.; Alavi, A.; Lee, M. H. A Density Functional Theory Study of Carbon Monoxide Oxidation on the Cu_3Pt(111) Alloy Surface: Comparison with the Reactions on Pt(111) and Cu(111). *J. Chem. Phys.* **2001**, *115*, 5272.
(23) Jewell, A. D.; Peng, G.; Mattera, M. F. G.; Lewis, E. A.; Murphy, C. J.; Kyriakou, G.; Mavrikakis, M.; Sykes, E. C. H. Quantum Tunneling Enabled Self-Assembly of Hydrogen Atoms on Cu(111). *ACS Nano* **2012**, *6*, 10115–10121.
(24) Bartels, L.; Meyer, G.; Rieder, K.-H.; Velic, D.; Knoesel, E.; Hotzel, A.; Wolf, M.; Ertl, G. Dynamics of Electron-Induced Manipulation of Individual CO Molecules on Cu(111). *Phys. Rev. Lett.* **1998**, *80*, 2004–2007.

6.6. Collaborations

Nanoparticle catalysts experiments were performed by Jilei Liu and the Stephanopoulos Group from the Department of Chemical and Biological Engineering at Tufts University.

Chapter 7: Altering H_2 Release from Pt-Cu Alloys with the Molecular Cork Effect

7.1. Introduction

Hydrogen and carbon monoxide are key species in many catalyzed conversions in the fuel industry, including Fisher Tropsch synthesis, methane steam reformation, and methanol/ethanol fuel cells. Typically a repulsion is observed between H and CO which impacts their uptake and release from a metallic surface.[1–8] Additionally, the strong adsorption of CO to metallic surfaces, renders CO a common catalytic poison.[9–11] Thus, understanding the interactions between H, CO, and the substrate is necessary for the design of new catalysts.

In previous works it has been shown that the co-adsorption of H and CO on bimetallic alloys produces unique desorption behaviors. On Pd-Cu(111) single atom alloys (SAAs), CO raises the desorption temperature of H_2 allowing hydrogen adatoms to remain on the surface beyond their normal desorption temperature, which we refer to as the *molecular cork effect.*[12] Similar behavior has been reported on $Pd_{70}Au_{30}$, where adsorbed CO traps H in the near-surface layer.[13] Although, for Pd-Au SAAs, H_2 desorbs from the alloyed surface at a lower temperature in the presence of CO. The repulsion between CO and H facilitates spillover of H from the Pd dissociation sites to Au terraces from where H_2 desorbs.[14] This is also observed on Co nanopoarticles supported on Cu(111) where CO exerts a two-dimensional pressure forcing H off the Co islands.[7] Thus, both the atomic surface structure and the nature of the adsorbed species impact the desorption temperatures. In this study, we further the understanding of co-adsorption of CO and H on SAAs by studying Pt-Cu alloys. We find that

Pt-Cu single atom alloys exhibit enhanced reactivity, selectivity, stability, and tolerance to CO poisoning as compared to monometallic catalysts;[15–17] they therefore represent promising candidates for overcoming the current limits of Pt-based catalysts.

To understand the interactions of H and CO with isolated Pt atoms, we studied their adsorption and desorption on Pt-Cu SAAs with atomic resolution. Using a combination of temperature programmed desorption (TPD), scanning tunneling microscopy (STM), and density functional theory (DFT), we probed the Pt active site to elucidate the energetics of hydrogen adsorption and desorption in the presence of CO. We show that CO increases desorption temperature of H for Pt-Cu SAAs and demonstrate the generality of the molecular cork effect with respect to SAAs.

7.2. Results and Discussion

Using model catalysts, we probed the interaction of H and CO on Pt-Cu SAAs in ultra-high vacuum (UHV). Pt atoms were deposited using physical vapor deposition onto a Cu(111) surface held at 380 K. Using this preparation condition, we have previously shown at low Pt concentrations (< 0.05 ML) Pt atoms exist as single isolated atoms in the surface layer of Cu.[17,18] As shown in Figure 7.1A, the Pt atoms appear in the STM ~ 20 pm higher than the surrounding Cu lattice and are well dispersed from one another. This high dispersion of Pt in Cu allows us to selectively probe the interactions of H and CO at isolated Pt atoms.

Using low-temperature STM, we directly probed the interaction of CO and H at the Pt active sites through molecular manipulation experiments using the STM tip (Figure 7.1 E-G). H and CO were co-adsorbed onto a 0.01 ML Pt-Cu(111) surface at 85 K before being cooled

to 5 K for imaging. We initially observed clusters of mobile depressions on the Cu terraces that we assigned to H adatoms (Figure 7.2B-D and Figure 7.2E). Previously, we demonstrated H adatoms that have spilled over from the Pt dissociation site can diffuse on Cu(111) at 5 K due to a low diffusion barrier (0.13 eV).[19] In the current experiments, we then deliberately and selectively remove H adatoms from the imaging window by applying a large bias (200 mV) to the STM tip while scanning. Most atoms readily diffused away as expected for hydrogen, but a few immobile depressions remained on the surface (Figure 7.1F) and required a high (5 V) local pulse to remove. Since 2.4 V pulses are needed to desorb CO atoms from metallic surfaces,[20] we identify those immobile depressions as CO molecules. Directly underneath the CO molecules we observed stationary surface protrusions, which are Pt atoms substituted into the Cu lattice (Figure 7.1G). These results demonstrate that the preferred adsorption site of CO is the isolated Pt atoms and H can diffuse away from the Pt site to the Cu lattice.

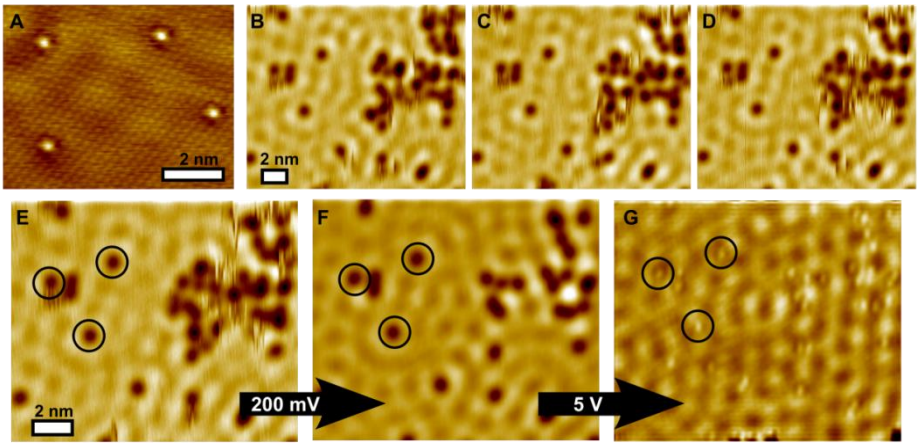

Figure 7.1. STM images of the co-adsorption of H and CO on 0.01 ML Pt-Cu(111) SAAs
(A) Atomic resolution image of individual isolated Pt atoms in Cu(111). Imaging conditions: 10 mV 150 nA imaged at 30 K. (B-D) Consecutive images of adsorbed H and CO showing H diffusion and stationary CO. Imaging conditions: 30 pA and 30 mV imaged at 5 K. (E-G) STM manipulation experiment to uncover the Pt active site. Image C is after adsorption of H and CO. Image D is after 200 mV scan to remove adsorbed H atoms. Image E is after local 5 V pulses to remove adsorbed CO. Three Pt sites are highlighted with circles. The images (B-F) were taken at 30 mV and 30 pA and image (G) 10 mV and 50 nA.

These Pt-Cu SAAs also exhibit unique H_2 adsorption and desorption behavior as compared to monometallic surfaces. As shown with TPD in Figure 7.2A, H desorbs from Pt-Cu SAAs at 230 K, which is 70 K lower than desorption temperature from either bare Cu(111) or Pt(111) (300 K). The isolated Pt atom in Cu reduces both the barrier for dissociative adsorption of H_2 relative to Cu(111) and the binding strength of H adatoms compared to Pt(111). Hence, we observe facile activation of H_2 at 85 K and low temperature desorption at 230 K. Additionally, microscopic reversibility states H_2 must adsorb and desorb via the same lowest-energy pathway, which is through the Pt monomers.[17,21]

We further explored the impact of CO adsorption on the uptake and release of H. At sub-saturation coverages of CO, H_2 desorbs from the surface at 230 K (Figure 7.2A). While we did not introduce CO deliberately, CO in the background of the UHV chamber always causes occupation of some Pt sites, but not all. Additional CO exposure allows us to saturate all Pt sites (0.01 ML) while producing a low coverage of excess CO on the Cu terraces (0.03 ML) (Figure 7.2B). When we co-adsorb H_2 and CO, the desorption traces are dependent on the order of gas exposure. If CO is adsorbed prior to H exposure, we do not observe any uptake of H (Figure 7.2C). CO blocks the Pt sites inhibiting the adsorption of H_2 despite the availability of Cu sites. When we adsorb H prior to CO, we observe H_2 desorption at 290 K, 60 K higher than the pure-component desorption temperature of H_2 on Pt-Cu SAAs (Figure 7.2D). We further observe that the full-width-half-max decreases from 35 K to 25 K in the presence of CO suggestive of a rapid recombination of H in the presence of CO.

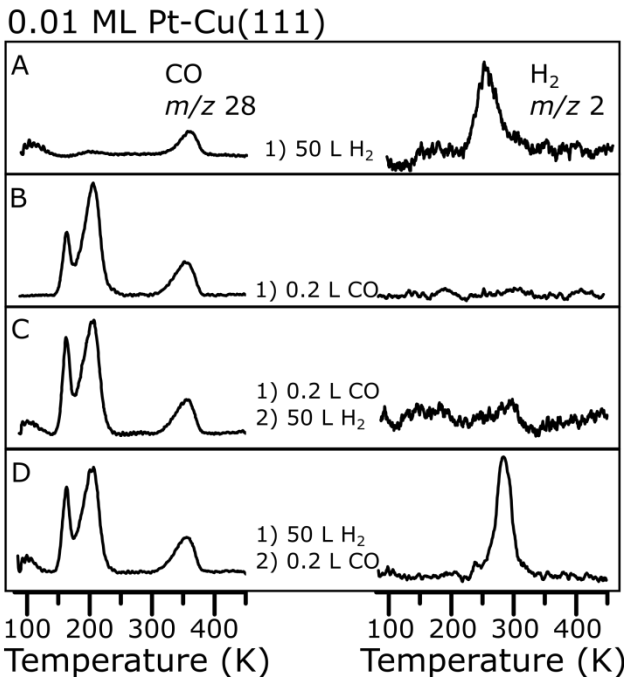

Figure 7.2. Co-adsorption of H and CO on Pt-Cu(111) SAAs
TPD traces for CO (*m/z* 28) and H_2 (*m/z* 2) for adsorption of (A) 50 L H_2, (B) 0.2 L CO, (C) 0.2 L CO followed by 50 L H_2 (D) 50 L H_2 followed by 0.2 L CO on 0.01 ML Pt.

Preliminary theoretical DFT calculations suggest two possible mechanisms for desorption of H_2 in the presence of CO. The first mechanism suggests an increased desorption barrier of H_2 from Pt sites in the presence of CO. DFT calculations show that in the absence of CO, H atoms recombine directly over the Pt site. When CO is present, CO selectively adsorbs to the Pt sites blocking the direct route for H_2 desorption. Therefore, in the presence of CO, H_2 desorbs from a bridge site between Pt and Cu suggesting H can recombine in the presence of CO. The second hypothesis suggests CO diffuses away from the Pt sites, thereby opening the desorption channel directly from the Pt atoms. Though the diffusion rate of CO from Pt to Cu is a non-activated process, it is highly an endothermic process.

7.3. Summary

In summary, we investigated the adsorption and desorption of H_2 in the presence and absence of CO to elucidate the energetics of adsorption at minority Pt sites. By using STM, we directly probed the interactions of H and CO at isolated Pt atoms in Cu to show that CO selectively adsorbs to the Pt sites. The preferential interaction of CO to Pt atoms blocks the adsorption and desorption of H_2. The selective adsorption of CO to minority Pt sites, traps H atoms on the surface beyond the typical desorption temperature demonstrating the generality of the molecular cork effect on single atoms alloys.

7.4. References

(1) Montano, M.; Bratlie, K.; Salmeron, M.; Somorjai, G. A. Hydrogen and Deuterium Exchange on Pt(111) and Its Poisoning by Carbon Monoxide Studied by Surface Sensitive High-Pressure Techniques. *J. Am. Chem. Soc.* **2006**, *128*, 13229–13234.

(2) Johansson, M.; Lytken, O.; Chorkendorff, I. The Sticking Probability for H_2 in Presence of CO on Some Transition Metals at a Hydrogen Pressure of 1 Bar. *Surf. Sci.* **2008**, *602*, 1863–1870.

(3) Wang, H.; Tobin, R. G.; Lambert, D. K. Coadsorption of Hydrogen and CO on Pt(335): Structure and Vibrational Stark Effect. *J. Chem. Phys.* **1994**, *101*, 4277.

(4) Hoge, D.; Tushaus, M.; Bradshaw, a. M. Island Formation during CO/H Coadsorption on Pt{111} Studied by IR Reflection-Absorption Spectroscopy. *Surf. Sci.* **1988**, *207*, L935–L942.

(5) Calaza, F.; Stacchiola, D.; Neurock, M.; Tysoe, W. T. Coverage Effects on the Palladium-Catalyzed Synthesis of Vinyl Acetate: Comparison between Theory and Experiment. *J. Am. Chem. Soc.* **2010**, *132*, 2202–2207.

(6) Richter, L. J.; Gurney, B. A.; Ho, W. The Influence of Adsorbate–adsorbate Interactions on Surface Structure: The Coadsorption of CO and H_2 on Rh(100). *J. Chem. Phys.* **1987**, *86*, 477–490.

(7) Lewis, E. A.; Le, D.; Jewell, A. D.; Murphy, C. J.; Rahman, T. S.; Sykes, E. C. H. Visualization of Compression and Spillover in a Coadsorbed System: Syngas on Cobalt Nanoparticles. *ACS Nano* **2013**, *7*, 4384–4392.

(8) Morkel, M.; Rupprechter, G.; Freund, H. J. Ultrahigh Vacuum and High-Pressure Coadsorption of CO and H_2 on Pd(111): A Combined SFG, TDS, and LEED Study. *J. Chem. Phys.* **2003**, *119*, 10853–10866.

(9) Cheng, X.; Shi, Z.; Glass, N.; Zhang, L.; Zhang, J.; Song, D.; Liu, Z.; Wang, H.; Shen, J. A Review of PEM Hydrogen Fuel Cell Contamination: Impacts, Mechanisms, and Mitigation. *J. Power Sources* **2007**, *165*, 739–

756.
(10) Baschuk, J. J.; Li, X. Carbon Monoxide Poisoning of Proton Exchange Membrane Fuel Cells. *Int. J. Energy Res.* **2001**, *25*, 695–713.
(11) Tang, D. C.; Hwang, K. S.; Salmeron, M.; Somorjai, G. A. High Pressure Scanning Tunneling Microscopy Study of CO Poisoning of Ethylene Hydrogenation on Pt(111) and Rh(111) Single Crystals. *J. Phys. Chem. B* **2004**, *108*, 13300–13306.
(12) Marcinkowski, M. D.; Jewell, A. D.; Stamatakis, M.; Boucher, M. B.; Lewis, E. A.; Murphy, C. J.; Kyriakou, G.; Sykes, E. C. H. Controlling a Spillover Pathway with the Molecular Cork Effect. *Nat. Mater.* **2013**, *12*, 523–528.
(13) Ogura, S.; Okada, M.; Fukutani, K. Near-Surface Accumulation of Hydrogen and CO Blocking Effects on a Pd − Au Alloy. *J. Phys. Chem. C* **2013**, *117*, 9366–9371.
(14) Lucci, F. R.; Darby, M. T.; Mattera, M. F. G.; Ivimey, C. J.; Therrien, A. J.; Michaelides, A.; Stamatakis, M.; Sykes, E. C. H. Controlling Hydrogen Activation, Spillover, and Desorption with Pd-Au Single Atom Alloys. *J. Phys. Chem. Lett.* **2016**, *7*, 480–485.
(15) Lucci, F. R.; Liu, J.; Marcinkowski, M. D.; Yang, M.; Allard, L. F.; Flytzani-Stephanopoulos, M.; Sykes, E. C. H. Selective Hydrogenation of 1,3-Butadiene on Platinum–Copper Alloys at the Single-Atom Limit. *Nat. Commun.* **2015**, *6*, 8550.
(16) Liu, J.; Lucci, F. R.; Yang, M.; Lee, S.; Marcinkowski, M. D.; Therrien, A. J.; Williams, C. T.; Sykes, E. C. H.; Flytzani-Stephanopoulos, M. Tackling CO Poisoning with Single Atom Alloy Catalysts. *J. Am. Chem. Soc.* **2016**, *138*, 6396–6399.
(17) Lucci, F. R.; Marcinkowski, M. D.; Lawton, T. J.; Sykes, E. C. H. Hydrogen Activation and Spillover on Catalytically Relevant Pt-Cu Single Atom Alloys. *J. Phys. Chem. C* **2015**, *119*, 24351–24357.
(18) Lucci, F. R.; Lawton, T. J.; Pronschinske, A.; Sykes, E. C. H. Atomic Scale Surface Structure of Pt/Cu(111) Surface Alloys. *J. Phys. Chem. C* **2014**, *118*, 3015–3022.
(19) Jewell, A. D.; Peng, G.; Mattera, M. F. G.; Lewis, E. A.; Murphy, C. J.; Kyriakou, G.; Mavrikakis, M.; Sykes, E. C. H. Quantum Tunneling Enabled Self-Assembly of Hydrogen Atoms on Cu(111). *ACS Nano* **2012**, *6*, 10115–10121.
(20) Bartels, L.; Meyer, G.; Rieder, K.-H.; Velic, D.; Knoesel, E.; Hotzel, A.; Wolf, M.; Ertl, G. Dynamics of Electron-Induced Manipulation of Individual CO Molecules on Cu(111). *Phys. Rev. Lett.* **1998**, *80*, 2004–2007.
(21) Kyriakou, G.; Boucher, M. B.; Jewell, A. D.; Lewis, E. A.; Lawton, T. J.; Baber, A. E.; Tierney, H. L.; Flytzani-Stephanopoulos, M.; Sykes, E. C. H. Isolated Metal Atom Geometries as a Strategy for Selective Heterogeneous Hydrogenations. *Science* **2012**, *335*, 1209–1212.

Chapter 8: Water Co-Catalyzed Selective Dehydrogenation of Methanol to Formaldehyde and H_2 on Pt-Cu *Single Atom Alloys*

This chapter was modified from an original publication of the same title by J. Shan, F. R. Lucci* et al. from Surface Science, volume 650, pages 121-129.*

8.1. Introduction

Formaldehyde is widely used as a precursor in the industrial synthesis of ethylene, glycol, dyes, drugs, and plastics.[1] Currently, it is synthesized via oxidative dehydrogenation of methanol using heterogeneous catalysts. However, the catalysts used in this process are unselective and produce unwanted byproducts including water, carbon monoxide, dimethyl ether, carbon dioxide, and formic acid.[2] Ideally, methanol dehydrogenation should selectively produce formaldehyde and H_2 (g). Chen *et al.* showed that a highly stepped Cu(210) surface is capable of catalyzing methanol to formaldehyde in the absence of O.[3] This surprising result contrasts most single crystal studies that suggest O adatoms or metal oxides are required to catalyze methanol dehydrogenation to formaldehyde and water.[4–7] Previously, we have shown that water on Cu(111) can also co-catalyze the reaction in the absence of O to selectively produce formaldehyde and H_2 and isolated Pd atoms in Cu can further enhance the reactivity.[8] Thus, opening a new route to produce formaldehyde and H_2 in an oxygen free environment.

In this work, we extended methanol dehydrogenation to Pt-Cu single atom alloys (SAAs) and observe that the addition of small amounts of highly dispersed isolated Pt atoms in Cu greatly enhance the water-catalyzed dehydrogenation of methanol to formaldehyde and H_2. We hypothesize that the isolated Pt atoms increase the initial production of methoxy, which then decomposes to formaldehyde and H_2. We also show that metallic Cu

nanoparticles can catalyze this reaction under realistic reaction conditions where the promotional effect observed on Pt-Cu nanoparticle catalysts is greater than that of Pd-Cu catalysts.

8.2. Results and Discussion

To investigate the methanol dehydrogenation reaction, we performed temperature programmed desorption/reaction (TPD/R) studies on model surfaces of Pt-Cu(111) in ultra-high vacuum (UHV). Figure 8.1 shows the TPD/R traces resulting from the adsorption of methanol-D onto Cu(111). In agreement with previously reported desorption of methanol from Cu(111),[3,9] we observe intact methanol-D (*m/z* 33) desorbing from Cu(111) terraces at 160 K and from Cu step edges at 200 K. Small amounts of reactively formed formaldehyde (*m/z* 30) desorbs from Cu(111) surface at 370 K. The fragmentation pattern of both methanol and formaldehyde include *m/z* 30, however, at 370 K, we observe desorption of *m/z* 30 independent of *m/z* 33 (methanol-D). Thus we conclude that reactively formed formaldehyde desorbs at higher temperatures. Additionally, water (*m/z* 18) from the chamber background is also observed desorbing from the surface at 150 K, though the surface coverage of water is small at a 0.2:1 water : methanol ratio. Water is known to co-catalyze the dehydrogenation of methanol on Cu in vacuum and will be discussed later.[8]

Interestingly, when methanol is adsorbed on a roughened Cu(111) surface (Figure 8.1A), the amount of reactively formed formaldehyde desorbing at 370 K increases. An increase in desorption of methanol-D at 200 K indicates that there is an increase in step sites on the roughened copper surface. Using scanning tunneling microscopy (STM), we imaged both a typical Cu(111) (Figure 8.1B) and a roughened Cu(111) surface (Figure 8.1C). Typically Cu(111) exhibits monoatomic steps separated by large terraces (30 – 100 nm). A

roughened surface prepared through Ar^+ sputtering without annealing, yields a highly stepped surface. Using CO titration, we estimate the concentration of step sites on the roughened Cu(111) surface is 5x that of a typical Cu(111) surface. From this experiment we conclude that the higher density of Cu step sites increases the conversion of methanol to formaldehyde.

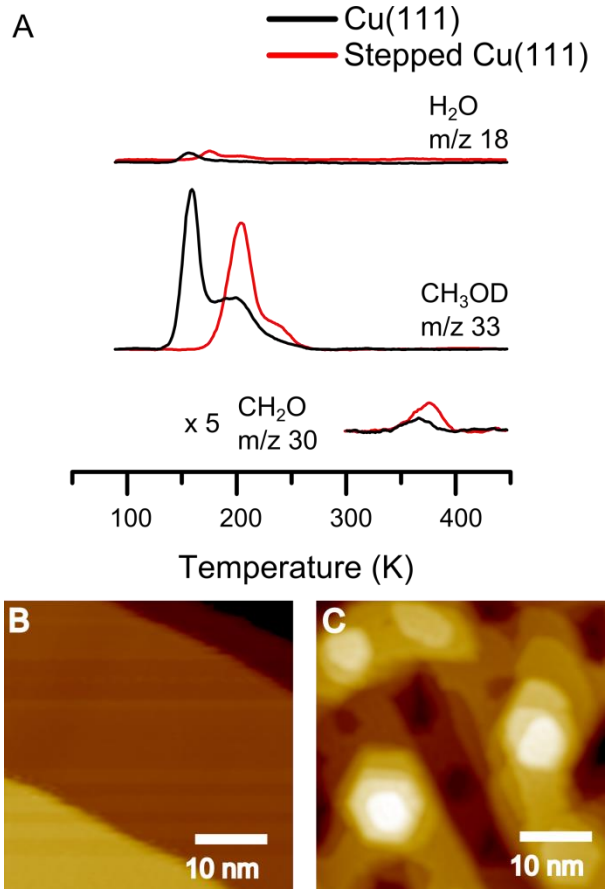

Figure 8.1. TPD/R traces for the adsorption of methanol on Cu(111) and a highly roughened Cu(111) surface
(A) Methanol-D (0.6 monolayer (ML)) was adsorbed onto the surfaces (water : methanol = 0.2:1). Desorption traces for reactants water (*m/z* 18) and methanol (*m/z* 33) and the product formaldehyde (*m/z* 30) are shown. STM images of a (B) typical Cu(111) surface and (C) roughened Cu(111) surface.

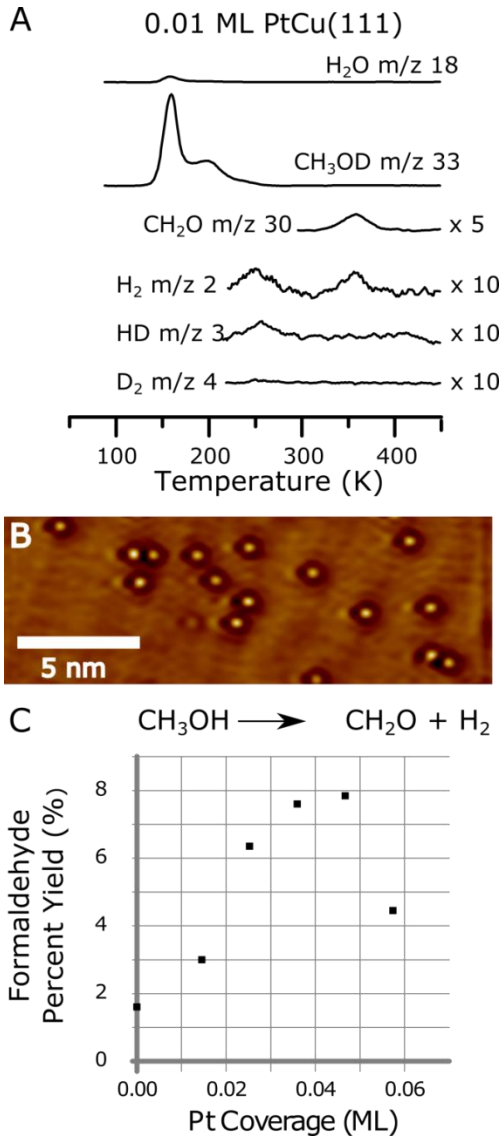

Figure 8.2. TPD/R traces for the adsorption of methanol on Pt-Cu(111) SAAs
(A) TPD/R traces of methanol on a Pt-Cu SAA. 0.6 ML methanol-D was adsorbed on 0.01 ML Pt-Cu(111) surface (water: methanol = 0.2:1). (B) STM image of Pt-Cu(111) SAA surface where the bright features are Pt atoms substituted into the Cu(111) surface. (C) Formaldehyde percent yield versus Pt concentration for adsorption of 0.6 ML methanol adsorbed onto varying surface coverages of Pt (water : methanol = 0.2:1).

To investigate if Pt atoms can enhance the reactivity of the Cu(111), we prepared Pt-Cu(111) SAAs and probed the methanol dehydrogenation reaction (Figure 8.2). We have previously characterized Pt-Cu(111) SAAs and showed that the Pt atoms exist as isolated species dispersed in the Cu terraces at low Pt coverages.[10,11] In Figure 8.2B, the Pt atoms

appear in STM images as single protrusions in the Cu(111) terrace. TPD/R for the adsorption of methanol-D on Pt-Cu(111) SAAs exhibits an increase in formaldehyde desorption (370 K) compared to Cu(111) surface (Figure 8.1A and 8.2A). Furthermore, the addition of Pt does not change the desorption temperature of methanol or formaldehyde; it only increases the production of formaldehyde. To further investigate the ability of Pt atoms to catalyze the reaction, we increased the concentration of Pt atoms in the Cu surface. The formaldehyde yield increases linearly as a function of Pt coverage in the single atom regime (< 0.05 ML Pt), but begins to decrease beyond 0.05 ML Pt where clusters greater than one Pt atom exist in the surface. Additionally, Pt-Cu SAAs exhibit high stability; the percent yield of formaldehyde remains constant at 9 % ± 1 for 7 consecutive reaction cycles on the same Pt-Cu SAA surface with 1:1 water to methanol ratio.

Furthermore, we do not observe reactively formed CO desorbing from Pt-Cu(111) SAA surfaces indicating that Pt-Cu SAAs cannot fully decompose methanol to CO resulting in 100 % selectivity to formaldehyde on the Pt-Cu SAA surface. After increasing the coverage of Pt to 0.3 ML, a significant decrease in the amount of reactively formed formaldehyde and unreactive methanol is observed, reducing the selectivity to formaldehyde. This is due to an ensemble effect at 0.3 ML Pt in Cu(111), our previous STM imaging data showed a heterogeneous atomic surface structure of Pt where linear clusters of Pt atoms were present on the surface.[10,12] We propose that these larger Pt ensembles are capable of decomposing formaldehyde or methanol since Pt(111) was observed to decompose methanol and formaldehyde.[13]

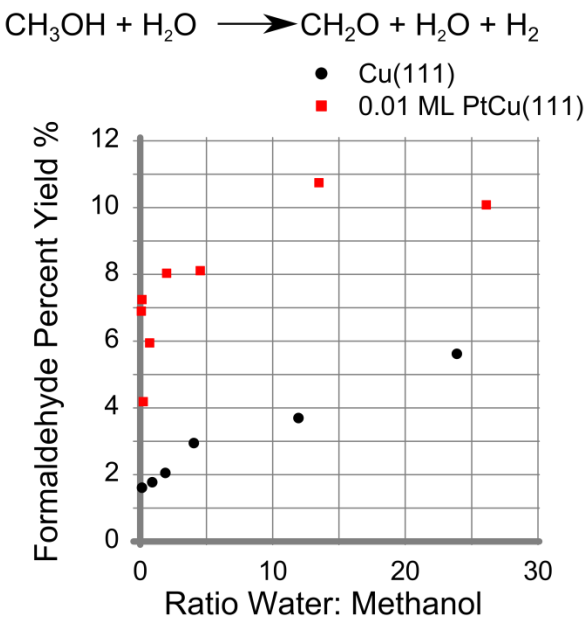

Figure 8.3. Formaldehyde yield versus the ratio of water to methanol for Cu(111) and Pt-Cu(111) SAA surfaces
Methanol was adsorbed prior to water and the methanol surface coverage was 0.6 ML for each trial.

To investigate the role of water in Pt-Cu SAA catalysts, we co-adsorbed water and methanol onto a Pt-Cu(111) SAA surface. Increasing the ratio of water : methanol led to an increase in the percent yield of formaldehyde on both Cu(111) and Pt-Cu(111) SAA (Figure 8.3) with Pt-Cu SAAs being more reactive than Cu(111). At maximum formaldehyde conversion, Pt-Cu SAAs are about twice as reactive as Cu(111). We previously reported that water co-catalyzes methanol dehydrogenation on Cu(111) surface.[8] Combing STM with TPD/R, we demonstrated that excess water is needed to convert methanol to formaldehyde on a Cu(111) surface. Since both water and methanol form hydrogen bonded clusters, we showed that the co-adsorption of methanol[14–16] and water[17,18] result in methanol-water networks that assist in the dehydrogenation of methanol to methoxy.

Through our surface science studies, we investigated the active sites for the dehydrogenation of methanol. Although Cu(111) terraces are incapable of converting

methanol to formaldehyde,[8] we demonstrate the we can dramatically increase the reactivity of Cu through producing additional active sites and utilizing the co-catalyst water. First, increasing the step density on a Cu(111) surface doubles the conversion of methanol to formaldehyde in agreement with previous studies that demonstrate the formation of methoxy on Cu steps.[8,19] Furthermore, addition of 0.01 ML isolated Pt atoms also doubles the conversion to formaldehyde. Both Cu steps and Pt-Cu SAAs catalyze the reaction via a similar mechanism. With our TPD/R studies, we elucidate the mechanism for dehydrogenation of methanol on Pt-Cu SAA surfaces. In order to identify desorption peaks for O-H versus C-H activation, we adsorbed methanol-D (CH_3OD) (Figure 8.2A). Intuitively, one would expect at low temperatures to observe the exclusive desorption of *m/z* 4 (D_2) from the initial O-D bond scission, however, we observe desorption of *m/z* 2 (H_2) and 3 (HD) at 250 K preceded by *m/z* 19 (HDO) at 160 K. Since at < 100 K methanol is initially dehydrogenated to methoxy on Cu steps, the D adatoms isotopically exchange with H_2O as previously reported by Mullins and co-workers on Au(111) or isotopic exchange occurs between H_2O and methanol-D,[7,20] because excess water co-catalyzes the reaction on Cu surfaces. Due to the competition between methoxy formation and methanol desorption, we hypothesize that isolated Pt atoms increase the formation of methoxy on the surface. The methoxy is then converted to formaldehyde at higher temperatures. The high temperature desorption of H_2 (*m/z* 2) that coincides with formaldehyde desorption, supports C-H activation as the rate limiting step to the formation of formaldehyde. This rate limiting step agrees with previous reports that C-H bond scission occurs at 430 K on Cu(111).[21] Furthermore, the overall process is reaction-rate-limited since formaldehyde desorption

occurs from Cu surfaces < 200 K.[5,22,23]

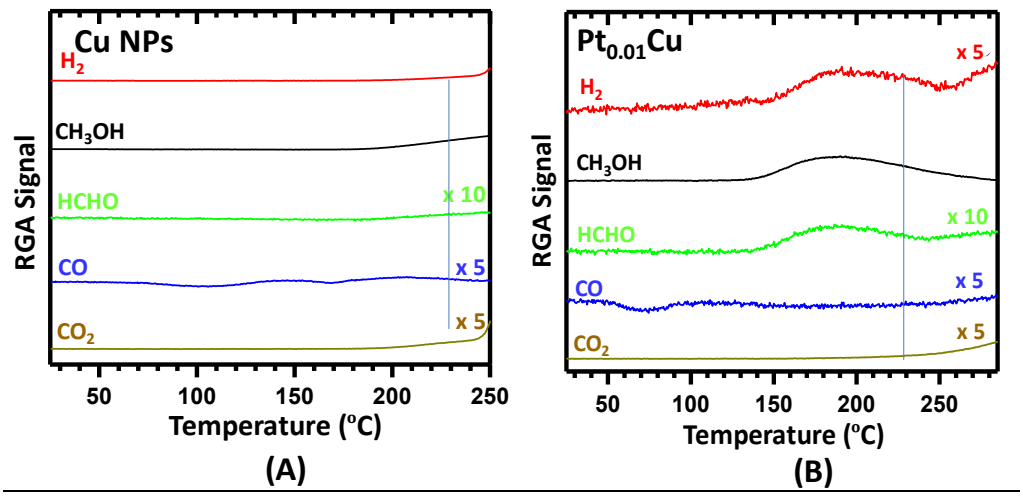

Figure 8.4. Temperature programmed surface reaction (TPSR) of methanol in the presence of water) on Pt-Cu supported nanoparticle catalysts
Water : methanol was 1:1 on (A) silica supported Cu nanoparticles and on (B) silica supported $Pt_{0.01}Cu$ SAA nanoparticles. Reaction conditions: 100mg catalyst, 3% methanol and 3% water balanced in He, He flow rate 10mL/min.

We also investigated water-catalyzed methanol dehydrogenation to formaldehyde on Cu surfaces under realistic reaction conditions (Figure 4) where silica supported Cu nanoparticles (A) and silica supported $Pt_{0.01}Cu$ SAA nanoparticles (B) catalyze methanol hydrogenation in the presence of water. In both cases, the water to methanol ratio was kept at 1:1 and formaldehyde is formed in both cases. The contribution from the methanol fragment was subtracted from the original *m/z* 30 signal prior to the analysis. At 230 °C the yield of formaldehyde on Cu nanoparticles is ~0.5 %; while the yield of formaldehyde on $Pt_{0.01}Cu$ SAA nanoparticles is ~7 %. At lower Pt loadings, a lower yield of formaldehyde (3 %) was observed for $Pt_{0.003}Cu$ SAA nanoparticles indicating that as expected, a higher concentration of single Pt atoms in Cu increases the conversion (Table 8.1). The formation of CO and CO_2 at 230 °C is negligible; hence the selectivity to formaldehyde at 230 °C on supported $Pt_{0.01}Cu$ SAA nanoparticles approaches 100 %. Higher Pt concentrations such as nanoparticles of

$Pt_{0.1}Cu$, catalyzed the full decomposition of methanol to CO and H_2 under the same reaction conditions (not shown here). This result is consistent with the formation of Pt clusters or nanoparticles, which are very active for the decomposition of formaldehyde.[24]

Table 8.1. The yield of formaldehyde at 230 °C from various catalysts operating with different water to methanol ratios

Sample	Water : methanol	Reaction conditions	Formaldehyde yield
Cu/SiO_2	1:1	100mg catalyst, 3 % methanol, 3 % water, 10mL/min	0.5 %
$Pt_{0.003}Cu/SiO_2$	1:1	100mg catalyst, 3 % methanol, 3 % water, 10mL/min	3 %
$Pt_{0.01}Cu/SiO_2$	1:1	100mg catalyst, 3 % methanol, 3 % water, 10mL/min	7 %
$Pt_{0.01}Cu/SiO_2$	1:5	100mg catalyst, 9 % methanol, 2 % water, 10mL/min	0
$Pt_{0.01}Cu/SiO_2$	3:1	100mg catalyst, 3 % methanol, 9 % water, 10mL/min	1.2 %
$Pt_{0.01}Cu/SiO_2$	7:1	100mg catalyst, 1 % methanol, 7 % water, 10mL/min	7 %
$Pd_{0.01}Cu/SiO_2$	1:1	100mg catalyst,3 % methanol, 3 % water, 10mL/min	0.8 %

Although water-catalyzed dehydrogenation of methanol has been observed on the Cu(111) surface under UHV conditions,[24] it is the first time that water-catalyzed methanol dehydrogenation has been observed under realistic reaction conditions. The promotion effect of water can be explained by the co-operative interactions of water and methanol facilitating the dehydrogenation of methanol to methoxy, thereby, increasing the formation of methoxy species. Methoxy can further dehydrogenate to formaldehyde by the activation of C-H bond.

Additionally, as observed in Figure 8.4, the stabilized methoxy can also undergo recombination with H atoms to desorb as methanol at higher temperature, which is kinetically more favorable in the absence of water. In the presence of water, however, stabilization of H atoms by water clusters increases the reaction barrier of recombination of methoxy and H and therefore allows the dehydrogenation of methoxy to formaldehyde via the C-H bond activation. Furthermore, we demonstrate that the catalytic activity of Cu surface originates from uncoordinated Cu atoms. Although the Cu(111) surface is active in the presence of water, the reactivity of Cu surface can be dramatically increased by increasing the step density of the Cu(111) surface.

Adding individual, isolated Pt atoms to a Cu surface also significantly promotes the reactivity of Cu in water-catalyzed methanol dehydrogenation. In TPSR measurements in the flow reactor, the yield of formaldehyde on silica-supported $Pt_{0.01}Cu$ SAA nanoparticles is 7 times larger than on supported Cu nanoparticles (Figure 8.4). In UHV conditions, depending on the concentration of water, the conversion of formaldehyde is 2 – 4 times higher than on Cu(111) at comparable water concentrations (Figure 8.3). Therefore, our data under both realistic reaction conditions and UHV support the dramatic increase of formation of formaldehyde by addition of single Pt atoms in Cu. We attribute this promotional effect to an increase in methoxy formation on Pt-Cu SAAs. As we previously demonstrated, isolated Pt atoms reduce the desorption temperature for H_2,[10,12] thereby facilitating the dehydrogenation of methanol to methoxy and increasing the surface coverage of methoxy, as well as allowing more conversion of methoxy to formaldehyde.

In a previous publication, we demonstrated that single Pd atoms in the Cu surface promote the water catalyzed methanol dehydrogenation.[8] In the current study, we found that

the promotional effect of Pt is much more pronounced than Pd. Under UHV conditions, at low water to methanol ratio (< 1) the formaldehyde yield on Pd-Cu(111) is almost the same as on Cu(111);[8] while the yield on Pt-Cu(111) is 4 times larger than on Cu(111) at the same water to methanol ratio. TPSR measurements in Table 8.1 also show that under reaction conditions the formaldehyde yield on $Pd_{0.01}Cu$ SAAs is approximately 0.8 % at 1:1 water to methanol ratio that is much lower than on $Pt_{0.01}Cu$ SAAs. We also performed tests with other Pd concentrations ($Pd_{0.003}Cu$ and $Pd_{0.05}Cu$) and observed that the yield of formaldehyde from these samples was similar to Cu. We propose that the increase reactivity for Pt-Cu SAAs can be rationalized based on the Brønsted-Evans-Polyani (BEP) relationship in terms of the adsorption strength of descriptor molecules affecting the reactivity.[25] For SAAs, Pt-Cu SAAs bind key descriptor molecules stronger than Pd-Cu SAAs and via the BEP would be expected to exhibit lower activation energies. We observed CO desorbing at a higher temperature from Pt-Cu(111) SAAs (350 K),[26] than Pd-Cu(111) SAAs (270 K),[27] despite similar desorption temperatures observed for Pd(111) and Pt(111) surfaces (450 K).[28,29] Additionally, Fu *et al.* predicts that Pt-Cu SAAs exhibit stronger binding of H atoms and a lower barrier for H_2 activation consistent with the BEP relationship.[30] Due to the stronger binding of these molecules to Pt-Cu SAAs, we propose that isolated Pt atoms are more reactive than Pd atoms, thereby enhancing methanol activation to methoxy.

8.3. Summary

In this work we demonstrate that Pt-Cu SAAs are active for methanol dehydrogenation to formaldehyde and hydrogen in the presence of water. Although Cu itself is also active, addition of single Pt atoms in the Cu surface significantly improves the reactivity where the yield of formaldehyde is strongly dependent on the water to methanol

ratio. The promotional effect of water is attributed to the stabilization of H atoms by water clusters that facilitate the dehydrogenation of methanol to methoxy, which can be further dehydrogenated to formaldehyde. Furthermore, Pt-Cu SAAs exhibit both high selectivity and stability in the water-catalyzed methanol dehydrogenation. The selectivity to formaldehyde on Pt-Cu SAA nanoparticle catalysts and on Pt-Cu(111) SAA model catalysts are both nearly 100 %. The findings of this work are a new manifestation of the utility of combining UHV surface science and high-pressure reactor experiments in exploring reaction mechanisms and guiding realistic catalyst designs.

8.4. Additional Experimental Methods

Cu(111) single crystals were cleaned with cycles of Ar^+ sputtering (1.5 keV, 15 μA) and annealing to 700 K. The roughened Cu(111) surface was prepared without the final anneal to 700 K. TPD/R experiments were performed after the model catalysts were cooled to 85 K with liquid nitrogen before reactants were deposited. Methanol (Alfa Aesar, ultrapure HPLC grade 99.8%), water (deionized H_2O), and methanol-D (Sigma-Aldrich, 99.5%) were further purified via freeze-pump-thaw cycles prior to deposition via a high precision leak valve. All exposures are quoted in Langmuirs (L) (1 L = 1 * 10^{-6} torr · s). Pt surface coverages and Cu step densities were quantified by CO (99.99% Airgas) titration after saturating the surface with CO (10 L). CO desorption from Cu terraces occurred at < 200 K, Cu step sites at 205 K, and Pt sites at > 300 K.

8.5. References

(1) Rounsaville, G. R. Ullmann's Encyclopedia of Industrial Chemistry, 1985, 619.
(2) G. Ertl, H. Knözinger, J. W. Handbook of Heterogeneous Catalysis, 1997, 3256.
(3) Chen, A. K.; Masel, R. Direct Conversion of Methanol to Formaldehyde

in the Absence of Oxygen on Cu(210). *Surf. Sci.* **1995**, *343*, 17–23.
(4) Bowker, M.; Madix, R. J. XPS, UPS, and Thermal-Desorption Studies of Alcohol Adsorption on Cu(11): I. Methanol. *Surf. Sci.* **1980**, *95*, 190–206.
(5) Wachs, I. E.; Madix, R. J. The Selective Oxidation of CH_3OH to H_2CO on a Copper(110) Catalyst. *J. Catal.* **1978**, *53*, 208–227.
(6) Bowker, M. Active Sites in Methanol Oxidation on Cu(110) Determined by STM and Molecular Beam Measurements. *Top. Catal.* **1996**, *3*, 461–468.
(7) Pan, M.; Pozun, Z. D.; Yu, W.; Henkelman, G.; Mullins, C. B. Structure Revealing H/D Exchange with Co-Adsorbed Hydrogen and Water on Gold. *J. Phys. Chem. Lett.* **2012**, *3*, 1894–1899.
(8) Boucher, M. B.; Marcinkowski, M. D.; Liriano, M. L.; Murphy, C. J.; Lewis, E. A.; Jewell, A. D.; Mattera, M. F. G.; Kyriakou, G.; Flytzani-Stephanopoulos, M.; Sykes, E. C. H. Molecular-Scale Perspective of Water-Catalyzed Methanol Dehydrogenation to Formaldehyde. *ACS Nano* **2013**, *7*, 6181–6187.
(9) Johnston, S. M.; Mulligan, A.; Dhanak, V.; Kadodwala, M. The Structure of Methanol and Methoxy on Cu(111). *Surf. Sci.* **2003**, *530* (1-2), 111–119.
(10) Lucci, F. R.; Marcinkowski, M. D.; Lawton, T. J.; Sykes, E. C. H. Hydrogen Activation and Spillover on Catalytically Relevant Pt-Cu Single Atom Alloys. *J. Phys. Chem. C* **2015**, *119*, 24351–24357.
(11) Lucci, F. R.; Lawton, T. J.; Pronschinske, A.; Sykes, E. C. H. Atomic Scale Surface Structure of Pt/Cu(111) Surface Alloys. *J. Phys. Chem. C* **2014**, *118*, 3015–3022.
(12) Lucci, F. R.; Liu, J.; Marcinkowski, M. D.; Yang, M.; Allard, L. F.; Flytzani-Stephanopoulos, M.; Sykes, E. C. H. Selective Hydrogenation of 1,3-Butadiene on Platinum–Copper Alloys at the Single-Atom Limit. *Nat. Commun.* **2015**, *6*, 8550.
(13) Gibson, K. D.; Dubois, L. H. Step Effects in the Thermal Decomposition of Methanol on Pt(111). *Surf. Sci.* **1990**, *233*, 59–64.
(14) Lawton, T. J.; Carrasco, J.; Baber, A. E.; Michaelides, A.; Sykes, E. C. H. Visualization of Hydrogen Bonding and Associated Chirality in Methanol Hexamers. *Phys. Rev. Lett.* **2011**, *107*, 256101.
(15) Lawton, T. J.; Carrasco, J.; Baber, A. E.; Michaelides, A.; Sykes, E. C. H. Hydrogen-Bonded Assembly of Methanol on Cu(111). *Phys. Chem. Chem. Phys.* **2012**, *14*, 11846–11852.
(16) Murphy, C. J.; Carrasco, J.; Lawton, T. J.; Liriano, M. L.; Baber, A. E.; Lewis, E. A.; Michaelides, A.; Sykes, E. C. H. Structure and Energetics of Hydrogen-Bonded Networks of Methanol on Close Packed Transition Metal Surfaces. *J. Chem. Phys.* **2014**, *141*, 014701.
(17) Mehlhorn, M.; Carrasco, J.; Michaelides, A.; Morgenstern, K. Local Investigation of Femtosecond Laser Induced Dynamics of Water Nanoclusters on Cu(111). *Phys. Rev. Lett.* **2009**, *103*, 1–4.
(18) Michaelides, A.; Morgenstern, K. Ice Nanoclusters at Hydrophobic Metal Surfaces. *Nat. Mater.* **2007**, *6*, 597–601.

(19) Russell, J. N.; Gates, S. M.; Yates, J. T. Reaction of Methanol with Cu(111) and Cu(111) + O(ads). *Surf. Sci.* **1985**, *163*, 516–540.
(20) Brush, A. J.; Pan, M.; Mullins, C. B. Methanol O–H Bond Dissociation on H-Precovered Gold Originating from a Structure with a Wide Range of Surface Stability. *J. Phys. Chem. C* **2012**, *116*, 20982–20989.
(21) Pöllmann, S.; Bayer, A.; Ammon, C.; Steinruck, H. P. Adsorption and Reaction of Methanol on Clean and Oxygen Precovered Cu(111). *Z. Phys. Chem.* **2004**, *218*, 957–971.
(22) Gomes, J. R. B.; Gomes, J. A DFT Study of the Methanol Oxidation Catalyzed by a Copper Surface. *Surf. Sci.* **2001**, *471*, 59–70.
(23) Gomes, J. R. B.; Gomes, J. A. N. F.; Illas, F. First-Principles Study of the Adsorption of Formaldehyde on the Clean and Atomic Oxygen Covered Cu(111) Surface. *J. Mol. Catal. A Chem.* **2001**, *170*, 187–193.
(24) Brown, J. C.; Gulari, E. Hydrogen Production from Methanol Decomposition over Pt/Al_2O_3 and Ceria Promoted Pt/Al_2O_3 Catalysts. *Catal. Commun.* **2004**, *5*, 431–436.
(25) Greeley, J.; Mavrikakis, M. Alloy Catalysts Designed from First Principles. *Nat. Mater.* **2004**, *3*, 810–815.
(26) Liu, J.; Lucci, F. R.; Yang, M.; Lee, S.; Marcinkowski, M. D.; Therrien, A. J.; Williams, C. T.; Sykes, E. C. H.; Flytzani-Stephanopoulos, M. Tackling CO Poisoning with Single Atom Alloy Catalysts. *J. Am. Chem. Soc.* **2016**, *138*, 6396–6399.
(27) Marcinkowski, M. D.; Jewell, A. D.; Stamatakis, M.; Boucher, M. B.; Lewis, E. A.; Murphy, C. J.; Kyriakou, G.; Sykes, E. C. H. Controlling a Spillover Pathway with the Molecular Cork Effect. *Nat. Mater.* **2013**, *12*, 523–528.
(28) Guo, X.; Yates, J. T. Dependence of Effective Desorption Kinetic Parameters on Surface Coverage and Adsorption Temperature: CO on Pd(111). *J. Chem. Phys.* **1989**, *90*, 6761–6766.
(29) Collins, D. M.; Spicer, W. E. The Adsorption of CO, O_2 and H_2 on Pt. *Surf. Sci.* **1977**, *69*, 85–113.
(30) Fu, Q.; Luo, Y. Catalytic Activity of Single Transition-Metal Atom Doped in Cu(111) Surface for Heterogeneous Hydrogenation. *J. Phys. Chem. C.* **2013**, *117*, 14618–14624.

8.6. Collaborations

Nanoparticle catalysts experiments were performed by Junjun Shan and the Stephanopoulos Group from the Department of Chemical and Biological Engineering at Tufts University.

Chapter 9: Controlling H_2 Activation, Spillover, and Desorption with Pd-Au *Single Atom Alloys*

This chapter was modified from an original publication of the same title by F. R. Lucci et al. from the Journal of Physical Chemistry Letters, volume 7, pages 480 - 485.

9.1. Introduction

A key requirement in the efficient use of heterogeneous catalysts, fuel cells and hydrogen storage devices is the ability to activate, uptake and release hydrogen easily.[1–3] Metallic surfaces that bind H weakly can exhibit high catalytic selectivity; however, these surfaces often have high activation barriers for H_2 dissociation which limits the activity of the catalysts.[4,5] One viable approach to produce weakly bound H atoms on the surface of catalysts is to use a bimetallic alloy that combines reactive catalytic metals with inert coinage metals.[6–9] This alloy combination includes a catalytic metal that exhibits facile H_2 dissociation and a coinage metal that can utilize the weakly bound H atoms to catalyze hydrogenation reactions.[10–14]

Au nanoparticles have been recently shown to catalyze highly selective hydrogenation and oxidation reactions due to the weak adsorption energy of H and O on Au.[15–18] The addition of Pd into Au changes the catalytic activity and selectivity for multiple reactions including vinyl acetate synthesis,[19] hydrogen peroxide synthesis,[20] hydrocarbon hydrogenation,[21,22] CO oxidation,[23] and oxidation of alcohols to aldehydes.[24] For many of these reactions, the size and dispersion of the Pd atom clusters have an impact on the observed chemistry; the so-called ensemble effect in alloy catalysis.[25,26] Selective synthesis of vinyl acetate[19,27] and hydrogen peroxide[20] relies on the inability of Pd monomers to activate O_2 while CO oxidation requires Pd dimers to dissociate O_2.[23] For H_2 activation on

Pd-Au, the necessary ensemble size has been debated. Yu *et al.* and Maroun *et al.* concluded that contiguous Pd atoms are required for H_2 activation.[28,29] But, density functional theory (DFT) calculations by Venkatachalam *et al.* indicated that Pd monomers may be capable of H_2 activation.[30] However, so far no experimental evidence exists demonstrating this single atom chemistry. Furthermore, CO is a common poison for catalysts. An understanding of CO interaction with adsorbed molecules and competition for actives sites is important when designing new catalysts. Hence, an atomic level understanding of reactive sites for CO adsorption and H_2 activation will elucidate the minimal Pd ensemble capable of activating H_2 and reveal the energetic landscape for uptake, spillover and release of H and CO.

9.2. Results and Discussion

To probe the ability of Pd monomers in Au to activate H2 and to induce spillover of H atoms onto Au, we studied the fundamental processes of dissociation, spillover, and desorption using the complementary techniques of scanning tunneling microscopy (STM), temperature programmed desorption (TPD) and density functional theory (DFT). STM enables direct visualization of the atomic composition of the active sites necessary for H_2 activation and TPD allows us to elucidate key parts of the energy landscape for activation, spillover and desorption. By studying dilute concentrations of Pd atoms ($\leq$5%) in Au, we observe facile dissociation and low temperature recombinative desorption of H_2 from isolated Pd atoms in Au(111). Our Pd-Au single atom alloy (SAA) data contrast with previous studies that suggested at least two contiguous Pd atoms are required for H_2 dissociation,[28,29] although this previous work lacked an atomic scale characterization of the alloy surface. Furthermore, we have discovered that the coadsorption of H and CO forces H to spill over from the active Pd sites to Au. By comparing H_2 and CO desorption temperatures to calculated adsorption

energies of H and CO, we elucidate the energetic pathway for the adsorption, spillover, and desorption of H with and without CO from Pd monomers in Au.

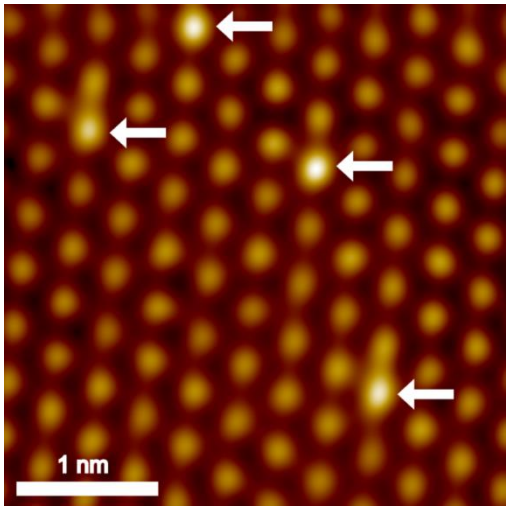

Figure 9.1. Pd-Au(111) SAA
Isolated Pd atoms (highlighted by arrows) substituted into the Au(111) surface appear slightly topographically higher than the Au host.

In order to determine if Pd monomers in Au are capable of H_2 activation, we first generated Pd-Au(111) alloys with isolated Pd atoms present in the surface layer (Figure 9.1). Pd-Au(111) alloys formed by the vapor deposition of Pd on Au(111) have been extensively characterized.[29,31–35] Depending on the surface temperature and flux of incoming Pd atoms during alloying, a range of structures can be formed from isolated atoms substituted into the surface and subsurface layers of Au to Pd rich nanoparticles on the surface.[31–33] At low Pd coverages (≤0.05 ML), Pd atoms exist as isolated atoms substituted into the Au lattice. Due to stronger heteroatom bonds, Pd atoms prefer to be surrounded by Au atoms and exist as isolated species at low coverages.[30,36,37] At Pd coverages > 0.05 ML, the Pd atoms begin to cluster due to a kinetic limitation on the dispersion of the Pd atoms in Au.[31] In the present study, all Pd-Au(111) alloys were prepared at 380 K yielding an alloyed surface where Pd atoms predominately exist as monomers in the Au surface at coverages below 0.05 ML.

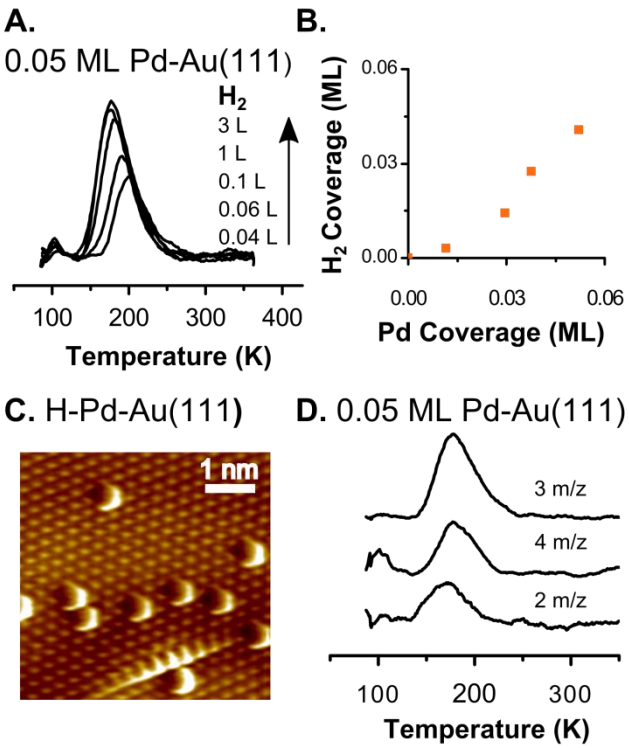

Figure 9.2. H_2 activation on Pd-Au SAAs
(A) TPD spectra of H_2 desorption from a 0.05 ML Pd-Au(111) SAA after exposure to H_2 at 85 K. (B) H_2 coverage on varying concentrations of Pd in the SAA regime. (C) STM image of Pd-Au(111) SAA exposed to H_2 and cooled to 5 K for imaging at -1 V and 1 nA. (D) Desorption traces for *m/z* 2, 3, and 4 from Pd-Au SAA with equivalent H_2 and D_2 coverages.

Using TPD, we investigated the ability of isolated Pd atoms to dissociate H_2 (Figure 9.2). We prepared Pd-Au(111) SAA with between 0.01 and 0.05 ML Pd and exposed them to H_2 at 85 K and observed the desorption of H_2 at 110 K and 175 K (Figure 9.2A). The predominant desorption peak at 175 K is due to H_2 desorption from single Pd atoms because increasing the Pd coverage leads to a linear increase in the area of the peak. In the absence of Pd atoms, no desorption of H_2 is observed from bare Au(111) after the same exposure to H_2. The desorption temperature of H_2 at 175 K indicates H_2 dissociates on the surface since molecular H_2 desorbs from metal surfaces at < 30 K.[38,39] Furthermore, our data shows that the desorption of H_2 from Pd monomers is significantly lower than the desorption of H_2 from Pd(111) which occurs at 310 K.[40] The small desorption peak seen in Figure 9.2A at 110 K is

due to desorption of H_2 from Au sites as previously reported by Pan *et al.* who adsorbed H atoms onto Au(111) using a H atom source in order to overcome the dissociation barrier.[41] Additionally, in order to determine the desorption order of H_2, we varied the surface coverage of H. With increasing H coverage, the desorption peaks shift to lower temperatures indicative of second order desorption as previously observed for disordered Pd-Au alloys.[28]

Figure 9.2B shows that in the single atom regime (≤0.05 ML), the amount of H_2 desorbing from the surface is proportional to the amount of Pd atoms present in the surface with an average of 1.4 ± 0.1 H atoms per Pd atom. One to three H atoms are predicted by DFT to be thermodynamically stable in the three-fold hollow sites surrounding Pd monomers in Au.[30] Small amounts of H atoms may spill over from the Pd sites to Au, but we are unable to quantify the amount of H_2 desorbing from Au since H_2 begins desorbing at the start of the temperature ramp. With STM we imaged Pd-Au(111) SAAs exposed to H_2 and observed localized protrusions in the vicinity of edge-dislocations where Pd atoms predominately reside (Figure 9.2C). In accord with our TPD results, we suggest the enlarged appearance of the Pd atoms is due to the presence of H atoms at the Pd monomer sites. DFT and STM experiments support the suggestion that H atoms are thermodynamically stable on Pd-Au alloys.[30,42,43]

To further probe the H_2 activation and H atom mobility on Pd-Au SAAs we co-adsorbed H_2 and D_2 onto Pd-Au SAA (Figure 9.2D). When H_2 and D_2 were deposited on the SAA, we observed desorption of H-D (*m/z* 3). This scrambling provides direct evidence that Pd-Au SAAs are indeed capable of H_2 activation at 85 K. Furthermore, when equal amounts of H_2 and D_2 were activated, the H_2:HD:D_2 product ratio was 1:2:1 demonstrating complete scrambling of H and D. In terms of the energetics of this scrambling, H atoms will diffuse

away from Pd sites onto Au by overcoming the diffusion barrier (0.244 eV or 0.302 eV depending on diffusion pathway) onto the Au surface (Table S1[57]). Once on Au, H and D atoms move very quickly due to the small diffusion barrier on Au (0.067 eV).[44] At 120 K (i.e. 5 K below the onset of the desorption peak of H_2/HD/D_2 from Pd sites on the surface) the rate of diffusion away from Pd sites is 640 or 2 Hz depending on diffusion pathway and assuming a pre-exponential factor of 10^{13}. Therefore, given the heating rate is 1 K/sec the H and D atoms at Pd sites would be statistically scrambled before desorption of H_2/HD/D_2 and hence the observed 1:2:1 ratio.

As a second probe of the surface chemistry of Pd-Au SAAs, we studied the adsorption of CO, a common catalyst poison. Figure 9.3 shows that after exposure of a Pd-Au SAA to CO, a CO desorption peak is observed at 270 K corresponding to an adsorption energy of -0.9 eV assuming a pre-exponential factor of 10^{15}.[45,46] DFT, with various exchange-correlation functionals, is known to overestimate CO adsorption strength and likewise our DFT predicts the adsorption energy to be -1.34 eV.[47,48] Most importantly, this is a significantly lower desorption temperature (270 K) than observed from pure Pd(111) (> 450 K).[49] CO is also seen to desorb from Au terraces at < 170 K and from Au step edges at 180 K.[50] Low temperature desorption of CO from Pd-Au alloys has been reported for isolated Pd atoms in Au-Pd(111)[32] and Au-Pd-Mo(110).[51] Ruff *et al.* reported that the low desorption temperature of CO from Pd-Au alloys is due to the size of the Pd ensembles in Au.[32] Larger Pd ensembles increase the adsorption energy of CO to the surface. The weak adsorption of CO to Pd-Au SAAs that we observe is important for both catalyst and fuel cells applications in which active site poisoning by CO can be a serious issue.

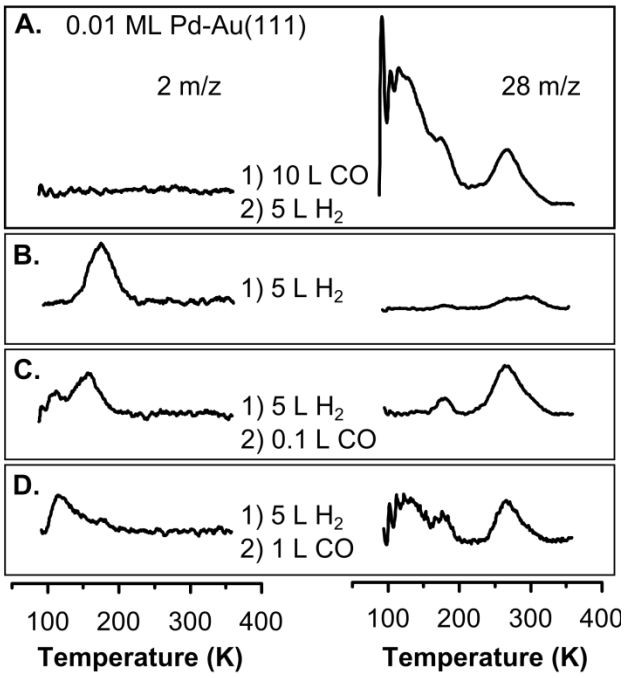

Figure 9.3. TPD traces for H_2 and CO from Pd-Au SAA
TPD traces for H_2 (left, *m/z* 2) and CO (right, *m/z* 28) desorption from Pd-Au SAA surfaces exposed to varying amounts of H_2 and CO. In panel A, 10 L CO is adsorbed and then 5 L H_2. In panel B, 5 L H_2 is exclusively adsorbed. In panel C, 5 L H_2 is adsorbed and then 0.1 L CO. In panel D, 5 L H_2 is adsorbed and then 1 L CO.

We discovered that CO can enhance the spillover of H atoms from Pd sites to Au where H_2 predominantly desorbs. Figure 9.3 shows TPD traces for the co-adsorption of H and CO where the desorption temperature of H_2 is dependent on the CO exposure. In the absence of CO, H_2 desorbs from Pd sites at 175 K (Figure 9.3B). At sub-saturation coverages of CO (0.1 L CO), we observed desorption of H_2 from both Pd (160 K) and Au (110 K) sites (Figure 9.3C). When the surface was exposed to 5 L H_2 followed by 1 L CO, all H_2 desorbs from the surface at 110 K since all the Pd atoms are saturated with CO (Figure 9.3D). Thus, it appears that when CO adsorbs on a H covered SAA surface, CO forces the H atoms on to the Au(111) terraces from where they desorb at a significantly lower temperature than otherwise observed in the absence of CO.

To further understand this desorption behavior, periodic DFT calculations were performed on unreconstructed Au(111) surfaces with the VASP 5.3.3[52,53] code employing the optB86b-vdW[54,55] exchange-correlation functional, which accounts for dispersion forces within the vdW-DF scheme of Dion et al[56] (see the Supporting Information[57] for more details of the computational setup and energy definitions). In our DFT calculations a variety of CO, H, and CO plus H adsorption structures were considered. With regard to the observed tendency of CO to drive H atoms away from the Pd sites of the SAA, our DFT calculations show that there is a strong repulsion between adsorbed CO and H. Specifically, when CO is adsorbed on the atop Pd site and H is in one of the adjacent three-fold hollow sites that surround the Pd atom there is a *ca.* 0.56 eV repulsion between CO and H (Table S4[57]). This repulsion can be reduced to only 0.01 -0.02 eV if the H atom moves away to a proximal hollow site surrounded by only surface Au atoms. Therefore, despite H atom spillover being unfavorable, when CO adsorbs to the Pd sites, it becomes favorable for H to move onto Au(111). Furthermore, if CO is adsorbed on the surface prior to H_2, no H_2 is observed desorbing from the surface. Therefore, CO binds to the Pd sites and blocks the adsorption and activation of H_2 which further supports our hypothesis that Pd atoms are the sites responsible for H_2 activation (Figure 9.3A). For a CO covered Pd(111), it has previously been shown that CO blocks the dissociative adsorption of H_2.[58] Also, related to these results, previous studies have demonstrated that the adsorption of CO on bimetallic alloys alters the desorption behavior of H_2. For $Pd_{70}Au_{30}$(110) alloys, the co-adsorption of CO and H increases the desorption temperature of H due to a trapping of near surface H.[59] A similar effect was observed for Pd-Cu alloys where CO selectively binds to the single Pd atoms in Cu and blocks the Pd entrance/exit sites for H_2 adsorption/desorption.[60] This mechanism,

called the *molecular cork effect*, allows H atoms to remain on the surface beyond their normal desorption temperature. Additionally, for Co nanoparticles supported on Cu(111), CO forces the spillover of H from Co to Cu sites via two-dimensional pressure.[61,62] However, the co-adsorption of CO on Pd-Au SAAs investigated in this study changes the H_2 desorption site. CO adsorption forces the H from the Pd sites to Au where it is weakly bound and it desorbs at 110 K; therefore, addition of CO alters the exit site for H_2 as shown in Figure 9.4.

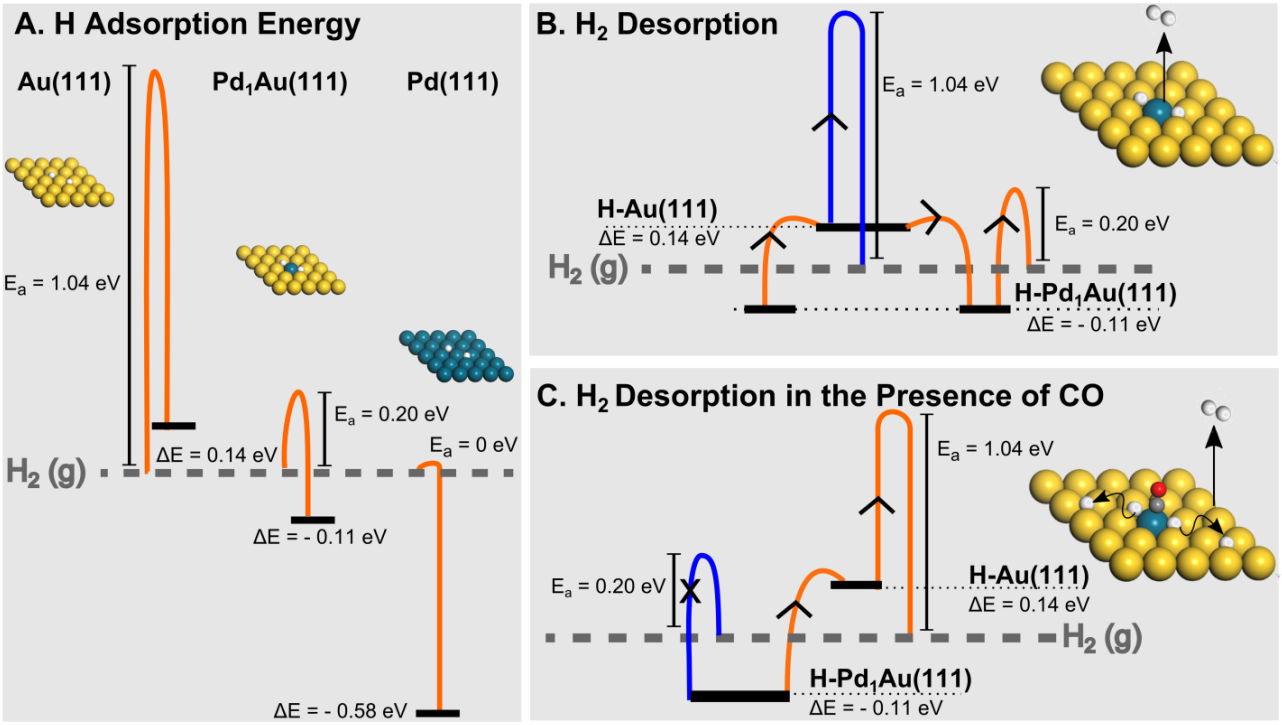

Figure 9.4. Schematics of the energy landscapes for H_2 adsorption and desorption from Pd-Au SAA

(A) H_2 activation energy (E_a) per H_2 molecule, and H adsorption energy (ΔE) per H atom in fcc sites on monometallic Au, Pd and Pd-Au SAA. Energetics of H_2 desorption for Pd-Au SAA (B) without and (C) with CO. Schematic illustrates the preferred active sites for H_2 dissociation as well as preferred adsorption sites for H and CO. Preferred and minor desorption pathways are displayed in orange and blue, respectively. In (B) the preferred pathway for H_2 desorption is via the Pd site. In (C) the Pd site is blocked by CO, so H atoms spillover to Au and then desorb from there. All energies are reported relative to H_2 in the gas phase, as noted by the dashed horizontal lines. Note that E_a for H_2 on Au(111) calculated by DFT (which doesn't account for quantum nuclear effects) may in fact be a large overestimate of the barrier, as experimentally H_2 desorbs from Au(111) at 110 K.

Combining our TPD results with DFT calculations (Table S1-S4[57]), we have elucidated the potential energy landscape for H_2 activation, diffusion and desorption from Pd-Au SAAs (Figure 9.4). The facile H_2 activation and weak adsorption of H atoms observed for Pd-Au SAAs are very different from those on monometallic Pd and Au surfaces (Figure 9.4A). On Au(111), H_2 activation and H adsorption is kinetically and thermodynamically unfavorable, respectively.[5,43,63] In order for H_2 from the gas phase to adsorb onto Au(111), it must overcome a large activation barrier, which we calculated to be 1.04 eV, in agreement with other DFT calculations.[5,63] Additionally, H adsorption on fcc sites of Au(111) is thermodynamically unfavorable with respect to gas phase H_2 by 0.14 eV, within the current computational set-up. H_2 adsorption onto Pd(111), however, is a non-activated (barrier-less) process, with the resulting H atoms adsorbing strongly at fcc sites of Pd(111) with an adsorption energy of -0.58 eV per H adatom. With Pd-Au SAAs, we observed facile H_2 activation compared to Au and low temperature desorption of H_2 compared to Pd. For dilute concentrations of Pd in Au, we report H_2 dissociation at 85 K indicating that Pd monomers greatly reduce the activation barrier for the dissociation of H_2 compared to Au(111). Our DFT calculations support a reduction in the activation energy on SAAs, since the transition state energy for H_2 adsorption on Pd-Au SAA is 0.20 eV compared to 1.04 eV for Au(111). However, it is important to note that the calculated transition state energies do not account for quantum nuclear effects which are likely to lower the barriers and make hydrogen dissociation more facile. This is what is observed experimentally as H_2 desorbs from Au(111) at 110 K which infers a barrier lower than that calculated by DFT. Indeed, previously we have shown with path-integral based DFT simulations for atomic and molecular hydrogen the effective free energy barrier for adsorption/desorption can be dramatically lowered due to

quantum mechanical tunneling.[64,65] After dissociation, H binds to a Pd-Au fcc site with a computed adsorption energy of -0.11 eV. The negative adsorption energies correspond to exothermic adsorption processes, which are significantly weaker than when H binds to pristine Pd(111) (-0.58 eV) (Figure 9.4). The smaller adsorption energy of H to Pd-Au sites compared to Pd(111) occurs mainly because H binds in 3-fold hollow sites composed of 1 Pd atom and 2 Au atoms.[32,66] In order to adhere to microscopic reversibility, the adsorption and desorption of H_2 must follow the lowest energy pathway which is via the isolated Pd atoms in Au. The total desorption barrier is dependent on the H_2 activation energy and H adsorption energy which is directly related to the observed desorption temperatures. In order for H_2 to desorb from Pd-Au SAA, H atoms overcome both the weak adsorption energy of H to the Pd-Au sites and the reduced H_2 activation barrier of Pd monomers (Figure 9.4B). Due to the thermodynamic instability of H atoms on Au, H atoms adsorb preferentially at Pd-Au sites, but a small quantity of H atoms exist on Au due to spillover from Pd-Au sites. The H atoms that exist on Au desorb directly from Au(111). Though the overall desorption temperature of H_2 from Au is less than the desorption temperature from Pd-Au sites, H_2 predominately desorbs from Pd-Au sites because they are more strongly bound there.

When we consider the co-adsorption of H and CO we find that the desorption pathway of H_2 from the alloyed surface is altered (Figure 9.4C). Our DFT calculations reveal a greater thermodynamic stability for CO to occupy Pd-Au sites instead of H atoms. The adsorption of CO (-1.34 eV) on Pd monomers is significantly stronger than the adsorption of H to Pd monomers (-0.11 eV). Therefore, when a H covered Pd-Au surface is exposed to CO at 85 K, the H atoms are forced from the Pd-Au to Au sites. Although it is thermodynamically unfavorable for H to adsorb on pure Au, the H_2 recombination barrier

traps it there until 110 K at which point H_2 desorbs from Au sites. CO changes the exit sites for H_2 from Pd atoms to Au sites without violating microscopic reversibility since the addition of CO makes the forward and reverse pathways non-equivalent. Interestingly, CO can force H atoms to spill over from a preferred site to a thermodynamically unstable site and remain trapped on the surface by the recombination barrier.

9.3. Summary

By utilizing well-defined Pd-Au model surfaces, we experimentally demonstrate that Pd monomers in a Au(111) surface can activate H_2, a process suggested by other experiments to require two contiguous Pd atoms. We clearly show by coupling high resolution STM with TPD, low concentrations of individual, isolated Pd atoms can dissociate H_2 since the concentration of adsorbed H atoms is proportional to the surface concentration of Pd atoms in Au. Combining TPD with DFT calculations, we elucidate the energetic landscape for H_2 adsorption, activation, and desorption from isolated Pd atoms revealing a low temperature pathway for H_2 activation and release through the Pd atoms with minimal spillover to Au. The co-adsorption of H_2 and D_2 leads to complete scrambling of H and D supporting the dissociation of H_2 and the transient existence of H atoms on Au. Additionally, Pd-Au SAAs bind CO significantly more weakly than Pd(111) (270 K vs. 450 K) which can potentially improve CO tolerance of the catalysts. The competitive adsorption of CO and H on the Pd atoms forces H atoms to spillover onto the Au surface altering the desorption pathway to an even lower temperature through Au (110 K vs. 175 K). Our work demonstrates that individual, isolated Pd atoms in Au allow for facile H_2 activation and weak adsorption of H atoms, a key requirement for efficient and selective hydrogenation catalysis.

9.4. Additional Experimental Details

Surfaces were exposed to H_2 (99.9 % Airgas) by backfilling the chamber to the required pressure through high precision leak valves while the sample was held at 85 K. H_2 coverages were determined by the saturation coverage of unity for H_2 adsorbed on 5 ML of Pt, assuming the surface terminates as Pt(111). Pt coverages were quantified by CO (99.99 % Airgas) titration by saturating with CO (10 L) and comparing the ratio between CO desorption from Cu sites (<200 K) and Pt sites (> 300 K). CO binds atop to isolated Pt atoms in Cu similar to CO binding to isolated Pt atoms in Au[67,68] and isolated Pd atoms in Cu.[60] We also accounted for the known saturation packing density of CO on Cu(111) (0.52 ML). [69]

9.5. References

(1) Hagen, J. *Industrial Catalysis*, 2nd ed.; Wiley-VCH Verlag GMbH & Co: Weinheim, 2006.

(2) Ritter, J. A.; Ebner, A. D. State-of-the-Art Adsorption and Membrane Separation Processes for Hydrogen Production in the Chemical and Petrochemical Industries. *Sep. Sci. Technol.* **2007**, *42*, 1123–1193.

(3) Graetz, J. New Approaches to Hydrogen Storage. *Chem. Soc. Rev.* **2009**, *38*, 73–82.

(4) Nørskov, J. K.; Bligaard, T.; Logadottir, A.; Bahn, S.; Hansen, L. B.; Bollinger, M.; Bengaard, H.; Hammer, B.; Sljivancanin, Z.; Mavrikakis, M.; et al. Universality in Heterogeneous Catalysis. *J. Catal.* **2002**, *209*, 275–278.

(5) Hammer, B.; Nørskov, J. K. Why Gold Is the Noblest of All the Metals. *Nature* **1995**, *376*, 238–240.

(6) Greeley, J.; Mavrikakis, M. Alloy Catalysts Designed from First Principles. *Nat. Mater.* **2004**, *3*, 810–815.

(7) Fu, Q.; Luo, Y. Catalytic Activity of Single Transition-Metal Atom Doped in Cu(111) Surface for Heterogeneous Hydrogenation. *J. Phys. Chem. C.* **2013**, *117*, 14618–14624.

(8) Skoplyak, O.; Barteau, M. A.; Chen, J. G. Reforming of Oxygenates for H2 Production: Correlating Reactivity of Ethylene Glycol and Ethanol on Pt(111) and Ni/Pt(111) with Surface D-Band Center. *J. Phys. Chem. B* **2006**, *110*, 1686–1694.

(9) Alayoglu, S.; Nilekar, A. U.; Mavrikakis, M.; Eichhorn, B. Ru-Pt Core-Shell Nanoparticles for Preferential Oxidation of Carbon Monoxide in

Hydrogen. *Nat. Mater.* **2008**, *7*, 333–338.
(10) Kyriakou, G.; Boucher, M. B.; Jewell, A. D.; Lewis, E. A.; Lawton, T. J.; Baber, A. E.; Tierney, H. L.; Flytzani-Stephanopoulos, M.; Sykes, E. C. H. Isolated Metal Atom Geometries as a Strategy for Selective Heterogeneous Hydrogenations. *Science* **2012**, *335*, 1209–1212.
(11) Boucher, M. B.; Zugic, B.; Cladaras, G.; Kammert, J.; Marcinkowski, M. D.; Lawton, T. J.; Sykes, E. C. H.; Flytzani-Stephanopoulos, M. Single Atom Alloy Surface Analogs in $Pd_{0.18}Cu_{15}$ Nanoparticles for Selective Hydrogenation Reactions. *Phys. Chem. Chem. Phys.* **2013**, *15*, 12187–12196.
(12) Pei, G. X.; Liu, X. Y.; Wang, A.; Li, L.; Huang, Y.; Zhang, T.; Lee, J. W.; Jang, B. W. L.; Mou, C.-Y. Promotional Effect of Pd Single Atoms on Au Nanoparticles Supported on Silica for the Selective Hydrogenation of Acetylene in Excess Ethylene. *New. J. Chem.* **2014**, *38*, 2043–2051.
(13) Zhang, L.; Wang, A.; Miller, T.; Liu, X.; Yang, X.; Wang, W.; Li, L.; Huang, Y.; Mou, C.; Zhang, T. Efficient and Durable Au Alloyed Pd Single-Atom Catalyst for the Ullmann Reaction of Aryl Chlorides in Water. *ACS Catal.* **2014**, *4*, 1546–1553.
(14) Cao, X.; Ji, Y.; Luo, Y. Dehydrogenation of Propane to Propylene by a Pd/Cu Single-Atom Catalyst: Insight from First-Principles Calculations. *J. Phys. Chem. C* **2015**, *119*, 1016–1023.
(15) Claus, P. Heterogeneously Catalysed Hydrogenation Using Gold Catalysts. *Appl. Catal.* **2005**, *291*, 222–229.
(16) Mcewan, L.; Julius, M.; Roberts, S.; Fletcher, J. C. Q. A Review of the Use of Gold Catalysts in Selective Hydrogenation Reactions. *Gold Bull.* **2010**, *43*, 298–306.
(17) Haruta, M. Size- and Support-Dependency in the Catalysis of Gold. *Catal. Today* **1997**, *861*, 153–166.
(18) Mohr, C.; Hofmeister, H.; Radnik, J.; Claus, P. Identification of Active Sites in Gold-Catalyzed Hydrogenation of Acrolein. *J. Am. Chem. Soc.* **2003**, *103*, 178–180.
(19) Chen, M.; Kumar, D.; Yi, C.; Goodman, D. W. The Promotional Effect of Gold in Catalysis by Palladium-Gold. *Science* **2005**, *310*, 291–293.
(20) Edwards, J. K.; Solsona, B.; Ntainjua N, E.; Carley, A. F.; Herzing, A. A.; Kiely, C. J.; Hutchings, G. J. Switching off Hydrogen Peroxide Hydrogenation in the Direct Synthesis Process. *Science* **2009**, *323*, 1037–1041.
(21) Choudhary, T. V; Sivadinarayana, C.; Datye, A. K.; Kumar, D.; Goodman, D. W. Acetylene Hydrogenation on Au-Based Catalysts. *Catal. Letters* **2003**, *86*, 1–8.
(22) Hugon, A.; Delannoy, L.; Krafft, J. M.; Louis, C. Selective Hydrogenation of 1,3-Butadiene in the Presence of an Excess of Alkenes over Supported Bimetallic Gold−palladium Catalysts. *J. Phys. Chem. C.* **2010**, *114*, 10823–10835.
(23) Gao, F.; Wang, Y.; Goodman, D. W. CO Oxidation over AuPd(100) from Ultrahigh Vacuum to near-Atmospheric Pressures: The Critical Role of

Contiguous Pd Atoms. *J. Am. Chem. Soc.* **2009**, *131*, 5734–5735.
(24) Enache, D. I.; Edwards, J. K.; Landon, P.; Solsona-Espriu, B.; Carley, A. F.; Herzing, A. A.; Watanabe, M.; Kiely, C. J.; Knight, D. W.; Hutchings, G. J. Solvent-Free Oxidation of Primary Alcohols to Aldehydes Using Au-Pd/TiO_2 Catalysts. *Science* **2006**, *311*, 362–365.
(25) Rodriguez, J. A.; Rodriguex, J. A. Physical and Chemical Properties of Bimetallic Surfaces. *Surf. Sci. Rep.* **1996**, *24*, 223–287.
(26) Groß, A. Reactivity of Bimetallic Systems Studied from First Principles. *Top. Catal.* **2006**, *37*, 29–39.
(27) Neurock, M.; Tysoe, W. T. Mechanistic Insights in the Catalytic Synthesis of Vinyl Acetate on Palladium and Gold/Palladium Alloy Surfaces. *Top. Catal.* **2013**, *56*, 1314–1332.
(28) Yu, W. Y.; Mullen, G. M.; Mullins, C. B. Hydrogen Adsorption and Absorption with Pd-Au Bimetallic Surfaces. *J. Phys. Chem. C* **2013**, *117*, 19535–19543.
(29) Maroun, F.; Ozanam, F.; Magnussen, O. M.; Behm, R. J. The Role of Atomic Ensembles in the Reactivity of Bimetallic Electrocatalysts. *Science* **2001**, *293*, 1811–1814.
(30) Venkatachalam, S.; Jacob, T. Hydrogen Adsorption on Pd-Containing Au(111) Bimetallic Surfaces. *PCCP* **2009**, *11*, 3010.
(31) Baber, A. E.; Tierney, H. L.; Sykes, E. C. H. Atomic-Scale Geometry and Electronic Structure of Catalytically Important Pd/Au Alloys. *ACS Nano.* **2010**, *4*, 1637–1645.
(32) Ruff, M.; Takehiro, N.; Liu, P.; Nørskov, J. K.; Behm, R. J. Size-Specific Chemistry on Bimetallic Surfaces: A Combined Experimental and Theoretical Study. *ChemPhysChem* **2007**, *8*, 2068–2071.
(33) Casari, C.; Foglio, S.; Siviero, F.; Li Bassi, A.; Passoni, M.; Bottani, C. Direct Observation of the Basic Mechanisms of Pd Island Nucleation on Au(111). *Phys. Rev. B* **2009**, *79*, 1–9.
(34) Barth, J. V.; Brune, H.; Ertl, G.; Behm, R. J. Scanning Tunneling Microscopy Observations on the Reconstructed Au(111) Surface: Atomic Structure, Long-Range Superstructure, Rotational Domains, and Surface Defects. *Phys. Rev. B* **1990**, *42*, 9307–9318.
(35) Meyer, J. A.; Baikie, I. D.; Kopatzki, E.; Behm, R. J. Preferential Island Nucleation at the Elbows of the Au(111) Herringbone Reconstruction through Place Exchange. *Surf. Sci.* **1996**, *365*, 647–651.
(36) Yudanov, I. V; Neyman, K. M. Stabilization of Au at Edges of Bimetallic PdAu Nanocrystallites. *Phys. Chem. Chem. Phys.* **2010**, *12*, 5094–5100.
(37) Yuan, D.; Gong, X.; Wu, R. Atomic Configurations of Pd Atoms in PdAu(111) Bimetallic Surfaces Investigated Using the First-Principles Pseudopotential Plane Wave Approach. *Phys. Rev. B* **2007**, *75*, 085428.
(38) Sugimoto, T.; Fukutani, K. Effects of Rotational-Symmetry Breaking on Physisorption of Ortho- and Para- H_2 on Ag(111). *Phys. Rev. Lett.* **2014**, *112*, 146101–1 – 5.
(39) Andersson, S.; Persson, M. Crystal-Face Dependence of Physisorption Potentials. *Phys. Rev. B* **1993**, *48*, 5685–5688.

(40) Gdowski, G. E.; Felter, T. E.; Stulen, R. H. Effect of Surface Temperature on the Sorption of Hydrogen on Pd(111). *Surf. Sci.* **1987**, *181*, L147–L155.
(41) Pan, M.; Flaherty, D. W.; Mullins, C. B. Low-Temperature Hydrogenation of Acetaldehyde to Ethanol on H-Precovered Au(111). *J. Phys. Chem. Lett.* **2011**, *2*, 1363–1367.
(42) Baber, A. E.; Tierney, H. L.; Lawton, T. J.; Sykes, E. C. H. An Atomic-Scale View of Palladium Alloys and Their Ability to Dissociate Molecular Hydrogen. *Chem. Cat. Chem* **2011**, *3*, 607–614.
(43) Tierney, H. L.; Baber, A. E.; Kitchin, J. R.; Sykes, E. C. H. Hydrogen Dissociation and Spillover on Individual Isolated Palladium Atoms. *Phys. Rev. Lett.* **2009**, *103*, 246102–1 – 4.
(44) Pan, M.; Pozun, Z. D.; Yu, W.; Henkelman, G.; Mullins, C. B. Structure Revealing H/D Exchange with Co-Adsorbed Hydrogen and Water on Gold. *J. Phys. Chem. Lett.* **2012**, *3*, 1894–1899.
(45) Campbell, C. T.; Sellers, J. R. V. The Entropies of Adsorbed Molecules. *J. Am. Chem. Soc.* **2012**, *134*, 18109–18115.
(46) Campbell, C. T.; Sellers, J. R. V. Enthalpies and Entropies of Adsorption on Well-Defined Oxide Surfaces : Experimental Measurements. *Chem. Rev.* **2013**, *113*, 4106–4135.
(47) Schimka, L.; Harl, J.; Stroppa, A.; Grüneis, A.; Marsman, M.; Mittendorfer, F.; Kresse, G. Accurate Surface and Adsorption Energies from Many-Body Perturbation Theory. *Nat. Mater.* **2010**, *9*, 741–744.
(48) Klimeš, J.; Michaelides, A. Perspective: Advances and Challenges in Treating van Der Waals Dispersion Forces in Density Functional Theory. *J. Chem. Phys.* **2012**, *137*, 120901.
(49) Guo, X.; Yates, J. T. Dependence of Effective Desorption Kinetic Parameters on Surface Coverage and Adsorption Temperature: CO on Pd(111). *J. Chem. Phys.* **1989**, *90*, 6761–6766.
(50) Kim, J.; Samano, E.; Koel, B. E. CO Adsorption and Reaction on Clean and Oxygen-Covered Au(211) Surfaces. *J. Phys. Chem. B* **2006**, *110*, 17512–17517.
(51) Yi, C.-W.; Luo, K.; Wei, T.; Goodman, D. W. The Composition and Structure of Pd-Au Surfaces. *J. Phys. Chem. B* **2005**, *109*, 18535–18540.
(52) Kresse, G.; Furthmüller, J. Efficiency of Ab-Initio Total Energy Calculations for Metals and Semiconductors Using a Plane-Wave Basis Set. *Comput. Mater. Sci.* **1996**, *6*, 15–50.
(53) Kresse, G.; Furthmuller, J. Efficient Iterative Schemes for Ab Initio Total-Energy Calculations Using a Plane-Wave Basis Set. *Phys. Rev. B* **1996**, *54*, 11169–11186.
(54) Klimes, J.; Bowler, D. R.; Michaelides, A. Chemical Accuracy for the Van Der Waals Density Functional. *J. Phys. Condens. Matter* **2010**, *22*, 22201.
(55) Klimes, J.; Bowler, D. R.; Michaelides, A. Van Der Waals Density Functionals Applied to Solids. *Phys. Rev. B* **2011**, *83*, 195131.
(56) Dion, M.; Rydberg, H.; Schroder, E.; Langreth, D. C.; Lundqvist, B. I. Van Der Waals Density Functional for General Geometries. *Phys. Rev.*

Lett. **2004**, *24*, 246401.
(57) Lucci, F. R.; Darby, M. T.; Mattera, M. F. G.; Ivimey, C. J.; Therrien, A. J.; Michaelides, A.; Stamatakis, M.; Sykes, E. C. H. Controlling Hydrogen Activation, Spillover, and Desorption with Pd-Au Single Atom Alloys. *J. Phys. Chem. Lett.* **2016**, *7*, 480–485.
(58) Rupprechter, G.; Morkel, M.; Freund, H.; Hirschl, R. Sum Frequency Generation and Density Functional Studies of CO–H Interaction and Hydrogen Bulk Dissolution on Pd(111). *Surf. Sci.* **2004**, *554*, 43–59.
(59) Ogura, S.; Okada, M.; Fukutani, K. Near-Surface Accumulation of Hydrogen and CO Blocking Effects on a Pd − Au Alloy. *J. Phys. Chem. C* **2013**, *117*, 9366–9371.
(60) Marcinkowski, M. D.; Jewell, A. D.; Stamatakis, M.; Boucher, M. B.; Lewis, E. A.; Murphy, C. J.; Kyriakou, G.; Sykes, E. C. H. Controlling a Spillover Pathway with the Molecular Cork Effect. *Nat. Mater.* **2013**, *12*, 523–528.
(61) Lewis, E. A.; Le, D.; Jewell, A. D.; Murphy, C. J.; Rahman, T. S.; Sykes, E. C. H. Visualization of Compression and Spillover in a Coadsorbed System: Syngas on Cobalt Nanoparticles. *ACS Nano* **2013**, *7*, 4384–4392.
(62) Lewis, E. A.; Marcinkowski, M. D.; Murphy, C. J.; Liriano, M. L.; Sykes, E. C. H. Hydrogen Dissociation, Spillover, and Desorption from Cu-Supported Co Nanoparticles. *J. Phys. Chem. Lett.* **2014**, *5*, 3380–3385.
(63) Campbell, C. T. Bimetallic Surface Chemistry. *Annu. Rev. Phys. Chem.* **1990**, *41*, 775–837.
(64) Davidson, E. R. M.; Klimeš, J.; Alfè, D.; Michaelides, A. Cooperative Interplay of van Der Waals Forces and Quantum Nuclear Effects on Adsorption: H at Graphene and at Coronene. *ACS Nano* **2014**, *10*, 9905–9913.
(65) Kyriakou, G.; Davidson, E. R. M.; Peng, G.; Roling, L. T.; Singh, S.; Boucher, M. B.; Marcinkowski, M. D.; Mavrikakis, M.; Michaelides, A.; Sykes, E. C. H. Significant Quantum Effects in Hydrogen Activation. *ACS Nano* **2014**, *8*, 4827–4835.
(66) Boscoboinik, J. A.; Calaza, F. C.; Garvey, M. T.; Tysoe, W. T. Identification of Adsorption Ensembles on Bimetallic Alloys. *J. Phys. Chem. C* **2010**, *114*, 1875–1880.
(67) Pedersen, M. Ø.; Helveg, S.; Ruban, A.; Stensgaard, I.; Lægsgaard, E.; Nørskov, J. K.; Besenbacher, F. How a Gold Substrate Can Increase the Reactivity of a Pt Overlayer. *Surf. Sci.* **1999**, *426*, 395–409.
(68) Eyrich, M.; Diemant, T.; Hartmann, H.; Bansmann, J.; Behm, R. J. Interaction of CO with Structurally Well-Defined Monolayer PtAu/Pt(111) Surface Alloys. *J. Phys. Chem. C* **2012**, *116*, 11154–11165.
(69) Raval, R.; Parker, S. F.; Pemble, M. E.; Hollins, P.; Pritchard, J.; Chesters, M. A. FT-RAIRS EELS LEED Studies of the Adsorption of Carbon Monoxide on Cu(111). *Surf. Sci.* **1988**, *203*, 353–377.

9.6. Collaborations

Density Function Theory experiments were performed by Matthew T. Darby and the Stamatakis Group from the Thomas Young Centre and Department of Chemical Engineering at University College London.

Chapter 10: Hydrogenation Attempts with Pd-Au *Single Atom Alloys*

10.1. Introduction

Pd-Au alloys are well known for their selective hydrogenation and oxidation reactions including vinyl acetate synthesis,[1] hydrogen peroxide synthesis,[2] hydrocarbon hydrogenation,[3,4] CO oxidation,[5] and oxidation of alcohols to aldehydes.[6] Although, they exhibit high selectivity, the ability to activate molecular H_2 and the mechanisms of the sequential hydrogenation reactions are not well understood. In Chapter 9, we showed that Pd monomers in Au(111) are capable of activating H_2, a process that does not occur on Au(111) in ultra-high vacuum (UHV).[7] In this chapter, we probe the desorption of CO and H_2 from various Pd-Au(111) alloy surfaces from 0.01 ML to 1 ML Pd. We show single atom alloys (SAA) have the lowest temperature desorption of H_2 and CO. Then, in order to probe the potential reactivity of Pd-Au SAA, we discuss unsuccessful attempts to hydrogenate a range of hydrocarbons including butadiene, acetaldehyde, acetylene, phenyl acetylene, and styrene. Though Pd-Au(111) SAAs can readily activate H_2 at low temperatures, the surface is unable to catalyze hydrogenation reactions in UHV.

10.2. Results and Discussion

Prior to hydrogenation reactions, H_2 and CO desorption from Pd-Au(111) alloys prepared at 380 K were extensively characterized using Temperature Programmed Desorption (TPD). CO desorption was used to extrapolated the alloy structure. As shown in Figure 10.1, at low coverages of Pd (< 0.01 monolayer (ML)), CO desorb at 270 K. With increasing Pd coverages, the CO trace broadens and a high temperature shoulder at 350 K

develops followed by another peak at 450 K at 0.08 ML. The peak at 450 K eventually saturates after depositing Pd for 60 min, thus we conclude 1 ML Pd is formed after 60 min of Pd deposition.

The structure of Pd-Au(111) alloys have been extensively characterized with STM.[8–13] Initially Pd atoms alloy into Au at the edge dislocations of the herringbone reconstruction. As the Pd coverage increases, small Pd clusters develop in the surface layer. The Pd clusters then serve as nucleation sites for Pd islands. Thus, we propose the peak at 270 K is due to isolated Pd atoms in Au, the peak at 350 K is due Pd clusters in the surface, and the peak at 450 K is Pd islands, a temperature identical to CO desorption from Pd(111).[14]

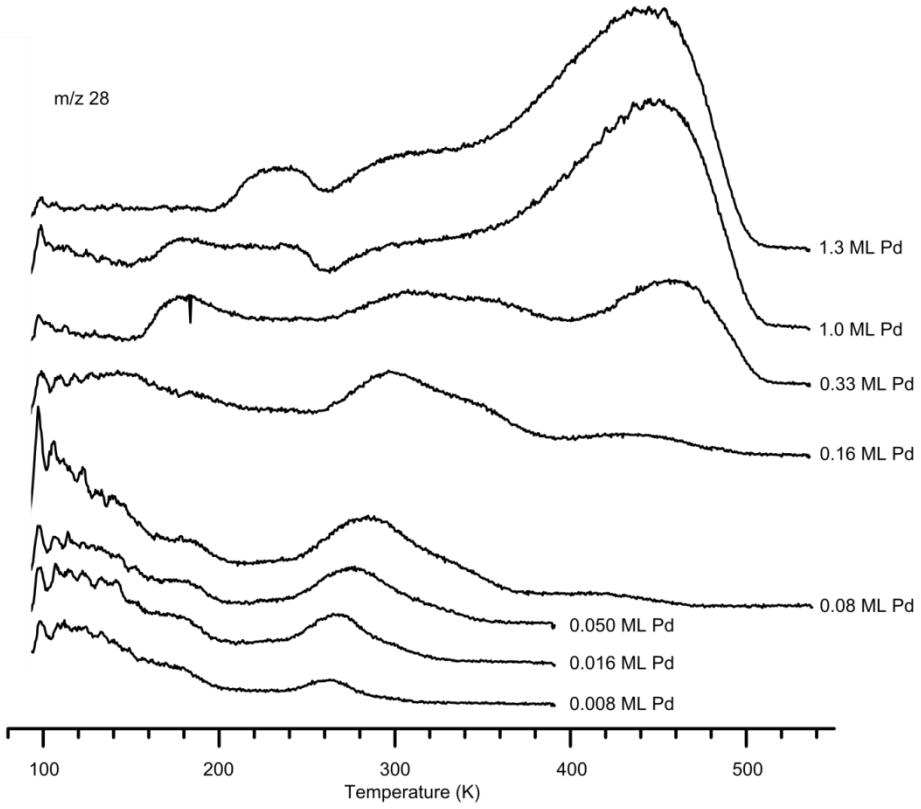

Figure 10.1. CO desorption from Pd-Au(111) alloys
Varying Pd coverages were deposited onto Au(111) at 380 K and exposed to 10 L CO.

On the various surface morphologies, we then probed H_2 desorption. Initially at low Pd coverages (< 0.05 ML Pd), a symmetrical H peak is observed desorbing at 175 K (Figure 10.2). With increasing Pd coverages, the peak continues to broaden. An additional peak develops at 300 K which saturates at 1 ML Pd. The H_2 desorption peak becomes asymmetrical at coverages > 0.05 ML Pd due to overlapping peaks, thus we conclude the single atom regime is < 0.05 ML. For high coverages of Pd, a low temperature H_2 peak is observed between 165 K and 190 K. The low temperature peak is due to subsurface H in Pd. Subsurface H_2 has been previously reported desorbing between 150 – 170 K for Pd(111) that was absorbed at temperatures as low as 90 K.[15]

Most importantly, after accounting for differences in ionization cross sections, the areas of the peaks for H_2 and CO from Pd-Au alloys are roughly proportional to one another. Since CO binds atop to isolated Pd atoms in Au, the CO coverage is directly correlated to the Pd surface concentration in the single atom regime (< 0.05 ML). Since H and CO are also proportional, we conclude that the Pd coverage directly dictates the H coverage. Since the ratio between H_2:CO:Pd is 1:1:1, we do not observe any H spillover from the Pd site activation sites to Au.

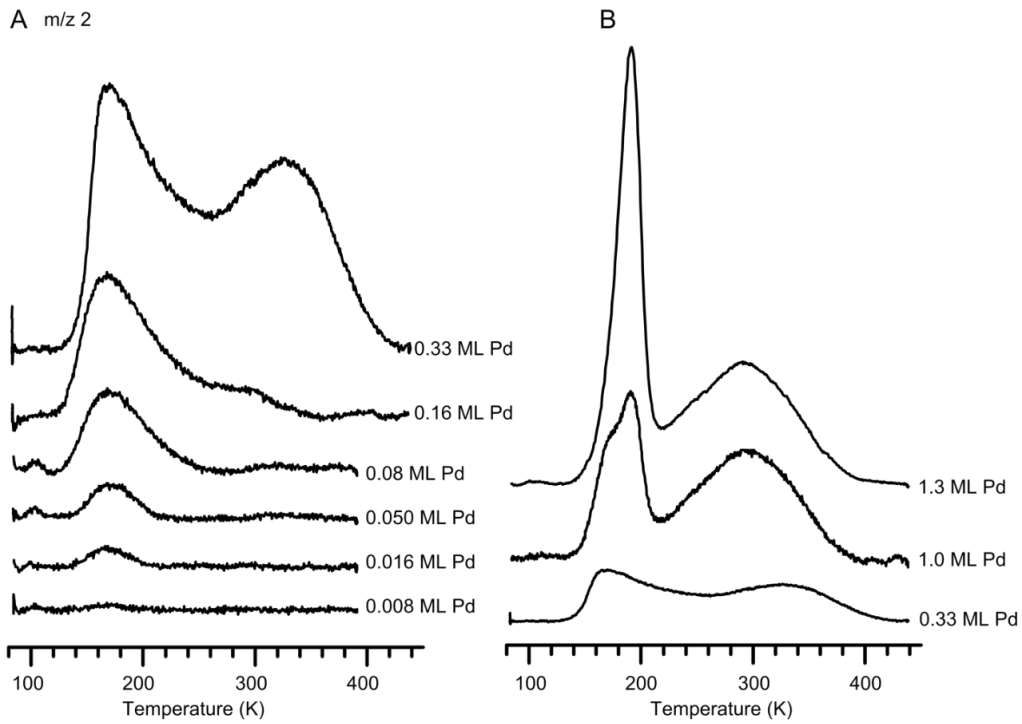

Figure 10.2. H_2 desorption from Pd-Au(111) alloys
Varying Pd coverages were deposited onto Au(111) at 380 K.

After extensively probing Pd-Au(111) alloys with H and CO, acetaldehyde hydrogenation was attempted using TPD/R (Figure 10.3A). Carbonyl groups exhibit faster hydrogenation kinetics in the gas phase compared to alkene since carbonyl groups are better able to stabilize intermediates states. Carbonyl groups, however, have stronger π bonds then alkenes as shown with π bond dissociation energies of ~85 kcal/mol (C=O) and ~65 kcal/mol (C=C), respectively. Thus, in order to probe the hydrogenation of aldehydes, sub-monolayer coverages of acetaldehyde were adsorbed onto Pd-Au(111) SAA and it desorbed at 150 K. When acetaldehyde was co-adsorbed with H, the hydrogenation product ethanol was not observed. Preliminary results by Matthew Marcinkowski also suggest that Pt-Cu(111) SAAs are unable to hydrogenate acetaldehyde in UHV.

Previously, Pan *et al* detected the hydrogenation of acetaldehyde to ethanol on Au(111) in UHV.[16] In that study, reactively formed ethanol was observed desorbing from the surface at 190 K. A complex hydrogenation mechanism was proposed where poly-acetaldehyde species were integrated with H atoms that then decomposed to ethanol and acetaldehyde. This mechanism was proposed because co-adsorption of H and acetaldehyde yielded a high temperature acetaldehyde peak (210 K) that desorbed concurrently with reactively formed ethanol.

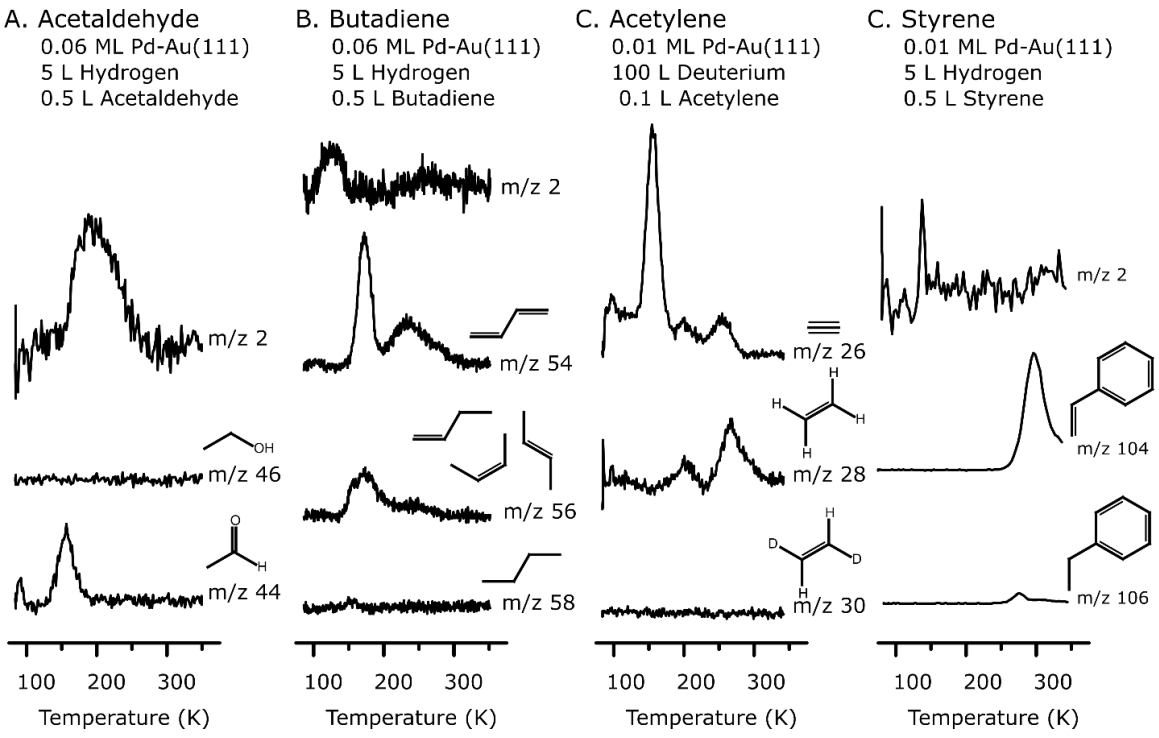

Figure 10.3. TPD/R for co-adsorption of H_2 and various hydrocarbons
Shown are traces for attempted hydrogenations of (A) acetaldehyde, (B) butadiene, (C) acetylene, and (D) styrene on Pd-Au SAAs.

Pan *et al.* also used an electron-beam-heated tungsten capillary to dissociate H_2 onto Au(111).[16] Therefore, higher H coverages (0.19 ML to 0.98 ML) than obtainable with Pd-Au SAAs were used by Pan *et al.* For Pd-Au SAAs, the H concentration is limited by the availability of Pd sites. In the current study, a higher concentration (0.06 ML) of Pd was

deposited onto a bare Au(111) surface in order to increase the H coverage (0.06 ML H_2). Although, the higher Pd concentration did facilitate more H adatoms on the surface (0.06 ML H), ethanol was still not detected. At 0.06 ML Pd, a heterogeneous Pd-Au alloyed surface is formed with mostly Pd monomers, but small Pd clusters are also present. Since the maximum H coverage obtainable within the single atom region is < 0.05 ML H, Pd was deposited at a higher Au surface temperature (420 K) to enhance the dispersion of Pd away from the Au edge-dislocations. The subsurface diffusion of Pd observed at higher temperatures prevented a significant increase in the number of isolated Pd atoms in the surface.

Finally for acetaldehyde hydrogenation, attempts were made to force H adatoms from the Pd activation sites to Au terraces by co-adsorbing H and CO. Unfortunately the hydrogenation product, ethanol was not observed again. When co-adsorbing H and CO, low temperature desorption (110 K) of H_2 from Au(111) is expected as shown in Chapter 9.[7] In these experiments, unreacted H_2 was not observed desorbing at 110 K possibly because at 0.06 ML Pd the alloyed surface is not exclusively Pd monomers, therefore, the preferential adsorption of both H and CO is no longer atop.

Next, butadiene hydrogenation was attempted in order to expand upon the work by Hugon *et*. al. who showed selective partial hydrogenation of butadiene with Pd-Au nanoparticles.[4] Using TPD, sub-monolayer coverages of butadiene desorbed from Pd-Au SAAs at 175 K and 230 K from terraces and steps, respectively (Figure 10.3B). Butenes were observed desorbing from Pd-Au SAAs at 155 K and 180 K in the presences and absence of H adatoms, suggesting H adatoms are not responsible for the observed hydrogenation products. Further investigation of survey spectra suggests butenes contaminations were present in the

butadiene source. Successive TPD experiments also yielded small increase in butenes desorption suggestive of self-hydrogenation/ polymerization.

Though, butadiene hydrogenation was not detected, the most interesting result for the co-adsorption of butadiene with H is a decrease in H_2 desorption (130 K) from Pd-Au SAAs. Typically, H_2 desorbs from Pd-Au SAAs at 175 K. Butadiene forces H from the Pd activation sites to Au in a similar to mechanisms observed for the co-adsorption of H and CO that was discussed in Chapter 9.[7]

For the next molecule acetylene, we attempted hydrogenations with D_2 because impurities in the acetylene source yielded convoluted desorption traces that often suggested desorption of hydrogenated species. TPD showed acetylene desorbing from Pd-Au(111) at 155 K and 250 K and ethene at 200 K and 265 K (Figure 10.3C). For the co-adsorption of acetylene with D, we do not observe any ethene-D, thus, we conclude we are not hydrogenating acetylene. We speculate that ethene desorption is due to self-hydrogenation/decomposition of acetylene. A similar process is observed on Cu(111) where the decomposition products are observed at 330 K.[17] We also tried phenylacetylene hydrogenation with similar results.

When utilizing D_2, it is difficult to obtain pure deuterium adsorption due to background adsorption of H. In these studies, the maximum obtainable D_2 coverage 30 % of the total coverage. In order to increase the adsorption of D_2 over H_2, the sample was flashed > 250 K and then cooled in a D_2 atmosphere by introducing $1 * 10^{-8}$ mbar of D_2 into the chamber. Additionally the kinetic isotope effect reduces the overall hydrogenation conversion when using D compared to H. For acetaldehyde[16], ~75 % decrease in conversion

for D compared to H was previously reported. Thus, at the low surface coverages of D obtainable by Pd-Au SAAs, the overall conversion with D might be below the limits of detection of the instrumentation.

The final hydrogenation attempt was styrene (Figure 10.3D). Sub-monolayer coverage of styrene was observed desorbing at 310 K and ethyl benzene was observed at 275 K. The ethyl benzene coverage was proportional to styrene coverage, but independent of the H coverage on the surface. Survey spectrum of the styrene source showed ethyl benzene contamination. Though styrene could not be hydrogenated with Pd-Au SAAs, styrene has been previously hydrogenated in UHV on Pd-Cu(111) SAAs.[18] However, Pd-Cu(111) SAAAs are capable of H spillover to Cu, which increased the surface coverage of H to 0.1 ML from 0.01 ML Pd.[19]

10.3. Summary

In conclusion, the co-adsorption of H and hydrocarbons on Pd-Au(111) SAAs do not yield hydrogenated products for butadiene, acetaldehyde, acetylene, phenyl acetylene, or styrene. Potentially, the low temperature desorption of H_2 from either Au(111) (110 K) or Pd-Au(111) SAAs (175 K) prevents hydrogenation because the barrier for hydrogenation of some of the alkenes tested is greater than the desorption barrier of H_2. Also, the hydrogenation products could be limited by the low coverages of H obtainable on Pd-Au(111) SAA since the H spillover mechanism is not observed on Au based alloys.

10.4. References

(1) Chen, M.; Kumar, D.; Yi, C.; Goodman, D. W. The Promotional Effect of Gold in Catalysis by Palladium-Gold. *Science* **2005**, *310*, 291–293.

(2) Edwards, J. K.; Solsona, B.; Ntainjua N, E.; Carley, A. F.; Herzing, A. A.; Kiely, C. J.; Hutchings, G. J. Switching off Hydrogen Peroxide

Hydrogenation in the Direct Synthesis Process. *Science* **2009**, *323*, 1037–1041.

(3) Choudhary, T. V; Sivadinarayana, C.; Datye, A. K.; Kumar, D.; Goodman, D. W. Acetylene Hydrogenation on Au-Based Catalysts. *Catal. Letters* **2003**, *86*, 1–8.

(4) Hugon, A.; Delannoy, L.; Krafft, J. M.; Louis, C. Selective Hydrogenation of 1,3-Butadiene in the Presence of an Excess of Alkenes over Supported Bimetallic Gold−palladium Catalysts. *J. Phys. Chem. C.* **2010**, *114*, 10823–10835.

(5) Gao, F.; Wang, Y.; Goodman, D. W. CO Oxidation over AuPd(100) from Ultrahigh Vacuum to near-Atmospheric Pressures: The Critical Role of Contiguous Pd Atoms. *J. Am. Chem. Soc.* **2009**, *131*, 5734–5735.

(6) Enache, D. I.; Edwards, J. K.; Landon, P.; Solsona-Espriu, B.; Carley, A. F.; Herzing, A. a; Watanabe, M.; Kiely, C. J.; Knight, D. W.; Hutchings, G. J. Solvent-Free Oxidation of Primary Alcohols to Aldehydes Using Au-Pd/TiO_2 Catalysts. *Science* **2006**, *311*, 362–365.

(7) Lucci, F. R.; Darby, M. T.; Mattera, M. F. G.; Ivimey, C. J.; Therrien, A. J.; Michaelides, A.; Stamatakis, M.; Sykes, E. C. H. Controlling Hydrogen Activation, Spillover, and Desorption with Pd-Au Single Atom Alloys. *J. Phys. Chem. Lett.* **2016**, *7*, 480–485.

(8) Barth, J. V.; Brune, H.; Ertl, G.; Behm, R. J. Scanning Tunneling Microscopy Observations on the Reconstructed Au(111) Surface: Atomic Structure, Long-Range Superstructure, Rotational Domains, and Surface Defects. *Phys. Rev. B* **1990**, *42*, 9307–9318.

(9) Baber, A. E.; Tierney, H. L.; Sykes, E. C. H. Atomic-Scale Geometry and Electronic Structure of Catalytically Important Pd/Au Alloys. *ACS Nano.* **2010**, *4*, 1637–1645.

(10) Ruff, M.; Takehiro, N.; Liu, P.; Nørskov, J. K.; Behm, R. J. Size-Specific Chemistry on Bimetallic Surfaces: A Combined Experimental and Theoretical Study. *ChemPhysChem* **2007**, *8*, 2068–2071.

(11) Maroun, F.; Ozanam, F.; Magnussen, O. M.; Behm, R. J. The Role of Atomic Ensembles in the Reactivity of Bimetallic Electrocatalysts. *Science* **2001**, *293*, 1811–1814.

(12) Casari, C.; Foglio, S.; Siviero, F.; Li Bassi, A.; Passoni, M.; Bottani, C. Direct Observation of the Basic Mechanisms of Pd Island Nucleation on Au(111). *Phys. Rev. B* **2009**, *79*, 1–9.

(13) Meyer, J. A.; Baikie, I. D.; Kopatzki, E.; Behm, R. J. Preferential Island Nucleation at the Elbows of the Au(111) Herringbone Reconstruction through Place Exchange. *Surf. Sci.* **1996**, *365*, 647–651.

(14) Guo, X.; Yates, J. T. Dependence of Effective Desorption Kinetic Parameters on Surface Coverage and Adsorption Temperature: CO on Pd(111). *J. Chem. Phys.* **1989**, *90*, 6761–6766.

(15) Gdowski, G. E.; Felter, T. E.; Stulen, R. H. Effect of Surface Temperature on the Sorption of Hydrogen on Pd(111). *Surf. Sci.* **1987**, *181*, L147–L155.

(16) Pan, M.; Flaherty, D. W.; Mullins, C. B. Low-Temperature Hydrogenation

of Acetaldehyde to Ethanol on H-Precovered Au(111). *J. Phys. Chem. Lett.* **2011**, *2*, 1363–1367.

(17) Kyriakou, G.; Kim, J.; Tikhov, M. S.; Macleod, N.; Lambert, R. M. Acetylene Coupling on Cu(111): Formation of Butadiene, Benzene, and Cyclooctatetraene. *J. Phys. Chem. B* **2005**, *109*, 10952–10956.

(18) Kyriakou, G.; Boucher, M. B.; Jewell, A. D.; Lewis, E. A.; Lawton, T. J.; Baber, A. E.; Tierney, H. L.; Flytzani-Stephanopoulos, M.; Sykes, E. C. H. Isolated Metal Atom Geometries as a Strategy for Selective Heterogeneous Hydrogenations. *Science* **2012**, *335*, 1209–1212.

(19) Boucher, M. B.; Zugic, B.; Cladaras, G.; Kammert, J.; Marcinkowski, M. D.; Lawton, T. J.; Sykes, E. C. H.; Flytzani-Stephanopoulos, M. Single Atom Alloy Surface Analogs in $Pd_{0.18}Cu_{15}$ Nanoparticles for Selective Hydrogenation Reactions. *Phys. Chem. Chem. Phys.* **2013**, *15*, 12187–12196.

Chapter 11: The Effect of Single Pd Atoms on the Energetics of Recombinative O_2 Desorption from Au(111)

11.1 Introduction

Heterogeneous catalysts that utilize isolated metal atoms are emerging as a promising approach for the efficient use of precious metal catalysts to enhance catalytic activity.[1,2] Both bimetallic *single atom alloys* and oxide supported single atoms have been shown to catalyze numerous reactions including water gas shift,[3,4] hydrogenation,[5–10] dehydrogenation, [11] oxidation,[12,13] hydrogenolysis,[14] and coupling reactions.[15] However, direct investigation of isolated atoms in real catalysts is often difficult due to the complexity of the catalyst structure. Recently, we developed the single atom alloy (SAA) approach for catalyst design where we initially studied the structure and chemistry of isolated atoms in single crystal model catalysts.[16–20] Over the years this work has informed the design of nanoparticle catalysts capable of catalyzing selective hydrogenation reactions with improved tolerance to CO poisoning under realistic operating pressures.[18,19] In order to expand the single atom alloy strategy beyond hydrogenation reactions, in this study we probe the adsorption and desorption of O from isolated Pd monomers in a Au(111) substrate.

Au nanoparticles and nanoporous Au are well known for highly selective oxidation reactions despite the high barrier for O_2 activation on Au.[21–26] The addition of Pd to Au catalysts increases the reactivity of Au and this alloy combination exhibits remarkable selectivity for catalyzing CO oxidation,[3] vinyl acetate synthesis,[27–29] alcohol oxidation,[30] and hydrogen peroxide synthesis.[31] In these reactions, the atomic ensemble of the Pd atoms in Au is critical to obtain the desired selectivity. It has been shown for CO oxidation that

contiguous Pd atoms are necessary for O_2 activation[32] and for vinyl acetate synthesis Pd monomers prevent the unwanted oxidation of products.[27,29] Despite the importance of the above reactions, the fundamental interaction between O and isolated Pd atoms in Au is not well understood. Previous studies by Li *et al.* and Yu *et al.* show extended Pd sites are required for the dissociative adsorption of O_2 on Au-Pd(100)[33,34] and Pd-Au(111), respectively. In both studies a dramatic decrease in O_2 uptake was observed at low concentrations of surface Pd atoms, suggesting a geometric ensemble effect for the adsorption and dissociation of O_2. Neither study, however, experimentally probed the capabilities of isolated metal geometries.

In the current work, we directly addressed the effects of single Pd atom geometries on the recombinative desorption of O_2 from Au(111). Since Au(111) is unable to dissociate O_2 in ultra-high vacuum (UHV), we used ozone to populate the surfaces with O. By using a combination of temperature programmed desorption, scanning tunneling microscopy, and density function theory, we probed the impact of isolated Pd atoms on the interactions O with the Au(111) surface. Our studies reveal that small amounts of Pd lead to a significant reduction in the O_2 desorption temperature at low O coverages. Since DFT calculations reveal that isolated Pd monomers in Au(111) very slightly increases (~10 meV) the barrier for dissociative adsorption of O_2 and recombinative desorption of O_2, we used STM to show that single Pd atoms prevent the formation of the 2D Au surface oxide from which O_2 is known to desorb. Since disordered O on Au(111) at low coverage is known to be more reactive, we speculate that small amounts of Pd, or other elements like Ni, may alter the initial oxidation of Au and hence be used to control the subsequent reactivity of the system.

11.2 Results and Discussion

In order to probe the desorption properties of O_2 from Pd-Au SAAs, oxidized Au(111) and Pd-Au(111) SAAs were prepared in UHV. Pd atoms were deposited onto Au(111) at 380 K using physical vapor deposition. The surface morphology of the alloy was characterized using STM (Figure 11.1) and has also been well described in the literature.[35–44] Briefly, at low Pd coverages, Pd atoms exist as isolated atoms in the Au surface due to stronger heteroatom bonds between Pd-Au than Pd-Pd or Au-Au (Figure 11.1B). During the place exchange of Pd atoms into the Au terraces, Au adatoms are ejected and nucleate into islands on the surface (Figure 11.1A). The surface layer of the islands are primarily composed of Au atoms due to the lower surface free energy of Au than Pd. Due to the large activation barrier of O_2 dissociative adsorption onto Au(111), O does not readily adsorb onto Au(111) surface in UHV. Thus, for these experiments, O was adsorbed onto Au(111) and Pd-Au(111) SAA by exposing the surface to ozone.

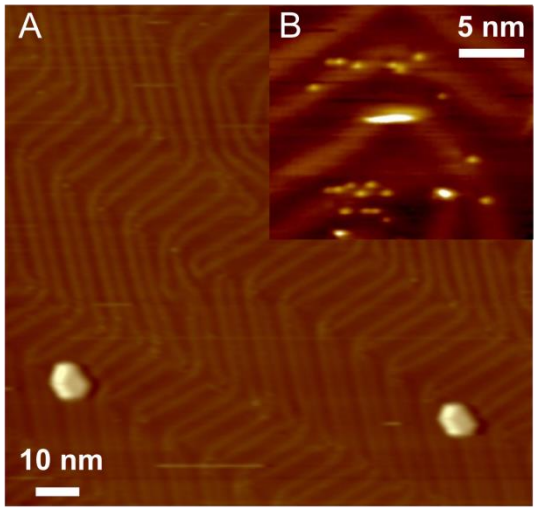

Figure 11.1. STM image of Pd-Au(111) SAAs
(A) Shown is a Pd-Au(111) alloy formed at 380 K with Au rich islands randomly dispersed across the surface. (B) High resolution images show Pd atoms exists as isolated monomers in Au terraces.

First, TPD experiments were performed to determine the desorption temperature of O_2 from Pd-Au SAAs. After exposure of Au(111) to ozone at 85 K, O_2 was observed desorbing at 510 K (ϒ1 peak in Figure 11.2). The desorption profiles of O_2 from Au(111) do not follow typical second order desorption trends suggesting the simple recombination of 2 O adatoms is not the rate limiting step. For the Pd-Au(111) SAA, O_2 desorbs at 470 K for low O coverages. At higher O coverages, a second desorption peak was observed at 510 K corresponding to desorption from the Au. Thus, the isolated Pd atoms open a low temperature O_2 desorption pathway from the surface.

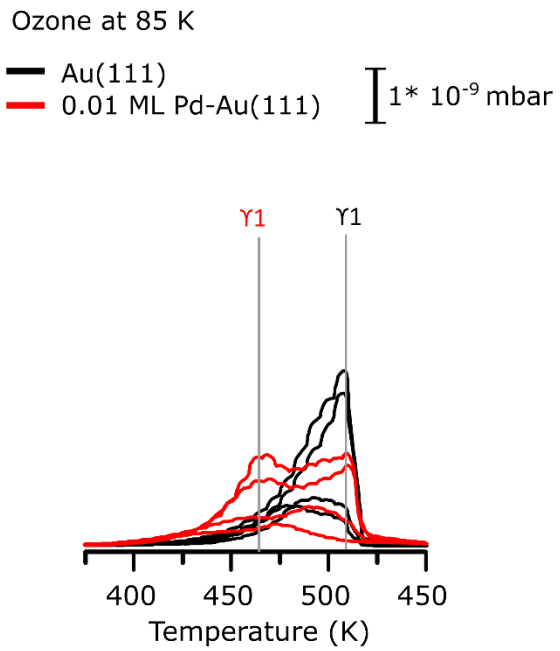

Figure 11.2. Recombinative O_2 desorption from Au(111) and Pd-Au(111) SAAs
TPD traces for O_2 desorption after exposing Au(111) and 0.01 ML Pd-Au(111) SAAs to ozone at 85 K.

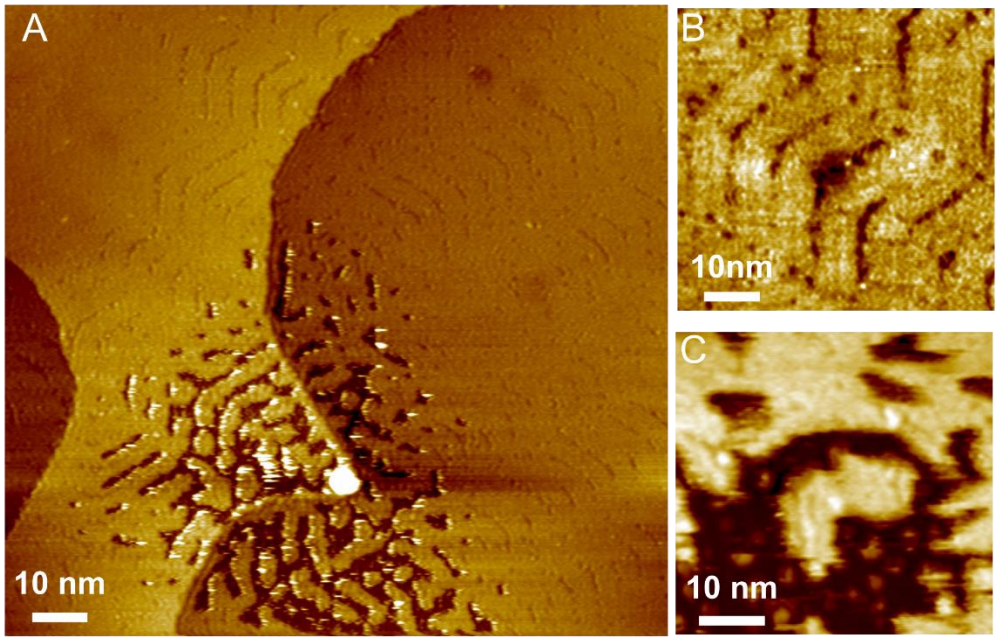

Figure 11.3. STM images of oxidation of Au(111) at 110 K
(A) Large scale images show both (B) depressions in registry with the herringbone reconstruction and (C) oxidized pits. Imaging conditions: 100 mV, 100 pA, imaged at 30 K.

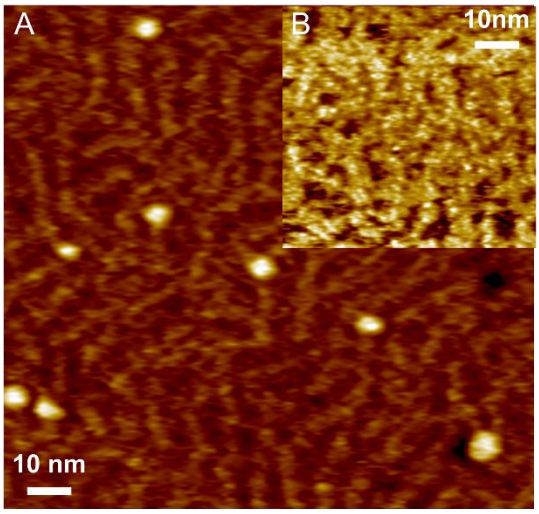

Figure 11.4. STM images of oxidation of Pd-Au(111) SAA at 110 K
STM images show a uniform oxide formed in sequence of the herringbone reconstruction. Au rich islands formed during the alloying of Pd are dispersed across the surface.

To determine morphology the surface, a Au surface oxidized at 110 K was imaged with STM. The STM imaging show dark amorphous stationary depressions in registry with the Au herringbone reconstruction (Figure 11.3A,B). Previously, it has been shown that

surface oxides appear darker than the surround metallic surface in STM images.[45] Localized regions of mobile pits are also observed whose mobility is probably influenced by the STM tip. (Figure 11.3C). The pits are ~390 nm deep which is greater than atomic layer of Au suggesting the pits are composed of an oxidized state of Au. This metastable state was only observed after preparation at 110 K. The mobility of the pits suggests weakly bound oxygen. For Pd-Au(111) SAAs exposed to ozone, the mobile pits were not observed suggesting Pd atoms prevent the formation of this weakly bound state (Figure 11.4). For the Pd-Au SAA, the amorphous stationary depressions in registry with the Au herringbone pattern was present similar to the Au(111).

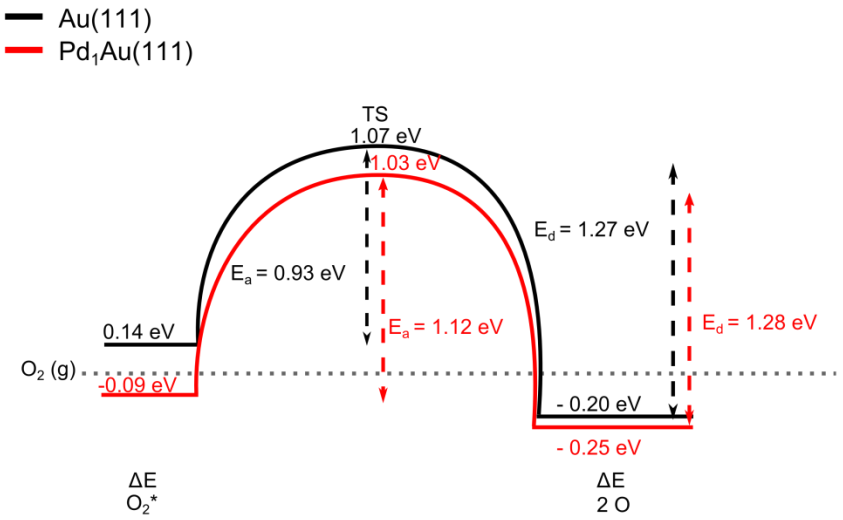

Figure 11.5. DFT calculated energy landscape for O_2 adsorption and desorption from Au and Pd-Au SAAs
Shown are adsorption energies (ΔE) of O_2 (0.14 eV and -0.09 eV) and 2 O (-0.20 eV and -0.25 eV), activation energy for dissociative adsorption of O_2 (E_a) and desorption energy for combinative desorption of O_2 (E_d) for both Au and PdAu surfaces.

In order to examine both the adsorption and desorption kinetics of O_2, we calculated the activation energy for dissociative adsorption and desorption energy for the recombinative desorption of O_2 with DFT (Figure 11.5). The recombinative desorption barrier of O_2 from a Pd-Au SAA (1.28 eV) is slightly higher than the recombinative desorption barrier from bare

Au(111) (1.27 eV) which is not consistent with the 40 K decrease in desorption temperature from Pd-Au(111) SAAs compared to Au(111). Although, according to Redhead analysis for a first order desorption process assuming a pre-exponential of $1*10^{15}$, the difference in desorption barriers for desorption from Au(111) (510 K, 1.64 eV) and Pd-Au(111) SAAs (470 K, 1.51 eV) should be ~0.1 eV. Thus, the DFT calculations do not account for the low temperature desorption observed in our TPD experiments. The DFT calculations show for O_2 adsorption, the activation energy is 0.19 eV larger on Pd-Au(111) than Au(111) since O_2 physisorption is exothermic on Au and endothermic on Pd-Au SAA. As a result the dissociative adsorption barrier is larger on Pd-Au SAAs than Au(111) which is certainly non-intuitive. This supports previous work on Pd-Au(111)[33] and Au-Pd(100)[34] which suggest isolated Pd atoms cannot activate O_2. These studies report low temperature physisorption of O_2 on extended Pd ensembles where the adsorbed coverage of O_2 is dependent on the surface concentration of Pd. Both studies report a non-linear decrease in O_2 uptake as a function of Pd coverage suggesting that geometric ensemble effects impact the physisorption of O_2 and sequential dissociation of O_2.

To further investigate the desorption of other oxide species from Au(111) and Pd-Au(111) SAAs, we exposed the surfaces to ozone at 290 K. For ozone exposure at 290 K, two distinct states were observed with STM including the dark depressions randomly dispersed across the Au surface and mobile clusters on the surface that exhibit pseudo-order on the surface (Figure 11.6). For Pd-Au SAA, the oxidized surfaces looks very different than \on Au(111) since an amorphous structure is observed on the Pd-Au SAA surface (Figure 11.7). The STM results suggests that Pd atoms alter the oxidation of the surface which potentially contributes to the low temperature desorption that we observed for O_2 from Pd-

Au SAAS. According to our x-ray photoelectron spectroscopy (XPS), neither observed oxide state is that of bulk oxide (Au_2O_3).

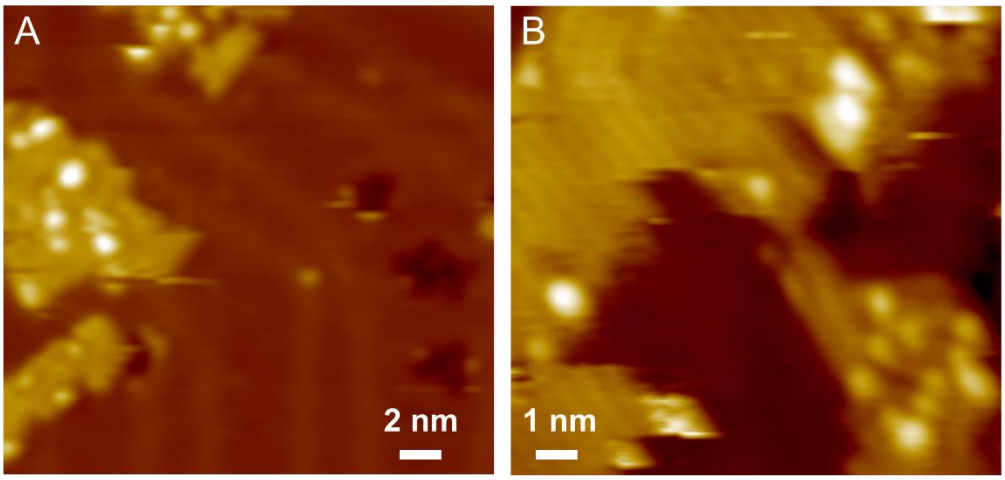

Figure 11.6. STM images of oxidized Au(111) at 290 K
(A,B) Shown are STM images after high temperature ozone exposure at 290 K. We postulate that the dark depressions are surface oxygen and (B) the bright features are Au-O complexes on the surface. Imaging conditions: 100 mV, 100 pA, 30 K.

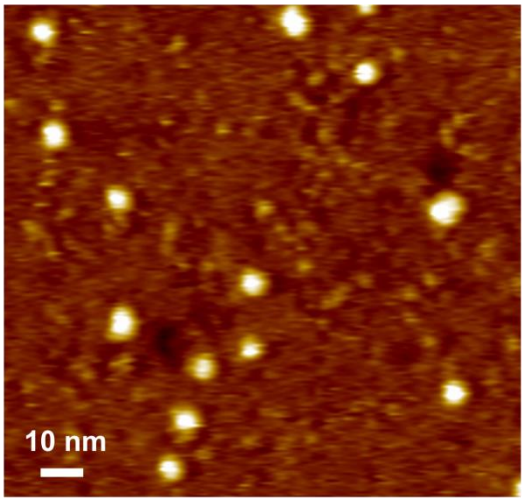

Figure 11.7. STM images of oxidized Pd-Au(111) SAA at 290 K.
Shown is STM image of the amorphous morphology after ozone exposure of the Pd-Au(111) at 290 K. Imaging conditions: 100 mV, 100 pA, 30 K.

Using TPD, we then determined the desorption temperature of the various surface coverages of O. For the desorption of low O coverages formed at low temperature (85 K), O_2 desorbs at 510 K from Au(111) and this ϒ1state saturates (Figure 11.2 and 11.8A). When we

increased the ozone exposure temperature to 290 K, two desorption peaks, ϒ2 and ϒ3, are observed at 510 K and 515 K, respectively (Figure 11.8B). At an ozone exposure temperature of 400 K, the ϒ3 peak continually broadens but does not saturate (Figure 11.8C). Due to the continuous broadening of the peak at higher exposure temperatures, we propose that there is more than one oxide state desorbing from the surface at ozone exposures ≥ 290 K. The desorption traces of ϒ2 and ϒ3 exposure Au(111) to ozone at 290 K are in agreement with Saliba *et al.* who report 2 distinct O_2 desorption features from Au(111) with desorption temperatures that favorably agree when accounting for difference is heating rates between the TPD experiments.[46] Oxidation of Au using oxygen sputtering yielded ϒ2 and ϒ3 peaks and two higher temperature peaks that were assigned as subsurface O atoms formed at a sputtering ion energy of 0.5 keV.[47]

O_2 desorption from the Pd-Au SAAs exhibits a unique desorption profile compared to Au(111) for both low temperature (85 K) and high temperature (290 K and 400 K) ozone exposure. After ozone exposure at 85 K, the ϒ1 state desorbs at 470 K and at 510 K (Figure 11.2 and 11.8A). When Pd-Au SAA is exposed to ozone at 290 K and 400 K, O_2 desorption occurs at 490 K for the ϒ2 peak. The ϒ2 peak continues to shift to higher temperatures with increasing O coverage. There is also a high temperature shoulder from ϒ3 at 515 K from Pd-Au(111) SAA (Figure11.8). At comparable O oxygen coverages, the O_2 desorption temperature from Pd-Au SAA decreases by 20 K compared to Au(111) (ϒ2 peak). Our STM experiments show that an amorphous oxidized surface structure is observed on the Pd-Au(111) surface suggesting that dilute Pd concentrations prevent the formation of the 2D oxide, which is known to be the rate limiting step of O_2 desorption from Au(111). We postulate that the low temperature desorption of O_2 from a Pd-Au SAA is due to Pd atoms

hindering the formation of the 2D oxide. The pronounced shift in O_2 desorption at low surface coverages suggests that Pd atoms only locally affects oxide formation on Au (Figure11.8).

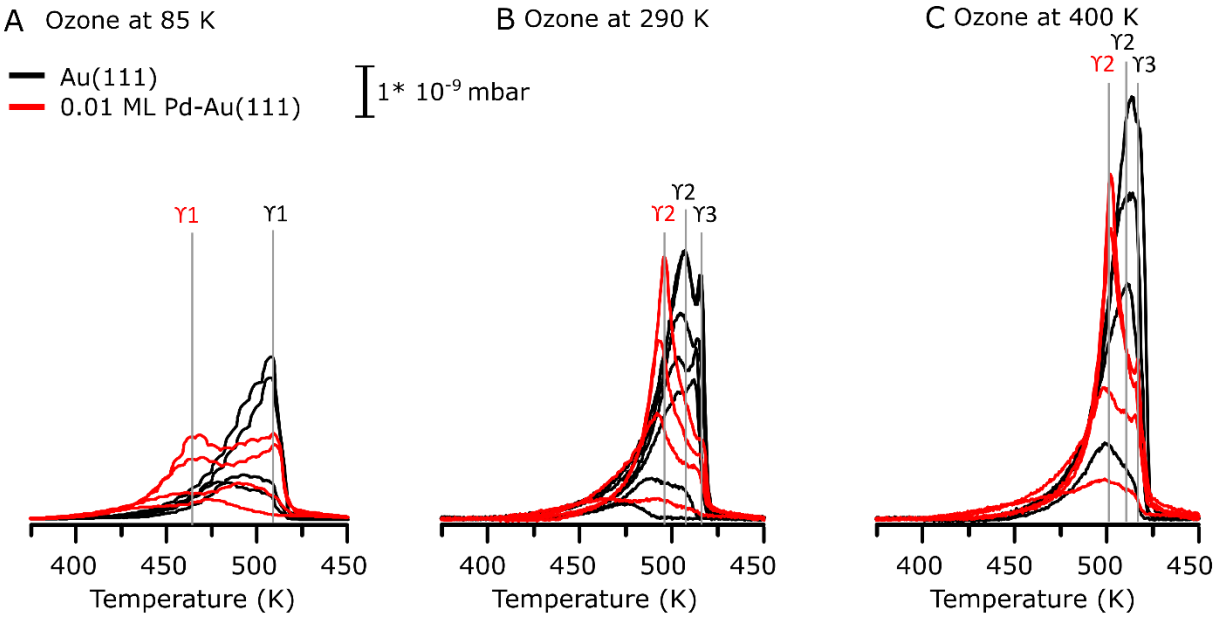

Figure 11.8. Desorption of O_2 form Au(111) and Pd-Au(111) SAAs
TPD traces for O_2 desorption from Au(111) and 0.01 ML Pd-Au(111) SAAs after low temperature ozone exposure at (A) 85 K and high temperature ozone exposures at (B) 290 K and (C) 400 K. All traces are plotted on the same y-scale.

11.3 Summary

By using ozone to populate a predominantly Au based surface with O, we can probe the energetics of O_2 desorption from dilute concentrations of Pd monomers in Au. We show that very small amounts of Pd (< 0.01 ML) in Au(111) alter the oxidation of the Au surface, which thereby dramatically reduces the desorption temperature of O_2. Specifically, isolated Pd atoms prevent the formation of the 2D surface oxide on Au(111) from which O_2 desorbs. Our TPD studies show that the greatest temperature shift (40 K) is observed at lower O coverages indicating that Pd monomers locally disrupt the formation of the 2D oxide. Using STM we directly visualize the surface morphology of both Pd-Au SAA and Au surface

structures to reveal an amorphous surface in the presence of Pd atoms. Since the amorphous Au surface structure has been suggested to be more reactive than the 2D oxide phase, the addition of trace amounts of Pd may be an interesting way to control the activity and/or selectivity of oxidation reactions using materials such as Au nanoparticles or nanoporous gold.

11.4 References

(1) Thomas, J. M.; Saghi, Z.; Gai, P. L. Can a Single Atom Serve as the Active Site in Some Heterogeneous Catalysts? *Top. Catal.* **2011**, *54*, 588–594.

(2) Thomas, J. M. The Concept, Reality and Utility of Single-Site Heterogeneous Catalysts (SSHCs). *Phys. Chem. Chem. Phys.* **2014**, *16*, 7647–7661.

(3) Zhai, Y.; Pierre, D.; Si, R.; Deng, W.; Ferrin, P.; Nilekar, A. U.; Peng, G.; Herron, J. A.; Bell, D. C.; Saltsburg, H.; et al. Alkali-Stabilized Pt-OHx Species Catalyze Low-Temperature Water-Gas Shift Reactions. *Science* **2010**, *329*, 1633–1636.

(4) Fu, Q.; Saltsburg, H.; Flytzani-Stephanopoulos, M. Active Nonmetallic Au and Pt Species on Ceria-Based Water-Gas Shift Catalysts. *Science* **2003**, *301*, 935–938.

(5) Vilé, G.; Albani, D.; Nachtegaal, M.; Chen, Z.; Dontsova, D.; Antonietti, M.; López, N.; Pérez-Ramírez, J. A Stable Single-Site Palladium Catalyst for Hydrogenations. *Angew. Chemie - Int. Ed.* **2015**, *54*, 11265–11269.

(6) Zhang, X.; Shi, H.; Xu, B.-Q. Catalysis by Gold: Isolated Surface Au^{3+} Ions Are Active Sites for Selective Hydrogenation of 1,3-Butadiene over Au/ZrO_2 Catalysts. *Angew. Chem. Int. Ed. Engl.* **2005**, *44*, 7132–7135.

(7) Pei, G. X.; Liu, X. Y.; Wang, A.; Li, L.; Huang, Y.; Zhang, T.; Lee, J. W.; Jang, B. W. L.; Mou, C.-Y. Promotional Effect of Pd Single Atoms on Au Nanoparticles Supported on Silica for the Selective Hydrogenation of Acetylene in Excess Ethylene. *New. J. Chem.* **2014**, *38*, 2043–2051.

(8) Pei, G. X.; Liu, X, Y.; Liu, Y.; Wang, A.; Lee, A. F.; Isaacs, M. A.; Li, L.; Pan, X.; Yang, X.; Wang, X.; et al. Ag Alloyed Pd Single-Atom Catalysts for Efficient Selective Hydrogenation of Acetylene to Ethylene in Excess Ethylene. *ACS Catal.* **2015**, *5*, 3717–3725.

(9) Aich, P.; Wei, H.; Basan, B.; Kropf, A. J.; Schweitzer, N. M.; Marshall, C. L.; Miller, J. T.; Meyer, R. Single-Atom Alloy Pd−Ag Catalyst for Selective Hydrogenation of Acrolein. *J. Phys. Chem. C* **2015**, *119*, 18140–18148.

(10) McCue, A. J.; Gibson, A.; Anderson, J. A. Palladium Assisted Copper/alumina Catalysts for the Selective Hydrogenation of Propyne, Propadiene and Propene Mixed Feeds. *Chem. Eng. J.* **2016**, *285*, 384–391.

(11) Cao, X.; Ji, Y.; Luo, Y. Dehydrogenation of Propane to Propylene by a Pd/Cu Single-Atom Catalyst: Insight from First-Principles Calculations. *J. Phys. Chem. C* **2015**, *119*, 1016–1023.
(12) Zhang, H.; Kawashima, K.; Okumura, M.; Toshima, N. Colloidal Au Single-Atom Catalysts Embedded on Pd Nanoclusters. *J. Mater. Chem.* **2014**, *2*, 13498.
(13) Cheng, X.; Zhao, Y.; Li, F.; Liu, Y. Catalytic Mechanisms of Au11 and Au_{11}-nPt_n (n=1–2) Clusters: A DFT Investigation on the Oxidation of CO by O2. *J. Mol. Model.* **2015**, *21*, 230.
(14) Yao, Y.; Goodman, D. W. New Insights into Structure–activity Relationships for Propane Hydrogenolysis over Ni–Cu Bimetallic Catalysts. *RSC Adv.* **2015**, *5*, 43547–43551.
(15) Zhang, L.; Wang, A.; Miller, T.; Liu, X.; Yang, X.; Wang, W.; Li, L.; Huang, Y.; Mou, C.; Zhang, T. Efficient and Durable Au Alloyed Pd Single-Atom Catalyst for the Ullmann Reaction of Aryl Chlorides in Water. *ACS Catal.* **2014**, *4*, 1546–1553.
(16) Kyriakou, G.; Boucher, M. B.; Jewell, A. D.; Lewis, E. A.; Lawton, T. J.; Baber, A. E.; Tierney, H. L.; Flytzani-Stephanopoulos, M.; Sykes, E. C. H. Isolated Metal Atom Geometries as a Strategy for Selective Heterogeneous Hydrogenations. *Science* **2012**, *335*, 1209–1212.
(17) Boucher, M. B.; Zugic, B.; Cladaras, G.; Kammert, J.; Marcinkowski, M. D.; Lawton, T. J.; Sykes, E. C. H.; Flytzani-Stephanopoulos, M. Single Atom Alloy Surface Analogs in $Pd_{0.18}Cu_{15}$ Nanoparticles for Selective Hydrogenation Reactions. *Phys. Chem. Chem. Phys.* **2013**, *15*, 12187–12196.
(18) Lucci, F. R.; Liu, J.; Marcinkowski, M. D.; Yang, M.; Allard, L. F.; Flytzani-Stephanopoulos, M.; Sykes, E. C. H. Selective Hydrogenation of 1,3-Butadiene on Platinum – Copper Alloys at the Single-Atom Limit. *Nat. Commun.* **2015**, *6*, 8550.
(19) Liu, J.; Lucci, F. R.; Yang, M.; Lee, S.; Marcinkowski, M. D.; Therrien, A. J.; Williams, C. T.; Sykes, E. C. H.; Flytzani-Stephanopoulos, M. Tackling CO Poisoning with Single Atom Alloy Catalysts. *J. Am. Chem. Soc.* **2016**, *138*, 6396–6399.
(20) Shan, J.; Lucci, F. R.; Liu, J.; El-Soda, M.; Marcinkowski, M. D.; Allard, L. F.; Sykes, E. C. H.; Flytzani-Stephanopoulos, M. Water Co-Catalyzed Selective Dehydrogenation of Methanol to Formaldehyde and Hydrogen. *Surf. Sci.* **2016**, *650*, 121–129.
(21) Claus, P. Heterogeneously Catalysed Hydrogenation Using Gold Catalysts. *Appl. Catal.* **2005**, *291*, 222–229.
(22) Mcewan, L.; Julius, M.; Roberts, S.; Fletcher, J. C. Q. A Review of the Use of Gold Catalysts in Selective Hydrogenation Reactions. *Gold Bull.* **2010**, *43*, 298–306.
(23) Haruta, M. Size- and Support-Dependency in the Catalysis of Gold. *Catal. Today* **1997**, *861*, 153–166.
(24) Mohr, C.; Hofmeister, H.; Radnik, J.; Claus, P. Identification of Active Sites in Gold-Catalyzed Hydrogenation of Acrolein. *J. Am. Chem. Soc.*

2003, *103*, 178–180.
(25) Hammer, B.; Nørskov, J. K. Why Gold Is the Noblest of All the Metals. *Nature* **1995**, *376*, 238–240.
(26) Wittstock, A.; Zielasek, V.; Biener, J.; Friend, C. M.; Bäumer, M.; Baeumer, M. Nanoporous Gold Catalysts for Selective Gas-Phase Oxidative Coupling of Methanol at Low Temperature. *Science* **2010**, *327*, 319–322.
(27) Neurock, M.; Tysoe, W. T. Mechanistic Insights in the Catalytic Synthesis of Vinyl Ccetate on Palladium and Gold/Palladium Alloy Surfaces. *Top. Catal.* **2013**, *56*, 1314–1332.
(28) Calaza, F.; Stacchiola, D.; Neurock, M.; Tysoe, W. T. Coverage Effects on the Palladium-Catalyzed Synthesis of Vinyl Acetate: Comparison between Theory and Experiment. *J. Am. Chem. Soc.* **2010**, *132*, 2202–2207.
(29) Chen, M.; Kumar, D.; Yi, C.; Goodman, D. W. The Promotional Effect of Gold in Catalysis by Palladium-Gold. *Science* **2005**, *310*, 291–293.
(30) Enache, D. I.; Edwards, J. K.; Landon, P.; Solsona-Espriu, B.; Carley, A. F.; Herzing, A. A.; Watanabe, M.; Kiely, C. J.; Knight, D. W.; Hutchings, G. J. Solvent-Free Oxidation of Primary Alcohols to Aldehydes Using Au-Pd/TiO_2 Catalysts. *Science* **2006**, *311*, 362–365.
(31) Beletskaya, A. V; Pichugina, D. A.; Shestakov, A. F.; Kuz 'menko, N. E. Formation of H_2O_2 on Au_{20} and $Au_{19}Pd$ Clusters: Understanding the Structure Effect on the Atomic Level. *J. Phys. Chem. A* **2013**, *117*, 6817–6826.
(32) Gao, F.; Wang, Y.; Goodman, D. W. CO Oxidation over AuPd(100) from Ultrahigh Vacuum to near-Atmospheric Pressures: The Critical Role of Contiguous Pd Atoms. *J. Am. Chem. Soc.* **2009**, *131*, 5734–5735.
(33) Yu, W.-Y.; Zhang, L.; Mullen, G. M.; Henkelman, G.; Mullins, C. B. Oxygen Activation and Reaction on Pd–Au Bimetallic Surfaces. *J. Phys. Chem. C* **2015**, *119*, 11754–11762.
(34) Li, Z.; Gao, F.; Tysoe, W. T. Carbon Monoxide Oxidation over Au / Pd (100) Model Alloy Catalysts. *J. Phys. Chem. C* **2010**, *114*, 16909–16916.
(35) Baber, A. E.; Tierney, H. L.; Sykes, E. C. H. Atomic-Scale Geometry and Electronic Structure of Catalytically Important Pd/Au Alloys. *ACS Nano.* **2010**, *4*, 1637–1645.
(36) Ruff, M.; Takehiro, N.; Liu, P.; Nørskov, J. K.; Behm, R. J. Size-Specific Chemistry on Bimetallic Surfaces: A Combined Experimental and Theoretical Study. *ChemPhysChem* **2007**, *8*, 2068–2071.
(37) Maroun, F.; Ozanam, F.; Magnussen, O. M.; Behm, R. J. The Role of Atomic Ensembles in the Reactivity of Bimetallic Electrocatalysts. *Science* **2001**, *293*, 1811–1814.
(38) Casari, C.; Foglio, S.; Siviero, F.; Li Bassi, A.; Passoni, M.; Bottani, C. Direct Observation of the Basic Mechanisms of Pd Island Nucleation on Au(111). *Phys. Rev. B* **2009**, *79*, 1–9.
(39) Barth, J. V.; Brune, H.; Ertl, G.; Behm, R. J. Scanning Tunneling Microscopy Observations on the Reconstructed Au(111) Surface: Atomic Structure, Long-Range Superstructure, Rotational Domains, and Surface

Defects. *Phys. Rev. B* **1990**, *42*, 9307–9318.
(40) Meyer, J. A.; Baikie, I. D.; Kopatzki, E.; Behm, R. J. Preferential Island Nucleation at the Elbows of the Au(111) Herringbone Reconstruction through Place Exchange. *Surf. Sci.* **1996**, *365*, 647–651.
(41) Venkatachalam, S.; Jacob, T. Hydrogen Adsorption on Pd-Containing Au(111) Bimetallic Surfaces. *PCCP* **2009**, *11*, 3010.
(42) Yudanov, I. V; Neyman, K. M. Stabilization of Au at Edges of Bimetallic PdAu Nanocrystallites. *Phys. Chem. Chem. Phys.* **2010**, *12*, 5094–5100.
(43) Yuan, D.; Gong, X.; Wu, R. Atomic Configurations of Pd Atoms in PdAu(111) Bimetallic Surfaces Investigated Using the First-Principles Pseudopotential Plane Wave Approach. *Phys. Rev. B* **2007**, *75*, 085428.
(44) Lucci, F. R.; Darby, M. T.; Mattera, M. F. G.; Ivimey, C. J.; Therrien, A. J.; Michaelides, A.; Stamatakis, M.; Sykes, E. C. H. Controlling Hydrogen Activation, Spillover, and Desorption with Pd-Au Single Atom Alloys. *J. Phys. Chem. Lett.* **2016**, *7*, 480–485.
(45) Hiebel, F.; Montemore, M. M.; Kaxiras, E.; Friend, C. M. Direct Visualization of Quasi-Ordered Oxygen Chain Structures on Au(110)-(1×2). *Surf. Sci.* **2015**, *650*, 5–10.
(46) Saliba, N.; Parker, D. H.; Koel, B. . Adsorption of Oxygen on Au(111) by Exposure to Ozone. *Surf. Sci.* **1998**, *410*, 270–282.
(47) Baber, A. E.; Torres, D.; Muller, K.; Nazzarro, M.; Liu, P.; Starr, D. E.; Stacchiola, D. J. Reactivity and Morphology of Oxygen-Modified Au Surfaces. *J. Phys. Chem. C* **2012**, *116*, 18292.

11.5 Collaborations

Density Function Theory experiments were performed by Graeme Henkelman's Group from Department of Chemistry and Biochemistry at The University of Texas at Austin.

Chapter 12: Surface Structure of Pt-Au(111) Alloys

12.1. Introduction

Understanding the alloying mechanism of bimetallic alloy formation is critical to selectively form single atom alloys. The general criteria that drive alloy formation include mixing enthalpy, surface free energy, atomic size and adatom diffusion. [1–5] Although extensive calculations have predicted the thermodynamic stability of alloyed surface, the kinetics associated with adatom diffusion is not well established for all metal interactions. Due to the industrial importance of Pt based alloys,[6,7] in this chapter, we explore the atomic structure of Pt-Au(111) surface alloys using scanning tunneling microscopy (STM). Pt-Au(111) alloys were prepared at varying Pt coverages and substrate temperatures. Preliminary results suggest that it is unfavorable for Pt atoms to exists as isolated monomers in the surface of Au(111). Low-temperature STM experiments for the co-adsorption of H and CO suggest that H and CO preferentially adsorb to the Pt sites.

12.2. Results and Discussion

In order to determine the surface morphology of sub monolayer coverages of Pt-Au(111) alloys, we used physical vapor deposition to deposit Pt atoms onto Au(111). The Au(111) herringbone reconstruction served as template for Pt alloying. Briefly, the Au(111) surface reconstructs due to under-coordination of the surface atoms.[8] In the surface layer, the Au atoms compress to form the "herringbone reconstruction" where 23 atoms compress into the space of 22 atoms in the bulk. As a result a (22 x $\sqrt{3}$) unit cell is observed. Domains of atoms sitting in hcp and fcc hollows are separated by pairs of soliton walls where the Au atoms sit in bridge sites and thus are topographically higher than neighboring atoms. In order

to relieve the tensile strain equally in all directions, the soliton walls periodically bend 120° at locations called elbows. At the elbows, edge dislocations occur from the misalignment of atomic rows and the atoms at the edge dislocations are under-coordinated, thus, they are preferential binding sites for adsorbates and adatoms.

Using STM, we characterized Pt-Au(111) surface morphology as a function of Pt coverage and Au(111) substrate temperature during deposition of Pt. Initially, we deposited Pt at 380 K. At a coverage of 0.05 ML, we observe small protrusions in the surface layer and monoatomic high islands (Figure 12.1). Atomic resolution shows the Pt atoms imaging as bright protrusions which are ~0.050 nm higher than the surrounding Au lattice (Figure 12.1B). Since the height of the protrusions is less than the atomic radius of Pt (0.277 nm) or Au (0.288 nm), we conclude the Pt atoms are substituted into the Au terrace. Pt atoms image topographically higher than the surrounding Au lattice since the electronic and topographic differences in Pt and Au are responsible for the contrast observed by STM.[9] At this deposition temperature (380 K) and Pt coverage (0.05 ML), the Pt atoms tend to cluster near the edge dislocations with heteroatom nearest-neighbor interactions (Figure 12.1B) in disagreement with Besenbacher *et al.* who observe isolated Pt atoms in Au.[10] The observed clustering of Pt atoms is consistent with DFT calculations[11] and Monte Carlo[12,13] simulations that predict favorable nearest-neighbor interactions between Pt-Pt atoms. According to Christensen *et al.* the solute and substrate identities influence the intermetallic mixing.[1] For Pt substituted into a Au lattice, the surface mixing energy (0.22 eV/atom) indicates mixing of the Pt and Au atoms. The reverse trend is predicted for Pt substitution into a Au lattice where surface mixing energy (-0.31 eV/atom) indicates segregation of the Pt and Au atoms. Experimentally, Bensenbacher *et al.* observed isolated Pt atoms in Au at coverages below

0.03 ML.[14] Since there is not a thermodynamic driving force for the formation of Pt monomers, possibly the Pt monomers observed at low coverages is an entropic effect due to the low probability of 2 Pt atoms existing as nearest neighbors at low concentrations. Furthermore, Pt is a group 6 transition metal; therefore, relativistic effects can impact its alloy formation. [1,15–17]

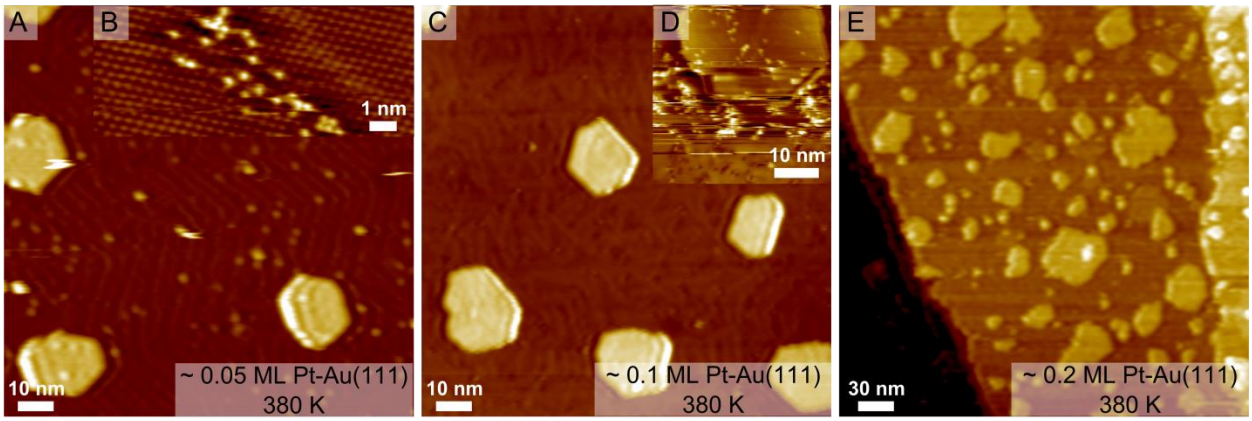

Figure 12.1. STM images of Pt-Au(111) surface alloys at varying Pt coverages
Shown are the surface structures of (A, B) 0.05 ML Pt, (C, D) 0.1 ML Pt, and (E) 0.2 ML Pt deposited at 380 K. (B) With atomic resolution the Pt atoms image higher than the Au lattice. (D) Higher resolution of an island shows disperse protrusions on the island. Images recorded at 30 K.

Additionally, monoatomic hexagonal islands are observed with an average size of ~200 nm^2 for 0.05 ML Pt. The islands are randomly dispersed across the Au terraces and their location is independent of edge dislocations. The dispersion of the islands is suggestive of Ostwald Ripening where the diffusion of Au atoms condense into larger Au clusters. Higher resolution imaging of the islands shows the dominance of the herringbone reconstruction with dispersed protrusions (Figure 12.1D and 12.2D). Thus, we conclude the islands are Au rich. The observance of Au rich islands is consistent with the greater surface free energy of Pt (2,203 J/m^2) than Au (1.63 J/m^2).[18] Despite the presence of Au rich islands

and substitution of Pt atoms into the Au lattice, the distance between the Au soliton walls is consistent with the separation observed on pure Au(111).

At higher Pt concentration of 0.1 ML, the density of the Au rich islands on the surface increases. The islands remain fairly uniform in size and maintain a hexagonal shape by equally expressing both (100) and (111) micro-facets step edges. The soliton walls on the underlying Au terraces, however, begin to run in irregular patterns. Then at 0.2 ML Pt, the concentration of islands increased and their shape is irregular suggesting slow diffusion kinetics of Pt and Au atoms.

At 380 K, the proposed alloying mechanism is as follows. The Pt atoms are randomly deposited onto the Au surface. Pt atoms diffuse until they come in contact with uncoordinated Au atoms at edge dislocations and potentially step edges. The Pt atoms then place exchange into the Au terraces. During the exchange process, Au atoms are ejected onto the surface. The ejected Au atoms and Pt adatoms nucleated into Au rich islands. Ostwald Ripening drives the Au rich islands to condense thereby reducing the concentration of under coordinated Au atoms. At higher Pt concentrations, these islands begin to incorporate deposited Pt atoms to a higher degree and become irregular in shape suggesting slow diffusion of adatoms. The proposed mechanism is consistent with the predominate alloying mechanism of other solute atoms with Au(111) surface including Pd[8,19–23], Ni[24], Fe[25], and Co[26].

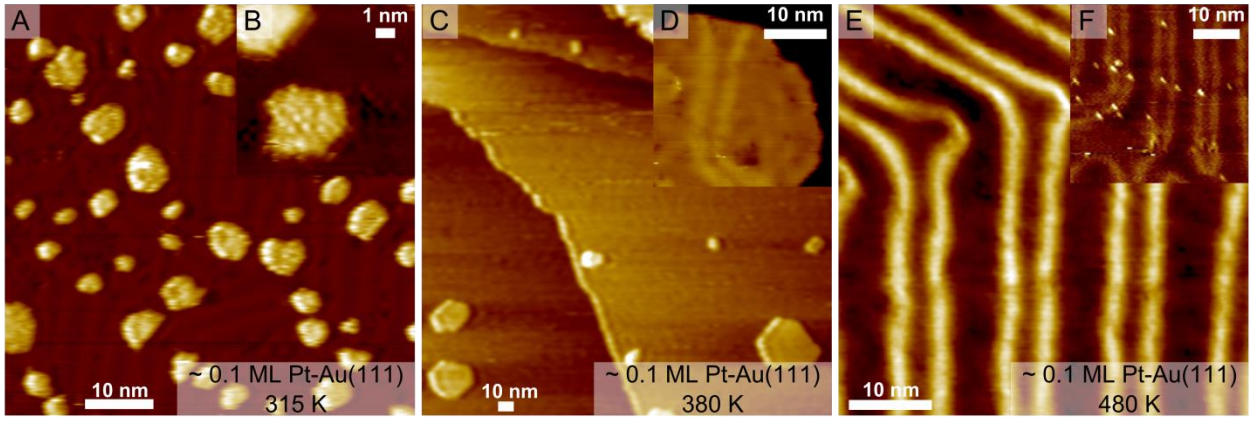

Figure 12.2. STM images of Pt-Au(111) surface alloys formed at varying temperatures Shown are STM images of 0.1 ML Pt deposited onto Au at (A, B) 315 K, (C, D) 380 K, and (E, F) 480 K. Shown are higher resolution images of the (B, D) islands on the Au surface and (F) Pt atoms dispersed across the Au surface. Images recorded at 30 K.

To further investigate the alloying mechanism, we varied the temperature of the Au(111) substrate during deposition of 0.1 ML Pt. At deposition temperature of 315 K, islands of varying sizes were dispersed across the surface (Figure 12.2). The islands appeared corrugated and the herringbone reconstruction was not visible on these islands. We propose that the islands formed at 315 K are a mixture of Pt and Au. As discussed above, when the deposition temperature is increased to 380 K, larger Au rich islands are present with Pt atoms substituted into the Au terraces. Then at deposition temperature of 480 K, a uniform surface was observed without any island features. The periodicity of soliton walls is increased to 6.8 nm which is larger than the typical separation of 6.3 nm. Though, atomic resolution was not obtained, the extension of the soliton walls suggest Pt atoms are substituted into the Au terrace. Depending on the tip state, dispersed protrusions can be observed on the Au surface, however, the resolution does not allow us to determine the size of the Pt ensembles or the location of the Pt atoms in the surface or subsurface layers. Further experimentation at the

higher deposition temperature (480 K) and low Pt concentration (< 0.01 ML Pt) might produce isolated Pt atoms in Au allowing for the formation of single atom alloys.

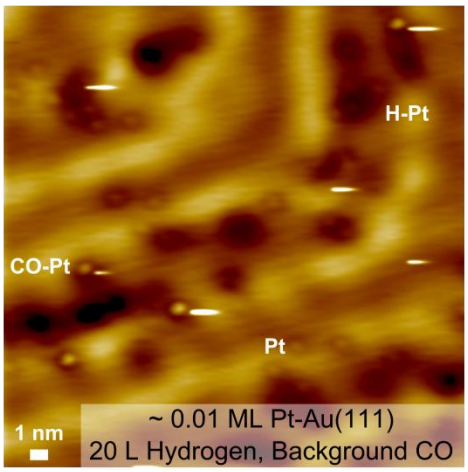

Figure 12.3. H and CO adsorption on Pt-Au alloys
STM image of H and CO adsorbed onto 0.01 ML Pt-Au(111). Images recorded at 5 K.

In order to probe the adsorption of H and CO on Pt-Au alloy systems, low-temperature STM (5 K) experiments were performed after the co-adsorption of H and CO on Pt-Au alloys. The Pt-Au alloys were prepared after depositing ~0.01 ML Pt on Au(111) at 380 K. The surface structure of the alloys was heterogeneous with isolated Pt atoms, short linear chains of Pt atoms and Au rich islands. The alloyed surface was exposed to 20 L H at 85 K and then cooled to 5 K for imaging. According to H_2 uptake on Pd-Au(111) alloys presented in Chapter 9 and 10, a 20 L dose would yield adsorption of background gases including CO and H_2O that could potentially block the adsorption of the H adatoms. After exposure to H_2, we observed 3 distinct features on the surface that I hypothesize are H adatoms, CO molecules, and Pt atoms. We propose that the dark depressions are H adatoms on Pt sites since H is known to image as depressions.[27,28] Furthermore, since it is thermodynamically unfavorable for H adatoms to diffuse onto Au, we propose the H atoms are localized at the Pt sites. The topographically larger protrusions are adsorbed CO. After

exposing the surface to 0.05 L CO, the concentration of these protrusions increased. Like H, CO selectively adsorbs to the Pt sites since the adsorption energy is -1.77 eV to Pt-Au SAA and -0.49 eV to Au(111). The less pronounced protrusions are Pt atoms substituted into the Au surface since these features are present before H or CO adsorption and remain stationary. Further experimentation, however, is necessary to confirm the assignments of the adsorbed species.

12.3. Summary/Future Directions

Using STM, we were able to characterize the surface structure of Pt-Au(111) alloys to elucidate the alloying mechanism. Adatoms condense into Au rich islands whose composition and size are dependent on the substrate temperature during preparation and Pt coverage. Atomically resolved images show that the Pt atoms tend to exist in small clusters in the surface layer. However, higher temperature preparation and lower Pt coverages may yield isolated Pt monomers in the Au surface.

Though it is thermodynamically favorable for Pt atoms to exist in small clusters in Au, Pt-Au alloys have the potential to catalyze various reactions. Of interest are selective oxidation reactions which typically exhibit higher activation energies due to strong O_2 bonds. Potentially, Pt-Au alloys can be utilized to catalyze selective oxidation reactions to a greater extent than Pd-Au alloys. Since Pt is able to bind reactants stronger than Pd, Pt based alloys may exhibit higher reactivity than Pd based alloys as we observed for methanol dehydrogenation on Pt-Cu and Pd-Cu alloys. The higher reactivity of Pt based alloys can be rationalized based on the Brønsted-Evans-Polyani (BEP) relationship which correlates adsorption strength of descriptor molecules to overall reactivity. As observed for SAAs, Pt-Cu SAAs bind key descriptor molecules such as H and CO stronger than Pd-Cu SAAs. For

example, we observed CO desorbing at a higher temperature from Pt-Cu(111) SAAs (350 K),[29] than Pd-Cu(111) SAAs (270 K),[30] the stronger binding suggests lower activation barriers that we observe for H_2 activation.[31,32] Due to the stronger binding of these molecules to Pt based SAAs, isolated Pt atoms may be more reactive than Pd atoms, thereby exhibiting higher catalytic activity. Some interesting oxidation reactions to explore with Pt-Au alloys include ammonia oxidation to N_2 and H_2O to remove ammonia from waste,[33] epoxidation of ethylene for the production of ethylene glycol, and propylamine oxidation to propionitrile.[34]

12.4. Additional Experimental Details

Pt was deposited onto the clean Au(111) sample held at varying surface temperatures using a flux monitored EFM 3 electron beam evaporator (Focus GmbH). Pt was deposited at a flux of 0.02 monolayer (ML) min^{-1} for varying amounts of time to obtain surface coverages between 0.01 and 5 ML Pt. Surface coverages are based on the calibration determined in Chapter 2 for Pt deposition onto Cu(111) at 380 K. STM experiments were performed using either a variable-temperature (VT) or low-temperature (LT) scanning tunneling microscope (Omicron Nanotechnology). Imaging of the bare Pt-Au surfaces was performed at 30 K with VT-STM. The VT-STM stage was cooled to 30 K prior to introducing the prepared sample and etched W tips were used to acquire images. In order to observe adsorbed H atoms, imaging was conducted using the LT-STM at 5 K after exposure to H_2 at 85 K and subsequent cooling to 5 K.

12.5. References

(1) Christensen, A.; Ruban, A. V.; Stoltze, P.; Jacobsen, K. W.; Skriver, H. L.; Nørskov, J. K.; Besenbacher, F. Phase Diagrams for Surface Alloys. *Phys. Rev. B* **1997**, *56*, 5822–5834.

(2) Groß, A. Reactivity of Bimetallic Systems Studied from First Principles. *Top. Catal.* **2006**, *37*, 29–39.

(3) Rodriguez, J. A.; Rodriguex, J. A. Physical and Chemical Properties of Bimetallic Surfaces. *Surf. Sci. Rep.* **1996**, *24*, 223–287.
(4) Brune, H.; Röder, H.; Bromann, K.; Kern, K.; Jacobsen, J.; Stoltze, P.; Jacobsen, K.; Nørskov, J. K. Anisotropic Corner Diffusion as Origin for Dendritic Growth on Hexagonal Substrates. *Surf. Sci.* **1996**, *6028*, L115–L122.
(5) Hwang, R. Q.; Schroder, J.; Gunther, C.; Behm, R. J. Fractal Growth of Two-Dimensional Islands: Au on Ru(0001). *Phys. Rev. Lett.* **1991**, *67*, 3279–3282.
(6) Stamenkovic, V. R.; Mun, B. S.; Arenz, M.; Mayrhofer, K. J. J.; Lucas, C. A.; Wang, G.; Ross, P. N.; Markovic, N. M. Trends in Electrocatalysis on Extended and Nanoscale Pt-Bimetallic Alloy Surfaces. *Nat. Mater.* **2007**, *6*, 241–247.
(7) Weitkamp, J.; Jacobs, P. A.; Martens, J. A. Isomerization and Hydrocracking of C_9 through C_{16} N-Alkanes on Pt/HZSM-5 Zeolite. *Appl. Catal. B* **1983**, *8*, 123–141.
(8) Barth, J. V.; Brune, H.; Ertl, G.; Behm, R. J. Scanning Tunneling Microscopy Observations on the Reconstructed Au(111) Surface: Atomic Structure, Long-Range Superstructure, Rotational Domains, and Surface Defects. *Phys. Rev. B* **1990**, *42*, 9307–9318.
(9) Varga, P.; Schmid, M. Chemical Discrimination on Atomic Level by STM. *Appl. Surf. Sci.* **1999**, *141*, 287–293.
(10) Besenbacher, F.; Chorkendorff, I.; Clausen, B. S.; Hammer, B.; Molenbroek, A. M.; Nørskov, J. K.; Stensgaard, I. Design of a Surface Alloy Catalyst for Steam Reforming. *Science* **1998**, *279*, 1913–1915.
(11) Stephens, J. A.; Ham, H. C.; Hwang, G. S. Atomic Arrangements of AuPt/Pt(111) and AuPd/Pd(111) Surface Alloys: A Combined Density Functional Theory and Monte Carlo Study. *J. Phys. Chem. C* **2010**, *114*, 21516–21523.
(12) Bergbreiter, A.; Alves, O. B.; Hoster, H. E. Entropy Effects in Atom Distribution and Electrochemical Properties of Au_xPt_{1-x}/Pt(111) Surface Alloys. *ChemPhysChem* **2010**, *11*, 1505–1512.
(13) Zoontjens, P.; Grochola, G.; Snook, I. K.; Russo, S. P. A Kinetic Monte Carlo Study of Pt on Au(111) with Applications to Bimetallic Catalysis. *J. Phys. Condens. Matter* **2011**, *23*, 015302.
(14) Pedersen, M. Ø.; Helveg, S.; Ruban, A.; Stensgaard, I.; Lægsgaard, E.; Nørskov, J. K.; Besenbacher, F. How a Gold Substrate Can Increase the Reactivity of a Pt Overlayer. *Surf. Sci.* **1999**, *426*, 395–409.
(15) Canzian, A.; Mosca, H. O.; Bozzolo, G. Atomistic Modeling of Pt Deposition on Cu(111) and Cu Deposition on Pt(111). *Surf. Rev. Lett.* **2004**, *11*, 235–243.
(16) Lu, Z. W.; Wei, S. H.; Zunger, A. Long-Range Order in Binary Late-Transition Metal Alloys. *Phys. Rev. Lett.* **1991**, *66*, 13–16.
(17) Sanyal, B.; Bose, S. K.; Drchal, V.; Kudrnovský, J. Ordering and Segregation in X Pt (X =V, Cu, and Au) Random Alloys. *Phys. Rev. B* **2001**, *64*, 134111–1 – 10.

(18) Tyson, W. R.; Miller, W. A. Surface Free Energies of Solid Metals Estimation from Liquid Surface Tension Measurments. *Surf. Sci.* **1977**, *62*, 267–276.
(19) Baber, A. E.; Tierney, H. L.; Sykes, E. C. H. Atomic-Scale Geometry and Electronic Structure of Catalytically Important Pd/Au Alloys. *ACS Nano.* **2010**, *4*, 1637–1645.
(20) Ruff, M.; Takehiro, N.; Liu, P.; Nørskov, J. K.; Behm, R. J. Size-Specific Chemistry on Bimetallic Surfaces: A Combined Experimental and Theoretical Study. *ChemPhysChem* **2007**, *8*, 2068–2071.
(21) Maroun, F.; Ozanam, F.; Magnussen, O. M.; Behm, R. J. The Role of Atomic Ensembles in the Reactivity of Bimetallic Electrocatalysts. *Science* **2001**, *293*, 1811–1814.
(22) Casari, C.; Foglio, S.; Siviero, F.; Li Bassi, A.; Passoni, M.; Bottani, C. Direct Observation of the Basic Mechanisms of Pd Island Nucleation on Au(111). *Phys. Rev. B* **2009**, *79*, 1–9.
(23) Meyer, J. A.; Baikie, I. D.; Kopatzki, E.; Behm, R. J. Preferential Island Nucleation at the Elbows of the Au(111) Herringbone Reconstruction through Place Exchange. *Surf. Sci.* **1996**, *365*, 647–651.
(24) Chambliss, D. D.; Wilson, R. J.; Chiang, S. Nucleation of Ordered Ni Island Arrays on Au(111) by Surface-Lattice Dislocations. *Phys. Rev. Lett.* **1991**, *66*, 1721–1724.
(25) Stroscio, J. A. Microscopic Aspects of the Initial Growth of Metastable FCC Iron on Au(111). *J. Vac. Sci. Technol. A Vacuum, Surfaces, Film.* **1992**, *10*, 1981–1985.
(26) Voigtländer, B.; Meyer, G.; Amer, N. M.; Voigtllnder, B.; Meyer, G.; Arner, N. M. Epitazial Growth of Thin Magnetic Cobalt Films on Au(111) Studied by Scanning Tunneling Microscopy. *Phys. Rev. B* **1991**, *44*, 10354–10357.
(27) Jewell, A. D.; Peng, G.; Mattera, M. F. G.; Lewis, E. A.; Murphy, C. J.; Kyriakou, G.; Mavrikakis, M.; Sykes, E. C. H. Quantum Tunneling Enabled Self-Assembly of Hydrogen Atoms on Cu(111). *ACS Nano* **2012**, *6*, 10115–10121.
(28) Lauhon, L. J.; Ho, W. Direct Observation of the Quantum Tunneling of Single Hydrogen Atoms with a Scanning Tunneling Microscope. *Phys. Rev. Lett.* **2000**, *85*, 4566–4569.
(29) Liu, J.; Lucci, F. R.; Yang, M.; Lee, S.; Marcinkowski, M. D.; Therrien, A. J.; Williams, C. T.; Sykes, E. C. H.; Flytzani-Stephanopoulos, M. Tackling CO Poisoning with Single Atom Alloy Catalysts. *J. Am. Chem. Soc.* **2016**, *138*, 6396–6399.
(30) Marcinkowski, M. D.; Jewell, A. D.; Stamatakis, M.; Boucher, M. B.; Lewis, E. A.; Murphy, C. J.; Kyriakou, G.; Sykes, E. C. H. Controlling a Spillover Pathway with the Molecular Cork Effect. *Nat. Mater.* **2013**, *12*, 523–528.
(31) Lucci, F. R.; Marcinkowski, M. D.; Lawton, T. J.; Sykes, E. C. H. H_2 Activation and Spillover on Catalytically Relevant Pt-Cu Single Atom Alloys. *J. Phys. Chem. C* **2015**, *119*, 24351–24357.

(32) Fu, Q.; Luo, Y. Catalytic Activity of Single Transition-Metal Atom Doped in Cu(111) Surface for Heterogeneous Hydrogenation. *J. Phys. Chem. C.* **2013**, *117*, 14618–14624.
(33) Gong, J.; Flaherty, D. W.; Ojifinni, R. A.; White, J. M.; Mullins, C. B. Surface Chemistry of Methanol on Clean and Atomic Oxygen Pre-Covered Au(111). *J. Phys. Chem. C.* **2008**, *112*, 5501–5509.
(34) Gong, J.; Yan, T.; Mullins, C. B. Selective Oxidation of Propylamine to Propionitrile and Propionaldehyde on Oxygen-Covered Gold. *Chem. Com.* **2009**, *7*, 761–763.